HOW PRIMATES INTERACT WITH THEIR ENVIRONMENT: ADAPTIVE GEOMETRY, DYNAMIC HOME RANGES, AND SPATIOTEMPORAL STRUCTURE IN BEHAVIOUR

MARCUS JACK DOSTIE
Masters of Science, University of Lethbridge, 2014

A thesis submitted
in partial fulfilment of the requirements for the degree of

DOCTOR OF PHILOSOPHY

in

BIOSYSTEMS AND BIODIVERSITY

Department of Geography & Environment
University of Lethbridge
LETHBRIDGE, ALBERTA, CANADA

HOW PRIMATES INTERACT WITH THEIR ENVIRONMENT: ADAPTIVE GEOMETRY, DYNAMIC HOME RANGES, AND SPATIOTEMPORAL STRUCTURE IN BEHAVIOUR

MARCUS JACK DOSTIE

Date of Defence: February 13, 2026

Dr. Louise Barrett	Professor	Ph.D.
Dr. Stefan Kienzle	Professor	Ph.D.
Thesis Co-Supervisors		
Dr. Peter Henzi	Professor	Ph.D.
Thesis Examination Committee Member		
Dr. Shawn Bubel	Professor	Ph.D.
Thesis Examination Committee Member		
Dr. Leslie Brown	Professor	Ph.D.
External Examiner		
University of South Africa		
Roodepoort, South Africa		
Dr. Josie Mills	Professor	Ph.D.
Chair, Thesis Examination Committee		

Dedication

This dissertation is dedicated to my wife Tina who supported me through the journey of going back to school for my doctorate.

I would also like to dedicate Chapter 2 to the memory of Parry M. R. Clarke whose extensive fieldwork at DeHoop, South Africa, provided the Baboon data for this study.

Abstract

The convergence of recent technical advances in spatial data collection and quantitative analysis offers new opportunities to generate explicitly spatial insights into problems faced by researchers across disciplines. In this context, I examine how social behaviour is shaped by the environment in which it occurs. Specifically, I address the following overarching questions: How do baboons adapt their spatial geometry to optimize foraging while maintaining dominance hierarchies? How can dynamic home range estimation, based on regularly updated kernel density estimates across time, improve our understanding of space use and its role in shaping social and ecological interactions, such as intertroop encounters in vervet monkeys? Is there a relationship between home ranges and intertroop encounters? Specifically, does proximity to the centre of one's home range influence the probability of winning, as suggested by patterns observed in white-faced capuchins (Crofoot et al., 2008)? Can dynamic home ranges, updated at fine temporal scales, reveal patterns missed by static approaches? Furthermore, what insights emerge when behaviours are analyzed in their absolute spatial and temporal contexts, independent of home range constructs? To answer these questions, I introduce two new methods for analyzing primate interactions with their environment: the *Dynamic Home Range Model*, which enables users to generate home ranges at variable temporal scales, including a single range, and the *Structure of Behaviour Analysis Model*, which predicts the spatiotemporal structure of observed behaviours as a three-dimensional point cloud. These models show that baboons are able to adapt their spatial and social geometry as they move through the landscape, in response to food availability and the structure of the environment (Chapter 2); home ranges measured at

smaller temporal scales offer greater detail about how animals are responding to seasonal trends in resource availability (Chapter 3); and that while the Samara population of Vervet monkeys does not show a connection between distance to home ranges and winning or loosing an inter-troop encounter, structure in behaviours (aggression and initiation) and outcomes (winning) can be modelled and demonstrate a spatial temporal component to ITE's (Chapter 4).

Contribution of Authors

Chapter 2: Proof of principle: The adaptive geometry of social foragers

Marcus J. Dostie: Conceptualisation, data analysis, writing and review. **David Lusseau**: Mathematical modelling. **Tyler Bonnell**: Data analysis, writing. **Parry M. R. Clarke**: Methodology, data collection. **George Chaplin**: Data analysis. **Stefan Kienzle**: Data analysis. **Louise Barrett**: Funding acquisition, methodology, conceptualisation, supervision, writing and review. **S. Peter Henzi**: Funding acquisition, methodology, conceptualisation, supervision, writing and review.

Preface

The overarching aim of this thesis research is to investigate how animals, in this case, two Old-World primate species, interact with their physical environment. This research does not start from a presumption of environmental determinism; in no way do I hypothesise that the environment determines behaviour. Instead, it is an exploration of the ways in which the environment structures behaviour and shapes interactions within and across groups.

For example, I do not argue that, as humans, cold weather predetermines a single coping strategy, such as putting on a jacket or turn up the heat. I do, however, argue that the cold must be engaged with, even if it means retreating indoors or dressing warmer. I also propose that while there is no single way to respond to the cold, there are common cultural responses to it.

Similarly, animals exhibit plasticity: the same species, even the same population, can express different phenotypes or adopt different reaction norms in response to environmental variation. This flexibility underscores that while behaviour is not predetermined, it is nonetheless shaped by ecological context. In this thesis, I focus on how groups, reflecting the actions of the individuals that comprise them, respond to their environment. In order to study these responses, I needed to gain an in-depth understanding of both the organism and the environment in which it lives. This foundational knowledge is integrated throughout the thesis.

Acknowledgements

I would like to thank Cape Nature for permission to undertake the study in Chapter 2. Thanks also to Dr. Matt Grove and two anonymous referees for comments and suggestions that improved the Chapter 2 manuscript substantially.

Thank you to the Samara Game Reserve for permission to undertake the studies in Chapter 3 and 4. Also, thank you to Asanta Sana Game Reserve, Richard, and Kitty for being excellent hosts to not only me but the entire BANZI Lab team during our many visits.

Finally, a special thanks to my committee, colleagues, BANZI lab mates, and friends and family who are too many to name but have all supported me along the way. I would also like to recognize the many hours that the researchers and research assistants of the BANZI lab put into collecting data in Samara, South Africa. Without their work much of my data would not exist.

This research was funded by grants from the Leakey Foundation, National Science and Engineering Research Council, Canada to S. Peter Henzi and Louise Berret and by the National Research Foundation, South Africa to S. Peter Henzi.

Table of Contents

List of Tables

List of Figures

List of Abbreviations

AIC – Akaike Information Criterion

AUC – Area Under the ROC Curve

BRMS – Bayesian Regression Models using Stan

CGIS – Canada Geographic Information Systems

CI – Credible Interval

DHR – Dynamic Home Range

DSS – Days Since Start

DSS_S or DSSs – Days Since Start Scaled and Centreed

ELPD – Expected Log Predictive Density

ELPD_Diff – Expected Log Predictive Density Difference

EOS – Earth Observing System

ESS - Effective Sample Size

GAM – Generalized Additive Model

GIS – Geographic Information Systems

GLMM – Generalized Linear Mixed Models

GME – Geospatial Modelling Environment

GPS – Global Positioning System

GSMap – Global Satellite Mapping of Precipitation

HMC – Hamiltonian Monte Carlo

ICC – Intraclass Correlation Coefficient

InitB – Initiation Binary

ITE – Inter Troop Encounters

JAXA – Japan Aerospace Exploration Agency

KDE – Kernel Density Estimation

l-95% – Lower 95% Credible Interval

LMM – Linear Mixed Model

LOOIC – Leave-One-Out Information Criterion

MODIS – Moderate Resolution Imaging Spectroradiometer

NASA – National Aeronautics and Space Administration

NDVI – Normalized Difference Vegetation Index

NIR – Near Infrared

NUTS – No-U-Turn Sampler

OR – Odds Ratios

Pd – Probability of Direction

Point Y, Y – Y Coordinates in WGS84 UTM 35S

Point_X, X – X Coordinates in WGS84 UTM 35S

Point_X_S, Xs – X Coordinates Scaled and Centreed

Point_Y_S, Ys – Y Coordinates Scaled and Centreed

PT – Picnic Troop

QTC – Qualitative Trajectory Calculus

R2 - Coefficient of Determination

RBM – River Bend Mob

ROC – Receiver Operating Characteristic

RST – River Side Troop

RW – Relative Width

SCV – Smoothed Cross-Validation

SD – Standard Distances

SDA – Spatial Data Analysis

SE – Standard Error

SE_Diff – Standard Error Difference

TDC – Troop Distance to Centre

TSA – Time Series Analysis

TSS – Time Since Start

u-95% – Upper 95% Credible Interval

VI – Vegetation Index

WinB – Winning Binary

ΔAgr – Difference in Aggression

ΔPart – Difference in Participation

σ - Standard Deviation

σ^2 – Group-Level Variance

Introduction and Literature Review

As a geographer with a focus on spatial analytics, my overarching objective in this thesis is to develop and apply techniques that address empirical issues in other domains. In other words, my goal is to demonstrate how the intersection of recent technical advances in spatial data gathering and the quantitative analyses of these data can provide explicitly spatial insights into problems confronted by researchers in other areas. Accordingly, I have chosen to explore ways to investigate how social behaviour is structured by the environment in which it occurs. As emphasized in a recent review of this topic (Webber et al., 2023), the consideration of social behaviour in the context of structuring environments is both timely, given the increasing availability of high-resolution data, and appropriate, given the evidence that behaviour has a demonstrably spatial aspect. To contribute to this emerging research paradigm, I have taken advantage of large and pertinent socio-spatial data sets that exist for two species of Old-World primate, the baboon (*Papio ursinus*) and the vervet monkey (*Chlorocebus pygerythrus*), for which comprehensive datasets exist from long-term study sites in South Africa.

The frameworks and specific background research from which I investigated the disparate social issues, derived in collaboration with domain experts, are elaborated in the relevant data chapters. Here, In Chapter 1, I take the opportunity to provide a broad overview of the geographical topics and statistical issues that informed my approach to the research questions I addressed.

Movement Analysis

The study of movement can be traced back in recorded history as far as Aristotle's treatise "*De Motu Animalium*", where he wrote in the opening chapter, "Now we must consider in general the common reason for moving with any movement whatever." (Aristotle, trans. 1985). Pliny the Elder also wrote on the subject of animal movement in a series of encyclopedia volumes called "*Naturalis Historia"* between 77 and 79 AD*,* in Volume Ten he queries the origin and destination of migrating birds (Pliny, trans. 1634). It is likely humans have studied the movement of not only animals, but also the stars and planets since our species' first days as subsistence hunters tracking prey or navigating by the stars (Andrienko et al., 2008).

For movement ecology, advances in tracking devices, computing power, statistical and mathematical methods, geographical information systems (GIS), and remote sensing data have led to ongoing (r)evolutionary progress in this field over many decades (Börger, 2016). I emphasize Börger's use of *evolutionary* combined with the *revolutionary* adjective because much of this technology did not exist the field of movement ecology until recently, with movement ecology having only been established as a an area of study in 2008 (Nathan et al., 2008), and Global Positioning Satellite data only becoming truly useful / available to consumers at the turn of the twenty-first century (Adrados et al., 2002).

A search for academic articles on animal movement in Web of Science (WoS) returns 63,561 results. To reduce false positives, such as physiology papers that use these words in unrelated contexts, the exact term "*animal movement"* was used, yielding 3,931 results. Of these, only eight predate 1976. After that, at least one article appeared every

year (except 1981) through to the present. Between 1976 and 1993, 45 articles were published, followed by another 83 between 1993 and 2000. From 2000 to 2008, publications increased nearly fourfold to 313, and since 2008, an additional 3,478 articles have been published (Figure 1.1).

These increases in scholarly output can be explained in the context of technological and methodological advances. In the mid 1960s, radio tracking systems practical for wildlife movement studies were developed (Cochran & Lord Jr, 1963; Marshall et al., 1962). In 1993, the Global Positioning System (GPS) reached its initial operational capability milestone and was released to civilian use, opening the doors for GPS tracking of wildlife (Rempel et al., 1995). The year 2000 marks what is probably one of the biggest technological changes in the field: the United States Department of Defense discontinued protective measures, referred to as *selective availability*, that restricted foreign nations from using GPS technology on the battlefield. This measure had degraded GPS accuracy by ~100 meters for receivers without the correct encryption and included the ability to "shut out" non-encrypted users. Prior to 2000, the primary method used to offset selective availability errors was differential GPS, which involved taking several readings at a location and then correcting positions through post-processing with base station data (Adrados et al., 2002).

Of the articles published prior to 2000, only six included the term *GPS*, which is not surprising given the impact selective availability had on consumer GPS accuracy. Since 2000, of the 3,808 articles published on animal movement, 2,579 (~68%) include the term GPS (Figure 1.1). While tracking technology has driven a proliferation of

publications on animal movement, the most recent advancement in the field was methodological: the creation of the movement ecology paradigm by Nathan et al. (2008).

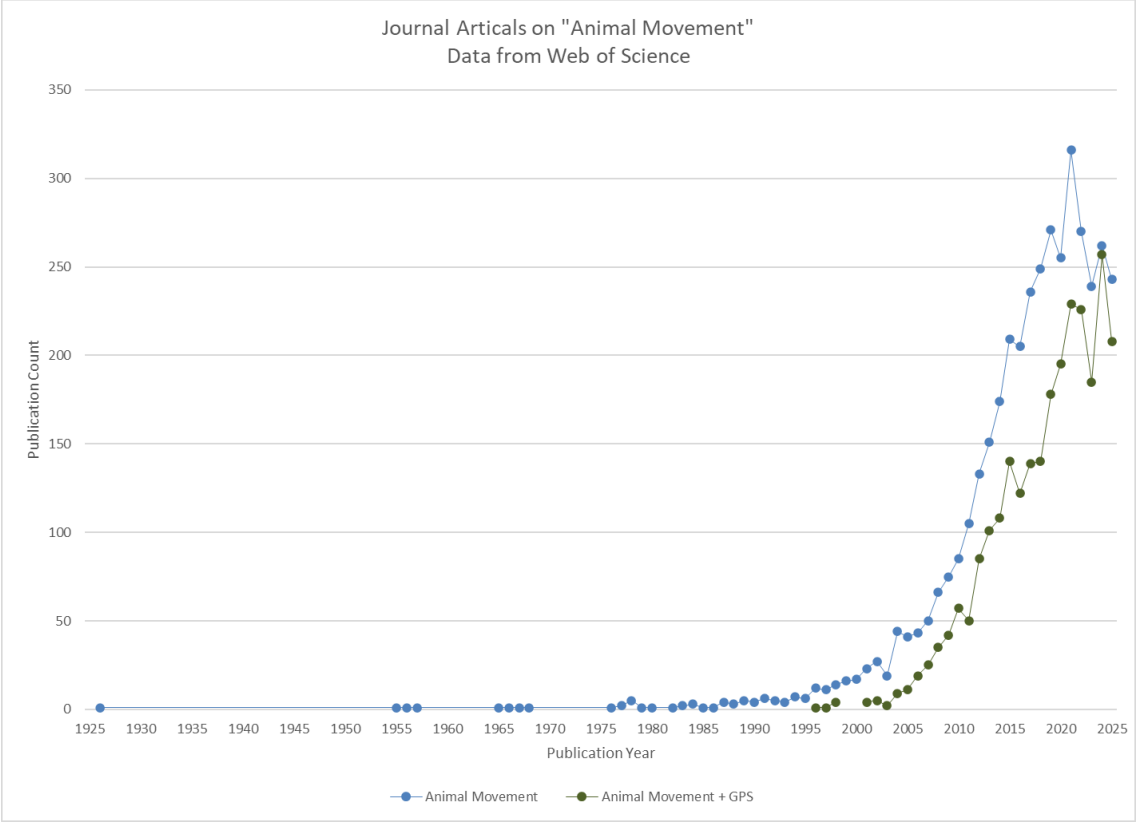

Figure 1.1: "Animal Movement" publications from the Web of Science Core Collection (Last Accessed: 06 Dec 2025).

Movement Ecology has seen a proliferation in the number of large, highly precise data sets available, due to advances in tracking technology like the GPS (Getz et al., 2007) and online databases for movement data like movebank.org which allow researchers to share and track movement data online (Wikelski, 2017). Access to highly accurate positioning data from GPSs still plays its role in the study of animal movement, but it is no longer a noteworthy advance in the field.

Movement Ecology Paradigm

In the 125th anniversary edition of *Science* the question "What don't we know?" appears at the top of every page. The article *So Much More to Know…* compiles a series

of questions that researchers still struggle to answer. One boxed inset at the bottom of the page poses the question: “How do migrating organisms find their way? Birds, butterflies, and whales make annual journeys of thousands of kilometers. They rely on cues such as stars and magnetic fields, but the details remain unclear ("So Much More to Know," 2005, p. 92). It is interesting to note that the movement of migrating birds was a strong focus in Pliny the Elders’ work (Pliny, trans. 1634) and continues to be a focus for human study nearly two centuries later. In 2006, *Science* released another article called “Inching Towards Movement Ecology” (Holden, 2006). This article served as an introduction for the Movement Ecology Group formed later that year who were tasked to develop a general theory of movement. This lead to a special edition in PNAS called *Movement Ecology* (Nathan, 2008; Nathan et al., 2008) in which the group laid out the foundations for the paradigm.

Prior to movement ecology, four major paradigms for the study of movement prevailed: the biomechanical paradigm, the cognitive paradigm, the random paradigm, and the optimality paradigm (Nathan et al., 2008). The biomechanical approach is concerned primarily with the mechanics of movement, energetics, and the physiological state of the organism. Researchers engaged in this approach provide good information on motion capacity, examining, for example, how changes in speed relate to gait transitions such as walking versus running (Vogel, 2013), but they generally do not address navigational capacity, movement paths, or environmental influences, since their studies are often conducted in controlled, static experimental conditions that do not generate full movement trajectories. The cognitive paradigm focuses on the how the organism and the brain make movement and navigation decision within its environment (Jeffery, 2003), but

is criticized for a lack of insight on how individuals implement these decisions and how their movement's interaction with the environment influence future motivations to move (Nathan et al., 2008). The random paradigm focuses primarily on random walk and diffusion models to explain movement, typically in the absence of any motivation, environmental factors, motion, or navigational capacities. Random walk models generate assumptions such as, organisms will randomly search for food (Turchin, 1998). Finally, the optimality approach focuses on problems such as determining the conditions that will prompt an animal to change a behaviour like foraging. It is primarily concerned with the internal state and external factors but rarely considers the movement path, motion, or navigational capacity of the organism. The movement ecology paradigm is not a replacement for these existing approaches, but an integration of the methods developed by all of them (Nathan et al., 2008).

Over the past couple decades, researchers have adopted the understanding that spatial changes in average population density cannot explain all population phenomena, and that individual movement behaviour plays an important role as well (Patterson et al., 2008). Individual movement behaviour must be considered with general behaviour (Morales & Ellner, 2002). Behaviour, and its influence on the internal state of the animal, could have direct or indirect effects on the animal's motivation to move. In other words, animals cannot be treated as simple particles which diffuse along the path of least resistance towards areas of 'low pressure', but as complex agents that have the ability to choose their path. Movement Ecology emphasizes this need to understand the movement of living organisms of all kinds in the context of their internal states, traits, constraints, and interactions between themselves and the environment (Nathan et al., 2008). This is

laid out as four basic components: (i) Internal state - also described as the ‘why’ or motivation for movement; (ii) Motion mechanisms - the ‘how ‘of movement; (iii) Navigation mechanisms - the ‘when’ and ‘where’; and (iv) External Factors - all other elements influencing movement.

While the internal state and motion mechanism of an organism can create a movement path in the absence of a navigation mechanism, when there is capacity to perceive the environment and make decisions, a navigation mechanism can be involved in the creation of a movement path. As an organism creates a movement path external, factors can create a feedback loop that can influence and cause changes in the internal state, motion mechanism, and navigation mechanism of the organism. Movement Ecology focuses on individuals, with the individual’s movement taken into consideration at various movement scales ranging from a single step, a movement phase, up to the lifetime (birth to death) of the organism. From these various scales, one can identify the basic mechanistic components of movement (Nathan et al., 2008), or possibly, the simple rules that govern movement (Barrett, 2011).

Eulerian vs. Lagrangian Approaches

Recent advances in the field of movement research have marked a shift from the more traditional Eulerian approach to the Lagrangian approach (Nathan et al., 2008; Schick et al., 2008; Turchin, 1998). These two approaches originate from fluid dynamics, where they describe different ways of conceptualizing motion, and they translate directly into the researcher’s perspective when studying movement. Adopting a Eulerian perspective means focusing on how conditions change at fixed locations in space, metaphorically similar to sitting on the riverbank and recording how water passes a

specific point, while the Lagrangian approach is analogous to floating down the river in a boat and experiencing the motion of the river directly. In animal movement, the Eulerian approach is often used to quantify population redistribution and can be thought of as the landscape-level perspective. A common Eulerian method is the diffusion model, which treats animal movement as a flow from areas of high density to areas of low density. For example, a simple diffusion model might describe how a population of small mammals spreads outward from a central release site over several days, as illustrated by the diffusion-like expansion of introduced muskrats across Europe in the early 20th century (Skellam, 1951). The Lagrangian approach is used to quantify the movement of individuals (Turchin, 1998), such as in simulations of wind-dispersed seeds (Muller-Landau et al., 2008; Wright et al., 2008) or the movement of individual monkeys in a foraging model (Bonnell, Clarke, et al., 2017). Wright's wind-dispersal model is also interesting because, instead of only considering external factors such as atmospheric conditions, Wright also considers the plant's internal state, showing how variation in key genetic traits, selected over the evolutionary history of the species, affect the timing and conditions under which seeds are released, directly influencing wind-dispersal patterns (Wright et al., 2008). The study of interactions between individuals not only gives ecologists more insight into population dynamics at different scales but has been used to understand the role of habitat loss and climate change, and model how these may impact future populations (Schick et al., 2008).

Random Walk Models

One method of understanding movement from the individual's perspective is to create movement models. Three movement models that have received much attention

from researchers studying movement are the Random Walk Model, the Correlated Random Walk Model, and the Levi Walk Model (Auger-Méthé et al., 2015; Turchin, 1998; Vickers et al., 2016). These models all incorporate a stochastic component to either the angular direction or the step length, which can vary from a uniform distribution to a probability distribution derived from observations. These random walk models find their origins in mathematics (Pearson, 1905) and physics, and are typically only concerned with the analysis of the moving object, in absence of the motivation for movement, the navigational capacity of the organisms, or the feedback of environmental factors (Nathan et al., 2008). For example, an animal foraging with no preference for direction or destination can be modeled as a simple random walk, taking steps in random directions that produce an overall diffusive path, as seen in ants during early-stage foraging, where movement patterns follow simple random walks before any directional bias emerges (Lecheval et al., 2024).

Individual Based Movement and Agent-Based Models

Individual Based Movement Models, originally referred to simply as computer simulations, were developed by ecologists to better understand the movement of individuals within a population and their environment (Jones, 1977; Siniff & Jessen, 1969). A basic assumption in an Individual Based Movement Model is that each action an organism takes is a mixture of stochastic and deterministic processes, allowing the modeler to incorporate environmental and life history factors, such as the location of food, sleep sites, predation, birth and death events, into the model to build a "feature-rich" environment. This can lead to very complex models that could be difficult to interpret (Turchin, 1998) and when first developed would have been computationally

cumbersome, requiring large amounts of computing power to run anything more than a simple model. This concept is over four decades old now and its universality in ecology has grown rapidly in the past twenty years, driven largely by advances in computational capacity. Today, it is more commonly referred to as agent-based modelling (DeAngelis & Grimm, 2014).

Agent-based models are used in movement research to create simulations of the animal's movement, in an attempt to answer questions such as: how do social influences shape individual movement choices in baboons (Bonnell et al., 2015), how do key resources in the environment influence disease transmission (Bonnell et al., 2010), or how does foraging memory shape home range formation (Van Moorter et al., 2009). In all three examples, a focus on biological or behavioural influences on movement is apparent. Rather than treating agents as particles in a physics experiment, individuals in the models are given agency; the ability to make choices based on environmental or social factors.

State-Space Models

Advances in computer hardware have facilitated the development of other new analytical tools, including state-space models of individual animal movement. State-space models are not new, but their use in movement ecology is relatively recent. Considered a statistical approach, state-space models combine observed data with predicted states of movement, with a state representing an attribute of the data, such as location, behavioural state, energetic, or physiological condition. Modelling the state space can reveal whether there is propensity for certain behaviours to occur at specific times or places (Patterson et al., 2008). Tracking data collected by ARGOS on hooded seals in the North Atlantic have proven difficult to analyze due to complex, non-Gaussian

error structures that vary in time, but have benefited from state-space models. Beyond dealing with non-Gaussian error structures, these models have also been successful in managing the complexity of behavioural processes and the temporal irregularity of observations (Jonsen et al., 2005).

Visual Analytics

Visual Analytics is another advance in the analysis of animal movement that has benefited from increased computational power, especially in the realm of computer graphics. Visual analytics rely on the human interpreter to make sense of patterns presented in a visual format that may be difficult to see or detect with traditional statistics because the human brain is good at detecting patterns (Yau, 2012). Andrienko et. al. (2013) tracked human test subjects as they walked together in a group. The data was transformed to a Cartesian coordinate system with the point of origin being the group centroid and the y-axis oriented along the direction of travel. This transformation was referred to as the group space. Once the data was converted to group space, it was possible to identify "leadership" behaviour by looking at how the group interacted relative to one another in this defined space, with a focus on which individuals tended to take up a central or forward position in the group space (Andrienko et al., 2013). This paper revisits an older concept called the space-time cube that has been seeing more use in geography and movement ecology recently (Hägerstrand, 1970; Kraak & Koussoulakou, 2005). Space-time cubes are a way of visualizing spatiotemporal data in 3D, with the coordinates in space in their traditional x- and y-location on the Cartesian plane, but instead of elevation being placed on the z-axis, time is place there. Space-time cubes make variables that are invisible in two dimensions, visible. Speed can be

interpreted from the slope of the line in the z-plane, and while colocation can be seen in 2D maps, one cannot tell if this colocation is simply spatial overlap or if it also occurred at the same time, collocation in space-time cubes become visible as the intersection of lines and/or points on all three planes.

Statistical Models

While visual analytics does not lend itself to easy statistical analysis, there are many purely statistical models that have been developed for movement ecology, such as work of Aureli et. al. (2012) to measure subgrouping of spider monkeys. This study used three statistical models, the biosocial model, the ecological model, and the socioecological model to measure the point of attraction between individuals, that is, the point at which an individual would try to still be considered a member of that group or subgroup. Statistical techniques such as the Monte Carlo method and jackknifing were used to test both the robustness of their models results and to assess the potential influence of samples on their parameter estimates. Of the three models, the socioecological model, which considers both biosocial and ecological factors, did the best at predicting the point of attraction for the monkeys (Aureli et al., 2012; Wu et al., 2014). Bayesian predictive models using space and time also provide an opportunity to gain insight into where and when behaviours occur.

Parametric and Nonparametric Kernel Methods

Home range estimation has seen advances in both parametric kernel methods, such as Brownian Bridge Movement Models (Horne et al., 2007), and nonparametric kernel methods, like the Local Convex Hull (LoCoH) (Getz et al., 2007). Brownian Bridge Movement Models are a stochastic movement model using a conditional random

walk, which is constrained by the start and end points of movement as well as the elapsed time between points, to generate a probability surface between the points. When multiple points are estimated together to represent longer periods of time, usage patterns begin to emerge that can be used to represent home range estimates (also referred to as utilization distributions) or the corridors between home ranges for migrating species. Their use in animal movement studies was first proposed by Bullard (Bullard, 1999) and later implemented in the R statistical program (Calenge, 2006; Nielson et al., 2011). An argument made against the use of parametric methods, like Brownian Bridge Movement Models or Kernel Density Estimates, is that they are sensitive to outliers. This can also be said about traditional Minimum Convex Polygons. The Local Convex Hull method is a non-parametric method that is less sensitive to outliers because it creates many smaller convex hulls around nearest neighbors, which are later put together to create the larger convex hull representing the home range. An alternate version of the LoCoH method is the TLoCoH method that considers not only spatial proximity of nearest neighbors but also their temporal proximity. These methods are meant to catch hard boundaries such as cliffs and coastlines that parametric methods may overestimate across or into (Getz et al., 2007).

Linear Models

Linear models have seen much use in Movement Ecology to fit observed behavioural variables to a linear distribution. Linear models can explain both positive and negative relationships and have the means to measure the quality of the models fit and how much variability each variable can account for in the model. It can be argued that this leads to two assumptions: (i) animal movement results from successive realizations

of static distributions (Dalziel et al., 2008); and (ii) patterns of animal movement are linear. The second assumption is easily addressed by testing normality in the distribution of data prior to running the model.

Flexible Machine Learning Methods

Flexible machine learning models are thought to be useful in understanding the mechanisms controlling animal movement, with the idea that animal movement results from interactions among elements of landscape structure and behaviour, motivating context-dependent movement probabilities (Dalziel et al., 2008). Flexible machine learning has been used to predict where humans look, utilizing eye tracking devices (Judd et al., 2009), while this seems to stray from the focus of movement ecology, recent research into how humans interact with maps and their environment to navigate in cities and high traffic environments have used eye tracking technology as well (Nevelsteen, 2013). Flexible machine learning gives us the potential to not just measure where people are looking as they navigate, but to predict where they might look in novel landscapes in the future.

Qualitative Trajectory Calculus (QTC)

When it is not necessary to measure the quantitative values that define moving objects but simply qualify their relationship, Qualitative Trajectory Calculus is a useful approach (Weghe et al., 2004). If our research question was, for example, how social-living animals react to a member of their group changing speed, it is not necessary to quantify the speed and movement vector of each animal; with Qualitative Trajectory Calculus this relationship is reduced to three symbols (-, 0, +) that explain the movement relationship between each animal. If we only consider the dimension of speed as an

example, one animal moving slower than another would be symbolized as (-), while maintaining the same speed would be (0), and moving faster would be assigned a (+). The first generation of Qualitative Trajectory Calculus was developed to work in one- and two-dimensional space. Recent work has been done to generalize this technique into three-dimensional space to facilitate the analysis of fish (AlZoubi et al., 2016). This three-dimensional analysis could be applied to the study of birds and even primates living in arboreal or semi-terrestrial habitats.

Technology

Much of the progress made in the field of Movement Ecology has been made possible or enhanced by advances in technology, both in the development of new technologies and in the miniaturization of older ones. Pervasive technology, such as the cellular phone, seems so commonplace now that many, especially younger generations, would probably have a hard time remembering when cell phones were not a part of their everyday life. Yet it is a new trend to use cellular networks to track not only humans but also animals (Anthony et al., 2012). New conferences like Mobile Tartu have been organized with the aim to facilitate the discussion of theoretical, methodological, and empirical aspects of research using mobile data, derived from mobile phones (MobileTartu, 2016). This newfound use for something considered commonplace and old is possible due to advances in cellphone technology that has miniaturized (mainly the batteries) them to a size that can be used on animals without weighing them down. As a rule of thumb the device should weigh less than 2% of the subjects body weight (Bridger & Booth, 2003; Cooke et al., 2004; Guillemette et al., 2002; Reynolds & Riley, 2002). The miniaturization of technology such as Lithium-Ion batteries has allowed another

commonplace technology to be used on smaller organisms. Global Positioning Satellite technology has benefited from battery technology advances that are now much lighter, as light as 1.1 grams, making them feasible for use on small songbirds such as Ovenbirds (Hallworth & Marra, 2015).

Biotelemetry is the measurement of an animal's physiology, behaviour, and energetic state remotely. Many devices fall into the biotelemetry category, but they tend to fall into one of three categories: receivers (GPS devices receive a signal from satellites to fix their location), transmitters (radio collars transmit a signal used to locate the device), or archival loggers (smart tags often record multiple variables such as temperature, tri-axial movement, and light levels which are saved locally on the data logger). Current biotelemetry variables that can be measured include, sound, vibrations, pressure (body cavities, depth in water, or barometric), acceleration, locomotor rhythms, activity/rest periods, salinity, blood flow rates, position and orientation of body parts, light levels, temperature, body chemistry, and neural activity (Cooke 2004).

Geographic Information Systems (GIS) have been around for over 50 years, since Roger Tomlinson created the first computer GIS called the Canada Geographic Information System (CGIS), but recent advances have made GIS more accessible to ecologists. Open-source GIS is not only more accessible, but many open-source GIS packages are comparable to expensive commercial GIS software like ArcGIS. New toolsets have been developed primarily for ecologists, such as HawthsTools and its most recent incarnation, the Geospatial Modelling Environment (GME), along with many spatial tools written for R. Remote Sensing Data like GIS has been around for a long time, but recent advances in sensor technology have given researchers access to

increasingly higher resolution imagery at lower costs, and in many cases even for free. MODIS imagery used to calculate a normalized difference vegetation index (NDVI), which can be used by ecologists to measure biomass, has a resolution of 250 meters per pixel, while newer satellites, like the European Union's Sentinel 2, have a resolution of 10 meters per pixel, giving ecologists a much more detailed picture of biomass, and Planet Labs Dove constellation can monitor the entire Earth every day at 3 meter resolution.

Movement ecology has benefited from both an influx of new technology and the miniaturization of older technology over the past two decades. New technology has facilitated a series of new approaches to the study of movement and helped shape the new Movement Ecology paradigm. Researchers have more detailed insight into the spatial behaviour of animals as well as their internal state or physiology. Environmental factors are being measured at increasingly higher spatial resolutions and with more precision as advances in remote sensors, both space-borne and ground-based, which contribute to a more detailed understanding of animal habitats. Advances in computer technology, both hardware and software, allows researchers to run more powerful models and simulations at increasingly faster speeds with each new generation of computer. Advances in both technology and methodology have allowed researchers to tackle questions that were previously left to speculation based on informed observation.

Stuart Altman's 1974 prediction about baboon foraging formations (Altmann, 1974), which he based on years of field observations and the intuition of a seasoned scholar, has only recently been tested, made possible by access to high resolution GPS data (at least relative to 1974 standards) and software advances in geographic information

science and statistics (Dostie et al., 2016). In that study, the following technological developments were central. The rapid ingestion and processing of ~60,000 baboon GPS locations provided the level of detail needed to revisit Altmann's ideas with quantitative precision, allowing the examination of group movement patterns at a temporal and spatial resolution that simply did not exist in the 1970s.

From this dataset, it was possible to perform directional and orientation analyses on hundreds of group formations, essentially reconstructing the spatial structure of foraging groups in ways that mirrored Altmann's qualitative descriptions with reproducible measurement. Using GIS-based workflows, individual positions, alignment, and spacing within each formation were quantified, generating empirical distributions of group configurations that could be directly compared to Altmann's predicted patterns.

Climate Change and Primates

While my thesis does not directly address climate change, I included this section to highlight the point that, as for all other animals, primates as a taxonomic order have been subject to natural selection in the context of fluctuating local conditions. This has been especially true for African species, such as vervets and baboons that have wide geographic distributions because of northern hemisphere ice sheet expansion and contraction. In this region especially we might expect animals to be tuned to variations in local resource availability and, as I note below, be capable of adaptive adjustments in the short-term. I address aspects of resource availability and distribution in each of the data chapters. Here, I simply provide a broad overview of climate change and flag the importance of anthropogenic factors for future work.

Over the course of the planet's ~4.5-billion-year history, the Earth has been much warmer than it is now, punctuated by six ice ages over the last ~2.3 billion years. The genus *Homo* evolved during the Quaternary Ice Age, which began ~2.6 million years ago, although the broader cooling trend following the Mid-Miocene Climatic Optimum that set up present-day conditions extends back ~15 million years.

Our current ice age —the Quaternary— has had anything but a uniform climate, with several oscillations in global temperature and ice cover, known as glacial and interglacial periods. These oscillations have increased in amplitude over the past ~2.6 million years, with the most dramatic increase over the past 800,000 years. We are currently experiencing an interglacial period that is predicted to be one of the warmest of the past 2.6 million years. For reference, the last interglacial period was 1°C to 3°C warmer and sea levels were as much as 6 meters above today's (Aguado & Burt, 2007).

The last three decades have each been successively warmer at the Earth's surface than any other decade since the start of instrumental records in 1850. It is estimated that the 30-year period from 1983 to 2012 was the warmest of the last 1400 years in the Northern Hemisphere (IPCC, 2014). Our planet is getting warmer, causing ice caps to melt and ocean levels to rise. Heat waves and drought are becoming more commonplace. The trends described above are collectively known as global warming, one of the conditions of natural climate change. What is different about this current cycle of global warming is the presence of unprecedented levels of greenhouse gases in the atmosphere (IPCC, 2014).

Like their namesake, greenhouse gases work like the glass of a greenhouse, in that they allow shortwave radiation from the sun to pass, and trap or absorb longwave

radiation as it is emitted from the surface of the Earth (Aguado & Burt, 2007), which is often referred to a radiative forcing (Notaro et al., 2007). Models of climate change predict with high confidence that by the end of this century (2100), global warming is likely to exceed 2°C, and has the potential to increase as much as ~5°C relative to 1850-1900 (IPCC, 2014).

In 1988, the World Meteorological Organization and the United Nations Environment Programme organized the Intergovernmental Panel on Climate Change to provide the world with a clear scientific view on the current state of knowledge in climate change and the potential environmental and socio-economic impacts (IPCC, 2017). Since the public address of Dr. James Hansen to the United States Congress (Hansen, 1989) in which he articulated the influence of man-made emissions on global warming, much attention has been given to this issue in both academic literature, (Bouwer, 2011; Ramanathan et al., 1985; Rosenzweig et al., 2008; Sarmiento et al., 1998) and popular media (Bowman, 2008; Emmerich, 2004; Guggenheim, 2006). The relationship between humans and climate change, whether we are causing it or making it worse, is referred to as anthropogenic climate change.

Climate change is caused by many factors, both natural and anthropogenic, these include biotic processes, including respiration and decomposition, and variations in solar radiation received by Earth, changes in axial tilt, wobbling of the planetary axis, plate tectonics, and volcanic eruptions. Anthropogenic activities such as the burning of fossil fuels, cement production, gas flaring, and harvesting rainforests have also been identified as significant factors in the recent global warming trend (IPCC, 2014). Not all factors contributing to climate change are direct causes; some can be regarded as feedback loops

that increase the rate of climate change. One of these feedback loops is the emission of carbon from arctic permafrost. As permafrost thaws carbon is released into the atmosphere as microbes of decomposed organic material. As the climate warms up, more permafrost thaws, thus more microbes flourish and are released (Christopherson et al., 2016).

Models of species distribution have shown that dispersal variables alone do a poor job of explaining species distribution, while models that incorporate climate and productivity have had more success (Field et al., 2009). Climate change has the potential to disrupt species distribution and abundance as changes in precipitation, temperature, habitat quality, and species interactions at the trophic level push species to adapt, evolve, move, or die (Jablonski, 2005; Van der Putten et al., 2010).

A Brief Note on the Study Species

Baboons and vervet monkeys have the widest latitudinal range of all non-human primates, extending throughout sub-Saharan Africa from the Sahel down to the continent's southern tip. The anatomical and physiological adaptations that underpin their ability to exploit increasingly open terrain means that they are able to take advantage of wide variations in resource availability, not only across geographic space but also, locally, through seasons. This feature of their relationship with their environments, which distinguishes them from other African monkeys, is most apparent in the higher latitudes of South Africa, where my particular study populations live. Here, they experience a generally lower resource base and increased resource seasonality that is exacerbated by marked seasonal variation in daylight (Hill et al., 2003) and by lower, declining rainfall and drought (McDougall et al., 2010) (Pasternak et al., 2013).

Baboons, being larger and fully terrestrial, cope with the lowered resource base not only by having a broad diet that includes the exploitation of underground items, but also by having large home ranges that are therefore uneconomical to defend against incursions by other baboon groups. Consequently, baboon troops have large overlapping home ranges and aggression between groups is directed at preventing male transfer from other groups and the possible exploitation of females as a reproductive resource (Henzi et al., 1998). As a corollary, their daily foraging movements, which may often be more than 10 km in length, expose them in the short-term to a wide range of shifting mosaics of local resources. Vervets, on the other hand, while also having a broad dietary range (Pasternak et al., 2013) are much smaller than baboons and because they rely on trees for protection from predators are semi-terrestrial. They utilise smaller home ranges and are in a position to defend these against exploitation by other vervet groups. They are, in other words, territorial. Not surprisingly, I use these differences in range use to address species-specific research questions in Chapters 2 and 4.

Socially, both vervets and baboons live in stable groups as an evolutionary response to predation risk (van Schaik, 1983). Females, other things being equal, spend their entire lives in their natal group, while males emigrate at sexual maturity in order to join another group where they can pursue reproductive opportunities with unrelated females. As more than one adult male may coexist in a group, both species are generally classified as living in multimale, female-bonded social groups (Van Schaik, 1983), where the bondedness refers to the presence of close social ties among female relatives. In both species, there is intra-group competition for access to resources (Van Schaik, 1983) and individuals differ in their priority of access. Where these differences are consistent and

relatively stable, we refer to them as differences in 'resource holding potential' (Parker, 1974) and quantify them as differences in rank, where the highest-ranking individual, usually designated as 1, is least likely to face competition for access. Interestingly, in baboon populations, where males are twice the size of females, all males are higher ranking than all females, a feature that is relevant to the analysis in Chapter 2. In vervets, on the other hand, sexual dimorphism is reduced and it is common for some females to outrank males (Young et al., 2017).

Thesis Research Objectives and Chapter Outline

My overarching aim is to apply an explicitly geographic perspective to study the relationship between two primate species and their socio-spatial environments. Following Webber et al.'s (2023) identification of the conjunction of spatial and social environments and spatial and social phenotypes and the ways in which these intersect, my research presented in Chapter 2 is an explicit consideration of the interaction between spatial phenotypes (including habitat preferences and movement patterns) and social phenotypes (social centrality and dominance rank) in baboons. I began with an assessment of Altmann's (1974) proposition about the consequences of resource distribution for baboon movement ecology and contextualized my work within Hamilton's (1971) concept of the geometry of the selfish group. In Chapter 3, I present the methodology I developed to determine ecologically and temporally appropriate estimates of home range size in vervet monkeys and demonstrate the utility of this approach. In Chapter 4, I build on my results to address the function of territoriality in vervet monkeys. In essence, I assess the argument that territoriality serves to protect a demarcated area (the 'territory') from intrusion by other groups to restrict access to necessary resources needed by the group. In

doing so, I describe the intersection of Webber et al.'s (2023) spatial environment (including habitat configuration) and social environment (group size and composition, intergroup competition). My final chapter brings these research deliverables together and concludes with ontological considerations and reflections.

Proof of Principle: The Adaptive Geometry of Social Foragers

This paper is published in Animal Behaviour Vol 119, 173-178, September 2016.

Authors

Marcus J. Dostie[a,b], David Lusseau[c], Tyler Bonnell[b,d], Parry M. R. Clarke[b], George Chapline, Stefan Kienzle[a,b], Louise Barrett[b,d] and S. Peter Henzi* [b,d]
[a] Department of Geography, University of Lethbridge, 4401 University Drive, Lethbridge T1K 3M4, Canada.
[b] Applied Behavioural Ecology and Ecosystems Research Unit, The University of South Africa Private Bag X6, Florida 1710, South Africa.
[c] Institute of Biological and Environmental Sciences, University of Aberdeen, Aberdeen AB24 2TZ, UK.
[d] Department of Psychology, University of Lethbridge, 4401 University Drive, Lethbridge T1K 3M4, Canada.
[e] Department of Anthropology, Pennsylvania State University, University Park, PA 16802, USA.
* Corresponding author

Abstract

The spatial configuration of a group of animals should reflect the ability of its members to respond to environmental contingencies. Under predation risk, the optimal position for an individual in a stationary group is at the group's centre. The resulting group geometry is circular, with individual placement determined by competitive ability. Where it compromises efficient foraging, a long-standing question has been whether this topology can deform adaptively in response to the local distribution of resources. Here we show that the shape described by a group of foraging baboons changes in response to habitat structure and that this promotes foraging efficiency while conserving the predation-risk-related distribution of group members. Adult baboons improve unimpeded access to the small, dispersed food items found in grassland by adjusting both their inter-individual distances and their relative positions along the line of movement in order to forage in rank formation. Dominant animals occupy the centre of the group and do so regardless of its geometry. Our results demonstrate that spatially explicit data can address

emergent group-level properties directly. This global approach complements analyses of individual action and can help direct the search for potential local rules of interaction.

Keywords: Collective action, Papio hamadryas, predation risk, selfish herd, spatial structure

Introduction

Principle Ten. A rank foraging formation will be favored whenever there is an advantage to remaining in a group and the group is foraging on slowly renewing resources that are of low overall density in the home range and are not locally abundant.

S.A. Altmann 1974 (p. 241).

The spatial configuration of a group of animals is the summation of the responses of its members to the local environment, made under the constraint of association (Parrish & Edelstein-Keshet, 1999). In mobile groups this emergent geometry is expected to deform adaptively as group members accommodate to local shifts in the relative salience of competing costs (Beecham & Farnsworth, 1999; Morrell et al., 2011).

Social species, such as primates, that form groups to reduce the risk of predation for their members (Hill & Dunbar, 1998; Shultz et al., 2011) do so at the expense of increasing local competition for resources (Majolo et al., 2008; Van Schaik, 1983). Heterogeneity in the distribution of these risks and costs both among group members (Koenig, 2002; Ron et al., 1996) and across the landscape (Willems & Hill, 2009), makes such groups well suited to investigating the environmental drivers of the spatial structure of social units (Krause et al., 2002; Morrell et al., 2011).

Under marginal predation, where animals on the edge of groups are more vulnerable to predators, those that are closer to the group's centre have smaller domains

of danger and are less exposed to risk (Hamilton, 1971; King et al., 2012; Morrell & Romey, 2008). Local adjustments in response to risk perception will then generate a group geometry that ideally, in two dimensions, is circular (Aurenhammer, 1991), with individual location determined by resource holding potential (Parker, 1974), which can be indexed as dominance rank. This configuration is likely to characterise the global structure of animal groups primarily where high-quality resources are clumped and can be defended, and marginal animals can balance increased predation risk against the possibility of improved foraging opportunities offered by a reduction in contest competition (Krause & Ruxton, 2002; Bumann, Krause, & Rubenstein 1997; Robinson 1981). The question, then, is whether the accommodation of this 'selfish herd' (Hamilton 1971) to changing cost potentials (Beecham & Farnsworth 1999) can be detected at the global level as a change in adaptive topology?

Savanna baboons (*Papio hamadryas*) have home ranges that encompass habitat mosaics and frequently forage in grasslands (Henzi & Barrett, 2005), which are typified by low quality, thinly dispersed, quickly consumed foods (Henzi et al., 1992). These induce scramble competition (Isbell, 1991), where the persistence of a circular formation would reduce foraging efficiency for all but those animals in the group's vanguard (Hirsch, 2007). In 1974, Altmann (1974) instantiated and extended Hamilton's general theoretical argument to predict that in grassland, where ephemeral resources are thinly distributed, group members will spread out to secure at least the minimum foraging swath that enables unimpeded foraging while adjusting their positions to keep abreast of their neighbours and thereby minimize the costs of scramble competition. The geometry of this foraging group is expected, therefore, to deform to a rank formation as animals encounter

low quality, dispersed resources, while the spread of the group will be constrained by continuing predation risk. As an implicit but necessary corollary, we also expect more dominant animals to continue to avoid the margins of the group as the shape shifts.

An assessment of these long-standing propositions can contribute to the development of a coherent group-level spatial ecology that complements current research on individual contributions to collective movement (Katz et al., 2011; Nagy et al., 2010; Parrish & Edelstein-Keshet, 1999; Strandburg-Peshkin et al., 2015; Sumpter et al., 2012), but has had to wait on the emergence of appropriate global positioning system (GPS) technologies and geospatial analytics (Tomkiewicz et al., 2010). Here, we use interpolated GPS data collected from individual adults to describe dynamic spatial relationships in a group of chacma baboons as it moves through its home range, which comprises a mix of open grassland and dense scrub (Kotze & Fairall, 2006).

Methods

Study Site and Data Collection

We collected 74 days of data - spread across 391 days - from a habituated group of chacma baboons (N≈45) at De Hoop Nature Reserve, South Africa (Barrett et al., 2004) during 2007 and early 2008. A single observer, using a handheld GPS-equipped data logger followed and recorded the spatial locations of all 14 adult members (NMales=3, NFemales=11). On-site calibration of the data loggers confirmed that they were absolutely accurate to within 2-5 m and relatively accurate to ~1 m (viz. the accuracy with which the distance between two points can be estimated). Beginning at one end of the group, the observer identified, stood next to, and collected a GPS record for each visible adult in turn. When the distal end of the group was reached, the observer

turned back along the line of travel while continuing to collect data. If an animal was not seen during two circuits of the troop, the observer interrupted data collection in order to locate it. We obtained 61,842 usable data points, with a mean of 63.98 points (+/-9.03 SD)/ individual/day. Foraging effort was determined from scan sample records of activity (N=5846), collected as standard procedure (Henzi et al., 2009) every 30 min from all visible, identified individuals, and expressed as the proportion of the group foraging. Animals were assigned an ordinal dominance rank derived from ad libitum records of all dyadic agonistic interactions over the study period, with participants identified as winners or losers. We used the Domicalc program (Schmid & de Vries, 2013) in R 3.2.1. (R Core Team, 2015) to confirm a high degree of linearity in the hierarchy ($h1 = 1$; $N = 704$; $P < 0.0001$).

Ethical note: All procedures were approved by the University of Lethbridge Animal Welfare Committee (Protocol #0702).

Interpolation and Estimates of Minimal Optimal Spread

While our spatial data collection procedure did not allow the simultaneous recording of all individual locations, the median time interval of 7 min between consecutive records for the same individual preserves sufficient information for analyses derived from individual points (Andrienko et al., 2013; Bonnell, Henzi, et al., 2017), giving us confidence in the use of interpolated data. We therefore estimated the positions of all group members for any given time using linear interpolation of trajectories between successive point samples. To confirm that our baboons were sensitive to both predation risk and foraging interference, we followed the approach detailed in Aureli et al (2012), extracting the inter-individual distances (IIDs. N=5204. Range: 0m-615m) of all animals

at 11am each day, when animals were consistently likely to be foraging, and fitting them to three models, with model selection based on the Akaike Information Criterion (AIC). These models were derived from the relative ability of (i) food distribution and predation risk (the Ecological model), (ii) foraging interference (the Biosocial model) or (iii) both (the Socioecological model) to predict observed IIDs. In summary, the Ecological model is an integrated estimate of the spatial distribution of important ecological factors (predation risk, food) in the habitat, with individual distribution following a Poisson process in response to this background heterogeneity. The Biosocial model assumes that individual distribution is governed solely by repulsion from others at close distances and attraction towards them at intermediate distances. The Socioecological model, therefore, is an extension of the Biosocial model that accounts explicitly for the ecological landscape (see Aureli et al. 2012 for detail and derivations) in predicting individual distributions. It should be noted that, for these analyses, we make the simplifying assumption that the extracted distances of repulsion and attraction do not vary significantly across habitats and individual group members (Aureli et al., 2012).

The Socioecological model provided the best fit to the data and consequently we doubled its estimate of the mean distance at which animals repelled one another to set the width of the swaths within which each animal might forage without interference. The degree to which individual swaths overlapped, estimated as a proportion of the distance along the x-axis (Figure 2.1), constituted our group-level estimate of the extent to which group spread reflected the predicted minimal requirements for unimpeded individual foraging in open country. The lower the overlap in foraging swaths, the more optimally the group was foraging. Where there was overlap in foraging swaths, we distinguished

between animals in front (no immediate scramble competition) from those further back, who might be expected to encounter less food as a consequence of foraging in another animal's path.

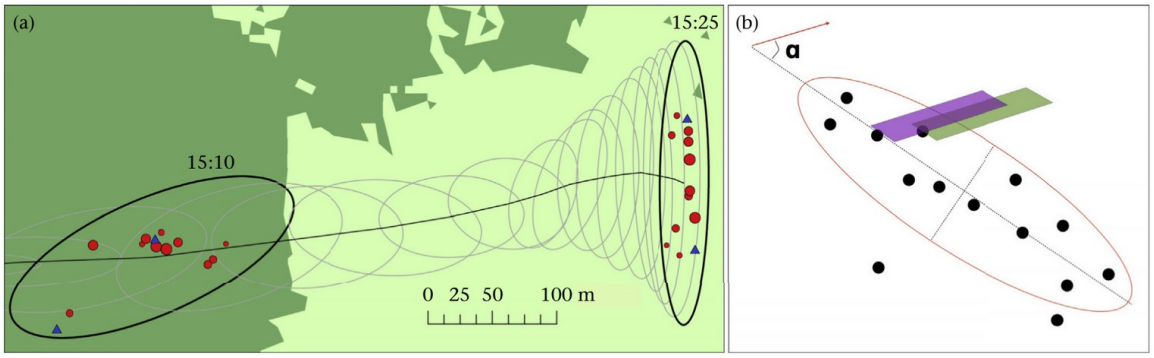

Figure 2.1: Transformation of baboon group geometry. (a) Shift to rank formation as the group moves from dense (dark green) scrub to grassland (light green). Individual group point clouds (Females: red circles; Males: Blue triangles) were used to generate ellipses, bounded for illustrative purposes at 2 SD, at 1 min intervals (grey), while analysis was restricted to those that were 15 min apart (black), with time indicated. The black line indicates travel direction. Larger circles reflect increasing female dominance rank. (b) Schematic of elements used to estimate group shape and foraging spread (see Methods). Dashed lines: short and long axes of ellipse; Purple and green bars: minimal expected optimal foraging swaths, illustrating suboptimal overlap for the purple swath; α: angle of orientation relative to travel direction (indicated by the red line).

Data Location Error and Temporal Independence

We constrained the data set to periods for which the average location error was predicted to be at or below 7.8 m, using a model of interpolation error derived from separately collected continuous tracks of individual baboons (Dostie et al., n.d.). This model estimated interpolation error by repeated subsampling of the continuous data and comparing the interpolated data generated in this way with the continuous data. We also measured autocorrelation in the dependent variable (i.e. group-level minimal optimal spread) by fitting a semi-variogram with the gstat package (Pebesma, 2004) in R. Point estimates of optimal foraging spread separated by 15 min offered the best trade-off between independence and sample size. Using these criteria, we were able to extract 349 group point clouds representing the estimated location of every individual at a particular moment.

Speed, Direction of Travel, Rotation, and Centring of Groups

Direction of travel (DoT) and speed of these group estimates were measured at the group level using the line between the group centroids (i.e. the mean x, y location of the group) at Time t and t+1. To simplify the measurement of group optimal spread across multiple samples with variable DoT orientations, group point clouds were rotated so that their DoT was set to 0°. In order to rotate the group point cloud, it was first centred on the Cartesian plane with the group centre at (0,0). This was done by subtracting the group mean centre from each individual's point. The point cloud was then rotated by applying the following formula to individual points within the centred point cloud:

$$X_r = X_z \cos R - Y_z \sin R \, , Y_r = X_z \sin R + Y_z \cos R \quad \textit{(Eq 2.1)}$$

where:

X_r and Y_r = Rotated x and y values

X_z and Y_z = The pre-rotation x and y values

R = Rotation in radians (difference between direction of travel and 0)

Group Geometry

A rank formation refers to one in which individuals are spread out along an x-axis which is perpendicular to the direction of travel. We estimated the extent to which group shape approximated a rank formation using the Directional Distribution (Standard Deviational Ellipse) tool in ArcGIS10.2, (ESRI, 2011) to generate ellipses around the group point clouds at each independent sample (Figure 2.1). Ellipses specified at different standard distances (SD) are centred at the same point, oriented in the same direction and retain the same proportions. Consequently, we arbitrarily bounded ellipses at 2 SD to

extract measurements with which to determine group shape. We used the orientation of the ellipse (i.e., the direction of the long axis) and the short and long axes to estimate rank formation as follows:

$$Shape = 1 - (\frac{s}{l}) \quad (Eq\ 2.2)$$

$$Perpedicularity = 1 - \left(\frac{90 - O_c}{90}\right) \quad (Eq.\ 2.3)$$

where:

s = length of short axis

l = length of long axis

O_c = Orientation of the long axis in relation to the direction of travel (0° to 180°)

While the resulting values that approach 0 can indicate either circles or files, only formations that are both linear and perpendicular to the DoT can approach 1.

Location Within the Group

Each animal's distance to the centre of the group (DtC) was expressed as its Euclidean distance to the centre of the ellipse.

Habitat Classification

At the time of the study, the home range consisted of dense fynbos scrub, recently burnt areas and grassland (Kotze & Fairall, 2006). This made it appropriate to classify the habitat as either closed (0) or open (1) and we used interactive, supervised classification in ArcGIS 10.2 (ESRI, 2011) to allocate each pixel in a high-resolution digital aerial photograph of the home range to one of the two categories. Training areas were assigned using geo-referenced photographs in conjunction with ground-truthing at the site. By overlaying point clouds on the photograph we could assign, for each independent sample

in the analysis, a habitat category to each subject's position. These were then used to generate a proportional measure, ranging between 0 and 1, for the group as a whole.

Statistical Analyses

Models were run in Stata 14 (StataCorp, 2015) and, after corroboration of the outcomes, goodness-of-fit was estimated for the LMM (Johnson, 2014) with the MuMin package (Barton & Barton, 2015) in R. Tests were two-tailed with α level set to 0.05. All continuous independent variables were centred. Test assumptions were controlled for by computation of variance inflation factors (all VIF <1.2) and visual inspection of scatterplots, histograms, and Q-Q plots of residuals.

Results

Distances of Attraction and Repulsion

After appropriate spatial interpolation, we modeled IIDs among troop members to assess the dimensionality of inter-individual interactions (Aureli et al., 2012). The Socioecological model (ΔAIC = 0), which models forces of attraction (a) and repulsion (r) among group members while accounting for environmental heterogeneity, explained IID distribution better than either the Biosocial (ΔAIC = 403) or the simple Ecological model (ΔAIC = 2743.2. Table 2.1). As required by the predictions (Altmann, 1974), therefore, these baboons were spatially constrained by both a reluctance to be too far away (model mean estimate: α = 71.3 m) or too close (model mean estimate: r = 3.9 m) to others.

Table 2.1: Parameter estimates for the three competing models of interindividual spacing

Parameter	Socioecological model	Biosocial model	Ecological model
p_a	0.0002 (0.0002–0.0002)	0.0002 (0.0002–0.0002)	
a	71.3 (70.8–71.8)	73 (72.5–73.5)	
p_r	0.065 (0.003–0.127)		
r	3.9 (1.9–5.9)	0.44 (0.43–0.45)	
β	3.8 (1.75–5.86)		2.6 (2.2–3.0)
AIC	−3740	−3591	−0.997

p_a: proportional contribution of attraction; p_r: proportional contribution of repulsion; a: range of attraction (m); r: range of repulsion (m); β is the inverse of λ, the mean of the spatial Poisson process explaining the distribution of individuals; AIC: Akaike information criterion. The estimated 95% confidence intervals for each parameter are provided in parentheses.

Foraging Spread, Group Shape and Habitat

We used the minimal foraging swath (2r = 7.8 m) and the extent of overlap of individual swaths as a group-level estimate of minimal optimal foraging spread, where less overlap indicates improved foraging for the group as a whole (Figure 2.2). As Altmann's principle expects group shape to promote efficiency in baboons foraging on widely dispersed, low-quality food items, we entered minimum optimal foraging spread as the response variable and habitat type, group shape and the proportion of the group foraging (indexing foraging effort) as predictors in a full-factorial linear model, with travel speed specified as a control variable. The results indicate that minimum optimal foraging spread was independently and positively associated with more open habitat, increasing rank formation, the proportion of the group that was foraging, as well as with the three-way interaction of these variables (Table 2.2). The foraging spread of our baboon group was therefore most likely to meet minimum requirements for optimality when it was in rank formation and foraging in open terrain (Figure 2.2).

Table 2.2: Minimal optimal foraging spread as a function of habitat structure, foraging effort and group formation.

Parameter	β	SE	t	P	95% CI
Speed	0.003	0.001	5.060	<0.0001	0.002 to 0.004
Habitat structure	0.130	0.019	6.720	<0.0001	0.092 to 0.168
Foraging effort	0.089	0.031	2.900	0.004	0.029 to 0.150
Group formation	0.405	0.038	10.770	<0.0001	0.331 to 0.479
Habitat structure * Foraging effort	0.008	0.090	0.090	0.928	−0.169 to 0.185
Habitat structure * Group formation	−0.099	0.114	−0.870	0.385	−0.323 to 0.125
Foraging effort * Group formation	0.247	0.164	1.500	0.134	−0.076 to 0.570
Habitat structure * Group formation * Foraging effort	1.146	0.532	2.150	0.032	0.099 to 2.193
Intercept	0.166	0.022	7.640	<0.0001	0.123 to 0.209

CI: confidence intervals. Whole model: $N = 349$, $F_{8,340} = 30.897$, $P < 0.0001$, adjusted $R^2 = 0.407$.

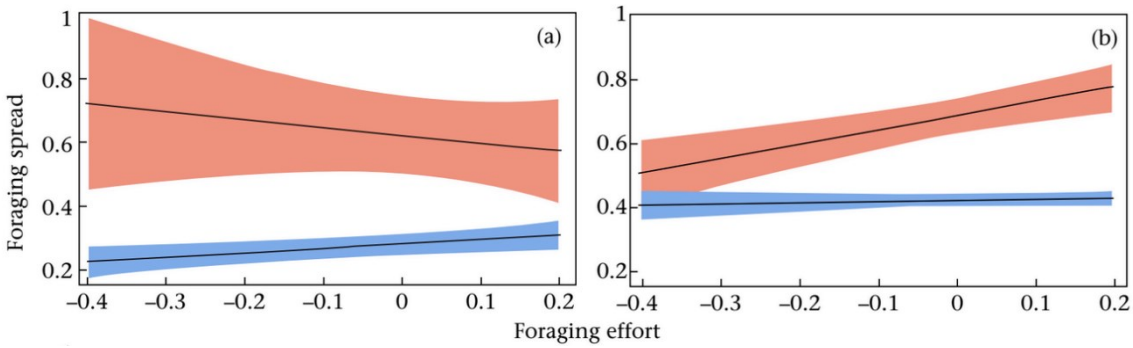

Figure 2.2: Modelling foraging spread. The relationship between the extent of minimum optimality in foraging spread and foraging effort (the number of animals foraging) in (a) Closed habitat and (b) Open habitat. Model predictions (+/- 95CI) in each are presented for high (red) and low (blue) rank formation.

Dominance Rank and Position Within the Group

We used a linear mixed model (LMM) to test the hypothesis that high-ranking animals were more likely to be closer to the group centre regardless of group geometry. We applied a square root transform to the dependent variable to improve the fit to normality. All adult chacma baboon males are dominant to all females (Henzi & Barrett, 2003), subordinate males avoid the alpha male (Bonnell, Henzi, et al., 2017) while, at twice the size of females, males are also less likely to avoid the margins of the group (Rhine et al., 1985). We therefore specified subject sex as a control variable and dominance rank and group shape as fixed effects (with interaction term). We specified subject ID as a random effect, with a random slope for the effect of spatial formation. With sex controlled, the results indicated that higher-ranking animals were closer to the centre of the group regardless of group geometry (Table 2.3. Figure 2.3).

Table 2.3: Distance from the group centre as a function of dominance and group formation.

Parameter	β	SE	Z	*P*	95% CI
Sex (Ref: Female)	1.172	0.185	6.340	<0.0001	0.809 to 1.534
Dominance rank	0.097	0.019	5.180	<0.0001	0.060 to 1.534
Group formation	−0.740	0.394	−1.880	0.060	−1.511 to 0.133
Rank * Formation	0.081	0.045	1.820	0.069	−0.006 to 0.169
Intercept	3.489	0.175	19.930	<0.0001	3.146 to 3.832

CI: confidence intervals. Whole model: $N = 4243$, log likelihood $= -8429.493$, Wald $X^2_4 = 52.40$, $P < 0.0001$, $R^2_{\text{Marginal}} = 0.045$, $R^2_{\text{Conditional}} = 0.058$.

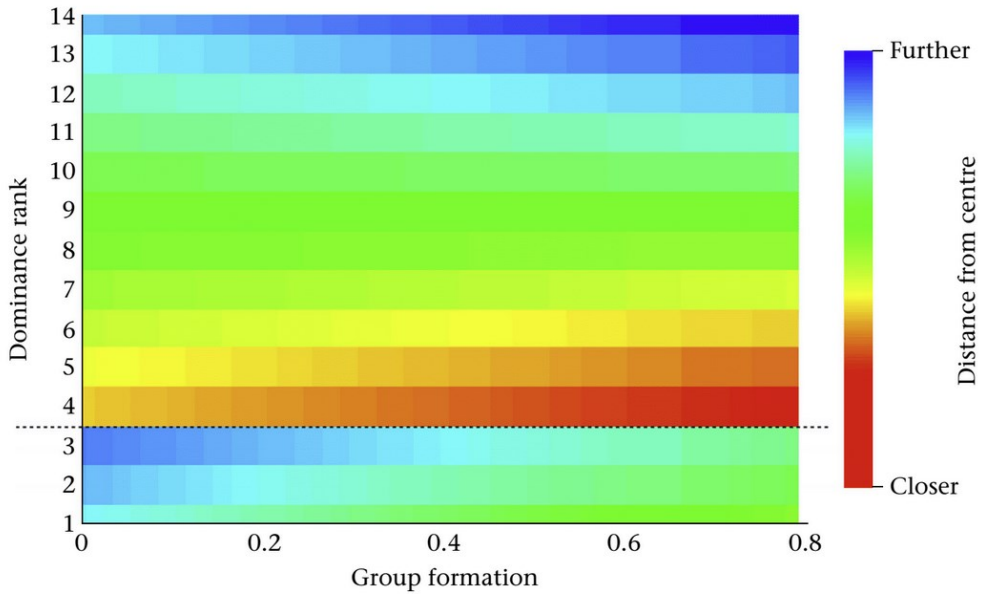

Figure 2.3: Dominance rank determines spatial location. The heat map indicates the LMM fit to the data for distance to the group centre in relation to rank (highest-ranking animal = 1) and group shape (rank formation = 1.0). The dashed line separates males (ranks 1 – 3) from females.

Discussion

Our results indicate that the shape described by a group of baboons as it traverses its home range conforms to that expected of a mobile selfish herd engaging adaptively with changing cost potentials in the environment (Altmann, 1974; Beecham & Farnsworth, 1999). Shifting priorities can therefore account for the absence of the file formation expected of a moving group under predation risk alone (Bumann et al., 1997). Topologically, the configuration of adults in the study troop was homeomorphic, with dominance rank determining individual location within each sex regardless of group shape. At the same time, high-ranking females were closer to the group's centre than were males. In general, therefore, this result confirms Altmann's expectations while also pointing to a need to consider more particularly the relative importance of other factors, such as vulnerability and reproductive competition, in explaining individual decisions about spatial location. It is probable, for instance, that the effect of rank on centrality in

males is driven by male-male competition and therefore only coincidentally mirrors the effect in females, which is more likely to be a consequence of perceived predation risk.

That said, it is clear that the goodness-of-fit of the model accounting for individual positioning is markedly poorer than that of the model describing foraging efficiency in relation to group shape. While this will be due partly to interpolation error and the coarse-grained characterisation of the environment (Josephs et al., 2016), we believe that the disparity reflects accurately the conditions faced by baboons at this field site. That is, while predators able to target baboons occur, they do so in very low numbers, and we have no evidence of either attempted or successful predation (Barrett et al., 2004). Not surprisingly, perceived risk, as indexed by the relatively large distance at attraction (71.3 m), is also low. Given this, the effect size in the configuration model serves as a gauge of perceived predation risk and we would anticipate it being larger in populations where predation is a more prominent source of mortality. At De Hoop, however, it seems that the cost potential encountered by the baboons as they move derives primarily from the effect of resource dispersion, with predation risk, given the absence of an interaction between centrality and group geometry, exerting a consistent but low-level, background effect on individual location, if only primarily for females.

This outcome confirms predictions of the emergence of adaptive shape (Parrish & Edelstein-Keshet, 1999) that were derived explicitly at the level of the group. Taken together, group geometry, together with the particular individual configurations that describe it, serves as a global indicator of individual decision-making without any a priori prescription as to the form of the decisions themselves. In so doing, it confirms the utility of a global-to-local trajectory in the modelling of collective behaviour (Sumpter et al.,

2012). It also offers the more general prospect that such sparse data sets, which are logistically simpler to assemble than the high-resolution equivalents generated by animal-mounted devices (Bonnell, Henzi, et al., 2017), can contribute to the development of this topic.

While not prescriptive, both the theory and the results generated at the global level certainly point to a circumscribed range of possible local rules that can be modeled and assessed empirically. The primary rules that describe spatial dynamics are those that govern the approach, avoidance and alignment of group members (Couzin et al., 2002; Eftimie et al., 2007), and a rule of preferential attraction to clusters of other group members has been shown to underpin collective movement and basal spatial coherence in baboons, both in Kenya (Strandburg-Peshkin et al., 2015) and at De Hoop (Bonnell, Henzi, et al., 2017). What our results suggest, however, is a need to consider the rules that are nested within this primary decision set that then govern the particular configurations of individuals under different ecological contexts. That is, while an undifferentiated attraction to the group's 'centre of mass' sustains spatial coherence and coordinated movement, subsequent positions are fine-tuned by rates at which food is encountered and the identities of neighbours and constrained by the perceived risk of predation.

Dynamic Home Ranges

Introduction

As outlined in Chapter 1, my general objective in this thesis is to interrogate the intersection of spatial and social phenotypes against the background of the larger spatial environment (Webber et al., 2023). To do so, I address questions requiring two levels of spatial analysis: namely (i) the movement patterns of individual animals within a group and (ii) the aggregate consequences of those movements expressed as the area that the group uses in order to satisfy its resource requirements (i.e. its 'home range'). Building on the study presented in Chapter 2, which involved the analysis of patterning of individual movement trajectories in baboons to examine the effects of social dominance rank and habitat quality on the structure of movement, here, I describe the development of a context-appropriate estimate of home range size and demonstrate its utility. This work is a contribution of broader value for movement ecology research and underpins the analyses of the spatial basis of territorial aggression in vervet monkeys that I present in Chapter 4.

Seton was the first to coin the term 'Home-Range' in his *Life History of Northern Animals* where he stated that: "No wild animal roams at random over the country; each has a home-region, even if it has not an actual home." (Seton, 1909, p. 26). The idea of a home range was later refined by Burt in 1943, where he included the idea that a home range estimate excluded occasional sallies outside its established boundaries, while also acknowledging that home ranges can be stationary or shifting; therewith a recognition that animal home ranges can change over time (Burt, 1943; Stickel, 2003). Cooper suggested that individuals of many species confine their movements to limited areas and

pointed out that early definitions of a home range fail to outline criteria by which their spatial and temporal limits could be determined (Cooper Jr, 1978). Although Brown defined a home range as the area an animal uses in its daily activities (Brown, 1962), Cooper also flagged the difficulty that arises when animals utilize distinct areas for different activities, which leads to the question: should we also consider cyclic usage such as diurnal or seasonal patterns? At the same time, it is not necessary for all group members to know where to find resources in their home range; as long as one individual holds this knowledge the rest of the group can follow that individual (Carter et al., 2016). Consequently, we can infer that as individuals die, a group's utilization of its area can change, especially in respect to areas of the home range that are used less.

Any ecologist who studies the movement of organisms likely understands that both the organisms being studied and the ecologists themselves, exist and move through both space and time simultaneously (Nathan et al., 2008). When mapping and analyzing spatial phenomena, a long-held tradition of freezing time has made it easier to focus on the spatial phenomenon itself and is typically less analytically complex. Spatial data analysis (SDA) (Amato et al., 2019; Pillay et al., 2023) treats spatial data as if they exist in a timeless space, while time series analysis (TSA) (Stockmayer, 2003; Vilette et al., 2022) treats a time series as if it were independent of space. Both SDA and TSA therefore fail to account for associations or dependencies between space and time (Wu et al., 2021), and do not recognise that spatiotemporal data are multi-dimensional. At minimum, any animal tracking data beyond a single observation are spatiotemporal data and could be represented on the cartesian plane as 3-dimensional, with the z-axis representing time rather than elevation.

Geographic Information Systems (GIS) tools that handle 3D typically expect elevation on the z-axis so time needs to be converted into a numeric format it will accept. Up until the past decade most time tools were limited and not well implemented in many GIS platforms, making it easier to treat time as a third dimension while simply ignoring elevation. Recently, geospatial analytical software such as ArcGIS Pro, QGIS, and libraries/packages in R and Python have been developed to better handle spatiotemporal data (Alam et al., 2022; Bivand et al., 2017; Henning Teickner et al., 2025; Lawler et al., 2023) although many are still in their infancy.

While it has been stated in the literature that home ranges can be stationary or shifting and that the criteria for spatial and temporal limits are poorly defined, home ranges are still largely treated as static areas that can cover large temporal periods, often measured in years (Isbell, Cheney, & Seyfarth, 1990). I postulate that changes to home ranges are often gradual and hard to see as animals adjust their 'normal' spatial behaviour over time to suit the conditions or pressures they face while also reflecting the group's current knowledge of their area. However, seasonal and climate change, as well as some oscillation between wet and dry years or hot and cold years, can cause shifts in a home range that are much easier to see and sometimes more extreme as resource availability changes and animals explore for new food/water sources. Internal and external pressures can cause a group to shift its home range or possibly split and slowly move apart (Aureli et al., 2008; Cords & Rowell, 1986). These shifts will not always look like sudden changes or the 'abandonment' of a home range but could involve many small adjustments over time as the group slowly moves into or abandons an area.

With this in mind, the idea that a home range can be described in terms of a static boundary seems less plausible. Recent research is therefore directed at the idea of dynamic species analysis, which incorporates both spatial and temporal analysis. Similar to how dynamic landscape analysis uses time series of landscapes to determine habitat suitability (Akçakaya et al., 2004), the goal of this analysis is to include time in the creation of home ranges to capture spatial usage changes that occur over short periods (days to weeks) during long-term studies. These changes can be hidden in the data when home ranges are generated from large data sets that span extended temporal periods such as years or even months.

To do this I explored a method to calculate home ranges using multiple iterations of kernel density estimations (KDE), which will be referred to as the Dynamic Home Range method (DHR). When estimating a home range, the KDE tool calculates the density of points around a grid cell in a raster that represent observations of the study species (Silverman, 2018). These raster cells are arranged in an even grid across the area being mapped. Once each cell has been calculated, the home range estimation will often emerge as a smooth area around the points. In profile these can be viewed as a hill with the higher (peak) density regions typically towards the centre and tapering off as it gets to the edge of the point cloud, and the lower density estimations are at the foot of the "hill". KDEs run on large data sets tend to smooth out spatial activities that occur at smaller temporal resolutions. For example, if a study group experiences drought for a few months and is forced to forage out farther than usual then, in a large data set that spans many years, these points will have less overall influence and will either become absorbed and obscured by the KDE or, worse, if they are excursions close to the edge, likely to be

removed once a 90% isopleth is applied. By running KDEs at shorter temporal resolutions, set to capture the scale of the phenomenon, these short-term details are more obvious and less likely to be cut off as 'outliers'. Essentially more is not always better, and I suggest that large datasets much like the one used in this study, with ~71,000 observations, be broken up into smaller temporal sets to capture more detail. Even datasets that span months or years, rather than nearly a decade could benefit from this analysis by allowing researchers the flexibility to choose smaller temporal periods that are better suited to particular questions about a group's broader spatial behaviour and its interactions with environmental and social landscapes (thermal regulation, food availability, inter-troop encounters, landscapes of fear). Consequently, my objectives here are to describe the estimation of dynamic home ranges and illustrate its application in reference to data from three groups of vervet monkeys (*Chlorocebus pygerythrus*).

Methods

Study Site

The study was conducted on the Samara Private Game Reserve in the Eastern Cape Province of South Africa (Figure 3.1) using data collected over a seven-year period (2011-2018). The reserve is located on ~27,000 ha of a semi-desert region called the Nama-Karoo (Mucina et al., 2006; Pasternak et al., 2013) on the edge of the Great Escarpment, which demarks the southern edge of South Africa's Central Plateau (Anhaeusser et al., 2016). The centre of the valley is delineated by the contrast between arid hillsides, with low growing shrubs and succulents (Mucina et al., 2006), and an *Vachellia* (formerly *Acacia*) *karroo* Riparian zone that flanks the Melk River, an

intermittent river that was subject to a high amount of variability during the study period due to drought (Figure 3.2).

Figure 3.1: Samara Game Reserve (green pointer), South Africa (Image is a screenshot from Google Earth Pro).

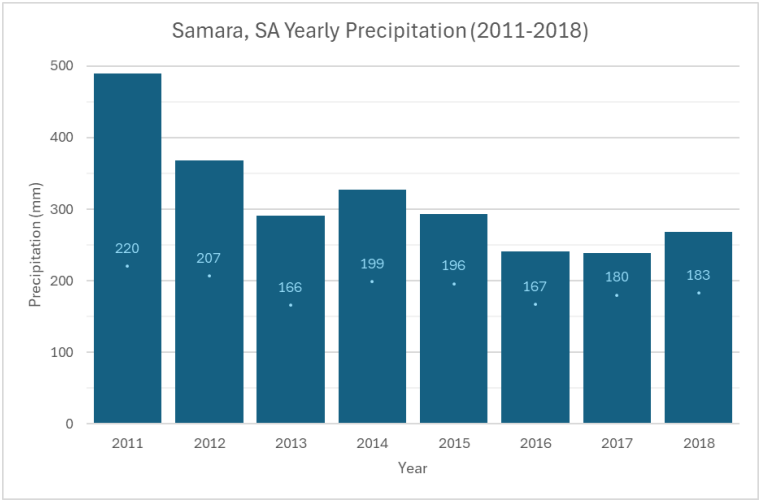

Figure 3.2: Global Satellite Mapping of Precipitation (GSMap) data was collected as year-round hourly observations by the Japan Aerospace Exploration Agency (JAXA) and have been aggregated to yearly rainfall (Blue Columns) and number of rainy days per year (Light Blue Point and Number).

Study Species

This study is focused on the spatial behaviour of three adjacent troops of vervet monkeys (*Chlorocebus pygerythrus*) that live the acacia riparian zone. All three troops (RST, RBM and PT) have been habituated to the presence of observers and are individually recognisable via natural markings. Vervet monkeys are generalists when it

comes to diet, with this population focusing on plant matter that makes up ~91% of their diet, and is primarily centred on *Vachellia karroo* (Pasternak et al., 2013). *Vachellia karroo* is evenly distributed in the riparian zone flanking the Melk River but quickly disperses further away from the river. Data used in this study were collected starting in October of 2011 for RBM and RST, while PT's data started after they were habituated in February of 2012. All data collection terminated in November of 2018 when the study site was closed.

Vervet Spatial Data

Troop level spatial data were collected every 30 minutes by research assistants using GPS-enabled data-loggers (Trimble Nomad and Trimble Juno) with 2-to-4-meter accuracy. During the study period, 70,910 geocoded scans were conducted at ~30-minute intervals over the course of 1,563 study days (Figure 3.3). Each of the troops in the study would typically have one or two researchers following the troop. A study day was ~10 hours long, starting with the troop being followed from their sleep site in the morning until they returned to their sleep site for the night.

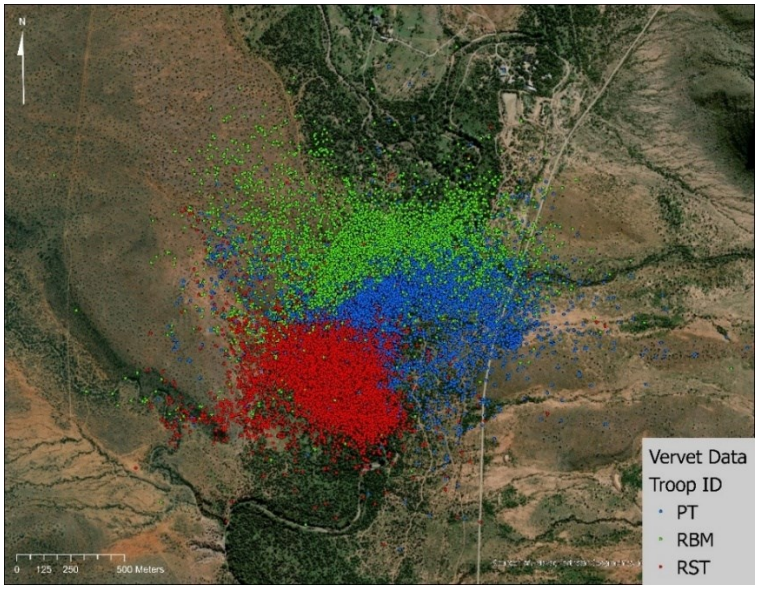

Figure 3.3: Map of 30-minute positional data collected by troop from October 2011 until November 2018.

Dynamic Home Ranges

Dynamic home ranges were generated by calculating a new KDE at a regular temporal interval. KDEs were estimated using R (R Core Team, 2015) in RStudio (Team, 2015), with the Kernel Smoothing ks package (Duong, 2018) and the smoothed cross-validation (SCV) bandwidth selector (Duong & Hazelton, 2005). Isopleth lines are commonly used to isolate a probability of occupation; a 50% isopleth line, for example, represents 50% of the highest estimates in the KDE. While it is recommended to use inner isopleths (50-80%) to avoid outlying data adversely overestimating utilization distributions (Anderson, 1982; D. E. Seaman et al., 1999), Börger has shown that 90% isopleths can produce unbiased home range estimates with smaller datasets, and that they do not suffer when sample sizes are smaller (Börger et al., 2006). For this analysis home ranges were defined as the KDE values falling within the 90% isopleth (Figure 3.4, Orange Line), the algorithm does allow the user to select values as high as 100%. I chose not to show the 100% isopleth as this is simply the minimum bounding box of the point cloud used to create the KDE's and provides no analytical utility.

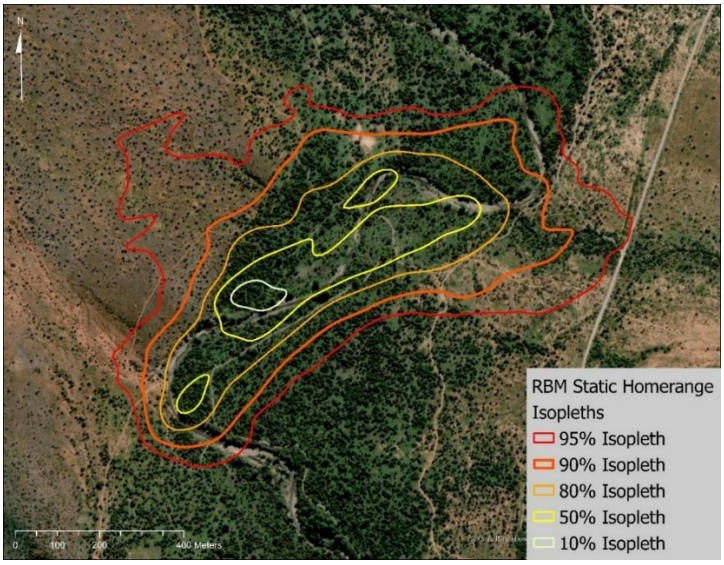

Figure 3.4: RBM static home range showing different isopleth levels, with 90% isopleth in thicker orange line. Samara, South Africa.

Point clouds were sampled using different temporal window sizes to determine how the home ranges changed based on the temporal scale used. For this study, I started by creating static home ranges (Figure 3.5) using all points collected from each troop (RST: 24,632 points; RBM: 24,584 points; PT: 21,694 points) as a baseline. I then subset the data down to yearly, then two-week (14-day) data sets to show how the same data would look in a more dynamic home range. The algorithm then iterated through the subsets to create home ranges at the given interval (yearly, weekly). For example, the data from each troop was then run through at an annual scale to produce home ranges from 2011 through to 2018 (2010 data were insufficient). Dates were converted to the `POSIXct` format to facilitate the use of the lubridate's `as.interval` function in R to create a temporal window that could be applied to a `dplyr` filter to extract observations within that window.

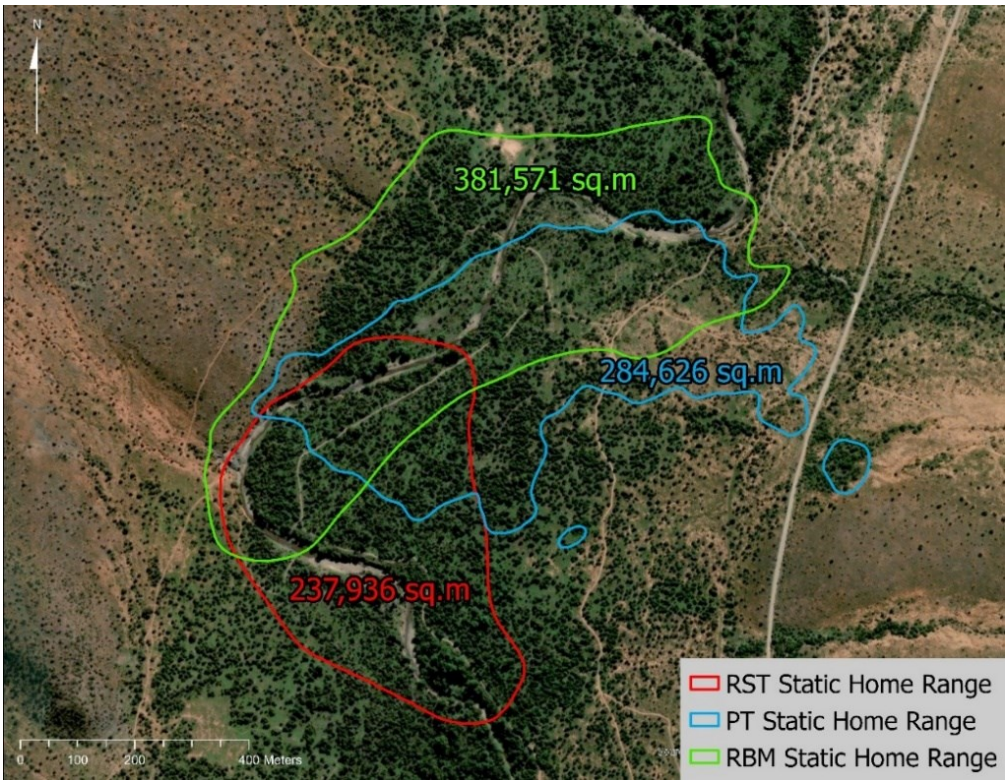

Figure 3.5: Static home ranges over the study period for RST (red), RBM (green), and PT (blue) troop as delineated by 90% isopleths. Samara, South Africa.

After each home range was created, the window was advanced, producing a new home range every **n** days, where **n** is the window size. The window size was set as a variable in R that could be selected by the user. At the same time, area was also extracted from each of the 90% isopleth polygons representing the home range using the `contourSizes` function from the `ks` package to allow the graphing of change in home range area.

Results

Dynamic home range calculations/models reveal that there is a high amount of spatial variability within a group of animals 'overall' home range when it is broken down to smaller temporal units. When we changed the temporal resolution from static to annual (Figure 3.6, Tables 3.1 & 3.2), then from annual to 14-day home ranges (Figure 3.7 & Table 3.3) the home range became more temporally defined. Home range overlap across the three groups does not show a significant change from static to annual home ranges until the temporal resolution drops to 14 days at which point the overlap between home ranges drops significantly (Table 3.4).

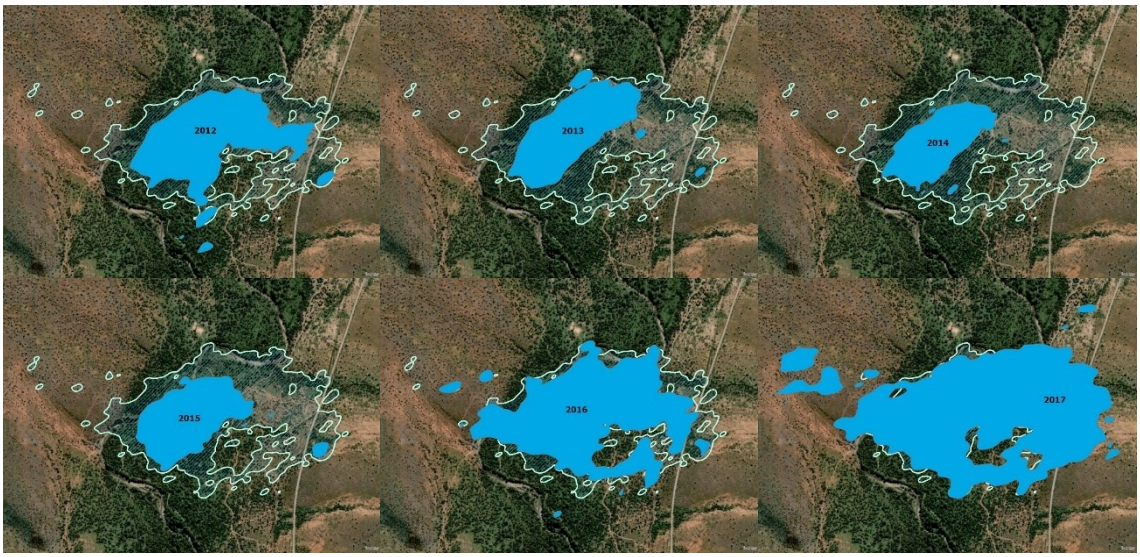

Figure 3.6: Yearly dynamic home ranges (solid blue) overlayed on the static home range (light blue border) for the PT troop. From left to right 2012 to 2017, years with less than 12 months of data (2011 & 2018) are not displayed.

Table 3.1: Static home range areas by Troop in square meters with sampling effort.

Static Areas		
Effort	**Area**	**Troop**
24,631	237,937	RST
24,581	381,572	RBM
21,693	284,627	PT

Table 3.2: Yearly home range areas by Troop in square meters with sampling effort.

Year	PT Troop		RBM Troop		RST Troop	
	Effort	Area	Effort	Area	Effort	Area
2011	-	-	311	326,063	235	304,698
2012	1247	158,571	2859	309,730	3627	216,464
2013	2053	121,280	2351	200,914	1673	164,457
2014	3383	75,570	3634	230,131	3131	145,563
2015	3877	94,573	4162	237,078	4235	173,210
2016	3988	257,872	4152	304,643	4526	191,436
2017	4348	472,446	4253	463,345	4354	284,405
2018	2797	536,766	2859	521,277	2850	267,837
Average	3,099	245,297	3,073	324,148	3,079	218,509
SD	1,045	173,673	1,240	106,322	1,391	56,165

Table 3.3: Summary of 14-day areas by Troop in square meters with sampling effort (full table in Appendix A).

	PT Troop		RBM Troop		RST Troop	
	Effort	Area	Effort	Area	Effort	Area
Minimum	21	21,660	24	60,616	23	49,111
Maximum	221	835,686	300	806,407	325	459,862
Average	131	162,204	139	254,056	138	157,067
SD	48	146,367	49	134,616	59	64,234

Table 3.4: Home Range overlap summary by Dyad for Static, Yearly, and 14-day periods (full tables in Appendix B).

Home Range Overlap by Dyad			
(sq.m)	**Static**	**Year Avg**	**14d Avg**
RBM/PT	276,121	259,358	103,446
RBM/RST	146,869	136,315	48,776
RST/PT	127,202	123,834	41,507

As we look at a higher temporal resolution (14 days) it starts to become obvious that there are core areas that the animals seem to be utilizing consistently throughout the year. There are also times of the year that we see the home ranges getting pushed out in what is likely exploratory movement to gather resources (Figure 3.7). The smallest home

range of 2017 was in January, with an area of ~88,000 m^2 (Figure 3.7 Frame 1). The largest expansion in 2017 happened in May (Figure 3.7 Frame 2) when PT troop expanded its home range to ~665,000 m^2, which followed a dry April (Figure 3.8 & Table 3.6) when only 3.7mm of rain fell. In June, PT's home range contracted to ~247,000 m^2 (Figure 3.7 Frame 3) after a wetter May with 15.9 mm of rainfall (Figure 3.8 & Table 3.6). The second largest expansion of the year was ~534,000 m^2 which occurred in July (Figure 3.7 Frame 4) following another dry month (June) that received less than 1 mm of rain (Figure 3.8 & Table 3.6). July was also a dry month at 1.4 mm of rainfall (Figure 3.8 & Table 3.6), which is likely why the home range expansion of July extends into August at ~475,000 m^2 (Figure 3.7 Frame 5). These expansions are substantial when compared to an average home range area for 2017 of ~284,000 m^2, Sept (Figure 3.7 Frame 6) which at ~279,000 m^2 is the closest home range to this average. In general, 2017 shows larger home range sizes compared to the overall 14-day average for PT troop of ~162,000 m^2 (Table 3.3). The largest expansion of a home range for not only PT but for all troops was ~835,000 m^2 in June of 2018 (Figure 3.9) during another dry month at 1.99 mm of rainfall (Table 3.6 & Figure 3.10). While it is not uncommon for June and July to be dry, these values were well below the 16 mm average observed between 2011 and 2018 (Table 3.5).

Expansion during or following a dry period suggests that the animals are moving out of their core areas to find food and water. This is reinforced by the fact that even marginally wetter months show contraction of the home ranges. These details of an animal's area of utilization are more obvious at a resolution measured in days and are lost within larger static or yearly home ranges, or smoothed out as outliers outside the 90%

isopleth, as we clutter the home range with months or years of data. Even annual home range variability is lost in a static home range, as years of broader usage bloat the static home range (Figure 3.6 last Frame). While Burt (1943) might have critiqued some of these as explorations or occasional sallies and excluded them from the home range, Brown's assessment that a home range reflects the area an animal uses in its daily activities seems better served in a dynamic system (Brown, 1962).

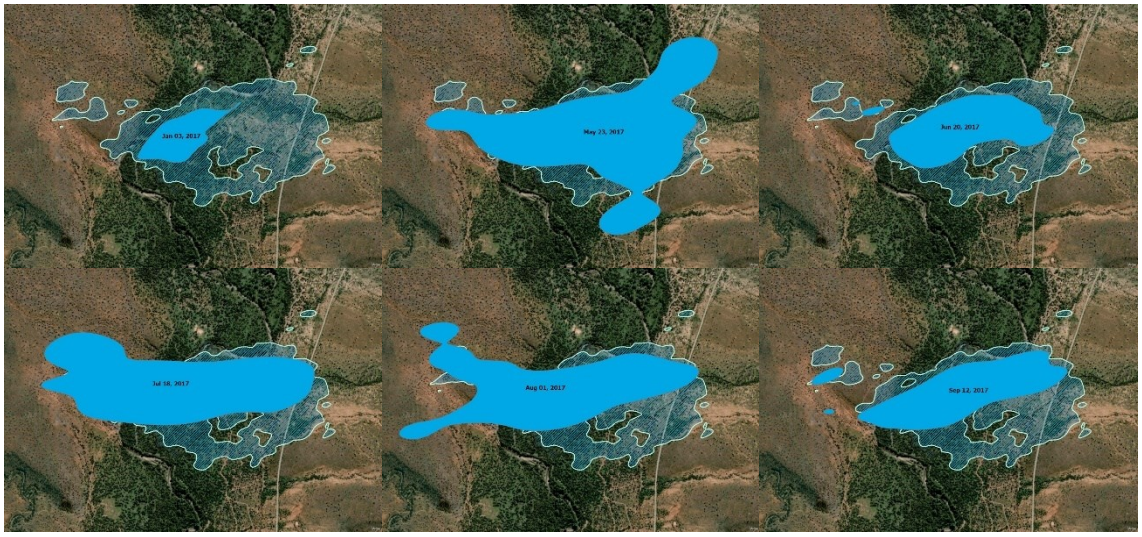

Figure 3.7: Six 14-day DHR's overlayed on 2017 DHR for PT troop illustrate changes during low rainfall periods (all 2017 images in Appendix C). From left to right: Jan 3rd, May 23rd, Jun 20th, Jul 18th, Aug 1st, Sep 12th.

Table 3.5: Minimum, Maximum, and Average Monthly rainfall values for Samara, South Africa from 2011 to 2018.

	Monthly Rainfall (mm)											
	Jan	**Feb**	**Mar**	**Apr**	**May**	**Jun**	**Jul**	**Aug**	**Sep**	**Oct**	**Nov**	**Dec**
Min	5	13	8	4	2	1	1	9	1	7	2	2
Max	91	88	82	40	54	37	53	31	41	52	65	80
Average	44	49	40	22	15	10	16	14	14	25	25	39

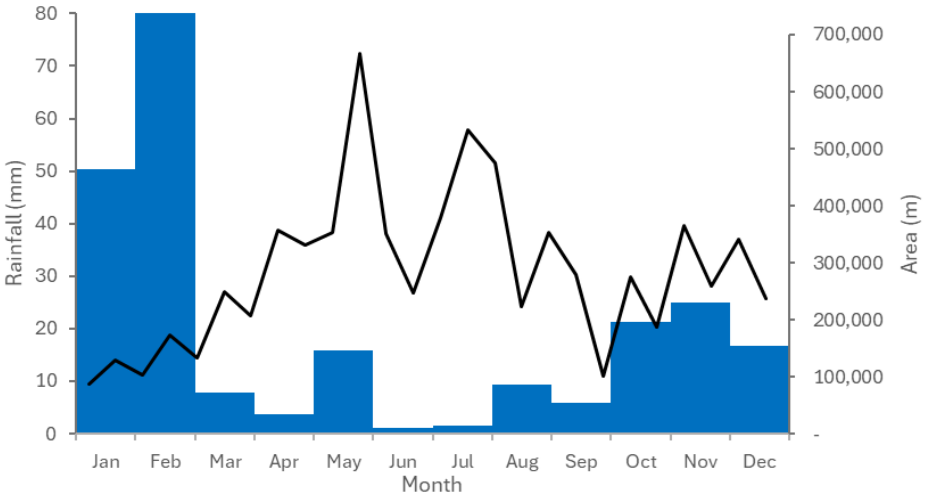

Figure 3.8: Monthly rainfall (blue columns) for Samara, South Africa in 2017, overlayed with 14-day home range areas for PT troop (black line). Precipitation data collected using the JAXA/NASA GSMap satellite.

Table 3.6: Monthly Precipitation for Samara, South Africa from 2011 to 2018.

	Precip (mm)							
Month	**2011**	**2012**	**2013**	**2014**	**2015**	**2016**	**2017**	**2018**
Jan	66.6	4.9	18.6	62.6	20.0	36.2	50.3	91.3
Feb	87.7	45.7	18.5	45.2	13.2	54.2	80.0	48.8
Mar	81.5	67.2	48.3	15.4	52.7	30.5	7.9	14.1
Apr	18.5	23.5	8.5	39.5	31.3	14.1	3.7	36.9
May	53.7	9.2	5.7	11.7	2.3	16.0	16.0	9.3
Jun	37.0	12.4	5.2	0.7	16.0	8.8	1.0	2.0
Jul	17.3	53.2	4.5	0.6	41.5	8.3	1.4	3.2
Aug	9.9	31.1	11.3	15.4	14.3	12.4	9.3	10.2
Sep	0.7	2.8	0.6	22.8	41.0	2.6	6.0	36.8
Oct	44.7	36.7	51.7	11.3	18.4	9.2	21.2	6.7
Nov	25.1	1.7	41.4	64.5	33.4	2.4	25.1	7.1
Dec	46.6	79.8	76.2	37.3	8.9	46.3	16.6	2.2

Figure 3.9: Kernel Density Estimation (KDE) dynamic home ranges calculated between May and August of 2018 for RBM show a short-term exploratory expansion which peaks in mid-June 2018.

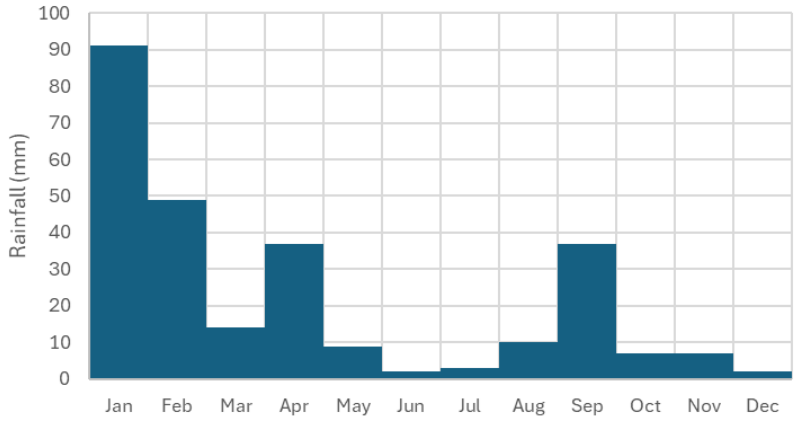

Figure 3.10: Monthly rainfall for Samara, South Africa in 2018. Data collected using the JAXA/NASA GSMap satellite.

Applications of DHRs

Area Change and Overlap

Dynamic Home Ranges can be used to quantify expansion and contraction by calculating area changes over time as animals are utilizing different parts of the site, as well as show how utilization can change depending on environmental factors such as drought. NOAA ranks the 2015/2016 drought in South Africa as one of the worst in 30 years, as many parts of the country received less than 80% of their normal rainfall. This was triggered by a strong El Niño event that ranked in the top three since 1950 (Di Liberto, 2016). Dynamic Home Ranges can also be used to look at the amount of overlap between troops as a metric for territoriality. A territory can be thought of as a fixed space which individuals or a group actively exclude competitors from the resources within (Maher & Lott, 2000). This exclusive use definition would expect a non-territorial species to have large areas of overlap with neighbouring groups, and territorial species to have less or no overlap (Lawes & Henzi, 1995; Pitelka, 1959; Strier, 2016).

Methods

With each iteration of the DHR algorithm each kernel representing the Home Range was trimmed at the 90% isopleth by assigning NA to any values in the raster that land outside the isopleth. To facilitate area and overlap calculations the newly trimmed rasters were then converted to polygons using the Reclassify and Raster to Polygon tools from the arcpy library in Python. Because the Raster to Polygon tool creates a separate polygon for each unique value in a raster, all pixels within a home range were reclassified as 1 to avoid having multiple polygons in the output. Each polygon was then run through the Calculate Geometry Attributes tool to calculate the home range area at each period for each troop.

The polygons of the home ranges were also iterated over with the Intersect tool, which only keeps overlapping areas. This was run on each of the three troop dyads, then once more with all of the troops together to give four overlap values at each time period: All Troops, RBM/RST dyad, RBM/PT dyad, and the RST/PT dyad. All overlaps polygons were also run through the Calculate Geometry tool to extract overlap area (Appendix B).

A high amount of variability was found in number of samples collected per day per troop. This variability was due to several factors, some days the animals were harder to find and may not have as many points, the number of research assistants available in the field varied over time, while environmental factors such as inclement weather could make data collection harder. To account for this, sampling effort was modeled to avoid bias due to variability in sampling effort over the course of the study, and to accommodate the comparison of the home range sizes over the study period (Börger et

al., 2006). Sampling effort was modeled with a Bayesian regression model using Stan (BRMS), running 1000 iterations across four chains and four cores with the gamma family. Model fit was confirmed using a graphical posterior predictive check:

$$Area \sim s(tss, by = Troop) + s(Size) + (1 \mid Troop)$$

Where: tss = Time since the start of the study measured in days, Size = the number of observations in any given home range kernel density estimation, with Troop entered as a random intercept.

In the histogram of sample sizes (Figure 3.11) used in 14-day kernel density estimations most home ranges were estimated using between 100 and 200 points (Appendix A). This was created by binning the number of samples used in every 14-day KDE. The output from the model shows that sample sizes below 100 tended to have lower area estimations and samples approaching 300 tended to have higher area estimations (Figure 3.12). The model output was then used to make predictions of the area as if sampling effort were equal across all predictions using the posterior_epred function in R set to 150 samples.

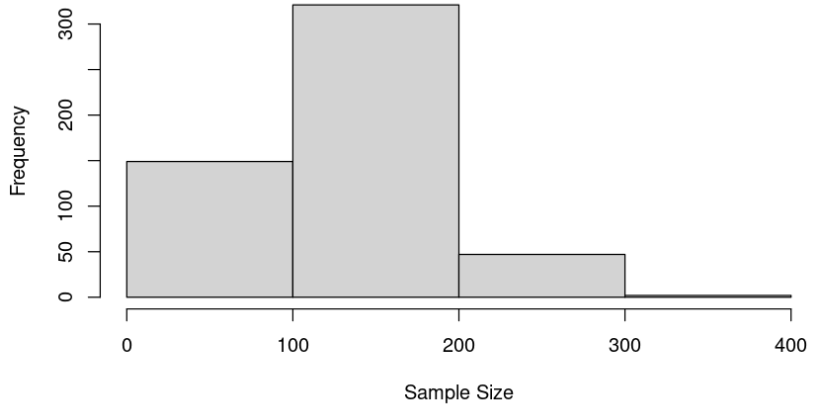

Figure 3.11: Histogram of sample sizes used in each kernel density estimation.

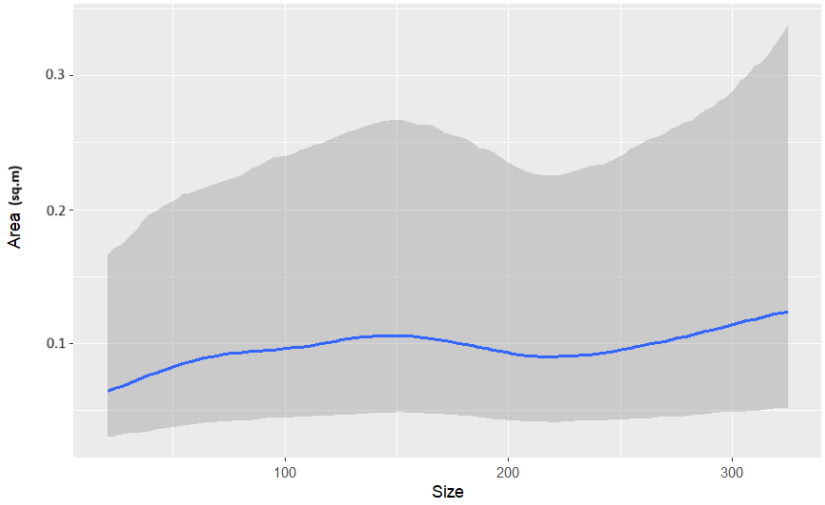

Figure 3.12: LOESS line of sampling effort to area estimates.

Overlap predictions by Dyad were also corrected for sampling effort using a similar model:

$$Overlap \sim s(tss, by = Dyad) + s(Size) + (1|Dyad) \quad \textit{(Eq. 3.1)}$$

Where: tss = Time since the start of the study measured in days, Size = the number of observations in any given overlap of a dyadic pairs home range kernel density estimations, and Dyad was entered as a random intercept. A sampling effort of 300 was used to represent the sampling effort of two troops.

Results

Area calculations show that the three troops show growth in home range area over the study period along with some cyclic variability over smaller time periods (Figure 3.13). These area changes are also visible when the home ranges are mapped out and can be used to highlight some of the short- (Figure 3.14) and long-term (Figure 3.15) changes to home range utilization.

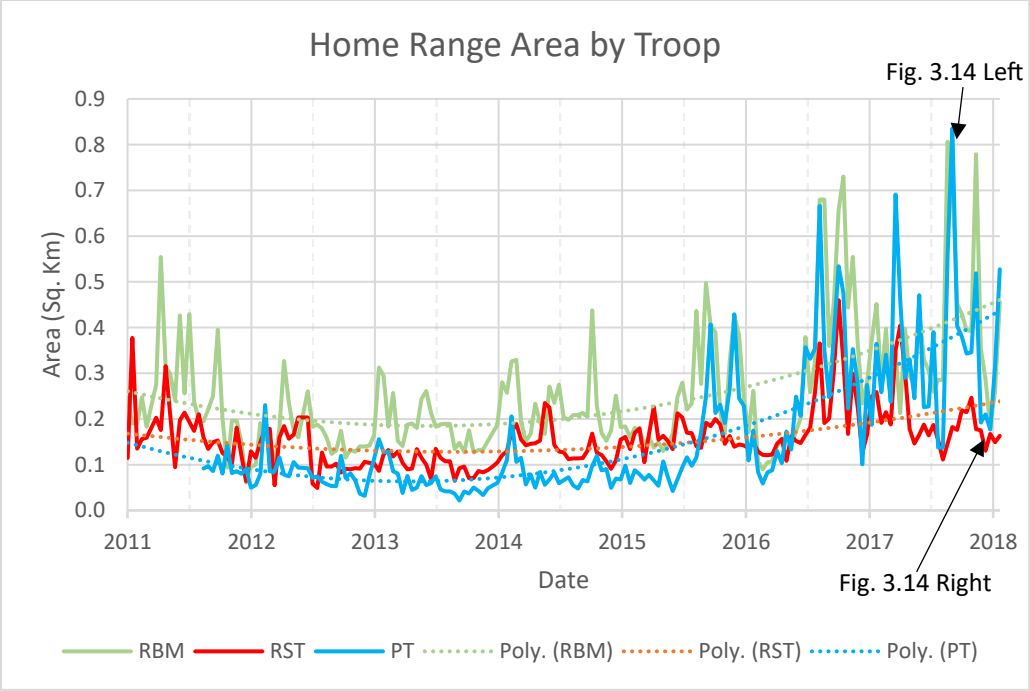

Figure 3.13: Home Range Area by Troop since 2011

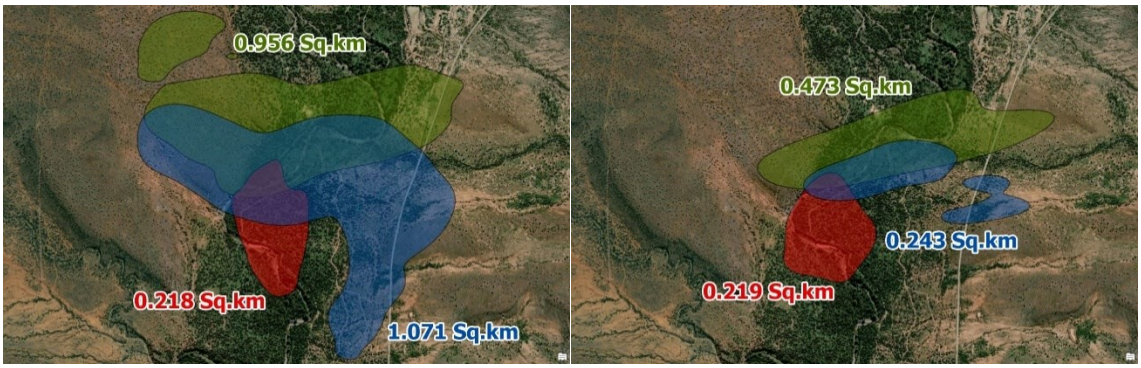

Figure 3.14: Fourteen-day home ranges. 19 June 2018 (left) 11 Sept 2018 (right).

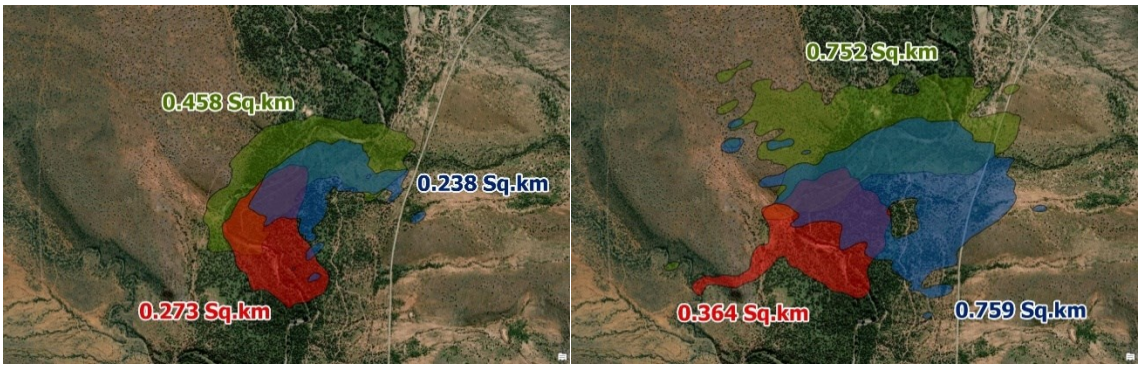

Figure 3.15: Yearly home ranges 2012 (left), and 2018 (right).

Area predictions by troop with a sampling effort modelled using 150-points per 14-day period are shown in Figure 3.16 using a smoothed line to reduce the noise of Figure 3.13. This clearly shows a slight shrinkage in all troop areas at the start of the study, then a large jump in area for PT and RBM troops and a smaller growth in area for RBM (Figure 3.16). The initial shrinkage by RBM and RST is likely due to the intrusion of PT between the two troops as they moved into the riparian zone around this time. Later expansions could be explained by the drought of 2015/2016 as pressure to find resources may have forced the troops to venture farther out.

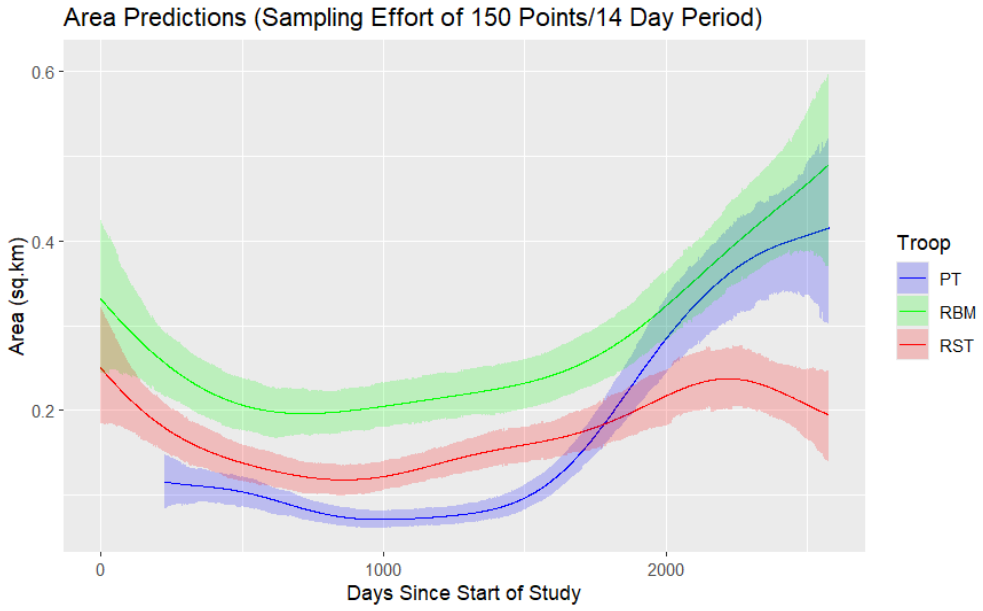

Figure 3.16: Area predictions by Troop corrected to a sampling effort of 150 points per KDE.

At the beginning of the study, based on sampling effort predictions of 300 samples, all dyads overlapped by between 0.01 and 0.06 km^2 (10,000-60,000 m^2), which grows considerably towards the end of the study as the drought of 2015/2016 forced troops to expand not only out but also across each others home ranges in an effort to gather resources, with overlap reaching as high as 0.22 km^2 (220,000 m^2) (Figure 3.17). This high amount of overlap also suggests that these three groups of vervets are not

excluding each other, as would be expected from Maher & Lott's exclusive use definition of territoriality (Maher & Lott, 2000). Overlap between dyads show variability that can be explained by a mix of proximity competition. Early intrusions of PT into the site would have initially been along the southeastern extent of RBM's home range then eventually push itself between RBM and RST, which would have increased overlap with PT and RBM and likely caused the drop in overlap between RBM and RST, and possibly PT and RST as RST area shrinks (Figures 3.16 & 3.17).

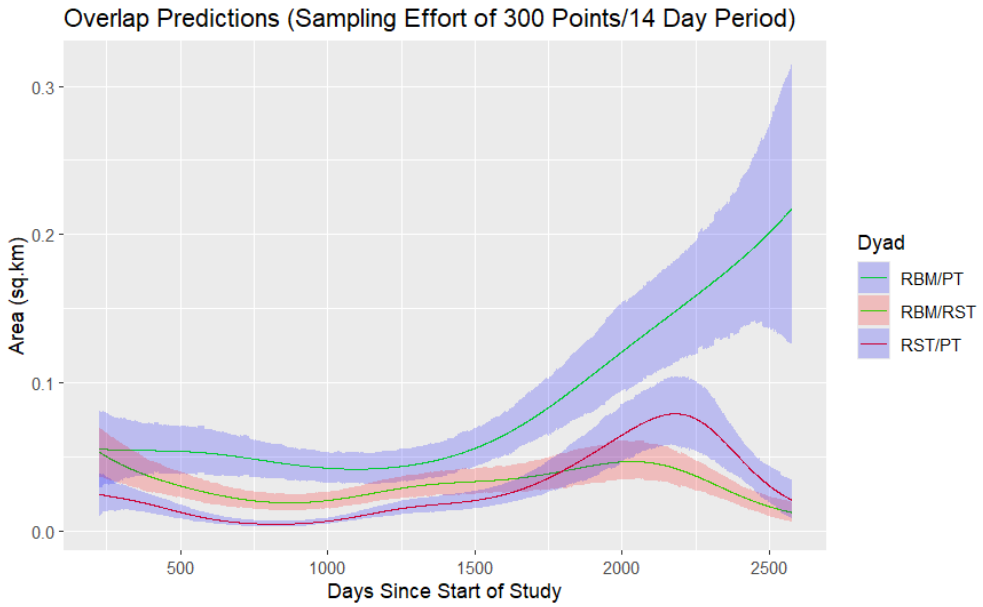

Figure 3.17: Overlap area predictions by Dyad corrected to a sampling effort of 300.

Home Range Productivity

Normalized Difference Vegetation Index (NDVI) has been shown to be an effective proxy for net primary productivity (Rasmussen, 1998), and has been used to measure vegetation health (Winnie et al., 2008). This makes NDVI a useful tool for evaluating habitat productivity (Arseneau et al., 2015). It has, more specifically, been shown to correlate strongly to food availability and shelter in vervet monkeys (E. P.

Willems et al., 2009). By using dynamic home ranges, it is possible to estimate the productivity of areas utilized by the animals at a given time by intersecting them with NDVI raster products.

Methods

For this application, I used a 16-day window for DHRs that coincided with the revisit time of Moderate Resolution Imaging Spectroradiometer (MODIS) Normalized Differences Vegetation Index (NDVI) data collection (Didan, 2015). MODIS data are collected by the Earth Observing System (EOS) satellites Terra (EOS AM-1) and Aqua (EOS PM-1) with a periodicity of 16 days (NASA, 2017). MODIS retrieves vegetation indices (VI) daily and applies a compositing method to retain only the highest quality pixels in the 16-day product. Spatial resolution varies from 250 m to 1 km products; the 250 m product was used in this analysis. NDVI is often referred to as a measure of 'greenness' but does not use the green part of the spectrum. Instead, it is calculated as the difference divided by the sum of the near-infrared (NIR) and red reflectance. High NDVI values indicate dense, healthy vegetation such as forests or crops, while low values suggest sparse or stressed vegetation; values near zero typically represent barren land or rock (Reed et al., 1994).

MODIS NDVI data were downloaded from NASA's Reverb|ECHO portal and imported into ArcGIS Pro. Each troop's DHR was represented as a regular grid of points (10 m spacing) rather than a polygon (Figure 3.18). To create this grid, an extent was defined that encompassed all known home ranges. Points within the 90% isopleth polygon of each troop's home range were then selected using the Selection by Location tool and the Intersect relationship, isolating points that represented the home range at a

given point in time. NDVI values were extracted to these points using the Extract Multi Values to Points tool and averaged to calculate an area-weighted NDVI for each home range, serving as a proxy for food availability given species' generalist diet. This process was repeated at 16-day intervals throughout the study period.

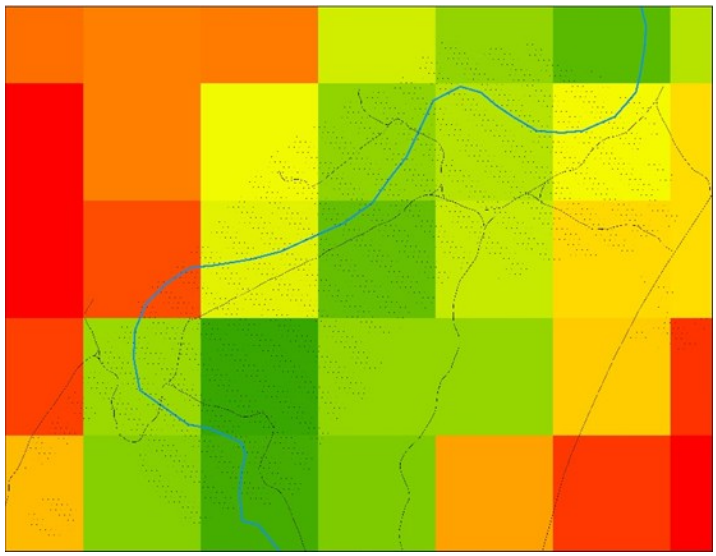

Figure 3.18: NDVI pixels (red for low, green for high) from MODIS overlayed with home range as a point grid (tiny black dots) for area weighted calculation of NDVI. River (blue) and road (black) lines are added for visualization only.

Results

When area and NDVI are plotted together over time using locally estimated scatterplot smoothing (LOESS) lines to reduce the noise, we can see that there is a tendency for troop home range area to increase as NDVI decreases, which may further indicate exploratory resource gathering. NDVI values do not vary much from troop to troop showing that food is generally evenly distributed within the riparian zone occupied by these three troops (Figure 3.19).

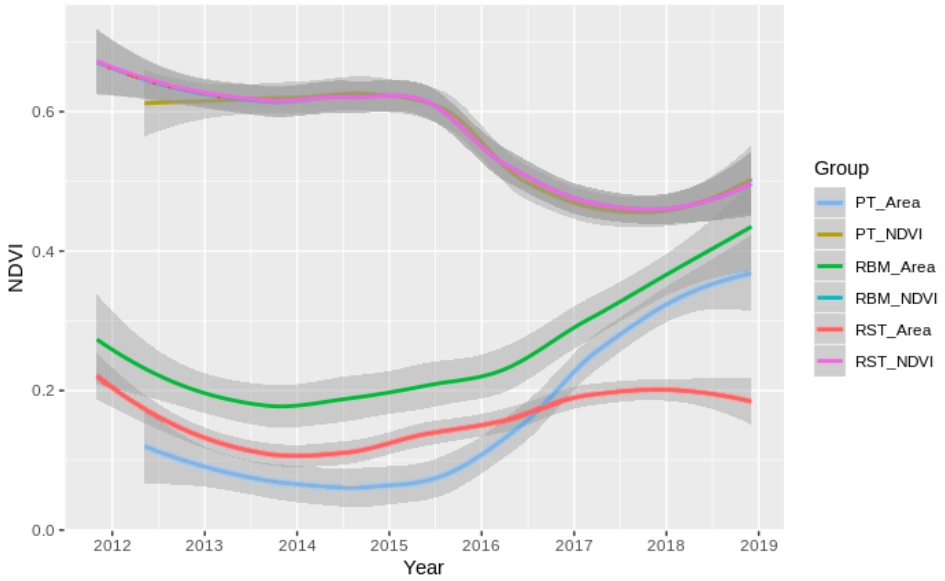

Figure 3.19: LOESS smoothed lines for troop area and NDVI values. RBM NDVI is hidden under the NDVI line for RST.

Discussion

Presenting the data using home ranges created with smaller temporal windows reveals that there is a great deal of variability within home ranges, not only in area but also in response to some of the drivers of home range size, such as food and water. Thus, dynamically produced home ranges offer a more accurate method for tracking and mapping these changes. DHRs can be used for a large variety of studies as they do not limit the user to a fixed temporal period. If a study requires a larger temporal window of months or even years, this method can accommodate it, just as it also allows smaller time periods of days and weeks. Its utility for extracting environmental data, such as NDVI at the home range scale in several papers (Blersch et al., 2023; Bonnell et al., 2022; Jarrett et al., 2020; Nord et al., 2022; Nord et al., 2021; Vilette et al., 2022, 2023) is clear and it shows promise for extracting other data such as Landsat Thermal data (10 m) or, in cases where home ranges are large enough, GSMap rainfall data (10 km). Dynamic mapping of home ranges also gives researchers the ability to look closer at area utilization (Henzi et

al., 2021) and the cyclic nature of home range utilization. This method is discussed in the next chapter, which presents how winning Inter Troop Encounters (ITE) might be tied to where they occur within a home range.

Intertroop Encounters

Introduction

Conflicts are a common occurrence among organisms, including primates (de Waal, 2000; García et al., 2022; Rusch & Gavrilets, 2020), and are thought to happen for a variety of reasons. These include access to food resources (Cheney, 1981; Crofoot & Wrangham, 2010; Henzi & Lucas, 1980), access to mates or mating opportunities (Cheney & Seyfarth, 1980; Henzi et al., 1998; Sicotte, 1993), and territorial disputes (Kitchen et al., 2004; Wilson et al., 2001). Territorial disputes have been categorized into three subtypes: incursions to "poach" resources, attempts to expand into neighbouring territory, and attempts to completely displace the current residents (Hinsch & Komdeur, 2017; Mitani et al., 2010; Wrangham, 1999). In some primate species, such as chimpanzees, intergroup conflicts have been described as resembling warfare, with the potential intent to kill or maim (Crofoot & Wrangham, 2010; Mitani & Watts, 2005; Wrangham & Glowacki, 2012).

The varied reasons for these conflicts, henceforth referred to as intertroop encounters (ITEs), must also be considered with both the physical and social environment in mind (García et al., 2022). Social interactions can influence whether two groups are likely to interact violently, particularly if previous interactions have led to violence (Crofoot, 2013). Likewise, the environmental pressure caused by resource clumping or seasonal availability can push groups to interact as they compete for access to these resources regardless of social relationships (Spiegel et al., 2016). Intragroup herding behaviour has been observed among primates during aggressive encounters (King et al., 2008), commonly in baboons. While herding has also been noted among vervets

(Struhsaker, 1967), it occurs at a relatively low rate of approximately 20% (Cheney, 1981).

Within the Samara population, there is little evidence that ITEs are driven by territoriality (E. Willems et al., 2009), and the defence of resources such as food or sleeping trees has yet to be shown as significant. It is possible that ITEs result simply from proximity (Lehmann et al., 2007), where an aggressive encounter occurs when one group discovers another in close spatial proximity. Testing this "proximity theory" is challenging, as it requires comprehensive data on all potential spatial interactions, including both violent and nonviolent encounters (Cheney, 1992). Moreover, spatial proximity may serve only as the proximate cause of an encounter, while ultimate causes could relate to other activities, such as foraging in a common location for resources (P. Henzi, personal communication, July 30, 2024).

Tinbergen (1963) laid out a framework for analyzing behaviour in biology, in which behavioural phenomena can be analyzed at two levels: the proximate (mechanism and development) and the ultimate (adaptive value and phylogeny) causes. Applied to ITEs, spatial proximity functions as the immediate trigger, or proximate cause, while resource competition serves as the ultimate cause, reflecting the evolutionary rationale for the interaction. The fact that groups encounter each other due to the spatial overlap of their home ranges does not preclude the influence of evolutionary pressures on their behaviour (Tinbergen, 1963).

In Samara, these evolutionary pressures are shaped by seasonal changes in resource abundance. During the mating season, food availability declines after the rainy period, leading individuals to spend less time foraging and more time travelling in search

of food (Barrett et al., 2004; McFarland et al., 2014). This seasonal ecology influences when and where groups move, which in turn can shape the timing and location of ITEs.

Some species employ active avoidance to minimize conflict. Wild baboons (*Papio cynocephalus*), for example, spend less time in close proximity than expected from a null model, suggesting deliberate avoidance behaviour (Crofoot & Gilby, 2012; Markham et al., 2013). This avoidance tactic does not seem to be the case with vervets in Samara, where it is common to have daily intertroop encounters.

In Section 1, I explore the relationship between ITEs and the participants' home ranges (Burt, 1943), aiming to determine whether the patterns observed in white-faced capuchin monkeys (*Cebus capucinus*) are also present in Samara vervets (Crofoot et al., 2008). Section 2 shifts the focus to the home range construct to address the limitations of static home ranges and to undertake a more detailed analysis of home range influence on ITEs. Specifically, Dynamic Home Ranges (DHR) introduced in the previous chapter are employed to evaluate whether higher temporal resolutions provide a more nuanced understanding of ITE dynamics. Sections 1 and 2 prompted further investigation into alternative approaches in Section 3, where I considered a framework that does not rely on the home range construct. This approach examines behaviours in their absolute locations in space and time and proposes a method for analyzing the structure of behaviours within ITEs across both spatial and temporal dimensions. By emphasizing the "*where"* and "*when"* of these encounters without tying them to human constructs, this framework aims to provide a more biologically meaningful perspective.

Methods

Study Groups

Data on naturally occurring intertroop encounters (ITEs) were collected by one to three observers from three habituated troops of vervet monkeys (*Chlorocebus pygerythrus*) occupying adjacent home ranges in semi-arid *Vachellia* (formerly *Acacia*) *karroo* riverine woodland in the Samara Game Reserve, Eastern Cape, South Africa (Pasternak et al., 2013). The three study groups, the River Bend Mob (RBM), River Side Troop (RST), and Picnic Troop (PT), consisted of individually recognisable members and had been under observation since 2008 (RBM, RST) or 2012 (PT).

Intertroop Encounter Data

Observations of ITEs were collected during 790 all-day follows between 20 November 2014 and 30 November 2018. During this period, 4,340 ITEs were recorded, yielding an average of 5.5 encounters per observation day across the three groups. Encounters involving groups outside the study population, or those with unknown initiators or winners, were excluded from the analysis. After filtering, 1,113 ITEs remained for analysis. Only encounters between the three focal troops (PT, RBM, and RST) where the initiator, winner, or a draw was clearly determined were included in analyses (Figure 4.1).

To ensure balanced representation during analysis, each ITE was duplicated in pre-processing such that each encounter was scored from the perspective of both participating troops, with each troop in turn constituting the "focal troop", or the troop whose perspective in the ITE is the focus of a given model. This controlled for potential recording bias (e.g., if one troop was preferentially listed first during data entry).

The initiator of an ITE was defined as the individual or group that first exhibited aggressive behaviour, while the winner was identified as the troop that either held its ground or successfully repelled the other group. From the focal troop's perspective, initiation and victory were coded as binary variables (InitB and WinB; 1 = yes, 0 = no). When ITEs were duplicated to include the other troops perspective, these values were inverted ($0 \longrightarrow 1$, $1 \longrightarrow 0$).

During each encounter, observers recorded the number and identity of participants, the maximum level of agonism recorded for each participant, and the GPS coordinates where the encounter took place. ITE Group size was defined as the number of individuals participating from each troop. Participation serves as a proxy for a group's potential to overwhelm an opponent and intimidate rivals, although other studies have found that smaller groups sometimes have a higher chance of winning (García et al., 2022). The difference in group size (ΔSize) was calculated as the focal troop's size minus that of the opposing troop, with positive values indicating a size advantage for the focal troop. When ITEs were duplicated (see below), both Aggression and Participation were multiplied by −1 to invert them accordingly.

Individual agonism scores were based on the highest level of aggression displayed during the encounter and classified into five mutually exclusive categories:

1. **Physical** – Direct physical contact with members of a rival troop.
2. **Active** – Non-contact aggressive movements (e.g., chasing, charging, lunging, swiping).
3. **Stationary** – Static aggressive displays, including vocalizations, eye-flashing, or bipedal threats.
4. **Victim Only** – Individuals that received physical or active aggression but did not retaliate.
5. **Non-Aggressive** – Individuals that altered behaviour during the encounter but neither displayed nor received aggression.

Group-level aggression for each troop was then estimated as the proportion of participating individuals that displayed Physical or Active aggression relative to the total number of participants from that troop in the ITE. The difference in group-level aggression between the opposing troops (ΔAggression) was computed as the focal troop's aggression minus that of the adversary, with positive values indicating greater aggression from the focal troop.

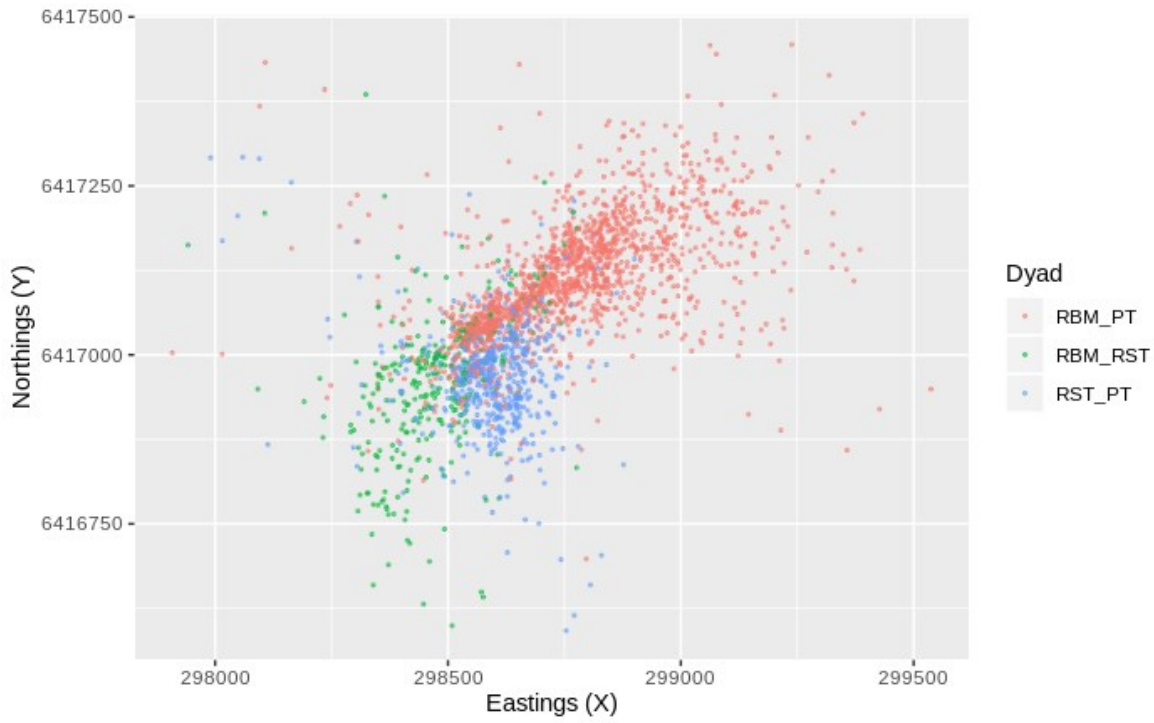

Figure 4.1: Point cloud of intertroop encounters (ITEs) colored by the dyad of troops involved. Dyads are non-directional and have been sorted from records representing both combinations of each dyad. RBM vs. PT (red), RBM vs. RST (green), RST vs. PT (blue).

Section 1: Troop Distance to Centre (TDC)

Yearly Home Range ITE Models

The annual home range of each troop was estimated using the Kernel Density Estimation `kde()` function from the `ks` package in R (Duong, 2024). The pixel with the highest value in the KDE, representing the densest part of the home range for the year,

was selected as the core, treating the home range space as relatively static. TDC was scaled and centred (TDCs) due to the larger potential distance values (in hundreds of meters) compared to other variables in the model that were either binary or small values (typically in tens rather than hundreds). This ensured that all predictors contributed comparably to the model, preventing larger magnitude variables from having a disproportionate influence on the results.

To test the prediction that ITE outcome is determined by a troop's location in relation to the centre of its home range (Figures 4.2, 4.3, 4.4), troop distance to centre (TDC) was calculated as the Euclidean distance between the ITE location and the centroid of the focal troop's home range. Home range centres were defined as the highest density point within each troop's range, and all coordinates were recorded in the WGS 1984 UTM Zone 35S projection to facilitate accurate distance calculations in R. TDC was calculated after duplication to ensure the correct troop's home-range centre was used.

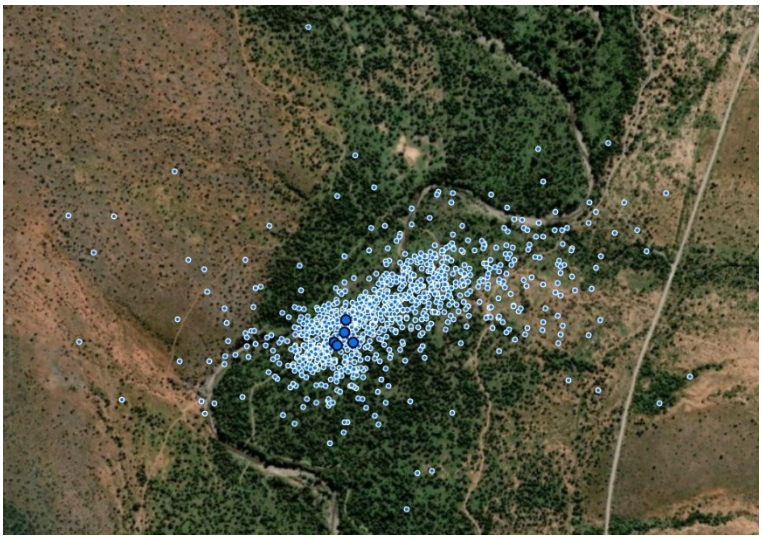

Figure 4.2: ITEs that PT are involved in (smaller blue points with white outline), relative to home range centres (larger blue points with black outline) give a sense of TDC relationship.

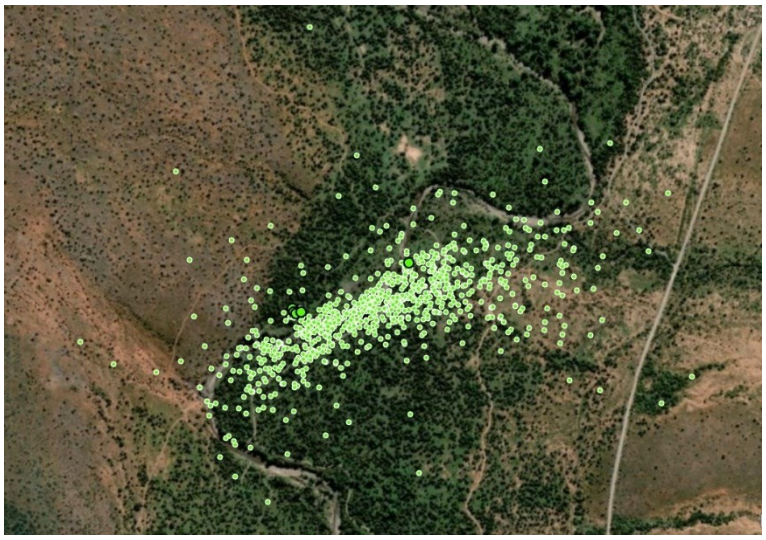

Figure 4.3: ITEs that RBM are involved in (smaller green points with white outline), relative to home range centres (larger green points with black outline) give a sense of TDC relationship.

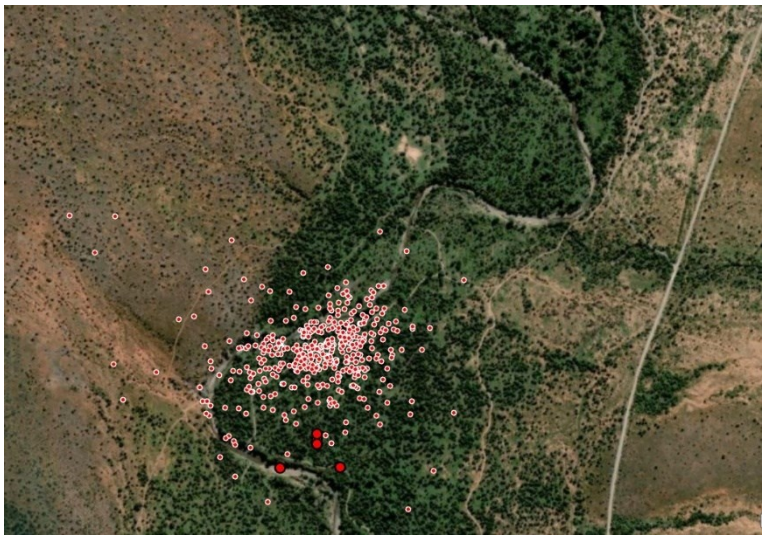

Figure 4.4: ITEs that RST are involved in (smaller red points with white outline), relative to home range centres (larger red points with black outline) give a sense of TDC relationship.

Statistical Methods

All models were run as Bayesian mixed-effects logistic regressions using the brm() function from the brms package in R. The brms package interfaces with Stan, a probabilistic programming language and computational framework for Bayesian statistical inference (Team, 2024). Stan uses a Hamiltonian Monte Carlo (HMC) sampler, which draws from the posterior distribution using gradient-based trajectories inspired by Hamiltonian physics. This allows for efficient exploration of high-dimensional parameter

spaces, outperforming simple Monte Carlo methods in complex models (Betancourt, 2017; Robert & Casella, 1999).

To avoid autocorrelation, each troop was modelled independently, including only ITEs involving the modelled troop and analysed from that troop's perspective. This approach ensured that TDC and other measures are always specific to the modelled troop.

Due to the binary nature of the response variable (1 = Win, 0 = Loss), the model was specified with a Bernoulli family. The opposing troop was included as a random effect. Model settings were chosen to reduce sampling issues: adapt_delta was set to 0.99, the number of iterations was set to 3000 to minimize divergent transitions, and weakly informative priors were used: set_prior("normal(0, 1)", class = "b") for regression coefficients (Bürkner, 2024). Each troop was modelled to see how well proximity to the home range centre predicted winning an ITE (Equation 1).

$$WinB \sim 1 + TDCs + DeltaAgr + DeltaPart + InitB + (1 \mid Adversary) \quad \text{(Eq. 1)}$$

To assist with the interpretation of results Interclass Correlation Coefficient (ICC), Relative Width (RW), Odds Ratios (OR), and Probability of Direction (pd) were calculated. The Intraclass Correlation Coefficient (ICC) quantifies the proportion of total variance in an outcome that is attributable to differences between groups, as captured by the standard deviation (σ) of the random effect. The ICC is calculated as the ratio of the group-level variance (σ^2) to the sum of group-level variance and the within-group (residual) variance (Equation 2). In a binomial (Bernoulli) model with a logit link, the residual variance is fixed at: $\pi^2/3 \approx 3.29$ (Nakagawa et al., 2017).

$$ICC = \frac{{\sigma^2}_{Adversary}}{{\sigma^2}_{Adversary} + \pi^2/3} \quad (Eq. 2)$$

Credible intervals (CIs) represent the range within the posterior distribution which contains a specific percentage of the probability mass (typically 95%). In Bayesian terms, this means that there is a 95% probability that the parameter falls within that range, given the data and priors (Edwards et al., 1963). A 95% CI excludes the tails of the distribution, leaving 2.5% of the probability mass in each tail, and is defined as the upper and lower bounds. Relative width (RW) quantifies the precision of a posterior distribution as the ratio of the distance between these bounds to the posterior mean (Equation 3), with zero representing very high precision, and one very low. This provides a normalized measure of interval width (Flegal & Gong, 2015; Kruschke, 2014).

$$RW = \frac{Upper\ CI - Lower\ CI}{Posterior\ Mean} \quad (Eq. 3)$$

Odds Ratios convert log-odds coefficients (logit scale) into a multiplicative effect on the odds, providing a more intuitive interpretation of each predictor's impact (Equation 4). This quantifies how the odds of an event change: OR = 1 indicates no change, OR = 0.5 halving of the odds, OR = 2 doubling of the odds, with OR values farther from 1 indicating a stronger effect (Chen et al., 2010; Fritz et al., 2012; Szumilas, 2010).

$$OR = e^{Coefficient} \quad (Eq. 4)$$

Probability of direction (pd) is a measure of how much of a distribution lies on the positive or negative side of zero. It ranges from 50% to 100% and can be interpreted as the probability that a parameter is positive or negative, based on its relationship to zero. The p_direction() function from the bayestestR package was used to quantify pd (Makowski et al., 2019).

Results

Proximity

Posterior means of the relationship of proximity (TDC) to the probability of winning an ITE were close to zero across all troops, with PT and RST exhibiting a negative relationship with winning, while RBM showed a positive relationship (Table 4.1; PT = −0.23, RBM = 0.23, RST = −0.16). Posterior distributions of TDCs for all troops were weakly constrained, with all relative widths greater than one (Table 4.1; PT = 1.65, RBM = 1.29, RST = 4.19). The odds ratios indicated a small negative effect for PT and RST and a small positive effect for RBM (Table 4.1; PT = 0.79, RBM = 1.26, RST = 0.85). Posterior distributions for PT and RBM crossed zero at the tails but did not enter the 95% credible interval (CI), whereas RST crossed inside the 95% CI (Figure 4.5). The probability of direction indicated 18.5% uncertainty that the direction of RST is negative (Table 4.1; PT = 99.2%, RBM = 99.8%, RST = 81.5%).

Participation

Posterior means of the difference in participation (ΔPart) and outcome were consistently low, with all troops exhibiting very small positive estimates (Table 4.1; PT = 0.03, RBM = 0.01, RST = 0.04). Posterior distributions of participation were generally weakly constrained, with low to very low precision. Based on relative widths (RW ≥ 1), all estimates were arguably of very low precision (Table 4.1; PT = 1.00, RBM = 4.00, RST = 1.00). Odds ratios for all troops were only slightly above one, where OR = 1 indicates no effect, suggesting a very weak positive effect (Table 4.1; PT = 1.03, RBM = 1.01, RST = 1.04). Posterior distributions for PT and RST crossed zero at the tails but did not enter the 95% CI, whereas RBM crossed inside the 95% CI (Figure 4.5). The

probability of direction indicated 10.9% uncertainty in the positive direction of RBM (Table 4.1; PT = 99.8%, RBM = 89.1%, RST = 99.9%).

Initiation

Posterior means of Initiation likelihood (InitB) and outcome were larger and consistently positive (Table 4.1; PT = 0.95, RBM = 1.51, RST = 0.95) compared to TDC and participation. Posterior distributions of initiation for all troops demonstrated low to moderate precision, with relative widths less than one for PT and RST and less than 0.50 for RBM (Table 4.1; PT = 0.68, RBM = 0.46, RST = 0.93). Odds ratios indicated a moderate positive effect for PT and RST and a strong positive effect for RBM (Table 4.1; PT = 2.59, RBM = 4.53, RST = 2.59). Posterior distributions for all troops were entirely above zero (Figure 4.5). The probability of direction was 100% for all distributions (Table 4.1), demonstrating a high degree of certainty in the positive direction of initiation.

Aggression

Posterior means of the severity of Aggression (ΔAgr) and outcome were, like initiation, larger and consistently positive (Table 4.1; PT = 0.84, RBM = 1.83, RST = 1.43). Posterior distributions of aggression demonstrated low to very low precision, with relative widths less than one for RBM and RST and greater than one for PT (Table 4.1; PT = 1.31, RBM = 0.62, RST = 0.93). Odds ratios indicated a moderate positive effect for PT and a strong positive effect for RBM and RST (Table 4.1; PT = 2.32, RBM = 6.23, RST = 4.18). Posterior distributions for RBM and RST were entirely above zero, while the tail for PT just touched it (Figure 4.5). The probability of direction was very high for

all distributions, demonstrating a high degree of certainty in the positive direction of aggression (Table 4.1; PT = 99.9%, RBM = 100%, RST = 100%).

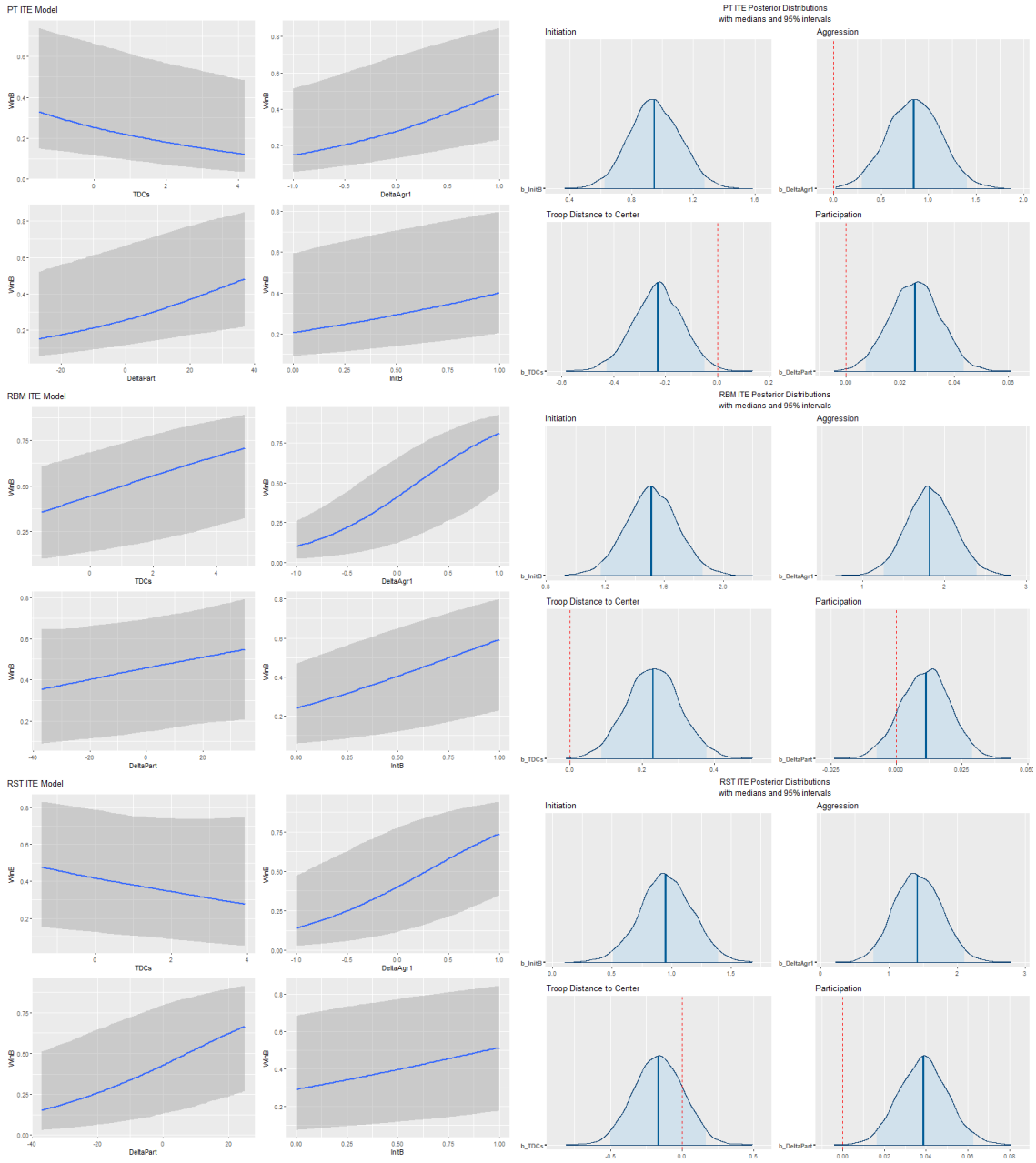

Figure 4.5: Conditional effects (left) give a visual interpretation of effect direction (+/-), intercept, slope, and linearity of the effects. Posterior distributions (right) offer a visual interpretation of the precision and magnitude of the effect, as well as the probability of direction. Sorted by troop: PT (top), RBM (middle), RST (bottom).

Table 4.1: The six metrics reported are: the mean of the posterior distribution (Estimate), the lower and upper bounds of the 95% credible interval (l-95%, u-95%), the relative width (RW), odds ratios (OR), and probability of direction (pd). Predictors include troop distance to the home range centre (TDCs), differences in aggression (ΔAgr), differences in participation (ΔPart), and initiation (InitB). Higher OR values and pd approaching 100% indicate stronger and more certain effects, whereas wide credible intervals and lower pd values suggest uncertainty.

Troop	Coefficient	Estimate	l-95%	u-95%	RW	OR	pd
PT	TDCs	-0.23	-0.43	-0.05	1.65	0.79	99.20%
	DeltaAgr	0.84	0.3	1.4	1.31	2.32	99.93%
	DeltaPart	0.03	0.01	0.04	1.00	1.03	99.82%
	InitB	0.95	0.62	1.27	0.68	2.59	100%
RBM	TDCs	0.23	0.09	0.38	1.26	1.26	99.80%
	DeltaAgr	1.83	1.26	2.4	0.62	6.23	100%
	DeltaPart	0.01	-0.01	0.03	4.00	1.01	89.13%
	InitB	1.51	1.17	1.86	0.46	4.53	100%
RST	TDCs	-0.16	-0.5	0.17	4.19	0.85	81.48%
	DeltaAgr	1.43	0.77	2.1	0.93	4.18	100%
	DeltaPart	0.04	0.02	0.06	1.00	1.04	99.90%
	InitB	0.95	0.51	1.39	0.93	2.59	100%

Random intercepts for Adversary indicated some variability in baseline winning probabilities across opponents. Intercepts for Adversary identity show the strongest effect for PT (0.96), the weakest effect for RBM (0.70), and RST falls in between (0.88). When converted to intraclass correlation coefficients (Equation 2), the adversary effect explains 22% of the variance in PT models, 13% in RBM, and 19% in RST (Table 4.2).

Table 4.2: Random intercept standard deviations and Intraclass Correlation Coefficients (ICC) for Adversary across three troops in yearly ITE models. The random intercept SD reflects variability in baseline outcomes between troops, while ICC quantifies the proportion of total variance in ITE outcomes attributable to differences between troops rather than within-troop variation. Higher ICC values indicate greater between-group influence on outcomes.

Troop	SD (Intercept)	ICC
PT	0.96	0.22
RBM	0.70	0.13
RST	0.88	0.19

Posterior predictive checks showed that simulated data distributions closely matched observed data, supporting model adequacy. Bayes R^2 values ranged from 0.10

(PT) to 0.23 (RBM), indicating modest but meaningful variance explained by the predictors (Table 4.3).

Table 4.3: R^2 estimates for yearly troop-level ITE models indicate how much of the variability in the data is explained by model predictors. Est. Error represents the estimated uncertainty in the R^2 value. Q2.5 and Q97.5 show the 95% credible interval for R^2 across model iterations.

	Estimate	Est.Error	Q2.5	Q97.5
PT	10.10%	1.78%	6.76%	13.76%
RBM	22.85%	2.01%	18.79%	26.64%
RST	12.48%	2.45%	7.76%	17.22%

Discussion

Yearly troop-level models of the Samara Vervet ITEs suggest that distance to the home range centre contributes little to a troop's ability to win an ITE. Across troops, PT and RST showed slightly negative relationships with winning, whereas RBM showed a slightly positive relationship; however, these effects were weak and uncertain. Together these findings suggest that proximity to the home range centre does not play a consistent or meaningful role in determining outcomes and indicates that TDC is not a major determinant of troop success when modelled using yearly home range estimates.

Participation was positively associated with winning an ITE, although the strength of the effect was consistently very weak and imprecise for all troops. The posterior distribution for RBM shows more uncertainty, with 10.9% of the distribution in the negative direction, whereas PT and RST only cross zero at the tails of their distributions, outside the 95% credible interval. This pattern suggests that increased participation may have a modest effect on a troop's likelihood of winning.

While the results for TDC and participation suggest intraspecific variation in behavioural responses among troops, the uncertainty surrounding these effects limits the ability to draw firm conclusions.

Initiation and aggression, in contrast, consistently show moderate to strong positive effects on a troop's chance of winning. The 95% CIs of their posterior distributions do not cross zero, indicating robust and reliable effects. Although the precision of these estimates varies from very low and moderate, this does not imply that the effects themselves are weak. Rather, there is some uncertainty in the exact magnitude of the effect. These results suggest that being the initiator in an ITE and exhibiting higher levels of aggression are key behavioural predictors of success across troops.

Overall, proximity to the home range appears to have little influence on ITE outcomes, while participation may have a modest positive effect. In contrast, initiating an ITE and exhibiting higher levels of aggression have the strongest, most consistent impact. These results highlight the central role of proactive and aggressive behaviours in determining ITE outcomes and, together with the absence of an effect of TDC, suggest that they are not determined by broad spatial location.

Section 2: Dynamic Home Range ITE Models

Statistical Methods

After proximity to home range centre (TDC) failed to predict ITE outcomes in annual models, it was hypothesised that static yearly home ranges might obscure spatiotemporal dynamics relevant to troop space use and conflict, and that a dynamic approach would better capture shifts in home range centres across time (Figure 4.6). For example, at a 14-day resolution, PT and RBM align along the river and road, while RST shows less directionality, centreing on a forested area known for its dense vegetation, but also partially aligned to the river as well.

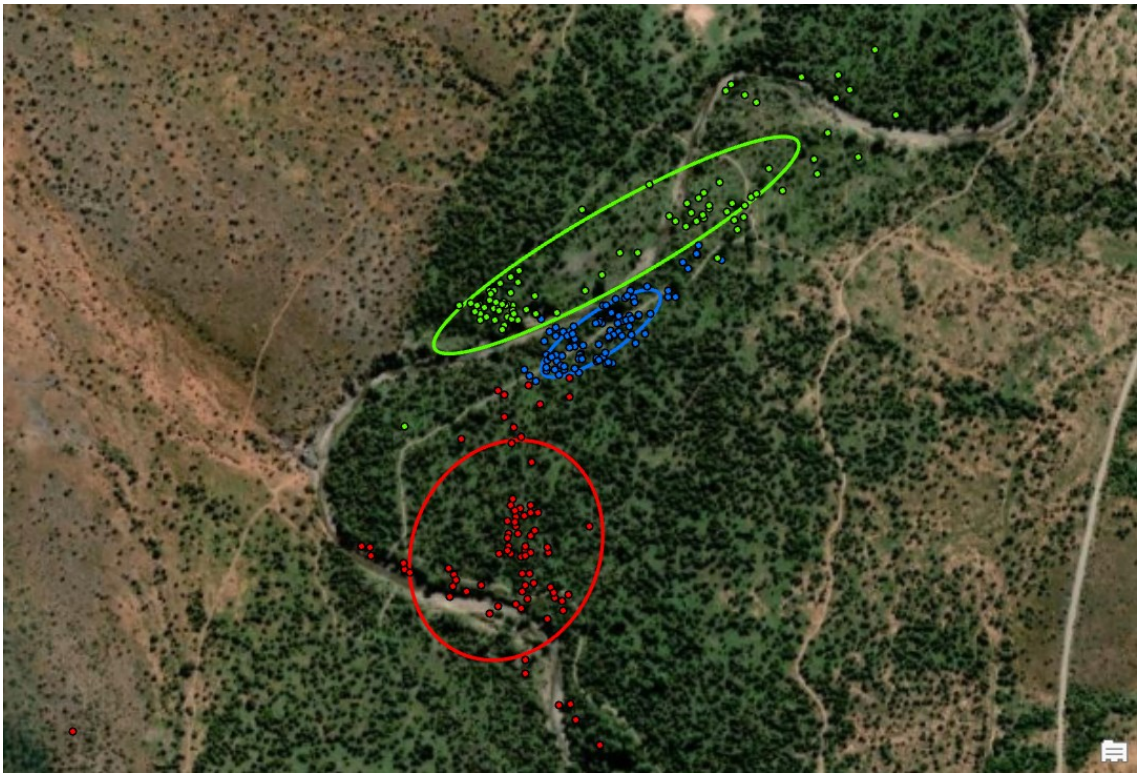

Figure 4.6: Centres of home ranges by troop (PT: blue, RBM: Green, RST: red), extracted from 14-day home ranges across 1,462 days. Standard Deviational Ellipses highlight directional trends over time.

As outlined in Chapter 3, static home ranges fail to represent temporal variation, including shifts in home range centres that affect the calculation of TDC. To address this, Dynamic Home Ranges (DHR) were estimated using temporal windows from 14 to 168 days at increments of seven days (or multiples thereof), specifically at 14, 21, 28, 35, 42, 84, and 168 days. Because a minimum of 30 to 50 points is recommended for stable contours (D. Seaman et al., 1999) and to reduce errors caused by both the KDE `ks::kde()` and bandwidth functions `ks::Hpi()`, a one-week model generally lacked enough points to estimate a home range reliably. This approach captured both short- and medium-term troop space use and produced home ranges reflecting current troop utilization at a local temporal scale rather than a global scale (years). Home range centres were extracted at all temporal scales (Appendix B), and TDC recalculated for each dataset.

Twenty-one hierarchical logistic regression models examined predictors of conflict outcomes (winning an ITE) in the three troops. Each model predicted the probability of winning a fight (WinB) as a function of troop proximity to the home range centre (TDCs), differences in aggression (DeltaAgr), participation (DeltaPart) during the fight, and whether the troop initiated the engagement (InitB). The same model structure and Bayesian framework were applied across all temporal windows, using datasets generated by the DHR method. For each run, the Euclidean distance between the newly derived DHR centres and ITEs was recalculated. All other variables remained unchanged, and troops were analyzed independently, with ITEs considered from the perspective of the focal troop.

Results

Proximity

Posterior means for proximity (TDC) ranged from -0.21 to 0.21 (PT: -0.21 to -0.12, RBM: 0.03 to 0.21, and RST: -0.10 to 0.17). Probability of direction for posterior distributions were higher for PT (90.20 to 98.52%), but highly variable for RBM and RST (RBM: 63.73 to 99.90%, and RST: 69.38 to 86.67%). Over two-thirds (17 of 21) of TDC distributions crossed zero inside the 95% CIs, but overall probability of direction (pd) showed that PT tended to be negative, while RBM and RST tended toward positive estimates (Table 4.4 & Appendix A).

Participation

Participation posterior means ranged from 0.01 to 0.04 (PT: 0.03, RBM: 0.01, and RST: 0.04). Posterior distributions for participation were consistently positive for PT and RST with pd values close to 100% (PT: 99.70 to 99.88% and RST: 99.92 to 100%),

but RBM consistently crossed zero, with pd values between 86.78 and 89.30% (Table 4.4 & Appendix A).

Initiation

Posterior means for initiation ranged from 0.94 to 1.56 (PT: 0.97 to 1.03, RBM: 1.50 to 1.56, and RST: 0.94 to 0.99). All posterior distributions for initiation were consistently positive with a pd of 100%, across all troops and temporal windows showing a strong propensity towards positive estimates (Table 4.4 & Appendix A).

Aggression

Posterior means for aggression ranged from 0.82 to 1.93 (PT: 0.82 to 0.86, RBM: 1.80 to 1.93, and RST: 1.37 to 1.41). All posterior distributions for aggression were consistently positive with pd estimates near 100% (99.98-100), across all troops and temporal windows (Table 4.4 & Appendix A).

Table 4.4: Posterior estimates and pd for four predictors of ITE outcomes across three troops (PT, RBM, RST). Rows represent predictors: initiation (InitB), differences in aggression (ΔAgr), differences in participation (ΔPart), and troop distance to the home range centre (TDC). For each troop, the range of posterior means summarizes estimates across seven Bayesian models run at different temporal windows, while pd indicates the probability that the effect is positive or negative relative to zero.

Predictor	Troop	Posterior Mean (range)	Probability of Direction (pd)
InitB	PT	0.97 → 1.03	100%
	RBM	1.50 → 1.56	100%
	RST	0.94 → 0.99	100%
ΔAgr	PT	0.82 → 0.86	99.88 → 100%
	RBM	1.80 → 1.93	100%
	RST	1.37 → 1.41	99.98 → 100%
ΔPart	PT	0.03	99.70 → 99.88%
	RBM	0.01	86.78 → 89.30%
	RST	0.04	99.92 → 100%
TDC	PT	-0.21 → -0.12	90.20 → 98.52%
	RBM	0.03 → 0.21	63.73 → 99.90%
	RST	-0.10 → 0.17	69.38 → 86.67%

Intercepts for Adversary identity show the strongest effect for PT (0.99-1.1), the weakest effect for RBM (0.71-0.77), and RST falls in between (0.82-0.91). When

converted to intraclass correlation coefficients (Equation 2), the adversary effect explains between 23-27% of the variance in PT models, 13 -15% in RBM models, and 17-20% in RST models (Table 4.5).

Table 4.5: Random intercept standard deviations and Intraclass Correlation Coefficients (ICC) for Adversary across three troops (PT, RBM, RST) for DHR ITE models. The random intercept SD reflects variability in baseline outcomes between troops, while ICC quantifies the proportion of total variance in ITE outcomes attributable to differences between troops rather than within-troop variation. Higher ICC values indicate greater between-group influence on outcomes.

Troop	SD (Intercept)	ICC
PT	0.99 - 1.10	0.23 - 0.27
RBM	0.71 - 0.77	0.13 - 0.15
RST	0.82 - 0.91	0.17 - 0.20

Model fit was low to moderate (Bayesian $R^2 \approx 0.09$-0.22), with PT at 9.9 to 10.1% of variance explained, RBM at 21.6 to 22.7%, and RST at 12.3 to 12.7% (Table 4.6). Posterior predictive checks showed that simulated data distributions closely matched observed data, supporting model adequacy (Appendix D). The baseline negative probability of the intercept (-1.20 to -0.89) suggests that, if all predictors are zero, the likelihood of winning is less than 50% (Appendix A).

Table 4.6: R^2 estimates for DHR troop-level ITE models indicate how much of the variability in the data is explained by model predictors. Est. Error, Q2.5 and Q97.5 values for individual models can be found in Appendix E.

Bayesian R^2	
PT	0.099 → 0.101
RBM	0.216 → 0.227
RST	0.123 → 0.127

The relative width (RW) of distributions (Equation 1) was calculated to facilitate interpretation of distribution precision. TDC has RW > 1 across all models, reflecting very low precision. Except for one RST model with RW > 1, participation for PT and RST has relative widths between 0.5 and 1, indicating low precision, while all RBM models show very low precision. Aggression exhibits very low precision for PT, and, aside from one RST model with RW > 1, the remaining RBM and RST models show low

precision. Initiation for RBM has relative widths between 0.2 and 0.5, indicating moderate precision, whereas PT and RST models are all low precision (Appendix C).

The magnitude of effects was calculated as an Odds Ratio (Equation 3). Odds Ratios for TDC in PT models were close to one but less than 0.88 indicating a small negative effect, RBM ranged from 1.03 to 1.23 indicating all but the highest OR were very weak positive effects, and the 1.23 is a small positive effect, most of RST's odds ratios indicated very weak positive effects (1.08-1.18), with the exception of one model with a very weak negative effect (0.9). Participation was a very weak positive effect across all models (1.01-1.04). Aggression was a moderate positive effect for PT (2.27-2.36), and a strong positive effect for RBM and RST (3.93-6.88). Initiation was a moderate positive effect for most PT and all RST models (2.56-2.69) and a strong positive effect for all RBM models (4.48-4.75), and one PT model (2.8) (Appendix C).

Discussion

These analyses support the findings of the yearly intertroop encounter (ITE) models: immediate behavioural strategies—such as initiating a fight and increased aggression during an encounter—are the primary drivers of success in vervet troop conflicts.

Participation by additional troop members showed only a very weak positive effect with low precision, offering a slight advantage at best. RBM posterior distributions indicated greater uncertainty, with 10.7-13.2% of posterior samples crossing zero, suggesting the opposite direction of effect. Conversely, PT and RST distributions crossed zero only at the tails.

Proximity to the home range centre appears to exert little consistent influence on outcomes, with low precision and variable effects across troops. Some models or temporal windows suggest a small effect for individual troops; however, the direction and strength of this effect are inconsistent. Uncertainty about direction varies widely across troops and temporal windows (PT = 1.5-9.8%, RBM = 0.1-36.3%, RST = 13.3-30.6%). The dynamic home range approach did not therefore meaningfully improve model fit over yearly home ranges, reinforcing that spatial proximity relative to the home range is secondary to behavioural dynamics.

Bayesian R^2 values mirrored those from the yearly home range ITE models, indicating that predictors—particularly behavioural factors—explain a modest but meaningful proportion of the variance in outcomes.

Overall, these findings underscore the importance of behavioural dynamics over spatial factors: being the initiator and behaving aggressively confer the strongest and most reliable advantage in ITEs. The observed variability in participation and TDC highlights potential intraspecific differences in behavioural strategies across troops, although these effects are generally less robust.

These findings suggest that spatial proximity to the home range centre had limited and inconsistent influence on ITE outcomes. This raises an important methodological consideration that home ranges are human-defined constructs that provide useful summaries of space use but are unlikely to reflect how animals perceive their environment. Our vervets are unlikely to experience a “boundary” or “centre” as humans conceptualize them; rather, their spatial experience may be shaped by gradients of familiarity or resource distribution (Powell, 2000), which calls into question the

biological significance of defining range use in terms of a 'territory' to be defended in relation to purely spatial parameters (see for example, Mitani & Rodman, 1979), a point also made glancingly by Lawes and Henzi (1995) in the context of the expectation of obligate defence of spatial boundaries (Lawes & Henzi, 1995).

Given this epistemological limitation, continuing to model success based on distance to a conceptual centre risks misrepresenting the ecological reality. The next step is to move beyond abstract spatial constructs and focus on predictive modelling grounded in the actual spatial distribution of behaviours such as winning, initiating, and aggression. This approach avoids assuming perceptual constructs that may not exist for the species while aligning the analysis with biologically meaningful patterns.

Section 3. Structure Models

Rationale

Given the lack of robust results supporting the hypothesis that proximity to the home range centre influences ITE outcomes and recognizing that this concept is based on a human-defined construct, I decided to shift the focus from explaining why certain behaviours occur to examining where they occur, with the aim of determining whether spatial patterns might shed light on the underlying causes. I wanted to test whether spatiotemporal structure exists and explore where such a structure originates if it is present. To investigate this issue, I needed to map behaviours across space and time. Are the spatial and temporal dimensions of a behaviour stochastic within a spatiotemporal framework, or do they exhibit structure?

In this context, *structure* refers to identifying locations across both space and time where predictable occurrences of specific behaviours can be mapped out. Structure also

implies that a point where a behaviour occurs in space and time should have other similar points adjacent to it, and if these points were connected, they would form a three-dimensional polygon. This approach assumes that Tobler's First Law of Geography applies: "everything is related to everything else, but near things are more related than distant things" (Tobler, 2004; Tobler, 1970). I extend this principle beyond the spatial plane to include the temporal dimension, expecting that behaviours occurring in space should be near similar behaviours in both space and time. In other words, I would hypothesize that if a troop wins in one location, the probability of winning in adjacent locations should be relatively high. Likewise, if a troop is likely to win there today, it should have a similar chance of winning there tomorrow.

To better understand where the sources of spatiotemporal structure arise during Intertroop Encounters (ITEs), we must confirm that such structure exists. At first glance, this seems straightforward: plotting a point cloud of all ITEs and coloring them by dyads reveals clusters that appear to emerge on the 2D map (Figure 4.1). This complexity increases when a third axis, time, is introduced. Clusters that appeared cohesive in two dimensions become dispersed, and the task shifts to identifying spatiotemporal clusters that may or may not exist within these 2D patterns (Figure 4.7).

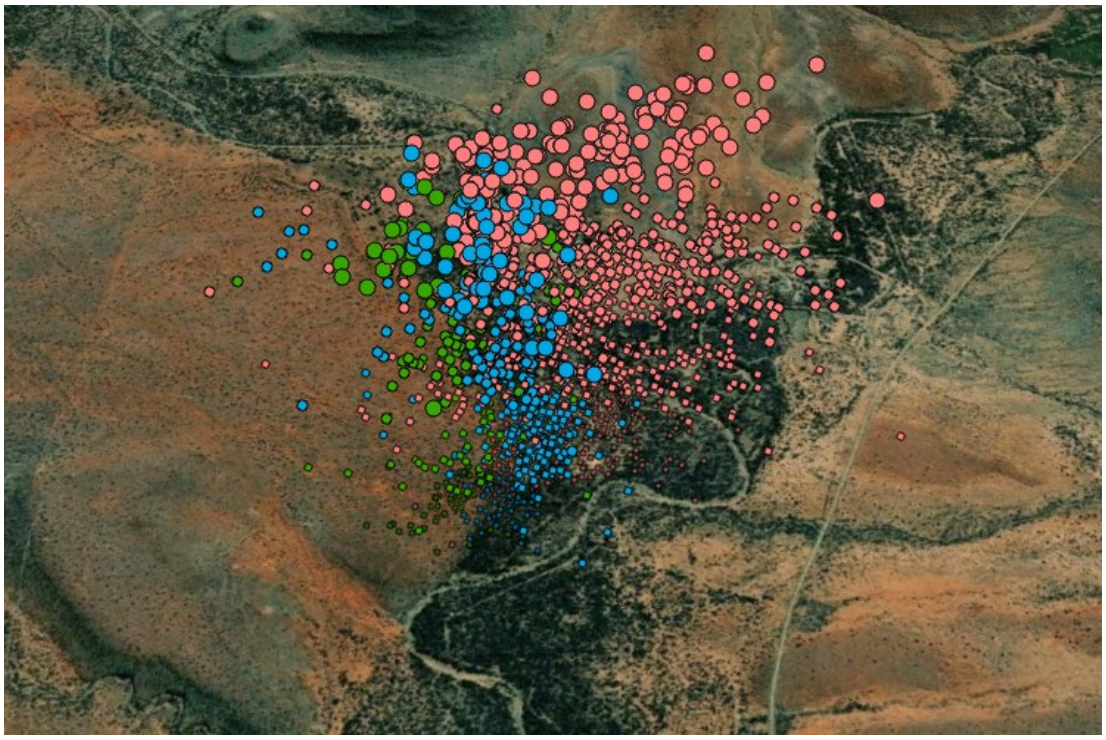

Figure 4.7: ITE Points sorted by dyad and time. Point size is classified chronologically into five categories using the Natural Breaks (Jenks) method, which identifies optimal groupings by minimizing within-group variation and maximizing differences between groups. Larger points represent later times (higher on the z-axis). Dyad colors correspond to the following non-directional dyads: RBM—PT (red), RST—PT (blue), and RBM—RST (green). The low oblique view creates the illusion that points extend north, but all remain within the river bend (Figure 4.1).

Statistical Methods

Models were created for three group-level behaviours observed during an ITE: winning, initiating, and aggression. The probability of those behavioural outcomes occurring during an intertroop encounter was then predicted across space and time. Probabilities were estimated using the same Bayesian framework as Sections 1 and 2; however, the models in this section are no longer generalized linear mixed models (GLMMs). Instead, they employ a more flexible Bayesian generalized additive model (GAM) structure with a tensor-product spline to capture non-linear spatial and temporal effects. GAMs allow the model to account for complex, non-linear interactions between spatial coordinates and temporal variables, which would be difficult to capture using a traditional GLMM. Tensor-product splines enable smooths across multiple dimensions,

in this case, space and time. This approach provides the flexibility to uncover localized patterns of behaviour and spatiotemporal trends that may indicate strategic clustering of behaviours or environmental influences on troop interactions, offering deeper insight into the mechanisms shaping intertroop dynamics.

The response variables for winning (WinNum) and initiating (InitNum) were binary, where 1 indicated winning or initiating and 0 indicated losing or not initiating. In a Bayesian model, this requires applying a Bernoulli likelihood with a logit link function.

Aggression (Agr) was calculated as the ratio of the sum of physical and active participants to the total number of participants, producing values between 0 and 1. Many zeros occurred due to non-aggressive ITEs, resulting in a zero-one inflated beta distribution.

Predictor variables included scaled and centred spatial coordinates (Point_Xs, Point_Ys) in WGS 1984 / UTM Zone 35S and scaled and centred days since the start of the study (DSSs). A tensor product of thin plate regression splines t2() was used to model a smooth 2D surface over space and a 1D smooth effect across time, allowing interactions between spatial location and study day.

Tensor product smooths were specified with marginal dimensions of two spatial and one temporal component (d = c(2,1)). Basis dimensions were initially set to k = c(25,10) for spatial and temporal splines, respectively, but in some models reduced to k = c(15,8) to improve convergence and minimize divergence, slightly reducing spline flexibility.

Models were run using brms (via Stan) with six chains of 2,000 iterations each. Sampling parameters were adjusted (adapt_delta = 0.95, max_treedepth = 12) to reduce the

probability of errors occurring. Posterior estimates were used to generate points indicating where a behavioural outcome (winning, initiating, or aggression) during an ITE would most likely occur, while accounting for non-linear spatiotemporal patterns.

To map out the structure of a behaviour, we must first generate a grid that predictions will be bound to. Because values for x and y (Point_X, Point_Y) are in UTM and time (DSS) represents the number of days since the start of the study, these were scaled and centre (Point_X_S, Point_Y_S, DSS_S) to avoid issues caused by differences in magnitude between the two set of numbers. The grid was created using the minimum and maximum bounds of Point_X_S and Point_Y_S (Figure 4.8, Lines 268—269), and DSS_S (Figure 4.8, Lines 266). To infill the grid with points, the expand.grid function (Figure 8, Lines 271—272) was used, which creates points at a set interval (pred.scale). This grid was then replicated across multiple time slices (Figure 8, Lines 274—277), again at a set interval (time.seq in Figure 4.8, Line 267), to create a 3D matrix resembling a space-time cube, where the z-axis (vertical) represents time rather than elevation (Figure 4.9). Predictions were then made with the fitted function using the grid for location data: fitted(<model>, newdata = <grid>, se.fit = TRUE). Setting se.fit = TRUE ensured that standard errors were reported in the output. Fitted predictions were bound back to the grid using cbind, then coordinates and time were unscaled and saved as a .csv to a to allow mapping of points in ArcGIS Pro.

```
265  # Create range variables for x,y,z axis
266  t.rng <- as.numeric(c(min(RST_Win_ST$data$DSS_S), max(RST_Win_ST$data$DSS_S)))
267  time.seq <- seq(t.rng[1],t.rng[2],by=time.scale)
268  x.range <- as.numeric(c(min(RST_Win_ST$data$Point_X_S), max(RST_Win_ST$data$Point_X_S)))
269  y.range <- as.numeric(c(min(RST_Win_ST$data$Point_Y_S), max(RST_Win_ST$data$Point_Y_S)))
270  # Create Grid surrounding the observed points and Expand
271  grd <- expand.grid(Point_X_S = seq(from = x.range[1], to = x.range[2], by = pred.scale),
272                     Point_Y_S = seq(from = y.range[1], to = y.range[2], by = pred.scale))
273  # Replicate grid at each time slice
274  for(i in 1:length(time.seq)){
275    grd$DSS_S <- time.seq[i]
276    grd.all <- rbind(grd.all, grd)
277  }
```

Figure 4.8: Cone block used to create a three-dimensional grid of points for predictions to be bound to.

The grids were added to ArcGIS Pro using the XY Table To Point tool, which converts tabular data with x, y coordinates into a point cloud. Once converted, the dataset initially appears as a flat rectangle because all points at the same location, but different times are collocated. To create a space—time cube, the dataset must be extruded in **Properties > Elevation** where the extrusion field is set to time (DSS). Features were also extruded **Relative to Ground** to prevent the data from being placed below the topography at 0m above sea level (Figure 4.9). Model adequacy was evaluated using LOOIC, Bayesian R^2, and posterior predictive checks. Z-scores were also calculated on LOOIC (Equation 5) results to give a measure of how meaningful the difference between time-only and space time models was (Table 4.7).

$$Z = \frac{Difference\ in\ ELPD}{Standard\ Error\ of\ Difference} \quad (Eq. 5)$$

Where: Z = the z-score of LOOIC differences, and ELPD = Expected Log Predictive Density

Table 4.7: Interpretation of z-scores for LOOIC differences. Z-scores measure how large the difference in expected log predictive density (ELPD) is relative to its uncertainty. This helps assess whether the observed difference is meaningful relative to uncertainty.

Z ≳ 2	The difference is clearly meaningful. The worse model has substantially lower predictive accuracy.
Z ≈ 1–2	The difference is noticeable but not overwhelming. There is moderate support for the better model, but uncertainty still plays a role.
Z < 1	Differences are small relative to uncertainty. Models have similar predictive performance.

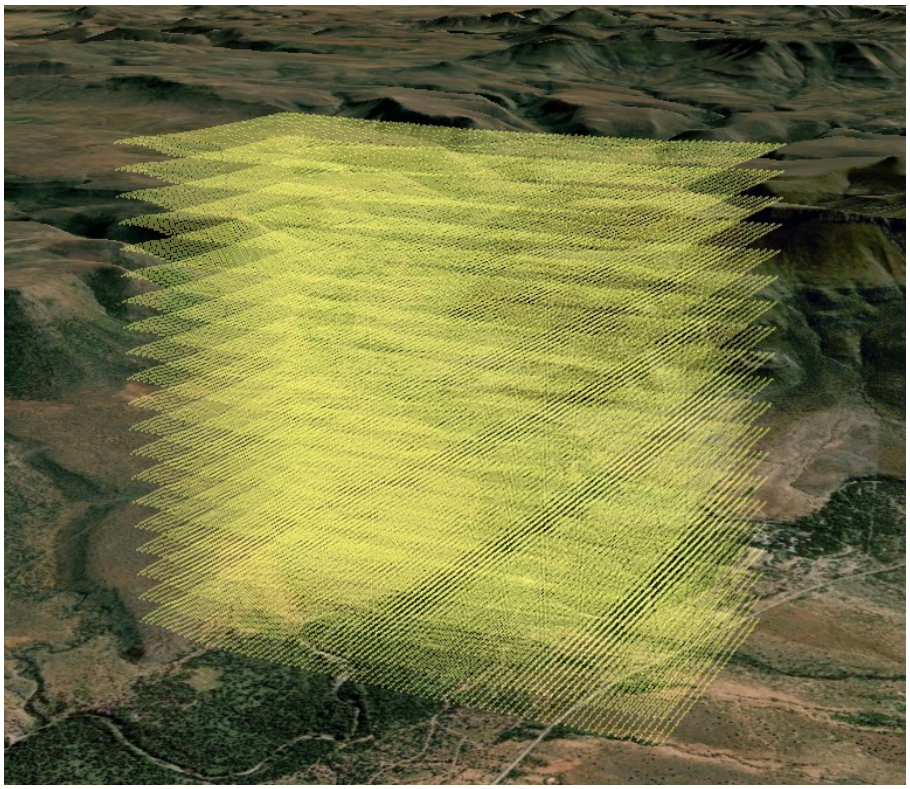

Figure 4.9: Three-dimensional grid (yellow) shows the spatiotemporal extent of predictions. This initial grid contains all predictions including false-positives and requires filtering to show meaningful results.

Once the prediction grid was imported, predictions had to be filtered to remove false positive or low-probability values. Predictions near the edge often contain increased error and could be filtered by Q2.5% > 0.1; however, methods grounded in ecological practice were chosen to determine the threshold for points to display. In the Bernoulli datasets (winning and initiating), false positives were removed using Receiver Operating Characteristic (ROC) analysis and Area Under Curve (AUC), while the aggression data set was filtered using change-point detection.

ROC analysis, combined with AUC, is widely used in ecological modelling as a threshold-dependent discrimination measure (Jiménez-Valverde, 2014; Liu et al., 2013; Pontius Jr & Parmentier, 2014). When paired with Youden's J Statistic (Liu et al., 2013; Piri Sahragard et al., 2018), ROC provides a data-driven threshold for visualizing 3D

point clouds in space-time. This approach was implemented in R using the roc() and auc() functions from the **pROC** package.

Because ROC is not applicable to continuous data such as aggression, change-point detection was employed to identify the natural breaks in the data, focusing on shifts in the ecological process (aggression) (Andersen et al., 2009; Toms & Lesperance, 2003). This method uses a piecewise or "broken-stick" regression to model segments of the data with different slopes (McZgee & Carleton, 1970; Quandt, 1958). Change-point detection was implemented in R using the segmented() function from the **segmented** package.

Winning

The first structure model created identified the likelihood of winning an ITE. Winning was mapped by troop to provide a baseline visualization of where this outcome occurred (Figure 4.10).

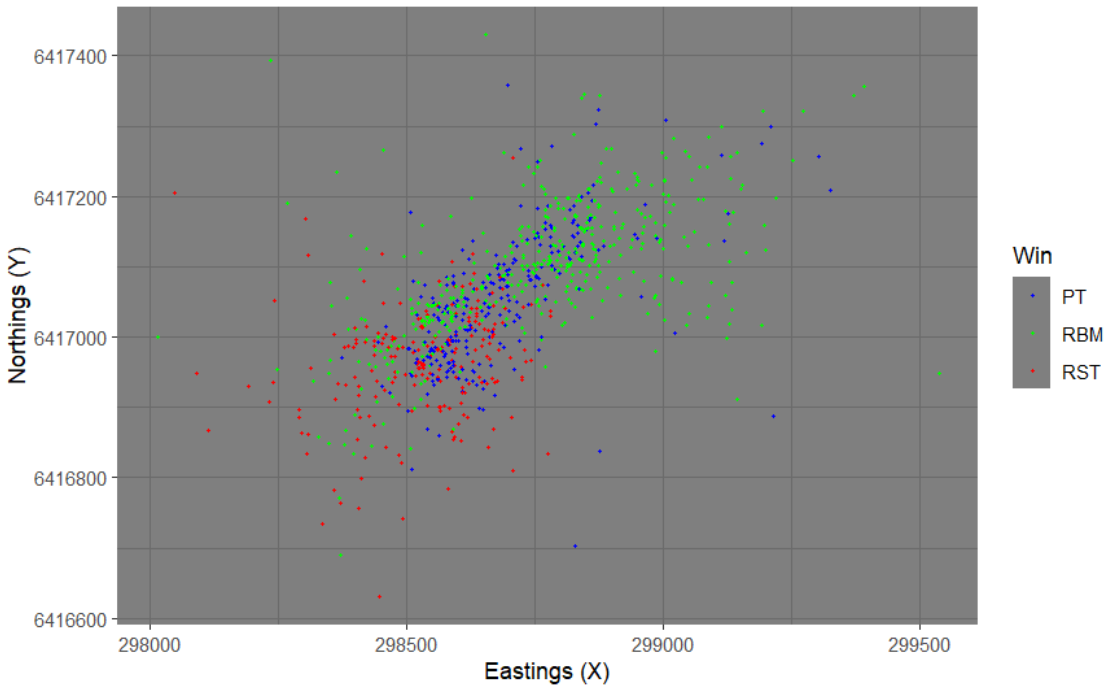

Figure 4.10: Map of ITE wins for each Troop.

Winning was first modelled using only time (Equation 6). Adding space to temporal models was then done using a Bayesian Generalized Additive Model (GAM) with a tensor product smooth (t2) for spatiotemporal effects (Equation 7).

$$WinNum \sim 1 + s(DSS_s, by = Troop) + Troop \quad (Eq.6)$$

$$WinNum \sim 1 + t2(X_s, Y_s, DSS_s, by = Troop) + Troop \quad (Eq.7)$$

Initiation

Initiation, like wins, was plotted out by troop to provide a baseline visualization of where initiation occurred by troop (Figure 4.11).

Figure 4.11: Map of ITE wins by Troop.

Initiation data like wins was first modelled using only time (Equation 8). Based on the structure of the initiation data (1 = initiated, 0 = did not initiate) the spatiotemporal model is the same structurally as the win model (Equation 9).

$$InitNum \sim 1 + s(DSS_s, \text{by} = \text{Troop}) + \text{Troop} \quad (Eq.8)$$

$$InitNum \sim 1 + t2(X_s, Y_s, DSS_s, by = Troop) + Troop \quad (Eq.9)$$

Aggression

The final structure model created was for aggression. Unlike wins and initiation, which can be attributed to only one of the two contesting groups, aggression is neither a binary variable nor limited to one or other of the groups. As such, maps visualizing where aggression occurs by troop are not informative, since both troops can display aggression at the same time. Histograms of aggression data show that, while values are continuous from zero to one, zeros are much more prevalent than other values (Figure 4.12).

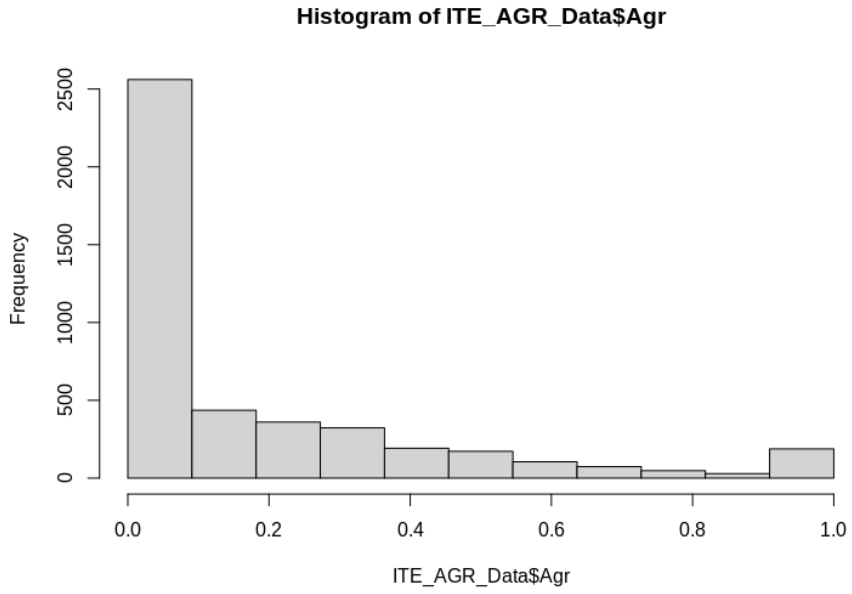

Figure 4.12: Histogram of Aggression Data.

Consequently, aggression was assessed using a Bayesian zero-one inflated beta regression model in the brms package in R to examine the effect that scaled and centreed time (DSSs) has on aggression. A smooth was applied to DSSs across all distributional parameters (Equation 10). Aggression in space-time was modelled with a tensor product smooth over all distributional parameters, and troop was set as a random effect (Equation 11).

$$Agr \sim 1 + s(DSS_s, by = Troop), zoi \sim 1 + s(DSS_s, by = Troop), coi \sim 1 + s(DSS_s, by = Troop), \varphi \sim 1 + s(DSSs, by = Troop) + Troop \quad (Eq. 10)$$

$$Agr \sim 1 + t^2(X_s, Y_s, DSS_s, by = Troop) + Troop, zoi \sim 1 + t^2(X_s, Y_s, DSS_s) + Troop, coi \sim 1 + t^2(X_s, Y_s, DSS_s) + Troop, \varphi \sim 1 + t^2(X_s, Y_s, DSS_s) + Troop \quad (Eq. 11)$$

Where: Agr = Aggression in an ITE, DSSs = Days Since Start [of study], zoi = zero-one inflation component, coi = conditional one inflation component, and φ (phi) = precision parameter.

Results

Full model summaries for both time and space-time models can be found in Appendix F.

Winning

The temporal model of winning had an R^2 value of 8.8%. Estimate plots show variability in winning across time, but based on R^2 values, account for little variance in winning (Figure 4.13).

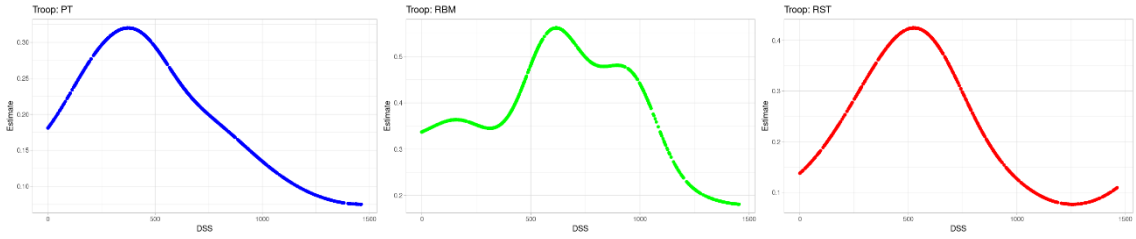

Figure 4.13: Temporal plots of winning. PT — Left, RBM — Middle, RST — Right.

Bayesian R^2 values for the spatiotemporal model of ITE wins was 23.3% (Table 4.8). LOOIC ranked the spacetime model as the better performer, with the time-only model showing a negative Expected Log Predictive Density under Leave-One-Out cross-validation (elpd_diff). An LOOIC z-score of 20.37 for the time-only structure model indicates a clearly meaningful difference between the time-only and spacetime

models (Table 4.9). Posterior predictive checks demonstrated that simulated data distributions closely matched observed data, supporting model adequacy.

Table 4.8: Bayesian R2 Estimations (Estimate) for Initiation structure models. WTM – Winning Time Model, WSTM – Winning Space Time Model. Estimated Error (Est.Error) and low/high Credible Intervals (Q2.5, Q97.5) are included.

Bayesian R^2				
Troop	Estimate	Est.Error	Q2.5	Q97.5
WTM	0.0881	0.0097	0.0694	0.1077
WSTM	0.2334	0.0129	0.2075	0.2583

Table 4.9: Leave-One-Out Information Criterion (LOOIC) indicates that the spacetime model ranked higher than the time-only model. Expected Log Predictive Density under Leave-One-Out cross-validation (elpd_diff), standard error of the difference in elpd between the two models (se_diff), and the z-scores are included.

Leave-One-Out Information Criterion			
Model	elpd_diff	se_diff	z-score
WSTM	0.0	0.0	-
WTM	-317.7	15.6	20.37

Point clouds of winning an ITE were visualized as 3D point clouds in space-time (Figure 4.14) and represent true positive predictions of winning across space and time, with false positives filtered out using a Youden J-derived threshold (PT—0.2294, RBM—0.3478, RST—0.2202).

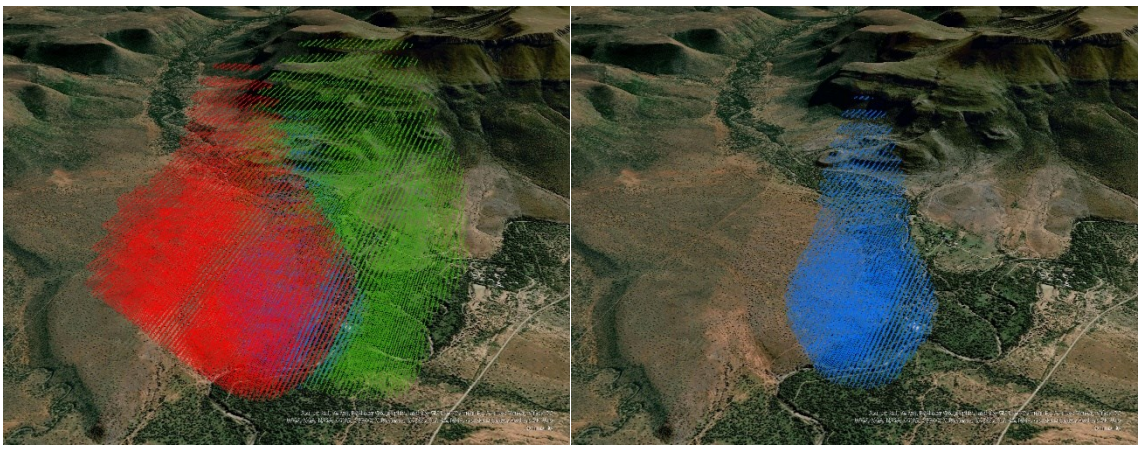

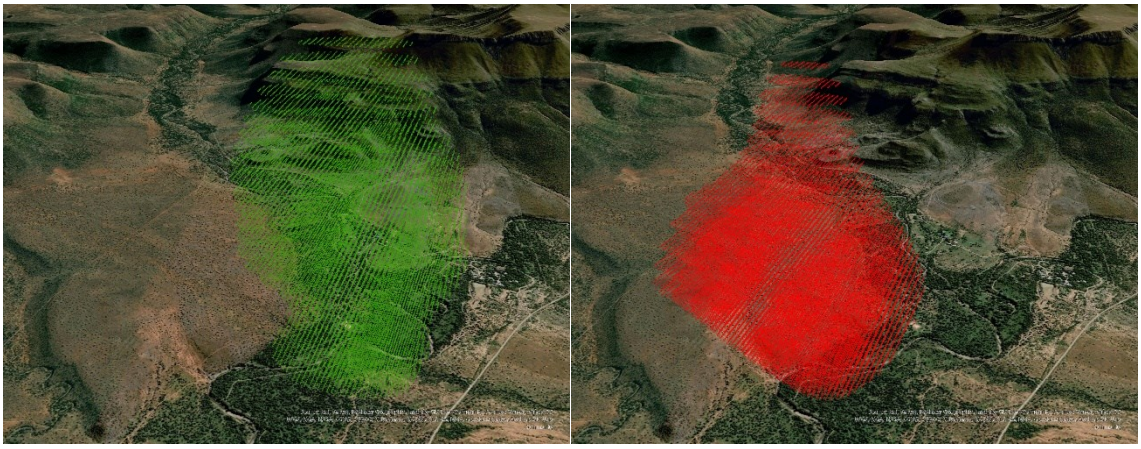

Figure 4.14: Visualization of 3D point clouds predicting where troops are likely to win an ITE across space and time. All troops (top left), PT (top right), RBM (bottom left), RST (bottom right).

Initiation

R^2 for the Initiation time-only models ranged was 10.2% (Table 4.10). Estimate plots of initiation again showed variability across time, but as with winning, R^2 values indicated that little variance in initiation was being explained by time alone (Figure 4.15).

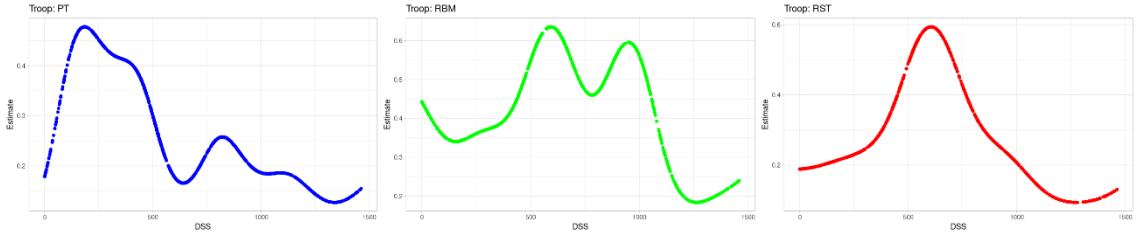

Figure 4.15: Temporal plots of initiating. PT — Left, RBM — Middle, RST — Right.

The spatiotemporal model of Initiation had a Bayesian R^2 value of 22% (Table 4.10). LOOIC ranked the initiation spacetime model as the better performer, with the time-only model showing a negative elpd_diff. An LOOIC z-score of 18.62 for the time-only structure model indicates a clearly meaningful difference between the time-only and spacetime models (Table 4.11). Posterior predictive check plots show that models are well fitted to the Bernoulli family.

Table 4.10: Bayesian R2 Estimations (Estimate) for Initiation structure models. ITM – Initiation Time Model, ISTM – Initiation Space Time Model. Estimated Error (Est.Error) and low/high Credible Intervals (Q2.5, Q97.5) are included.

Bayesian R^2				
Troop	Estimate	Est.Error	Q2.5	Q97.5
ITM	0.1024	0.0087	0.0853	0.1193
ISTM	0.2197	0.0098	0.2005	0.2391

Table 4.11: Leave-One-Out Information Criterion (LOOIC) indicates that the spacetime model ranked higher than the time-only model. Expected Log Predictive Density under Leave-One-Out cross-validation (elpd_diff), standard error of the difference in elpd between the two models (se_diff), and the z-scores are included.

Leave-One-Out Information Criterion			
Model	elpd_diff	se_diff	z-score
ISTM	0.0	0.0	-
ITM	-370.6	19.9	18.62

Point clouds of initiating an ITE were visualized as 3D point clouds in space-time (Figure 4.16) and represent true positive predictions of initiating across space and time, with false positives filtered out using a Youden J-derived threshold (PT—0.2954, RBM—0.4768, RST—0.3351).

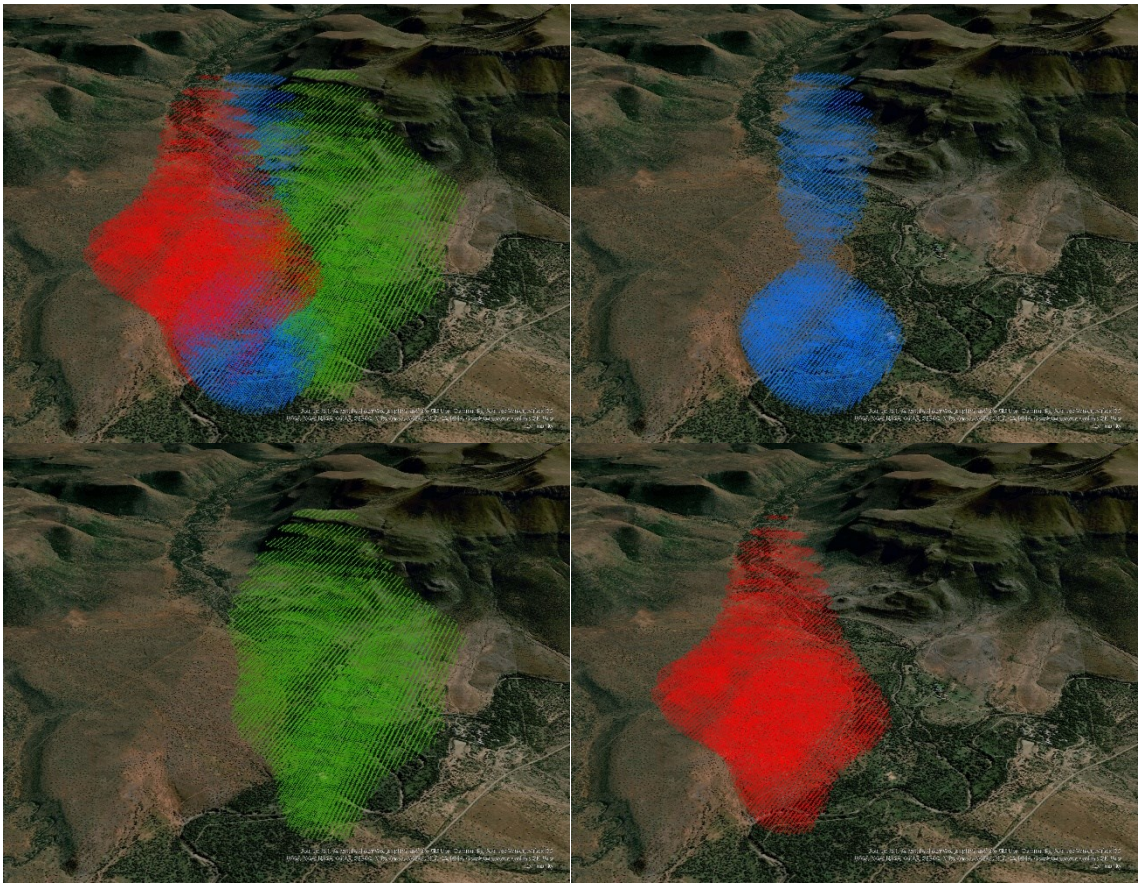

Figure 4.16: Visualization of 3D point clouds predicting where troops are likely to initiate an ITE across space and time. All troops (top left), PT (top right), RBM (bottom left), RST (bottom right).

Aggression

The temporal model of ITE aggression had an R^2 value of 2.2% (Table 4.12). Estimate plots indicate variability in aggression over time. However, consistent with the temporal models for winning and initiation, the R^2 value suggest that time alone explains little variance in aggression (Figure 4.17).

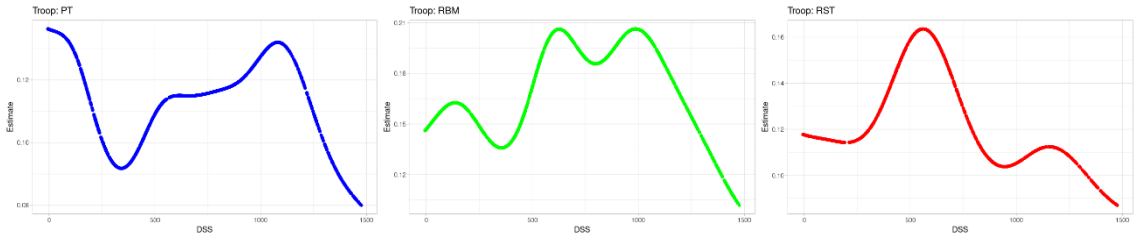

Figure 4.17: Temporal plots of aggression (PT—blue, RBM—green, RST—red.

This spatiotemporal model of ITE wins had R^2 value of 12.3% (Table 4.12). Posterior predictive check plots show that models are well fitted to the Bernoulli family. LOOIC ranked the initiation spacetime model as the better performer across all troop models, with the time-only models showing a negative elpd_diff. An LOOIC z-score of 3.41 for the time-only structure model indicates a clearly meaningful difference between the time-only and spacetime models (Table 4.13).

Table 4.12: Bayesian R2 Estimations (Estimate) for Initiation structure models. ITM – Initiation Time Model, ISTM – Initiation Space Time Model. Estimated Error (Est.Error) and low/high Credible Intervals (Q2.5, Q97.5) are included.

Bayesian R^2				
Model	Estimate	Est.Error	Q2.5	Q97.5
ATM	0.0221	0.0036	0.0159	0.0295
ASTM	0.1234	0.0228	0.0886	0.1793

Table 4.13: Leave-One-Out Information Criterion (LOOIC) indicates that the spacetime model ranked higher than the time-only model. Expected Log Predictive Density under Leave-One-Out cross-validation (elpd_diff), standard error of the difference in elpd between the two models (se_diff), and the z-scores are included.

Leave-One-Out Information Criterion			
Model	elpd_diff	se_diff	z-score
ASTM	0.0	0.0	-
ATM	-23995.8	7028.8	3.41

Point clouds of aggression in an ITE were visualized as 3D point clouds in space-time (Figure 4.18) with graduated colours showing levels of aggression (darker = higher aggression, lighter = lower aggression). Edge points and low probability estimates were filtered out using change-point detection to identify the natural breaks in each troops predicted point cloud (PT—0.135581, RBM—0.223733, RST—0.182840).

Figure 4.18: Visualization of 3D point clouds predicting where troops are likely to have be more aggressive during an ITE across space and time. All troops (top left), PT (top right), RBM (bottom left), RST (bottom right).

Discussion

Structure models show that where a troop wins and initiates an ITE, along with its aggression level during an ITE, there is a spatial component and it exhibits structure in space and time. R^2 values for spatiotemporal structure models range from approximately 12 to 30%, which is consistent with expectations for probabilistic models of binary outcomes and reflects the inherent complexity of ecological systems. These systems exhibit cross-scale interactions, emergent behaviours, and agent-driven variability, making complete predictability unattainable (Allen et al., 2014; Anand et al., 2010; Lin & Wiegand, 2023; Low-Décarie et al., 2014). Results from LOOIC, Bayesian R^2, and posterior predictive checks together indicate strong predictive performance and confirm that spacetime models provide a more reliable representation of behavioural patterns across space and time. ITE models using measures of proximity to Home Ranges or Dynamic Home Ranges explained very little variability in the data, and results were often weak and imprecise for the Samara vervet population. Structure models remove any reliance on the human construct of a home range and instead predict behaviours independently across space and time.

Functionally a home range is derived from a point cloud of animal locations. This point cloud is then distilled into a home range using tools such as kernel density or convex hull (Lichti & Swihart, 2011). And while a home range is based on location data from the animals, we do not know how an animal perceives its own home range (Powell, 2000). It is doubtful that any animal, likely even humans, perceives a boundary where the home range ends. Humans rely on maps or physical indicators to identify boundaries in their environment. Some boundaries may be natural, such as rivers, ridgelines, and other

environmental features, but many, if not most, are man-made, such as fences, roads, or a city boundary sign. In some cases, boundaries are purely mental constructs, such as the border between Canada and the U.S. where it crosses the Great Lakes. Powel suggests that animals may perceive their home range as a form of cognitive map, and some research supports the use of cognitive maps by animals (Peters, 1978). However, even if vervets possess a cognitive map to navigate, it is no more likely that they perceive the edge of their home range than a person perceives a city limit when leaving town, because there is no physical manifestation of this boundary. At best both species likely use landmarks (trees, city limits signs, etc.), but Powell's initial assertion remains, we simply do not know. The concept of a home range is a human construct used to delineate where animals have been observed and provides a useful approximation of where they are likely to be found in the field.

While home ranges are still useful for modelling where an animal spends its time and the area it utilizes, it is highly unlikely that the animals recognize this construct. Therefore, any measure of proximity to the home range that assumes animals understand this concept is flawed. Simply stated, isopleths are not lines in the sand that animals recognize, and it is arguable that even humans would struggle to recognize these constructs without some physical manifestation of them in their environment.

Structure analysis examines where behaviours occur absolutely, rather than relative to the home range. By analyzing behaviours without the bias of the home range, we may gain deeper insight into not only the "why "but also the "why there".

Conclusion

While the environment, both physical and psychological (e.g., the "landscape of fear"), does not determine behaviour, it does strongly influence behavioural patterns and coping strategies. This influence interacts with the inherent plasticity of animals. The same species, even the same population, can express different phenotypes or adopt different reaction norms in response to environmental variation.

The results presented in this dissertation were made possible by statistical (R, RStudio) and spatial modelling approaches (ArcGIS Pro, R, RStudio) designed to extract biologically meaningful patterns from complex, heterogeneous, and temporally uneven field data. Across all analytical chapters, the central objective of the computational framework was not to impose prescriptive structures on animal behaviour, but to allow spatial and temporal patterns to emerge from the data at scales relevant to the ecological context and behavioural interactions.

Throughout the analytical chapter, the computational and technological framework enabled inference at multiple biological scales: individual interactions, group-level organization, space use dynamics, and inter-group behavioural outcomes. Spatial interpolation, dynamic home range modelling, Bayesian modelling, sampling-effort correction, integration of remote sensing data, and spatiotemporal structure modelling collectively provided the analytical resolution required to detect patterns that would not be visible under static, coarse, or analytically imposed spatial constructs.

The interpretative results are therefore inseparable from these methodological choices. The results depend not only on the behavioural data themselves, but on

analytical approaches that allow spatial and temporal structure to emerge without assuming how animals perceive home ranges.

Chapter 2 examined how predation risk shaped the internal organization of a baboon group by applying Hamilton's Selfish Herd theory. Using spatial interpolation of individual locations, inter-individual distances (IIDs) were quantified and used to model group structure, allowing dominant females' consistently central positions to be assessed across varying troop formations and terrain types. Model-comparison frameworks applied to IID distributions evaluated whether social, ecological, or socioecological processes best explained observed spatial organization, allowing attraction and repulsion forces among individuals to be estimated directly from spatial data while accounting for interactions with a complex spatial environment.

Empirically estimated attraction and repulsion parameters provided the foundation for determining foraging spread, which in turn facilitated analyses of group geometry and individual positioning. Importantly, the derivation of a minimal foraging swath from estimated repulsion distances enabled group level foraging efficiency to be evaluated without reliance on assumed spatial thresholds. Linear modelling of foraging spread incorporated terrain type, group shape, foraging effort, and their interactions, while controlling for movement speed.

The effect of dominance rank and sex on the spatial positioning of individuals across varying group configurations was assessed in a mixed effects model, explicitly accounting for repeated sampling of individuals. This analysis revealed that terrain, also affected the troop formation as members interacted with different land-cover types. Fynbos, with its dense shrub-like vegetation, reduced visibility but provided abundant

food, allowing the group to maintain a tighter formation for safety while still accessing resources. In contrast, in more open karsts and rocky post-fire terrain where food was dispersed but visibility was high, the group spread out to reduce resource competition while remaining able to see conspecifics and potential threats.

Together, these methods enabled group shape and internal configuration to be interpreted as outcomes of interacting social and ecological constraints rather than as fixed or assumed properties of the troop.

Chapter 3 extended this theme by examining space use as a dynamic, environmentally responsive process rather than a fixed spatial envelope. Dynamic home range (DHR) modelling was used to move beyond static representations of space use by calculating home ranges across multiple temporal resolutions (static, annual, and sub-monthly). This framework captured variability in space use that would otherwise be obscured by temporal aggregation. Kernel density estimation, combined with trimming at defined isopleths and conversion to polygonal representations, enabled consistent quantification of area and overlap across time and temporal scale.

A critical component of the area and overlap application of the DHR framework was the explicit modelling of sampling effort. Bayesian regression models were used to correct area and overlap estimates for uneven sampling intensity, allowing meaningful comparisons across time periods and troops. This correction was essential for interpreting changes in home range size, overlap, and temporal trends as ecological signals rather than artefacts in how data were collected.

The integration of remotely sensed environmental data further extended the DHR approach. Dynamic home ranges were intersected with MODIS NDVI raster products to

extract area-weighted vegetation productivity estimates aligned with the temporal resolution of space use. By synchronizing DHR windows with satellite revisit intervals, the analysis provided an environmentally grounded context for observed expansions and contractions in home range area.

Using this framework, Chapter 3 demonstrated that vervet home range patterns shifted across fine and broader temporal scales in response to climatic phenomena such as El Niño. Troops foraged farther during or shortly after months of low rainfall, expanding their home ranges, but contracted space use when rainfall increased, indicating a flexible spatial response to environmentally driven changes in resource availability.

While scholars agree that the environmental context can shape behavioural responses to external pressures, it is important to recognize that animals, like humans, have agency in how they respond to ecological and social constraints (Tinbergen, 1963), and their choices can generate more meaningful outcomes in certain contexts than environmental pressures alone. Chapter 4 examined this agency by mapping and evaluating individual decisions to initiate intergroup encounters (ITEs), as well as the group's aggregated aggression level during these encounters. These behavioural variables proved more conclusive predictors of encounter outcomes than spatial proximity to the home range centre, challenging assumptions that spatial position alone governs success.

Chapter 4 represents an analytical evolution over the course of my PhD, in which earlier linear models gave way to Bayesian approaches and ultimately to the development of a novel approach for examining the structure of behaviour during ITEs. Initial analyses employed Bayesian models to evaluate behavioural and spatial predictors of encounter outcomes. Bayesian inference was used consistently to quantify effect sizes, uncertainty,

and directionality through posterior distributions, credibility intervals, odds ratios, and probabilities of direction. This approach was particularly well-suited to the relatively sparse and noisy nature of ITE data, allowing weak, moderate, and strong effects to be distinguished probabilistically without reliance on binary significance thresholds.

Mixed-effects structures with random intercepts for adversary identity accounted for differences in encounter difficulty among opponents and allowed variance to be partitioned between troop-level and adversary-level sources. Models were evaluated using posterior predictive checks, Bayesian R^2 values, and leave-one-out cross-validation (LOOIC), providing an assessment of the explanatory power and predictive performance of each model.

Importantly, this modelling framework was applied consistently across analyses using static home range metrics, dynamic home ranges, and subsequently behaviour-centric spatiotemporal representations. This consistency allowed direct comparison of how different spatial representations influenced explanatory power, revealing the relative limitations of proximity-based metrics, such as distance to the centre of the home range, because these metrics are derived from a construct that is not biologically meaningful to the animals.

The final analytical step replaced proximity-based predictors with spatiotemporal structure models that treated winning, initiation, and aggression as behaviours distributed across continuous space and time. These models jointly incorporated spatial coordinates and temporal information to identify structured patterns without reference to predefined boundaries or centres. Comparisons between time-only and spatiotemporal models demonstrated substantial improvements in explained variance when spatial information

was included, with LOOIC consistently favouring spatiotemporal models and posterior predictive checks indicating adequate fit. Bayesian R^2 values, while necessarily modest given the probabilistic nature of behavioural outcomes, nonetheless revealed meaningful structure across space and time.

Model predictions were visualized as three-dimensional point clouds, providing an explicit representation of where behaviours were most likely to occur across the landscape and through time. Thresholding procedures and change-point detection were applied to remove low-probability and false positive predictions, ensuring that visualization reflected informative structure rather than background noise. By modelling behaviours directly in space and time, this approach avoided reliance on human-defined spatial constructs and instead allowed patterns of initiation, aggression, and success to emerge from the data themselves.

Human constructs, both scientific and cultural, should be avoided or, when used, applied with caution. Researchers should bear in mind that these constructs, such as territory boundaries and home ranges, are unlikely to be perceived the same way by animals, let alone other humans. An animal's internal state is opaque to us, and our understanding of how they perceive these constructs, if at all, is incomplete. In Chapter 4, I discussed how home ranges represented as lines or points on a map are not concepts, we should expect an animal to perceive, especially when humans themselves often struggle to perceive their own position or boundaries without technological aids (e.g., borders through water or desert). A home range is a scientific construct, and while useful for quantifying where animals have been within a home range, it is not something we should expect the animals to conceptualize. In fact, the idea of a boundary for an animal is more

likely to exist as a gradient of familiarity and comfort rather than a line on a map or a point that represents a sleeping tree, but even this concept of a boundary as a gradient of comfort is conjecture on my part. Territorial boundaries as "lines in the sand" are cultural constructs rooted in the Colonial Age of human history and have even been compared to the "territorial law in man" (Seton, 1909). It may be fine as an analogy but should be avoided in any analysis of animal home ranges or territoriality as it anthropomorphizes the behaviour.

Analysis of spatial behaviour should be conducted without relying on human constructs because correlating animal behaviour to human behaviour risks erasing the critical difference between similarity and equivalence. That is, between resemblance and actual sameness. For example, while chimpanzee conflicts may resemble warfare, we must avoid interpreting them as such in a human sense or attributing intentions such as maiming or killing. As a former career soldier, I can attest to the complexity of human warfare: while individual soldiers are trained to kill an enemy combatant when required, in many countries they are also bound by rules of engagement, and all are accountable to international humanitarian law. Maiming is not an acceptable intent even if it is an unfortunate byproduct of armed conflict. There is also a political component to warfare that is often overlooked: politicians who make war and soldiers who fight them. With this in mind, saying that an animal's behaviour resembles warfare is a gross oversimplification. Attempting to correlate an outcome or behaviour to a human construct such as a home range, even when based on the animal's own positional data, seems less biologically meaningful in my assessment than first mapping the behaviour in space and time and then identifying the drivers behind it. This approach places behaviour before the

construct, and while analysis may reveal that a construct plays a role, this must not be presumed at the outset.

Throughout this dissertation I have tried to maintain two fundamental movement ecology principles: first, not to compartmentalize movement, and second to look at it through a holistic lens. Where possible, I consider how internal state, motion capacity, navigation, and external factors interact to produce movement. Movement is therefore treated as an emergent behaviour shaped by decisions made through time in response to ecological and social pressures. The use of spatiotemporal structure and dynamic home ranges reflects my contribution to the view that movement is inherently multidimensional, and that movement ecology was explicitly developed as a framework to integrate multiple paradigms into a unified perspective. Movement, therefore, cannot be reduced to a single analytical approach (Nathan et al., 2008).

Chapter 2 applies movement-ecology mechanisms such as inter-individual distances, attraction and repulsion, and group cohesion versus spacing, drawing on approaches common to agent-based models, collective motion theory, and self-organized movement systems (Nathan et al., 2008; Parrish & Edelstein-Keshet, 1999). Motion capacity is operationalized through constraints on proximity, navigation is expressed as the maintenance of cohesion without excessive overlap, and external pressures are incorporated through habitat structure and its effects on group spacing and formation.

In Chapter 3, dynamic home ranges are treated as summaries of movement through time rather than as containers enclosing observed locations. These representations respond dynamically to external pressures such as rainfall, resource distribution, and drought, whereas static approaches remove much of this movement

variability. As such, dynamic home ranges are not explanatory in themselves; they are descriptive aggregations that reflect accumulated movement decisions across time.

Consistent with Nathan's (2008) movement ecology framework, space use is therefore interpreted as an emergent outcome of movement decisions rather than as movement occurring within a defined area. Animals are not assumed to move within home ranges, but rather through landscapes of opportunity, risk, and interaction. The structure models presented in Chapter 4 do not assume any relationship to centres or boundaries; instead, they treat movement as a continuous trajectory punctuated by behavioural events. Behaviour is embedded within movement, and movement becomes the carrier of behavioural outcomes. The resulting three-dimensional space–time point clouds can thus be understood as movement paths enriched with behavioural state, providing a behaviour-first representation of movement in space and time.

As a whole, the analyses presented throughout this dissertation reflect my original intent, which was to approach primate behaviour through an explicitly geographic and movement-ecology lens. Rather than treating space use, social structure, or behaviour as separable components, I have consistently examined how they emerge through movement as animals interact with complex environments and social contexts over time. Taken together, the analyses presented in this dissertation reflect my intent to understand movement not as something that occurs within space, but as the process through which spatial and social patterns are produced, consistent with the movement ecology paradigm that treats space use as an emergent outcome of movement decisions.

Future work will include submitting Chapter 3 as a methods paper, alongside developing the Dynamic Home Range (DHR) code into a dedicated R package. I also

plan to expand the spatiotemporal structure analysis in Chapter 4 to address the question of “why there”, with the aim of publishing this work as a separate paper. In addition, I will complete a thermal landscape analysis that was originally intended as a chapter in this dissertation but was deferred as the research trajectory evolved.

References

Adrados, C., Girard, I., Gendner, J.-P., & Janeau, G. (2002). Global positioning system (GPS) location accuracy improvement due to selective availability removal. *Comptes Rendus Biologies*, *325*(2), 165-170.

Aguado, E., & Burt, J. E. (2007). *Understanding Weather and Climate* (4th ed.). pearson Education.

Akçakaya, H. R., Radeloff, V. C., Mladenoff, D. J., & He, H. S. (2004). Integrating landscape and metapopulation modeling approaches: viability of the sharp-tailed grouse in a dynamic landscape. *Conservation Biology*, *18*(2), 526-537.

Alam, M. M., Torgo, L., & Bifet, A. (2022). A survey on spatio-temporal data analytics systems. *ACM Computing Surveys*, *54*(10s), 1-38.

Altmann, S. A. (1974). Baboons, space, time, and energy. *American Zoologist*, *14*(1), 221-248.

AlZoubi, A., Dickinson, P., Pike, T. W., & Al-Diri, B. (2016). Analysing Fish Behaviours Using Three-Dimensional Qualitative Trajectory Calculus.

Amato, K. R., Sanders, J. G., Song, S. J., Nute, M., Metcalf, J. L., Thompson, L. R., Morton, J. T., Amir, A., McKenzie, V. J., & Humphrey, G. (2019). Evolutionary trends in host physiology outweigh dietary niche in structuring primate gut microbiomes. *The ISME journal*, *13*(3), 576-587.

Andersen, T., Carstensen, J., Hernández-García, E., & Duarte, C. M. (2009). Ecological thresholds and regime shifts: approaches to identification. *Trends in ecology & evolution*, *24*(1), 49-57.

Anderson, D. J. (1982). The home range: a new nonparametric estimation technique: ecological archives e063-001. *Ecology*, *63*(1), 103-112.

Andrienko, N., Andrienko, G., Barrett, L., Dostie, M., & Henzi, P. (2013). Space Transformation for Understanding Group Movement. *IEEE Transactions on Visualization and Computer Graphics*, *19*(12), 2169-2178. https://doi.org/10.1109/TVCG.2013.193

Andrienko, N., Andrienko, G., Pelekis, N., & Spaccapietra, S. (2008). Basic Concepts of Movement Data. In F. Giannotti & D. Pedreschi (Eds.), *Mobility, Data Mining and Privacy: Geographic Knowledge Discovery* (pp. 15-38). Springer Berlin Heidelberg. https://doi.org/10.1007/978-3-540-75177-9_2

Anhaeusser, C. R., Viljoen, M. J., & Viljoen, R. (2016). *Africa's Top Geological Sites: 35th International Geological Congress Commemorative Volume*. Struik Publishers.

Anthony, D., Bennett, W. P., Vuran, M. C., Dwyer, M. B., Elbaum, S., Lacy, A., Engels, M., & Wehtje, W. (2012). Sensing through the continent: towards monitoring migratory birds using cellular sensor networks. Information Processing in Sensor Networks (IPSN), 2012 ACM/IEEE 11th International Conference on,

Aristotle. (trans. 1985). De Motu Animalium (M. C. Nussbaum, Trans.). In *Aristotle's De Motu Animalium: Text with translation, commentary, and interpretive essays*. Princeton: Princeton University Press.

Arseneau, T. J. M., Taucher, A.-L., van Schaik, C. P., & Willems, E. P. (2015). Male monkeys fight in between-group conflicts as protective parents and reluctant recruits. *Animal behaviour*, *110*, 39-50. https://doi.org/https://doi.org/10.1016/j.anbehav.2015.09.006

Auger-Méthé, M., Derocher, A. E., Plank, M. J., Codling, E. A., & Lewis, M. A. (2015). Differentiating the Lévy walk from a composite correlated random walk. *Methods in Ecology and Evolution*, *6*(10), 1179-1189.

Aureli, F., Schaffner, C. M., Asensio, N., & Lusseau, D. (2012). What is a subgroup? How socioecological factors influence interindividual distance. *Behavioral Ecology*, ars122.

Aureli, F., Schaffner, C. M., Boesch, C., Bearder, S. K., Call, J., Chapman, C. A., Connor, R., Fiore, A. D., Dunbar, R. I., & Henzi, S. P. (2008). Fission-fusion dynamics: new research frameworks. *Current Anthropology*, *49*(4), 627-654.

Aurenhammer, F. (1991). Voronoi diagrams—a survey of a fundamental geometric data structure. *ACM Computing Surveys (CSUR)*, *23*(3), 345-405.

Barrett, L. (2011). *Beyond the brain: How body and environment shape animal and human minds*. Princeton University Press.

Barrett, L., Gaynor, D., Rendall, D., Mitchell, D., & Henzi, S. (2004). Habitual cave use and thermoregulation in chacma baboons (Papio hamadryas ursinus). *Journal of Human Evolution*, *46*(2), 215-222.

Barton, K., & Barton, M. K. (2015). Package 'mumin'. *Version*, *1*(18), 439. ftp://155.232.191.229/cran/web/packages/MuMIn/

Beecham, J., & Farnsworth, K. (1999). Animal group forces resulting from predator avoidance and competition minimization. *Journal of theoretical Biology*, *198*(4), 533-548.

Betancourt, M. (2017). A conceptual introduction to Hamiltonian Monte Carlo. *arXiv preprint arXiv:1701.02434*.

Bivand, R., Rowlingson, B., Diggle, P., Petris, G., Eglen, S., & Bivand, M. R. (2017). Package 'splancs'. *R package version*, 2.01-40.

Blersch, R. A., Bonnell, T. R., Clarke, M., Dostie, M. J., Lucas, M., Jarrett, J., McFarland, R., Nord, C., Takahashi, A., & Varsanyi, S. (2023). Maternal social position and survival to weaning in arid-country vervet monkeys. *American Journal of Biological Anthropology*, *181*(1), 3-9.

Bonnell, T. R., Clarke, P. M., Henzi, S. P., & Barrett, L. (2017). Individual-level movement bias leads to the formation of higher-order social structure in a mobile group of baboons. *PeerJ Preprints*, *5*, e2808v2801.

Bonnell, T. R., Henzi, S. P., & Barrett, L. (2015). Sparse movement data can reveal social influences on individual travel decisions. *arXiv preprint arXiv:1511.01536*.

Bonnell, T. R., Henzi, S. P., & Barrett, L. (2017). Direction matching for sparse movement data sets: determining interaction rules in social groups. *Behavioral Ecology*, *28*(1), 193-203.

Bonnell, T. R., Henzi, S. P., & Barrett, L. (2022). Using network synchrony to identify drivers of social dynamics. *Proceedings of the Royal Society B*, *289*(1977), 20220537.

Bonnell, T. R., Sengupta, R. R., Chapman, C. A., & Goldberg, T. L. (2010). An agent-based model of red colobus resources and disease dynamics implicates key resource sites as hot spots of disease transmission. *Ecological Modelling*, *221*(20), 2491-2500.

Börger, L. (2016). EDITORIAL: Stuck in motion? Reconnecting questions and tools in movement ecology. *Journal of Animal Ecology*, *85*(1), 5-10.

Börger, L., Franconi, N., De Michele, G., Gantz, A., Meschi, F., Manica, A., Lovari, S., & Coulson, T. (2006). Effects of sampling regime on the mean and variance of home range size estimates. *Journal of Animal Ecology*, 1393-1405.

Bouwer, L. M. (2011). Have disaster losses increased due to anthropogenic climate change? *Bulletin of the American Meteorological Society*, *92*(1), 39-46.

Bowman, R. (2008). *Six Degrees Could Change the World* National Geographic.

Bridger, C., & Booth, R. (2003). The effects of biotelemetry transmitter presence and attachment procedures on fish physiology and behavior. *Reviews in Fisheries Science*, *11*(1), 13-34.

Brown. (1962). Home range in small mammal communities. *Survey of biological progress*, *4*, 131-179.

Bullard, F. (1999). *Estimating the home range of an animal: a Brownian bridge approach. Johns Hopkins University* Master thesis].

Bumann, D., Krause, J., & Rubenstein, D. (1997). Mortality risk of spatial positions in animal groups: the danger of being in the front. *Behaviour*, *134*(13), 1063-1076.

Bürkner, P. (2024). *brms: Bayesian multilevel models using Stan*. CRAN. https://cran.r-project.org/package=brms

Burt, W. (1943). Territoriality and home range concepts as applied to mammals. *Journal of mammalogy*, *24*(3), 346-352.

Calenge, C. (2006). The package "adehabitat" for the R software: a tool for the analysis of space and habitat use by animals. *Ecological modelling*, *197*(3), 516-519.

Carter, A. J., Tico, M. T., & Cowlishaw, G. (2016). Sequential phenotypic constraints on social information use in wild baboons. *eLife*, *5*, e13125.

Chen, H., Cohen, P., & Chen, S. (2010). How big is a big odds ratio? Interpreting the magnitudes of odds ratios in epidemiological studies. *Communications in Statistics—simulation and Computation®*, *39*(4), 860-864.

Cheney, D. (1981). Intergroup Encounters among Free-Ranging Vervet Monkeys. *Folia Primatologica*, *35*(2-3), 124-146. https://doi.org/10.1159/000155970

Cheney, D., & Seyfarth, R. (1980). Vocal recognition in free-ranging vervet monkeys. *Animal behaviour*, *28*(2), 362-367.

Cheney, D. L. (1992). Intragroup cohesion and intergroup hostility: the relation between grooming distributions and intergroup competition among female primates. *Behavioral Ecology*, *3*(4), 334-345.

Christopherson, W. R., Birkeland, G. H., Byrne, M.-L., & Giles, P. T. (2016). *Geosystems: An Introduction to Physical Geography* (4th Canadian Edition ed.). Pearson Education Limited.

Cochran, W. W., & Lord Jr, R. D. (1963). A radio-tracking system for wild animals. *The Journal of Wildlife Management*, 9-24.

Cooke, S. J., Hinch, S. G., Wikelski, M., Andrews, R. D., Kuchel, L. J., Wolcott, T. G., & Butler, P. J. (2004). Biotelemetry: a mechanistic approach to ecology. *Trends in ecology & evolution*, *19*(6), 334-343.

Cooper Jr, W. E. (1978). Home range criteria based on temporal stability of areal occupation. *Journal of theoretical Biology*, *73*(4), 687-695.

Cords, M., & Rowell, T. (1986). Group fission in blue monkeys of the Kakamega Forest, Kenya. *Folia Primatologica*, *46*(2), 70-82.

Couzin, I. D., Krause, J., James, R., Ruxton, G. D., & Franks, N. R. (2002). Collective memory and spatial sorting in animal groups. *Journal of theoretical Biology*, *218*(1), 1-11.

Crofoot, M. (2013). The cost of defeat: Capuchin groups travel further, faster and later after losing conflicts with neighbors. *American journal of physical anthropology*, *152*(1), 79-85.

Crofoot, M., & Gilby, I. (2012). Cheating monkeys undermine group strength in enemy territory. *Proceedings of the National Academy of Sciences*, *109*(2), 501-505.

Crofoot, M., Gilby, I., Wikelski, M., & Kays, R. (2008). Interaction location outweighs the competitive advantage of numerical superiority in Cebus capucinus intergroup contests. *Proceedings of the National Academy of Sciences*, *105*(2), 577-581.

Crofoot, M., & Wrangham, R. (2010). Intergroup Aggression in Primates and Humans: The Case for a Unified Theory. In P. M. Kappeler & J. Silk (Eds.), *Mind the Gap* (pp. 171-195). Springer Berlin Heidelberg.

Dalziel, B. D., Morales, J. M., & Fryxell, J. M. (2008). Fitting probability distributions to animal movement trajectories: using artificial neural networks to link distance, resources, and memory. *The American Naturalist*, *172*(2), 248-258.

de Waal, F. (2000). Primates--a natural heritage of conflict resolution. *Science*, *289*(5479), 586-590.

DeAngelis, D. L., & Grimm, V. (2014). Individual-based models in ecology after four decades. *F1000Prime Rep*, *6*(39), 6.

Di Liberto, T. (2016). A not so rainy season: drought in southern Africa in January 2016. *Edited by MICHELLE L'HEUREUX and STEVEN FUHRMAN, NOAA Climate. gov*, *7*.

Didan, K. (2015). MOD13Q1 MODIS/Terra vegetation indices 16-day L3 global 250m SIN grid V006. *NASA EOSDIS Land Processes DAAC*.

Dostie, M., Bonnell, T., Barrett, L., & Henzi, S. (n.d.). *Estimating interpolation error in the individual movement trajectories of chacma baboons* (

Dostie, M. J., Lusseau, D., Bonnell, T., Clarke, P. M., Chaplin, G., Kienzle, S., Barrett, L., & Henzi, S. P. (2016). Proof of principle: the adaptive geometry of social foragers. *Animal behaviour*, *119*, 173-178.

Duong, T. (2018). *ks: Kernel Smoothing*. In https://CRAN.R-project.org/package=ks

Duong, T. (2024). *ks: Kernel smoothing* (Vol. 1.14.3). CRAN. https://CRAN.R-project.org/package=ks

Duong, T., & Hazelton, M. L. (2005). Cross-validation bandwidth matrices for multivariate kernel density estimation. *Scandinavian Journal of Statistics*, *32*(3), 485-506.

Edwards, W., Lindman, H., & Savage, L. J. (1963). Bayesian statistical inference for psychological research. *Psychological review*, *70*(3), 193.

Eftimie, R., De Vries, G., Lewis, M. A., & Lutscher, F. (2007). Modeling group formation and activity patterns in self-organizing collectives of individuals. *Bulletin of mathematical biology*, *69*(5), 1537-1565.

Emmerich, R. (2004). *The Day After Tomorrow*

Field, R., Hawkins, B. A., Cornell, H. V., Currie, D. J., Diniz-Filho, J. A. F., Guégan, J. F., Kaufman, D. M., Kerr, J. T., Mittelbach, G. G., & Oberdorff, T. (2009). Spatial species-richness gradients across scales: a meta-analysis. *Journal of Biogeography*, *36*(1), 132-147.

Flegal, J. M., & Gong, L. (2015). Relative fixed-width stopping rules for Markov chain Monte Carlo simulations. *Statistica Sinica*, 655-675.

Fritz, C. O., Morris, P. E., & Richler, J. J. (2012). Effect size estimates: current use, calculations, and interpretation. *Journal of experimental psychology: General*, *141*(1), 2.

García, M. G., de Guinea, M., Bshary, R., & van de Waal, E. (2022). Drivers and outcomes of between-group conflict in vervet monkeys. *Philosophical Transactions of the Royal Society B*, *377*(1851), 20210145.

Getz, W. M., Fortmann-Roe, S., Cross, P. C., Lyons, A. J., Ryan, S. J., & Wilmers, C. C. (2007). LoCoH: nonparameteric kernel methods for constructing home ranges and utilization distributions. *PloS one*, *2*(2), e207.

Guggenheim, D. (2006). *An Inconvenient Truth* L. Bender, S. Burns, L. David, & L. Chilcott; Paramount Classics.

Guillemette, M., Woakes, A. J., Flagstad, A., & Butler, P. J. (2002). Effects of data-loggers implanted for a full year in female common eiders. *The condor*, *104*(2), 448-452.

Hägerstrand, T. (1970). What about people in Regional Science? *Papers of the Regional Science Association*, *24*(1), 6-21. https://doi.org/10.1007/BF01936872

Hallworth, M. T., & Marra, P. P. (2015). Miniaturized GPS tags identify non-breeding territories of a small breeding migratory songbird. *Scientific reports*, *5*, 11069.

Hamilton, W. D. (1971). Geometry for the selfish herd. *Journal of theoretical Biology*, *31*(2), 295-311.
Hansen, J. E. (1989). The greenhouse effect: Impacts on current global temperature and regional heat waves. *IN: The Challenge of Global Warming. Island Press, Washington, DC. 1989. p 35-43, 3 fig, 7 ref.*
Henning Teickner, Benedikt Gräler, & Pebesma, E. (2025). *sftime*. In https://r-spatial.github.io/sftime/articles/sftime.html
Henzi, P., & Barrett, L. (2003). Evolutionary ecology, sexual conflict, and behavioral differentiation among baboon populations. *Evolutionary Anthropology: Issues, News, and Reviews: Issues, News, and Reviews*, *12*(5), 217-230.
Henzi, S., Bonnell, T., Pasternak, G., Freeman, N., Dostie, M., Kienzle, S., Vilette, C., & Barrett, L. (2021). Keep calm and carry on: reactive indifference to predator encounters by a gregarious prey species. *Animal behaviour*, *181*, 1-11.
Henzi, S., Byrne, R., & Whiten, A. (1992). Patterns of movement by baboons in the Drakensberg mountains: primary responses to the environment. *International Journal of Primatology*, *13*(6), 601-629.
Henzi, S., Lusseau, D., Weingrill, T., Van Schaik, C., & Barrett, L. (2009). Cyclicity in the structure of female baboon social networks. *Behavioral ecology and sociobiology*, *63*(7), 1015-1021.
Henzi, S., Lycett, J., & Weingrill, T. (1998). Mate guarding and risk assessment by male mountain baboons during inter-troop encounters. *Animal behaviour*, *55*(6), 1421-1428.
Henzi, S. P., & Barrett, L. (2005). The historical socioecology of savanna baboons (Papio hamadryas). *Journal of Zoology*, *265*(03), 215-226.
Henzi, S. P., & Lucas, J. W. (1980). Observations on the Inter-Troop Movement of Adult Vervet Monkeys (Cercopithecus aethiops). *Folia Primatologica*, *33*(3), 220-235. https://doi.org/10.1159/000155936
Hill, R., Barrett, L., Gaynor, D., Weingrill, T., Dixon, P., Payne, H., & Henzi, S. (2003). Day length, latitude and behavioural (in) flexibility in baboons (Papio cynocephalus ursinus). *Behavioral ecology and sociobiology*, *53*(5), 278-286.
Hill, R. A., & Dunbar, R. I. (1998). An evaluation of the roles of predation rate and predation risk as selective pressures on primate grouping behaviour. *Behaviour*, *135*(4), 411-430.
Hinsch, M., & Komdeur, J. (2017). What do territory owners defend against? *Proceedings of the Royal Society B: Biological Sciences*, *284*(1849), 20162356. https://doi.org/10.1098/rspb.2016.2356
Hirsch, B. T. (2007). Costs and benefits of within-group spatial position: a feeding competition model. *The Quarterly review of biology*, *82*(1), 9-27.
Holden, C. (2006). Inching Toward Movement Ecology. *Science*, *313*(5788), 779-782. https://doi.org/10.1126/science.313.5788.779
Horne, J. S., Garton, E. O., Krone, S. M., & Lewis, J. S. (2007). Analyzing animal movements using Brownian bridges. *Ecology*, *88*(9), 2354-2363.
IPCC. (2014). *Climate Change 2014: Synthesis Report. Contribution of Working Groups I, II and III to the Fifth Assessment Report of the Intergovernmental Panel on Climate Change* (R. Pachauri, L. Meyer, & C. W. Team, Eds. AR5 ed.). IPCC.
IPCC. (2017). *IPCC Organization*. https://www.ipcc.ch/organization/organization.shtml
Isbell, L. A. (1991). Contest and scramble competition: patterns of female aggression and ranging behavior among primates. *Behavioral Ecology*, *2*(2), 143-155.

Jablonski, N. G. (2005). 16 Primate diversity and environmental seasonality in historieal perspeetive. *Seasonality in Primates: Studies of Living and Extinct Human and Non-Human Primates*, *44*, 465.

Jarrett, J. D., Bonnell, T., Jorgensen, M. J., Schmitt, C. A., Young, C., Dostie, M., Barrett, L., & Henzi, S. P. (2020). Modeling variation in the growth of wild and captive juvenile vervet monkeys in relation to diet and resource availability. *American journal of physical anthropology*, *171*(1), 89-99.

Jeffery, K. J. (2003). *The neurobiology of spatial behaviour*. Oxford University Press Oxford.

Jiménez-Valverde, A. (2014). Threshold-dependence as a desirable attribute for discrimination assessment: implications for the evaluation of species distribution models. *Biodiversity and Conservation*, *23*(2), 369-385. https://doi.org/10.1007/s10531-013-0606-1

Johnson, P. C. (2014). Extension of Nakagawa & Schielzeth's R2GLMM to random slopes models. *Methods in Ecology and Evolution*, *5*(9), 944-946.

Jones, R. (1977). Movement patterns and egg distribution in cabbage butterflies. *The Journal of Animal Ecology*, 195-212.

Jonsen, I. D., Flemming, J. M., & Myers, R. A. (2005). Robust state–space modeling of animal movement data. *Ecology*, *86*(11), 2874-2880.

Josephs, N., Bonnell, T., Dostie, M., Barrett, L., & Henzi, S. P. (2016). Working the crowd: sociable vervets benefit by reducing exposure to risk. *Behavioral Ecology*, arw003.

Judd, T., Ehinger, K., Durand, F., & Torralba, A. (2009). Learning to predict where humans look. Computer Vision, 2009 IEEE 12th international conference on,

Katz, Y., Tunstrom, K., Ioannou, C. C., Huepe, C., & Couzin, I. D. (2011). Inferring the structure and dynamics of interactions in schooling fish. *Proc Natl Acad Sci U S A*, *108*(46), 18720-18725. https://doi.org/10.1073/pnas.1107583108

King, A., Douglas, C., Huchard, E., Isaac, N., & Cowlishaw, G. (2008). Dominance and affiliation mediate despotism in a social primate. *Current Biology*, *18*(23), 1833-1838.

King, A. J., Wilson, A. M., Wilshin, S. D., Lowe, J., Haddadi, H., Hailes, S., & Morton, A. J. (2012). Selfish-herd behaviour of sheep under threat. *Current Biology*, *22*(14), R561-R562.

Kitchen, D., Seyfarth, R., & Cheney, D. (2004). Factors mediating inter-group encounters in savannah baboons (Papio cynocephalus ursinus). *Behaviour*, *141*(2), 197-218. https://doi.org/10.1163/156853904322890816

Koenig, A. (2002). Competition for resources and its behavioral consequences among female primates. *International Journal of Primatology*, *23*(4), 759-783.

Kotze, I. J. D. F., & Fairall, N. (2006). Using Landsat TM imagery to map fynbos plant communities : a case study : research article. *South African Journal of Wildlife Research - 24-month delayed open access*, *36*(1), 75-87. https://journals.co.za/content/wild/36/1/EJC117226

Kraak, M.-J., & Koussoulakou, A. (2005). A visualization environment for the space-time-cube. In *Developments in spatial data handling* (pp. 189-200). Springer.

Krause, J., Ruxton, G. D., & Ruxton, G. D. (2002). *Living in groups*. Oxford University Press.

Kruschke, J. (2014). Doing Bayesian data analysis: A tutorial with R, JAGS, and Stan.

Lawes, M. J., & Henzi, S. P. (1995). Inter-group encounters in blue monkeys: How territorial must a territorial species be? *Animal behaviour*, *49*(1), 240-243.

Lawler, E., Field, C., & Mills Flemming, J. (2023). starve: An R package for spatio-temporal analysis of research survey data using nearest-neighbour Gaussian processes. *Methods in Ecology and Evolution*, *14*(3), 817-830.

Lecheval, V., Robinson, E. J. H., & Mann, R. P. (2024). Random walks with spatial and temporal resets can explain individual and colony-level searching patterns in ants. *Journal of the Royal Society Interface*, *21*(216), 20240149.

Lehmann, J., Korstjens, A., & Dunbar, R. (2007). Group size, grooming and social cohesion in primates. *Animal behaviour*, *74*(6), 1617-1629.
Lichti, N., & Swihart, R. (2011). Estimating utilization distributions with kernel versus local convex hull methods. *The Journal of Wildlife Management*, *75*(2), 413-422.
Liu, C., White, M., & Newell, G. (2013). Selecting thresholds for the prediction of species occurrence with presence-only data. *Journal of Biogeography*, *40*(4), 778-789.
Maher, C. R., & Lott, D. F. (2000). A review of ecological determinants of territoriality within vertebrate species. *The American Midland Naturalist*, *143*(1), 1-29.
Majolo, B., de Bortoli Vizioli, A., & Schino, G. (2008). Costs and benefits of group living in primates: group size effects on behaviour and demography. *Animal behaviour*, *76*(4), 1235-1247.
Makowski, D., Ben-Shachar, M. S., & Lüdecke, D. (2019). bayestestR: Describing effects and their uncertainty, existence and significance within the Bayesian framework. *Journal of open source software*, *4*(40), 1541.
Markham, A., Guttal, V., Alberts, S., & Altmann, J. (2013). When good neighbors don't need fences: temporal landscape partitioning among baboon social groups. *Behavioral ecology and sociobiology*, *67*(6), 875-884. https://doi.org/10.1007/s00265-013-1510-0
Marshall, W. H., Gullion, G. W., & Schwab, R. G. (1962). Early summer activities of porcupines as determined by radio-positioning techniques. *The Journal of Wildlife Management*, *26*(1), 75-79.
McDougall, P., Forshaw, N., Barrett, L., & Henzi, S. (2010). Leaving home: Responses to water depletion by vervet monkeys. *Journal of Arid Environments*, *74*(8), 924-927.
McFarland, R., Barrett, L., Boner, R., Freeman, N., & Henzi, S. (2014). Behavioral flexibility of vervet monkeys in response to climatic and social variability. *American journal of physical anthropology*, *154*(3), 357-364.
McZgee, V. E., & Carleton, W. T. (1970). Piecewise regression. *Journal of the american statistical association*, *65*(331), 1109-1124.
Mitani, J., & Watts, D. (2005). Seasonality in hunting by nonhuman. *Seasonality in primates: studies of living and extinct human and non-human primates. Cambridge University Press, Cambridge*, 215-241.
Mitani, J. C., & Rodman, P. S. (1979). Territoriality: the relation of ranging pattern and home range size to defendability, with an analysis of territoriality among primate species. *Behavioral ecology and sociobiology*, *5*, 241-251.
Mitani, J. C., Watts, D. P., & Amsler, S. J. (2010). Lethal intergroup aggression leads to territorial expansion in wild chimpanzees. *Current Biology*, *20*(12), R507-R508.
MobileTartu. (2016). *Mobile Tartu 2016*. http://mobilitylab.ut.ee/mobiletartu/2016/
Morales, J. M., & Ellner, S. P. (2002). Scaling up animal movements in heterogeneous landscapes: the importance of behavior. *Ecology*, *83*(8), 2240-2247.
Morrell, L. J., & Romey, W. L. (2008). Optimal individual positions within animal groups. *Behavioral Ecology*, *19*(4), 909-919.
Morrell, L. J., Ruxton, G. D., & James, R. (2011). Spatial positioning in the selfish herd. *Behavioral Ecology*, *22*(1), 16-22.
Mucina, L., Rutherford, M. C., Palmer, A. R., Milton, S. J., Scott, L., Lloyd, J., Van der Merwe, B., Hoare, D., Bezuidenhout, H., & Vlok, J. (2006). Nama-Karoo Biome. *The vegetation of South Africa, Lesotho and Swaziland. Strelitzia*, *19*, 324-347.
Muller-Landau, H. C., Wright, S. J., Calderón, O., Condit, R., & Hubbell, S. P. (2008). Interspecific variation in primary seed dispersal in a tropical forest. *Journal of Ecology*, *96*(4), 653-667.

Nagy, M., Akos, Z., Biro, D., & Vicsek, T. (2010). Hierarchical group dynamics in pigeon flocks. *Nature*, *464*(7290), 890.

Nakagawa, S., Johnson, P. C., & Schielzeth, H. (2017). The coefficient of determination R 2 and intra-class correlation coefficient from generalized linear mixed-effects models revisited and expanded. *Journal of the Royal Society Interface*, *14*(134), 20170213.

Nathan, R. (2008). An emerging movement ecology paradigm. *Proceedings of the National Academy of Sciences*, *105*(49), 19050-19051.

Nathan, R., Getz, W. M., Revilla, E., Holyoak, M., Kadmon, R., Saltz, D., & Smouse, P. E. (2008). A movement ecology paradigm for unifying organismal movement research. *Proceedings of the National Academy of Sciences*, *105*(49), 19052-19059.

Nevelsteen, K. (2013). Attention allocation of traffic environments of international visitors during virtual city walks. Eye Tracking for Spatial Research, Proceedings of the 1st International Workshop (in conjunction with COSIT 2013),

Nielson, R., Sawyer, H., & McDonald, T. (2011). BBMM: Brownian bridge movement model for estimating the movement path of an animal using discrete location data. *R package version*, *22*.

Nord, C., Bonnell, T., Roth, D., Clarke, M., Dostie, M., Henzi, P., & Barrett, L. (2022). Fear of missing out? Personality and plasticity in food neophilia by wild vervet monkeys, Chlorocebus pygerythrus. *Animal behaviour*, *191*, 179-190.

Nord, C. M., Bonnell, T. R., Dostie, M. J., Henzi, S. P., & Barrett, L. (2021). Tolerance of muzzle contact underpins the acquisition of foraging information in vervet monkeys (Chlorocebus pygerythrus). *Journal of Comparative Psychology*, *135*(3), 349.

Notaro, M., Vavrus, S., & Liu, Z. (2007). Global vegetation and climate change due to future increases in CO2 as projected by a fully coupled model with dynamic vegetation. *Journal of Climate*, *20*(1), 70-90.

Parker, G. A. (1974). Assessment strategy and the evolution of fighting behaviour. *Journal of theoretical Biology*, *47*(1), 223-243.

Parrish, J. K., & Edelstein-Keshet, L. (1999). Complexity, pattern, and evolutionary trade-offs in animal aggregation. *Science*, *284*(5411), 99-101.

Pasternak, G., Brown, L. R., Kienzle, S., Fuller, A., Barrett, L., & Henzi, S. P. (2013). Population ecology of vervet monkeys in a high latitude, semi-arid riparian woodland. *Koedoe*, *55*, 01-09. http://www.scielo.org.za/scielo.php?script=sci_arttext&pid=S0075-64582013000100001&nrm=iso

Patterson, T. A., Thomas, L., Wilcox, C., Ovaskainen, O., & Matthiopoulos, J. (2008). State–space models of individual animal movement. *Trends in ecology & evolution*, *23*(2), 87-94.

Pearson, K. (1905). The problem of the random walk. *Nature*, *72*(1865), 294.

Pebesma, E. J. (2004). Multivariable geostatistics in S: the gstat package. *Computers & Geosciences*, *30*(7), 683-691.

Peters, R. (1978). Communication, cognitive mapping, and strategy in wolves and hominids. In *Wolf and man* (pp. 95-107). Elsevier.

Pillay, K. R., Streicher, J. P., & Downs, C. T. (2023). Home range and habitat use of vervet monkeys in the urban forest mosaic landscape of Durban, eThekwini Municipality, KwaZulu-Natal, South Africa. *Urban Ecosystems*, *26*(6), 1769-1782.

Piri Sahragard, H., Ajorlo, M., & Karami, P. (2018). Modeling habitat suitability of range plant species using random forest method in arid mountainous rangelands. *Journal of Mountain Science*, *15*(10), 2159-2171.

Pitelka, F. A. (1959). Numbers, breeding schedule, and territoriality in Pectoral Sandpipers of northern Alaska. *The condor*, *61*(4), 233-264.

Pliny, t. E. (trans. 1634). Naturalis Historia (P. Holland, Trans.). In *The history of the world, commonly called the Naturall historie of C. Plinius Secundus*. London: A. Islip.

Pontius Jr, R. G., & Parmentier, B. (2014). Recommendations for using the relative operating characteristic (ROC). *Landscape Ecology*, *29*(3), 367-382.

Powell, R. A. (2000). Animal home ranges and territories and home range estimators. *Research techniques in animal ecology: controversies and consequences*, *442*, 65-110.

Quandt, R. E. (1958). The estimation of the parameters of a linear regression system obeying two separate regimes. *Journal of the american statistical association*, *53*(284), 873-880.

R Core Team. (2015). *R: A language and environment for statistical computing.* In R Foundation for Statistical Computing. https://www.R-project.org/.

Ramanathan, V., Cicerone, R. J., Singh, H. B., & Kiehl, J. T. (1985). Trace gas trends and their potential role in climate change. *Journal of Geophysical Research: Atmospheres*, *90*(D3), 5547-5566.

Rasmussen, M. S. (1998). Developing simple, operational, consistent NDVI-vegetation models by applying environmental and climatic information: Part I. Assessment of net primary production. *International Journal of Remote Sensing*, *19*(1), 97-117. https://doi.org/10.1080/014311698216459

Reed, B. C., Brown, J. F., VanderZee, D., Loveland, T. R., Merchant, J. W., & Ohlen, D. O. (1994). Measuring phenological variability from satellite imagery. *Journal of vegetation science*, *5*(5), 703-714.

Rempel, R. S., Rodgers, A. R., & Abraham, K. F. (1995). Performance of a GPS animal location system under boreal forest canopy. *The Journal of Wildlife Management*, 543-551.

Reynolds, D., & Riley, J. (2002). Remote-sensing, telemetric and computer-based technologies for investigating insect movement: a survey of existing and potential techniques. *Computers and Electronics in Agriculture*, *35*(2), 271-307.

Rhine, R., Bioland, P., & Lodwick, L. (1985). Progressions of adult male chacma baboons (Papio ursinus) in the Moremi Wildlife Reserve. *International Journal of Primatology*, *6*(2), 115-122.

Robert, C., & Casella, G. (1999). *Monte Carlo statistical methods* (Vol. 2). Springer.

Ron, T., Henzi, S. P., & Motro, U. (1996). Do female chacma baboons compete for a safe spatial position in a southern woodland habitat? *Behaviour*, *133*(5), 475-490.

Rosenzweig, C., Karoly, D., Vicarelli, M., Neofotis, P., Wu, Q., Casassa, G., Menzel, A., Root, T. L., Estrella, N., & Seguin, B. (2008). Attributing physical and biological impacts to anthropogenic climate change. *Nature*, *453*(7193), 353-357.

Rusch, H., & Gavrilets, S. (2020). The logic of animal intergroup conflict: A review. *Journal of Economic Behavior & Organization*, *178*, 1014-1030.

Sarmiento, J. L., Hughes, T. M., Stouffer, R. J., & Manabe, S. (1998). Simulated response of the ocean carbon cycle to anthropogenic climate warming. *Nature*, *393*(6682), 245-249.

Schick, R. S., Loarie, S. R., Colchero, F., Best, B. D., Boustany, A., Conde, D. A., Halpin, P. N., Joppa, L. N., McClellan, C. M., & Clark, J. S. (2008). Understanding movement data and movement processes: current and emerging directions. *Ecology letters*, *11*(12), 1338-1350.

Schmid, V. S., & de Vries, H. (2013). Finding a dominance order most consistent with a linear hierarchy: an improved algorithm for the I&SI method. *Animal behaviour*, *86*(5), 1097-1105.

Seaman, D., Millspaugh, J., Kernohan, B., Brundige, G., Raedeke, K., & Gitzen, R. (1999). Effects of sample size on kernel home range estimates. *The Journal of Wildlife Management*, 739-747.

Seaman, D. E., Millspaugh, J. J., Kernohan, B. J., Brundige, G. C., Raedeke, K. J., & Gitzen, R. A. (1999). Effects of sample size on kernel home range estimates. *The Journal of Wildlife Management*, 739-747.

Seton, E. T. (1909). *Life-histories of northern animals: an account of the mammals of Manitoba* (Vol. 1). Scribner.

Shultz, S., Opie, C., & Atkinson, Q. D. (2011). Stepwise evolution of stable sociality in primates. *Nature*, *479*(7372), 219-222.

Sicotte, P. (1993). Inter-group encounters and female transfer in mountain gorillas: influence of group composition on male behavior. *American journal of primatology*, *30*(1), 21-36.

Silverman, B. W. (2018). *Density estimation for statistics and data analysis*. Routledge.

Siniff, D. B., & Jessen, C. (1969). A simulation model of animal movement patterns. *Advances in ecological research*, *6*, 185-219.

Skellam, J. G. (1951). Random dispersal in theoretical populations. *Biometrika*, *38*(1/2), 196-218.

So Much More to Know. (2005). *Science*, *309*(5731), 78-102. https://doi.org/doi:10.1126/science.309.5731.78b

Spiegel, O., Leu, S. T., Sih, A., & Bull, C. M. (2016). Socially interacting or indifferent neighbours? Randomization of movement paths to tease apart social preference and spatial constraints. *Methods in Ecology and Evolution*, *7*(8), 971-979.

Stickel, L. (2003). Home range and travels. *Biology of Peromyscus (Rodentia*, 373-411.

Stockmayer, G. E. (2003). *Statistical Time Series Analysis of a Howler Monkey Population* University of California, Berkeley].

Strandburg-Peshkin, A., Farine, D. R., Couzin, I. D., & Crofoot, M. C. (2015). Shared decision-making drives collective movement in wild baboons. *Science*, *348*(6241), 1358-1361.

Strier, K. B. (2016). *Primate Ethnographies*. Routledge.

Struhsaker, T. (1967). Social Structure Among Vervet Monkeys (Cercopithecus Aethiops). *Behaviour*, *29*(2-4), 83-121. https://doi.org/10.1163/156853967X00073

Sumpter, D. J. T., Mann, R. P., & Perna, A. (2012). The modelling cycle for collective animal behaviour. *Interface Focus*, *2*(6), 764-773. https://doi.org/10.1098/rsfs.2012.0031

Szumilas, M. (2010). Explaining odds ratios. *Journal of the Canadian academy of child and adolescent psychiatry*, *19*(3), 227.

Team, R. (2015). *RStudio: Integrated Development for R*. In RStudio, Inc. http://www.rstudio.com/

Team, S. D. (2024). *Stan Modeling Language Users Guide and Reference Manual, Version 2.33*. In (Version Version 2.33) Stan Development Team. https://mc-stan.org

Tinbergen, N. (1963). On aims and methods of ethology. *Zeitschrift für tierpsychologie*, *20*(4), 410-433.

Tobler, W. (2004). On the first law of geography: A reply. *Annals of the association of American geographers*, *94*(2), 304-310.

Tobler, W. R. (1970). A computer movie simulating urban growth in the Detroit region. *Economic geography*, *46*(sup1), 234-240.

Tomkiewicz, S. M., Fuller, M. R., Kie, J. G., & Bates, K. K. (2010). Global positioning system and associated technologies in animal behaviour and ecological research. *Philos Trans R Soc Lond B Biol Sci*, *365*(1550), 2163-2176. https://doi.org/10.1098/rstb.2010.0090

Toms, J. D., & Lesperance, M. L. (2003). Piecewise regression: a tool for identifying ecological thresholds. *Ecology*, *84*(8), 2034-2041.

Turchin, P. (1998). *Quantitative analysis of movement: measuring and modeling population redistribution in animals and plants* (Vol. 1). Sinauer Associates Sunderland.

Van der Putten, W. H., Macel, M., & Visser, M. E. (2010). Predicting species distribution and abundance responses to climate change: why it is essential to include biotic interactions across trophic levels. *Philosophical Transactions of the Royal Society of London B: Biological Sciences*, *365*(1549), 2025-2034.

Van Moorter, B., Visscher, D., Benhamou, S., Börger, L., Boyce, M. S., & Gaillard, J. M. (2009). Memory keeps you at home: a mechanistic model for home range emergence. *Oikos*, *118*(5), 641-652.

Van Schaik, C. P. (1983). Why are diurnal primates living in groups? *Behaviour*, *87*(1), 120-144.

Vickers, M., Schwarzkopf, L., Woods, H. A., & Bronstein, J. L. (2016). A Random Walk in the Park: An Individual-Based Null Model for Behavioral Thermoregulation. *The American Naturalist*, *187*(4), 000-000.

Vilette, C., Bonnell, T., Dostie, M., Henzi, S., & Barrett, L. (2022). Network formation during social integration in juvenile vervet monkeys. *Animal behaviour*, *194*, 205-223.

Vilette, C., Bonnell, T., Dostie, M., Henzi, S., & Barrett, L. (2023). Strong ties formation, composition and processes at play during the developmental period of juvenile vervet monkeys. *Animal behaviour*, *201*, 137-156.

Vogel, S. (2013). *Comparative biomechanics: life's physical world*. Princeton University Press.

Webber, Q. M., Albery, G. F., Farine, D. R., Pinter-Wollman, N., Sharma, N., Spiegel, O., Vander Wal, E., & Manlove, K. (2023). Behavioural ecology at the spatial–social interface. *Biological Reviews*, *98*(3), 868-886.

Weghe, N. V. d., Cohn, A. G., & Maeyer, P. D. (2004). A qualitative representation of trajectory pairs. Proceedings of the 16th European Conference on Artificial Intelligence,

Wikelski, M. (2017). *Movebank: For Animal tracking Data*. Retrieved 2/26/2017 from https://www.movebank.org/

Willems, E., Barton, R., & Hill, R. (2009). Remotely sensed productivity, regional home range selection, and local range use by an omnivorous primate. *Behavioral Ecology*, *20*(5), 985-992.

Willems, E. P., Barton, R. A., & Hill, R. A. (2009). Remotely sensed productivity, regional home range selection, and local range use by an omnivorous primate. *Behavioral Ecology*, arp087.

Willems, E. P., & Hill, R. A. (2009). Predator-specific landscapes of fear and resource distribution: effects on spatial range use. *Ecology*, *90*(2), 546-555.

Wilson, M., Hauser, M., & Wrangham, R. (2001). Does participation in intergroup conflict depend on numerical assessment, range location, or rank for wild chimpanzees? *Animal behaviour*, *61*(6), 1203-1216.

Winnie, J. A., Cross, P., & Getz, W. (2008). Habitat quality and heterogeneity influence distribution and behavior in African buffalo (Syncerus caffer). *Ecology*, *89*(5), 1457-1468.

Wrangham, R., & Glowacki, L. (2012). Intergroup aggression in chimpanzees and war in nomadic hunter-gatherers: Evaluating the chimpanzee model. *Human nature*, *23*(1), 5-29.

Wrangham, R. W. (1999). Evolution of coalitionary killing. *American journal of physical anthropology*, *110*(S29), 1-30.

Wright, S. J., Trakhtenbrot, A., Bohrer, G., Detto, M., Katul, G. G., Horvitz, N., Muller-Landau, H. C., Jones, F. A., & Nathan, R. (2008). Understanding strategies for seed dispersal by wind under contrasting atmospheric conditions. *Proceedings of the National Academy of Sciences*, *105*(49), 19084-19089.

Wu, F., Lei, T. K. H., Li, Z., & Han, J. (2014). Movemine 2.0: Mining object relationships from movement data. *Proceedings of the VLDB Endowment*, *7*(13), 1613-1616.

Wu, J., He, J., & Christakos, G. (2021). *Quantitative Analysis and Modeling of Earth and Environmental Data: Space-Time and Spacetime Data Considerations*. Elsevier Science. https://books.google.ca/books?id=qQAAEAAAQBAJ

Yau, N. (2012). *Visualize this!* John Wiley & Sons.

Young, C., McFarland, R., Barrett, L., & Henzi, S. P. (2017). Formidable females and the power trajectories of socially integrated male vervet monkeys. *Animal behaviour*, *125*, 61-67.

Appendices

Appendix A — 14-Day Area Table

Table 7.1: Complete 14-Day Area and Effort Table

Date	PT Troop		RBM Troop		RST Troop	
	Effort	Area	Effort	Area	Effort	Area
18-10-2011	-	-	118	246,689	39	115,052
01-11-2011	-	-	89	190,010	96	377,280
15-11-2011	-	-	-	-	31	135,104
29-11-2011	-	-	73	247,515	26	156,517
13-12-2011	-	-	27	182,954	43	158,933
10-01-2012	-	-	122	275,510	106	202,784
24-01-2012	-	-	101	554,292	89	175,724
07-02-2012	-	-	110	313,976	133	315,671
21-02-2012	-	-	90	298,637	85	207,583
06-03-2012	-	-	85	240,435	97	94,633
20-03-2012	-	-	81	426,386	147	197,479
03-04-2012	-	-	203	255,938	198	214,076
17-04-2012	-	-	300	429,417	205	193,649
01-05-2012	-	-	173	238,564	325	173,888
15-05-2012	-	-	176	197,343	303	210,287
29-05-2012	71	91,809	171	195,026	253	159,224
12-06-2012	143	97,085	202	221,028	217	134,531
26-06-2012	162	86,347	168	250,458	170	149,275
10-07-2012	108	119,620	88	395,130	265	153,098
24-07-2012	70	80,568	96	203,126	83	125,775
07-08-2012	62	143,357	38	93,616	133	117,144
21-08-2012	81	81,496	136	196,182	77	101,744
04-09-2012	46	85,707	-	-	70	181,188
18-09-2012	90	80,234	99	149,671	95	119,510
02-10-2012	81	90,781	94	60,616	100	64,006
16-10-2012	60	49,661	84	96,357	108	129,203
30-10-2012	47	55,449	115	99,752	131	115,328

13-11-2012	96	79,734	60	191,037	98	149,333
27-11-2012	39	230,240	48	155,617	123	178,426
11-12-2012	56	85,384	-	-	-	-
25-12-2012	-	-	24	101,929	23	55,108
08-01-2013	111	115,989	121	179,838	88	159,323
22-01-2013	92	78,229	98	327,055	106	184,684
05-02-2013	141	74,550	146	235,788	96	156,904
19-02-2013	99	105,798	122	174,835	130	165,615
05-03-2013	110	93,560	125	159,582	67	203,545
02-04-2013	93	92,452	84	260,368	-	-
16-04-2013	74	71,221	108	183,223	26	58,465
30-04-2013	133	74,810	128	187,716	34	49,111
14-05-2013	112	62,661	144	179,133	40	126,688
28-05-2013	47	57,602	87	158,505	36	96,015
11-06-2013	70	53,411	60	123,648	-	-
25-06-2013	-	-	53	131,276	62	102,350
09-07-2013	60	119,390	81	173,942	38	82,939
23-07-2013	85	70,992	81	115,555	78	91,005
06-08-2013	99	81,148	61	132,651	73	89,954
20-08-2013	50	65,440	58	128,325	70	92,634
03-09-2013	44	36,541	43	140,033	46	91,570
17-09-2013	48	31,941	46	139,795	88	106,354
01-10-2013	99	76,236	73	141,893	76	103,949
15-10-2013	93	113,053	99	164,191	49	102,909
29-10-2013	74	155,977	99	312,614	66	86,416
12-11-2013	53	127,622	74	294,245	46	122,671
26-11-2013	76	128,473	140	183,146	107	132,183
10-12-2013	141	85,360	132	256,953	128	117,964
24-12-2013	71	80,431	95	151,869	98	128,931

07-01-2014	126	38,412	121	140,710	89	103,924
21-01-2014	133	75,420	154	187,631	159	90,069
04-02-2014	147	45,063	138	190,159	97	91,403
18-02-2014	121	49,749	122	180,180	131	134,126
04-03-2014	176	75,003	186	244,021	129	115,078
18-03-2014	191	55,573	167	261,195	151	99,940
01-04-2014	184	59,801	158	213,032	145	68,115
15-04-2014	128	74,954	137	183,467	125	134,890
29-04-2014	84	45,814	125	188,313	117	115,146
13-05-2014	98	41,709	96	189,489	103	107,695
27-05-2014	36	41,593	-	-	-	-
10-06-2014	62	36,352	71	134,546	25	65,020
24-06-2014	32	21,660	59	147,838	38	92,565
08-07-2014	95	41,471	104	127,475	66	96,092
22-07-2014	101	37,129	133	175,425	57	70,309
05-08-2014	118	50,139	180	126,859	95	70,946
19-08-2014	96	42,662	162	131,901	126	86,202
02-09-2014	122	33,872	93	132,931	118	83,460
16-09-2014	102	48,454	178	152,065	147	88,223
30-09-2014	168	54,716	178	169,811	164	95,846
14-10-2014	207	60,068	202	187,065	191	104,728
28-10-2014	194	82,414	192	280,403	190	120,628
11-11-2014	207	110,743	185	257,383	199	129,731
25-11-2014	184	205,703	185	325,715	158	172,381
09-12-2014	174	105,987	182	329,307	193	189,203
23-12-2014	95	115,076	98	195,776	114	155,596

06-01-2015	173	56,673	192	151,630	165	142,654
20-01-2015	148	78,811	196	167,110	190	145,786
03-02-2015	142	49,735	139	233,580	149	146,960
17-02-2015	137	84,060	177	193,236	189	152,551
03-03-2015	123	56,128	160	167,286	160	234,834
17-03-2015	146	67,638	144	271,097	164	225,091
31-03-2015	140	82,762	163	235,249	141	143,143
14-04-2015	171	59,508	194	275,073	196	128,971
28-04-2015	203	66,121	193	203,229	210	127,145
12-05-2015	185	72,608	205	198,015	200	112,073
26-05-2015	167	54,751	180	208,642	180	113,730
09-06-2015	21	48,047	-	-	-	-
23-06-2015	183	66,448	183	213,365	184	114,512
07-07-2015	202	63,334	209	204,884	212	130,455
21-07-2015	103	96,958	118	437,515	117	167,972
04-08-2015	208	119,545	195	228,145	195	126,177
18-08-2015	145	87,737	186	169,242	164	121,132
01-09-2015	120	90,566	94	152,349	144	107,601
15-09-2015	202	49,608	181	174,230	188	91,166
29-09-2015	140	69,840	181	251,130	155	109,000
13-10-2015	176	67,574	160	182,564	178	155,167
27-10-2015	144	98,070	169	183,723	169	160,823
10-11-2015	156	60,129	165	159,193	158	134,115
24-11-2015	106	87,894	163	180,679	144	169,808
08-12-2015	118	79,092	117	175,180	164	179,471

22-12-2015	80	67,212	78	144,076	80	105,614
05-01-2016	160	77,644	144	160,823	142	167,040
19-01-2016	144	65,652	128	137,358	165	226,549
02-02-2016	159	54,182	178	149,205	169	154,794
16-02-2016	159	107,252	160	130,084	162	163,288
01-03-2016	120	71,841	116	144,671	164	151,402
15-03-2016	63	42,421	125	167,403	111	134,243
29-03-2016	147	68,158	143	248,353	182	212,550
12-04-2016	180	94,133	179	279,257	194	203,407
26-04-2016	160	116,298	180	220,664	206	169,928
10-05-2016	162	97,876	163	234,201	210	168,959
24-05-2016	37	115,188	64	436,399	85	140,559
07-06-2016	101	172,883	118	276,470	124	137,055
21-06-2016	176	248,139	151	497,501	190	191,794
05-07-2016	149	407,205	135	405,404	128	184,588
19-07-2016	180	213,324	165	390,002	167	200,064
02-08-2016	182	231,132	185	215,657	198	187,930
16-08-2016	164	191,001	156	167,621	181	145,685
30-08-2016	182	264,630	184	324,338	205	162,921
13-09-2016	143	429,214	165	426,426	208	139,516
27-09-2016	184	244,921	160	383,495	193	144,296
11-10-2016	137	228,743	183	244,718	165	142,071
25-10-2016	181	109,267	206	170,780	198	136,230
08-11-2016	202	174,644	191	261,466	193	148,151
22-11-2016	184	83,265	189	106,766	201	128,583
06-12-2016	184	58,773	217	89,566	210	121,520
20-12-2016	148	83,540	146	105,596	155	120,712
03-01-2017	193	88,049	193	106,776	196	122,071
17-01-2017	190	129,985	209	140,140	215	145,831
31-01-2017	203	103,392	206	152,405	220	156,626
14-02-2017	200	172,626	200	162,118	216	108,749
28-02-2017	201	133,272	188	141,454	211	162,562
14-03-2017	196	248,811	185	173,146	189	151,810

28-03-2017	174	207,080	192	201,680	192	147,274
11-04-2017	221	357,079	211	378,940	204	165,147
25-04-2017	206	332,000	204	258,250	213	180,250
09-05-2017	143	353,080	139	322,881	163	256,922
23-05-2017	137	665,977	120	679,936	104	365,278
06-06-2017	64	350,644	-	-	40	191,269
20-06-2017	121	247,388	101	359,306	59	200,893
04-07-2017	160	379,379	199	453,623	159	303,630
18-07-2017	168	534,023	173	656,735	180	459,862
01-08-2017	187	475,707	150	729,884	198	325,312
15-08-2017	135	222,499	132	443,386	170	167,299
29-08-2017	185	352,849	174	554,283	155	299,314
12-09-2017	199	279,283	185	367,585	189	227,717
26-09-2017	175	100,825	142	233,958	156	125,463
10-10-2017	165	274,495	180	281,169	176	166,175
24-10-2017	112	187,347	114	371,901	88	248,585
07-11-2017	165	364,414	157	451,479	168	259,219
21-11-2017	195	258,411	200	276,156	192	191,601
05-12-2017	157	340,606	201	397,295	203	215,036
19-12-2017	96	237,726	78	239,005	98	187,991
02-01-2018	100	690,670	93	343,710	80	350,381
16-01-2018	140	461,086	104	212,921	115	404,115
30-01-2018	107	289,949	153	397,777	139	303,717
13-02-2018	111	330,340	148	293,956	174	178,014
27-02-2018	143	245,554	206	275,954	174	146,502
13-03-2018	179	470,839	161	435,402	209	165,535
27-03-2018	172	225,899	206	330,750	184	187,841
10-04-2018	141	227,410	129	305,081	131	164,286
24-04-2018	168	390,025	181	258,916	221	186,935
08-05-2018	105	137,772	105	285,694	130	154,234
22-05-2018	-	-	-	-	24	111,241
05-06-2018	139	555,167	143	806,407	104	145,965
19-06-2018	143	835,686	147	715,647	163	182,390
03-07-2018	145	403,615	119	451,505	125	176,129
17-07-2018	136	380,490	151	430,128	101	219,201
31-07-2018	164	343,162	115	394,069	120	215,118
14-08-2018	173	345,737	124	392,235	132	246,615
28-08-2018	51	518,710	38	779,104	52	177,985
11-09-2018	54	192,356	49	353,495	71	174,928
25-09-2018	85	210,210	118	287,692	94	130,592
09-10-2018	89	176,701	63	182,477	60	167,251
23-10-2018	91	316,042	101	261,634	93	149,134
06-11-2018	98	527,262	105	455,052	101	163,084

Average	131	162,204	139	254,056	138	157,067
SD	48	146,367	49	134,616	59	64,234

Appendix B — Overlap Tables

Table 7.2: Yearly and Static Overlap of RBM and PT

Yearly and Static Overlap of RBM and PT					
Period	Area (sq.m)			Overlap (%)	
	Overlap	RBM	PT	RBM	PT
2012	232,922	645,800	337,100	36%	69%
2013	184,525	416,900	247,100	44%	75%
2014	108,114	423,200	165,700	26%	65%
2015	129,482	471,100	208,300	27%	62%
2016	277,401	592,300	529,900	47%	52%
2017	442,690	970,400	850,400	46%	52%
2018	440,373	1,060,500	1,070,900	42%	41%
Static	276,121	587,300	464,400	47%	59%

Table 7.3: Yearly and Static Overlap of RBM and RST

Yearly and Static Overlap of RBM and RST					
Period	Area (sq.m)			Overlap (%)	
	Overlap	RBM	RST	RBM	RST
2011	163,995	431,400	363,400	38%	45%
2012	166,413	645,800	387,100	26%	43%
2013	108,609	416,900	286,200	26%	38%
2014	95,112	423,200	264,100	22%	36%
2015	125,946	471,100	342,800	27%	37%
2016	115,534	592,300	346,000	20%	33%
2017	209,102	970,400	587,400	22%	36%
2018	105,810	1,060,500	513,800	10%	21%
Static	146,869	587,300	333,600	25%	44%

Table 7.4: Yearly and Static Overlap of RST and PT

Yearly and Static Overlap of RST and PT					
Period	Area (sq.m)			Overlap (%)	
	Overlap	RST	PT	RST	PT
2012	108,356	387,100	337,100	28%	32%
2013	56,097	286,200	247,100	20%	23%
2014	49,746	264,100	165,700	19%	30%
2015	72,087	342,800	208,300	21%	35%
2016	123,321	346,000	529,900	36%	23%
2017	233,454	587,400	850,400	40%	27%
2018	223,776	513,800	1,070,900	44%	21%
Static	127,202	333,600	464,400	38%	27%

Table 7.5: 14-Day Overlap Complete Table

14 Day Overlap Areas				
Date	**All**	**RBM/RST**	**RBM/PT**	**RST/PT**
18-10-2011	-	17,311	-	-
01-11-2011	-	196,625	-	-
15-11-2011	-	-	-	-

29-11-2011	-	98,133	-	-
13-12-2011	-	67,733	-	-
27-12-2011	-	-	-	-
10-01-2012	-	110,025	-	-
24-01-2012	-	161,279	-	-
07-02-2012	-	152,254	-	-
21-02-2012	-	121,156	-	-
06-03-2012	-	10,315	-	-
20-03-2012	-	93,433	-	-
03-04-2012	-	52,719	-	-
17-04-2012	-	101,239	-	-
01-05-2012	-	73,633	-	-
15-05-2012	-	91,359	-	-
29-05-2012	20,850	53,858	47,845	30,048
12-06-2012	13,307	52,466	66,759	18,888
26-06-2012	8,807	22,177	51,899	16,922
10-07-2012	29,386	62,013	112,981	34,833
24-07-2012	13,639	43,988	46,624	20,894
07-08-2012	15,749	16,474	57,955	36,844
21-08-2012	14,859	20,930	65,903	20,866
04-09-2012	-	-	-	28,368
18-09-2012	4,843	33,655	60,476	5,456
02-10-2012	32	10,168	22,897	19,840
16-10-2012	19,635	30,725	29,879	32,489
30-10-2012	12,548	45,184	31,097	20,663
13-11-2012	10,410	59,691	29,123	22,316
27-11-2012	25,674	66,783	93,402	38,473
11-12-2012	-	-	-	-
25-12-2012	-	21,054	-	-
08-01-2013	13,645	60,994	94,969	19,665
22-01-2013	25,098	115,527	75,843	28,051
05-02-2013	14,649	59,473	74,874	14,825
19-02-2013	17,757	85,199	69,700	28,143
05-03-2013	12,951	61,344	54,802	37,073
19-03-2013	-	-	-	-
02-04-2013	-	-	100,448	-
16-04-2013	4,901	13,645	56,152	5,192
30-04-2013	9,364	37,788	47,416	11,629
14-05-2013	9,096	54,897	45,853	14,463
28-05-2013	1,003	17,065	34,022	7,700
11-06-2013	-	-	34,458	-
25-06-2013	-	10,189	-	-
09-07-2013	22	16,807	115,024	335

23-07-2013	4,080	9,292	67,282	9,239
06-08-2013	243	10,353	39,440	2,887
20-08-2013	-	746	27,283	921
03-09-2013	-	7,402	33,544	-
17-09-2013	56	8,961	23,976	128
01-10-2013	669	5,112	44,064	8,152
15-10-2013	8,377	26,616	107,512	9,454
29-10-2013	2,373	23,593	164,796	2,663
12-11-2013	6,095	16,651	115,951	11,850
26-11-2013	5,983	25,506	110,119	14,322
10-12-2013	1,693	31,528	85,475	3,600
24-12-2013	155	17,645	54,447	2,047
07-01-2014	-	29,372	29,482	-
21-01-2014	3,103	23,256	63,162	10,999
04-02-2014	7,428	34,478	62,114	7,514
18-02-2014	5,050	51,119	47,974	5,949
04-03-2014	1,675	53,013	70,205	1,675
18-03-2014	8,943	59,816	61,911	10,044
01-04-2014	1,853	17,646	48,919	5,096
15-04-2014	11,766	29,928	62,583	21,939
29-04-2014	3,604	24,819	36,444	5,727
13-05-2014	2,076	19,557	31,483	4,659
27-05-2014	-	-	-	-
10-06-2014	-	-	4,001	5,615
24-06-2014	2,231	27,729	8,328	9,320
08-07-2014	334	4,650	14,832	5,994
22-07-2014	2,509	13,567	26,703	6,808
05-08-2014	5,102	11,628	20,007	10,557
19-08-2014	5,649	17,569	23,540	12,847
02-09-2014	2,651	21,553	20,880	3,151
16-09-2014	1,286	19,938	29,672	13,410
30-09-2014	4,755	26,804	37,962	16,568
14-10-2014	3,206	21,190	45,791	11,500
28-10-2014	15,856	69,081	79,124	32,857
11-11-2014	24,233	47,271	101,438	39,726
25-11-2014	17,437	71,868	140,499	35,761
09-12-2014	27,948	88,439	109,649	38,341
23-12-2014	7,177	31,643	72,937	46,139
06-01-2015	8,578	58,905	37,045	22,849
20-01-2015	4,030	36,882	54,260	19,610
03-02-2015	5,723	38,124	41,009	12,784
17-02-2015	7,614	37,766	72,604	28,615
03-03-2015	9,848	69,838	42,022	24,534

17-03-2015	20,966	85,903	58,069	41,820
31-03-2015	25,018	58,461	92,927	38,656
14-04-2015	10,736	56,458	64,543	17,897
28-04-2015	6,538	42,560	51,675	21,674
12-05-2015	9,467	57,574	52,746	32,201
26-05-2015	16,516	62,135	51,888	27,940
09-06-2015	-	-	-	-
23-06-2015	10,357	47,567	58,069	21,688
07-07-2015	8,532	39,046	46,410	19,663
21-07-2015	25,181	42,599	105,280	28,201
04-08-2015	24,938	51,361	77,077	36,559
18-08-2015	12,780	33,195	52,177	30,460
01-09-2015	2,320	4,553	43,912	30,057
15-09-2015	4,285	15,874	34,016	11,046
29-09-2015	10,965	37,062	62,825	19,071
13-10-2015	12,242	41,865	51,856	20,474
27-10-2015	31,053	93,539	84,736	43,837
10-11-2015	4,359	25,201	33,354	14,493
24-11-2015	16,035	43,678	71,136	24,996
08-12-2015	10,442	32,803	54,574	16,630
22-12-2015	3,268	24,513	39,379	9,192
05-01-2016	18,771	41,021	48,590	37,559
19-01-2016	21,570	65,743	41,081	44,967
02-02-2016	12,222	52,817	33,507	28,530
16-02-2016	21,011	47,748	72,406	49,627
01-03-2016	8,956	36,143	48,983	19,578
15-03-2016	7,798	31,015	39,052	10,597
29-03-2016	34,292	79,038	80,224	47,821
12-04-2016	41,279	103,135	102,198	49,853
26-04-2016	28,622	65,699	102,277	53,170
10-05-2016	47,713	108,066	94,458	63,358
24-05-2016	32,262	81,893	88,865	37,763
07-06-2016	31,166	55,847	94,733	52,183
21-06-2016	48,459	78,626	172,927	52,479
05-07-2016	42,549	47,268	245,032	68,815
19-07-2016	69,481	94,048	173,562	77,851
02-08-2016	35,648	76,112	161,505	74,944
16-08-2016	22,070	36,285	152,965	51,584
30-08-2016	24,365	56,740	175,959	40,192
13-09-2016	31,502	31,502	244,818	74,622
27-09-2016	23,969	23,969	150,119	57,412
11-10-2016	11,447	11,447	115,919	46,839
25-10-2016	1,891	1,891	53,810	20,873

08-11-2016	20,112	28,714	115,035	40,683
22-11-2016	3,904	3,904	42,942	20,777
06-12-2016	2,762	2,762	20,420	13,544
20-12-2016	4,000	9,902	29,751	23,951
03-01-2017	7,533	11,113	48,428	26,112
17-01-2017	8,436	13,057	68,102	20,565
31-01-2017	16,263	32,393	68,066	26,281
14-02-2017	14,109	20,656	118,259	30,421
28-02-2017	17,508	67,423	73,682	31,257
14-03-2017	24,222	46,643	120,170	44,587
28-03-2017	23,620	37,653	134,007	49,321
11-04-2017	62,400	78,081	247,431	90,695
25-04-2017	61,892	97,632	189,312	90,997
09-05-2017	65,997	130,221	177,043	109,204
23-05-2017	163,860	207,939	362,622	198,956
06-06-2017	-	-	-	117,724
20-06-2017	62,622	91,713	144,256	101,492
04-07-2017	143,936	170,016	246,983	236,185
18-07-2017	112,213	130,172	238,086	271,150
01-08-2017	106,432	112,336	313,962	191,789
15-08-2017	61,477	73,703	214,835	66,331
29-08-2017	73,342	74,316	260,758	138,608
12-09-2017	48,767	53,963	184,532	89,563
26-09-2017	19,669	31,998	123,654	20,162
10-10-2017	34,104	39,415	193,023	83,226
24-10-2017	35,666	65,593	217,941	62,398
07-11-2017	65,924	78,913	264,909	97,086
21-11-2017	59,250	68,120	177,881	88,574
05-12-2017	78,656	107,371	192,014	128,575
19-12-2017	27,304	40,152	116,971	57,115
02-01-2018	66,907	67,239	125,386	127,442
16-01-2018	31,744	68,062	130,674	98,680
30-01-2018	47,543	99,167	168,540	82,694
13-02-2018	42,801	56,233	144,718	86,840
27-02-2018	19,115	40,112	135,604	51,790
13-03-2018	22,535	23,729	228,644	83,584
27-03-2018	33,435	51,036	157,892	63,820
10-04-2018	10,761	11,108	161,102	52,774
24-04-2018	11,364	11,364	169,664	83,426
08-05-2018	22,725	28,443	134,953	42,166
22-05-2018	-	-	-	-
05-06-2018	9,211	9,211	281,906	49,778
19-06-2018	36,627	36,627	421,147	101,875

03-07-2018	50,884	51,219	245,129	82,223
17-07-2018	32,767	36,126	244,814	69,661
31-07-2018	35,194	35,194	213,347	79,570
14-08-2018	27,996	29,221	223,534	92,589
28-08-2018	8,569	10,853	328,647	23,026
11-09-2018	13,501	13,501	119,485	28,941
25-09-2018	9,862	9,862	162,493	12,693
09-10-2018	1,599	1,599	104,306	21,561
23-10-2018	3,762	3,762	150,972	13,700
06-11-2018	22,438	36,480	222,872	25,006
Min	22	746	4,001	128
Max	163,860	207,939	421,147	271,150
Average	22,078	48,776	103,446	41,507
SD	25,470	37,220	77,472	42,367

Appendix C — 14-Day DHR's for PT Troop in 2017

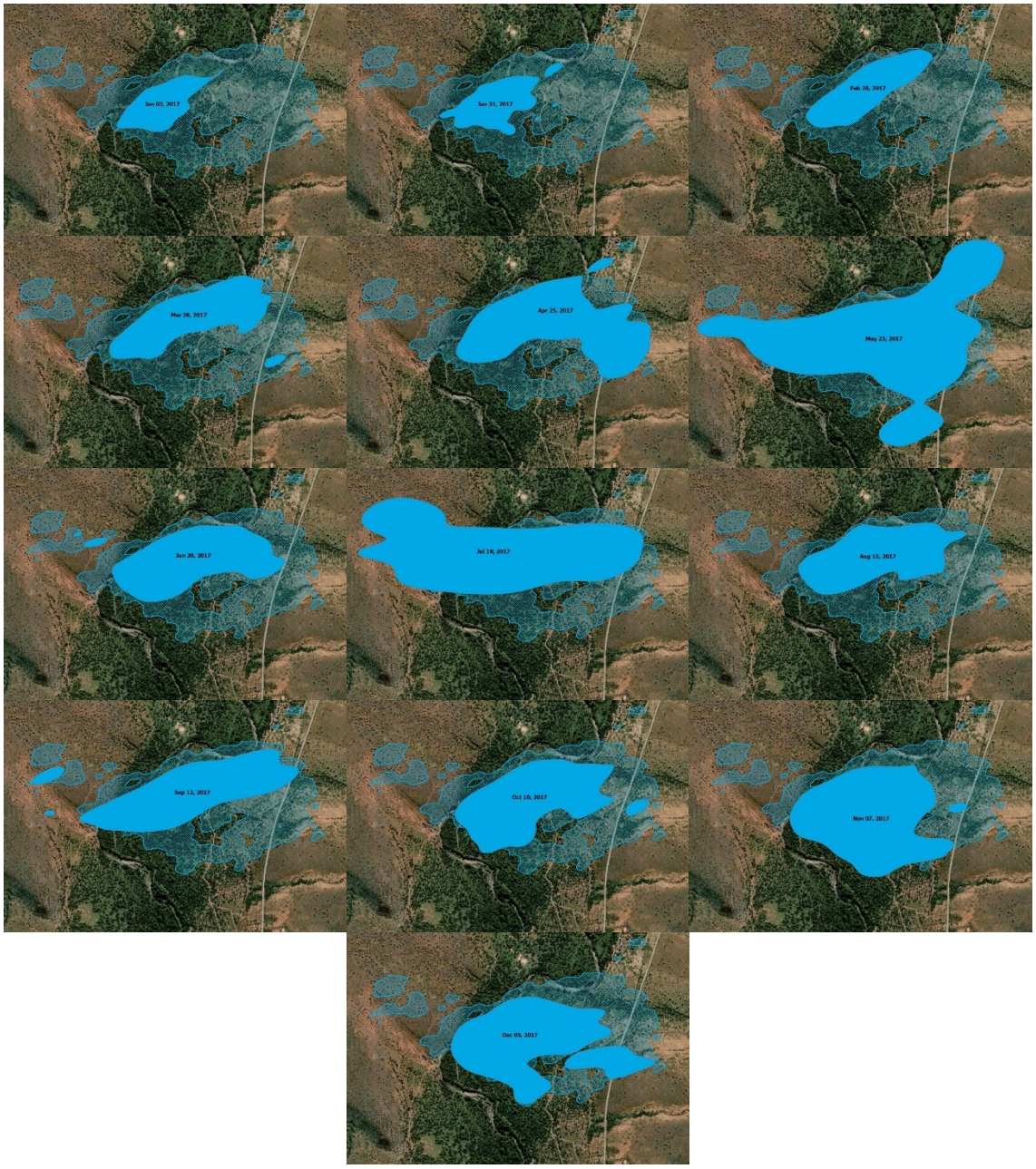

Figure 7.1: 14-day dynamic home ranges for all of 2017. From left to right and top to bottom: Jan 03, Jan 17, Jan 31, Feb 14, Feb 28, Mar 14, Mar 28 Apr 11, Apr 25, May 09, May 23, Jun 06, Jun 20, Jul 04, Jul 18, Aug 01, Aug 15, Aug 29, Sep 12, Sep 26, Oct 10, Oct 24, Nov 07, Nov 21, Dec 05, Dec 19

Appendix D: Summaries for Yearly Models

PT ITE Model

```
Family: bernoulli
  Links: mu = logit
Formula: WinB ~ TDCs + DeltaAgr1 + DeltaPart + InitB + (1 | Adversary)
   Data: PT.ITE (Number of observations: 959)
  Draws: 4 chains, each with iter = 3000; warmup = 1500; thin = 1;
         total post-warmup draws = 6000

Multilevel Hyperparameters:
~Adversary (Number of levels: 3)
              Estimate Est.Error l-95% CI u-95% CI Rhat Bulk_ESS Tail_ESS
sd(Intercept)     1.00      0.90     0.07     3.34 1.00     1571     2016

Regression Coefficients:
          Estimate Est.Error l-95% CI u-95% CI Rhat Bulk_ESS Tail_ESS
Intercept    -1.22      0.73    -2.44     0.63 1.00     1682     1926
TDCs         -0.23      0.10    -0.42    -0.04 1.00     4682     4058
DeltaAgr1     0.84      0.27     0.30     1.39 1.00     4740     4316
DeltaPart     0.03      0.01     0.01     0.04 1.00     5136     4414
InitB         0.95      0.17     0.63     1.27 1.00     4809     3927

Draws were sampled using sampling(NUTS). For each parameter, Bulk_ESS
and Tail_ESS are effective sample size measures, and Rhat is the potential
scale reduction factor on split chains (at convergence, Rhat = 1).

    Estimate  Est.Error      Q2.5     Q97.5
R2 0.1010324 0.01780945 0.0675535 0.1375783

Probability of Direction

Parameter   |     pd
--------------------
(Intercept) | 94.07%
TDCs        | 99.20%
DeltaAgr1   | 99.93%
DeltaPart   | 99.82%
InitB       |   100%
```

RBM ITE Model

```
Family: bernoulli
  Links: mu = logit
Formula: WinB ~ TDCs + DeltaAgr1 + DeltaPart + InitB + (1 | Adversary)
   Data: RBM.ITE (Number of observations: 837)
  Draws: 4 chains, each with iter = 3000; warmup = 1500; thin = 1;
         total post-warmup draws = 6000

Multilevel Hyperparameters:
~Adversary (Number of levels: 3)
              Estimate Est.Error l-95% CI u-95% CI Rhat Bulk_ESS Tail_ESS
sd(Intercept)     0.66      0.80     0.01     2.94 1.00     1461     1949

Regression Coefficients:
          Estimate Est.Error l-95% CI u-95% CI Rhat Bulk_ESS Tail_ESS
Intercept    -1.39      0.56    -2.72    -0.32 1.00     1564     1330
TDCs          0.23      0.08     0.09     0.38 1.00     4908     3807
DeltaAgr1     1.83      0.29     1.29     2.42 1.00     4047     3718
DeltaPart     0.01      0.01    -0.01     0.03 1.00     4955     4201
InitB         1.51      0.18     1.16     1.87 1.00     4054     4097

Draws were sampled using sampling(NUTS). For each parameter, Bulk_ESS
and Tail_ESS are effective sample size measures, and Rhat is the potential
scale reduction factor on split chains (at convergence, Rhat = 1).

    Estimate Est.Error      Q2.5      Q97.5
R2 0.2284926  0.020102 0.1878997 0.2664346

Probability of Direction

Parameter   |     pd
--------------------
(Intercept) | 98.73%
TDCs        | 99.80%
DeltaAgr1   |   100%
DeltaPart   | 89.13%
InitB       |   100%
```

RST ITE Model

```
Family: bernoulli
  Links: mu = logit
Formula: WinB ~ TDCs + DeltaAgr1 + DeltaPart + InitB + (1 | Adversary)
   Data: RST.ITE (Number of observations: 430)
  Draws: 4 chains, each with iter = 3000; warmup = 1500; thin = 1;
         total post-warmup draws = 6000

Multilevel Hyperparameters:
~Adversary (Number of levels: 2)
              Estimate Est.Error l-95% CI u-95% CI Rhat Bulk_ESS Tail_ESS
sd(Intercept)     0.88      1.04     0.02     3.86 1.00     1345     2251

Regression Coefficients:
          Estimate Est.Error l-95% CI u-95% CI Rhat Bulk_ESS Tail_ESS
Intercept    -0.88      0.72    -2.49     0.63 1.00     1884     1713
TDCs         -0.16      0.18    -0.52     0.18 1.00     5108     3647
DeltaAgr1     1.42      0.36     0.73     2.13 1.00     4779     4140
DeltaPart     0.04      0.01     0.01     0.06 1.00     5051     3752
InitB         0.95      0.22     0.53     1.40 1.00     5232     3698

Draws were sampled using sampling(NUTS). For each parameter, Bulk_ESS
and Tail_ESS are effective sample size measures, and Rhat is the potential
scale reduction factor on split chains (at convergence, Rhat = 1).
   Estimate Est.Error       Q2.5    Q97.5
R2 0.124778 0.0244806 0.07758384 0.172205
              prior     class      coef     group resp dpar nlpar lb ub       source
         normal(0, 1)         b                                          user
         normal(0, 1)         b DeltaAgr1                          (vectorized)
         normal(0, 1)         b DeltaPart                          (vectorized)
         normal(0, 1)         b     InitB                          (vectorized)
         normal(0, 1)         b      TDCs                          (vectorized)
 student_t(3, 0, 2.5) Intercept                                         default
 student_t(3, 0, 2.5)        sd                                0         default
 student_t(3, 0, 2.5)        sd          Adversary                 0    (vectorized)
 student_t(3, 0, 2.5)        sd Intercept Adversary                0    (vectorized)

Probability of Direction

Parameter   |     pd
---------------------
(Intercept) | 92.40%
TDCs        | 81.48%
DeltaAgr1   |   100%
DeltaPart   | 99.90%
InitB       |   100%
```

Appendix E: DHR Tables

Model Variables

Table 7.6: Multiday Win Models from 14 to 168 day windows.

Model	Troop	Days	Divergent	Adversary SD	ICC	R^2 (Mean)	Intercept	pd(Inter)
PT.Win_14d	PT	14	0	1.06	0.25	0.099525	-1.2	94.53%
PT.Win_21d	PT	21	1	1.10	0.27	0.099775	-1.2	93.00%
PT.Win_28d	PT	28	0	1.09	0.27	0.098743	-1.13	92.40%
PT.Win_35d	PT	35	0	1.03	0.24	0.099016	-1.19	94.33%
PT.Win_42d	PT	42	0	0.99	0.23	0.101086	-1.21	94.62%
PT.Win_84d	PT	84	0	1.08	0.26	0.098890	-1.17	93.08%
PT.Win_168d	PT	168	1	1.09	0.27	0.101430	-1.2	93.47%
RBM.Win_14d	RBM	14	13	0.71	0.13	0.215993	-1.4	98.42%
RBM.Win_21d	RBM	21	4	0.76	0.15	0.226152	-1.46	98.50%
RBM.Win_28d	RBM	28	10	0.71	0.13	0.220755	-1.43	98.67%
RBM.Win_35d	RBM	35	4	0.71	0.13	0.226735	-1.48	98.75%
RBM.Win_42d	RBM	42	3	0.77	0.15	0.225102	-1.47	97.97%
RBM.Win_84d	RBM	84	7	0.71	0.13	0.219737	-1.41	98.58%
RBM.Win_168d	RBM	168	10	0.72	0.14	0.220462	-1.39	98.28%
RST.Win_14d	RST	14	4	0.88	0.19	0.123933	-0.87	92.30%
RST.Win_21d	RST	21	0	0.82	0.17	0.124911	-0.82	92.55%
RST.Win_28d	RST	28	3	0.87	0.19	0.125548	-0.84	92.47%
RST.Win_35d	RST	35	1	0.84	0.18	0.126504	-0.87	93.12%
RST.Win_42d	RST	42	0	0.86	0.18	0.122614	-0.82	92.12%
RST.Win_84d	RST	84	1	0.82	0.17	0.125136	-0.8	90.97%
RST.Win_168d	RST	168	0	0.91	0.20	0.125588	-0.89	92.22%

Model	TDCs	TDCs CIs		pd(TDCs)	ΔAgr	ΔAgr CIs		pd(ΔAgr)	ΔPart	ΔPart CI		pd(ΔPart)	InitB	InitB		pd(InitB)
PT.Win_14d	-0.15	-0.34	0.03	95.12%	0.86	0.32	1.42	99.92%	0.03	0.01	0.04	99.70%	0.97	0.65	1.30	100%
PT.Win_21d	-0.17	-0.35	0.01	96.47%	0.86	0.35	1.38	100.00%	0.03	0.01	0.04	99.72%	0.98	0.65	1.30	100%
PT.Win_28d	-0.14	-0.32	0.04	93.30%	0.86	0.33	1.41	99.95%	0.03	0.01	0.04	99.72%	0.98	0.66	1.31	100%
PT.Win_35d	-0.16	-0.35	0.02	96.00%	0.85	0.33	1.39	99.92%	0.03	0.01	0.04	99.80%	0.98	0.67	1.29	100%
PT.Win_42d	-0.21	-0.40	-0.02	98.52%	0.85	0.32	1.38	99.90%	0.03	0.01	0.04	99.80%	0.97	0.64	1.31	100%
PT.Win_84d	-0.18	-0.39	0.01	96.78%	0.84	0.34	1.38	99.90%	0.03	0.01	0.04	99.88%	0.97	0.64	1.29	100%
PT.Win_168d	-0.12	-0.31	0.06	90.20%	0.82	0.29	1.34	99.88%	0.03	0.01	0.04	99.85%	1.03	0.70	1.36	100%
RBM.Win_14d	0.03	-0.12	0.17	63.73%	1.93	1.38	2.48	100%	0.01	-0.01	0.03	87.92%	1.5	1.17	1.84	100%
RBM.Win_21d	0.2	0.06	0.34	99.65%	1.9	1.31	2.48	100%	0.01	-0.01	0.03	88.83%	1.51	1.17	1.83	100%
RBM.Win_28d	0.11	-0.04	0.25	92.17%	1.91	1.35	2.49	100%	0.01	-0.01	0.03	88.20%	1.52	1.18	1.87	100%
RBM.Win_35d	0.21	0.07	0.34	99.90%	1.88	1.33	2.45	100%	0.01	-0.01	0.03	88.35%	1.51	1.18	1.87	100%
RBM.Win_42d	0.17	0.04	0.31	99.42%	1.89	1.32	2.46	100%	0.01	-0.01	0.03	89.30%	1.51	1.18	1.86	100%
RBM.Win_84d	0.1	-0.05	0.24	91.45%	1.9	1.35	2.48	100%	0.01	-0.01	0.03	88.42%	1.51	1.16	1.86	100%
RBM.Win_168d	0.1	-0.03	0.24	92.12%	1.8	1.23	2.38	100%	0.01	-0.01	0.03	86.78%	1.56	1.20	1.91	100%
RST.Win_14d	0.12	-0.16	0.39	78.90%	1.41	0.73	2.11	100%	0.04	0.02	0.06	100.00%	0.94	0.51	1.36	100%
RST.Win_21d	0.12	-0.16	0.39	80.50%	1.41	0.76	2.13	100%	0.04	0.02	0.06	99.98%	0.94	0.52	1.37	100%
RST.Win_28d	0.15	-0.13	0.44	84.75%	1.38	0.69	2.09	100%	0.04	0.02	0.06	99.98%	0.96	0.54	1.40	100%
RST.Win_35d	0.17	-0.12	0.47	86.67%	1.39	0.72	2.09	100%	0.04	0.02	0.07	99.95%	0.96	0.52	1.42	100%
RST.Win_42d	0.08	-0.22	0.38	69.38%	1.4	0.71	2.10	100%	0.04	0.02	0.06	99.92%	0.94	0.50	1.39	100%
RST.Win_84d	0.16	-0.12	0.44	86.42%	1.4	0.72	2.10	100%	0.04	0.02	0.06	100%	0.94	0.52	1.36	100%
RST.Win_168d	-0.1	-0.46	0.25	71.20%	1.37	0.69	2.06	100%	0.04	0.02	0.06	99.98%	0.99	0.56	1.41	100%

Precision Table

Table 7.7: Precision Table for Multiday Win Models

Model	TDCs Rel Width	ΔAgr Rel Width	ΔPart Rel Width	Init Rel Width	TDCs Precision	ΔAgr Precision	ΔPart Precision	Init Precision
PT.Win_14d	2.47	1.28	1.00	0.67	Very low precision	Very low precision	Low precision	Low precision
PT.Win_21d	2.12	1.20	1.00	0.66	Very low precision	Very low precision	Low precision	Low precision
PT.Win_28d	2.57	1.26	1.00	0.66	Very low precision	Very low precision	Low precision	Low precision
PT.Win_35d	2.31	1.25	1.00	0.63	Very low precision	Very low precision	Low precision	Low precision
PT.Win_42d	1.81	1.25	1.00	0.69	Very low precision	Very low precision	Low precision	Low precision
PT.Win_84d	2.22	1.24	1.00	0.67	Very low precision	Very low precision	Low precision	Low precision
PT.Win_168d	3.08	1.28	1.00	0.64	Very low precision	Very low precision	Low precision	Low precision
RBM.Win_14d	9.67	0.57	4.00	0.45	Very low precision	Low precision	Very low precision	Moderate precision
RBM.Win_21d	1.40	0.62	4.00	0.44	Very low precision	Low precision	Very low precision	Moderate precision
RBM.Win_28d	2.64	0.60	4.00	0.45	Very low precision	Low precision	Very low precision	Moderate precision
RBM.Win_35d	1.29	0.60	4.00	0.46	Very low precision	Low precision	Very low precision	Moderate precision
RBM.Win_42d	1.59	0.60	4.00	0.45	Very low precision	Low precision	Very low precision	Moderate precision
RBM.Win_84d	2.90	0.59	4.00	0.46	Very low precision	Low precision	Very low precision	Moderate precision
RBM.Win_168d	2.70	0.64	4.00	0.46	Very low precision	Low precision	Very low precision	Moderate precision
RST.Win_14d	4.58	0.98	1.00	0.90	Very low precision	Low precision	Low precision	Low precision
RST.Win_21d	4.58	0.97	1.00	0.90	Very low precision	Low precision	Low precision	Low precision
RST.Win_28d	3.80	1.01	1.00	0.90	Very low precision	Very low precision	Low precision	Low precision
RST.Win_35d	3.47	0.99	1.25	0.94	Very low precision	Low precision	Very low precision	Low precision
RST.Win_42d	7.50	0.99	1.00	0.95	Very low precision	Low precision	Low precision	Low precision
RST.Win_84d	3.50	0.99	1.00	0.89	Very low precision	Low precision	Low precision	Low precision
RST.Win_168d	7.10	1.00	1.00	0.86	Very low precision	Low precision	Low precision	Low precision

Effect Size Table

Table 7.8: Effect Size Table for Multiday Win Models

Model	exp(TDCs)	exp(ΔAgr)	exp(ΔPart)	exp(Init)	TDCs Strength	ΔAgr Strength	ΔPart Strength	Init Strength
PT.Win_14d	0.8607	2.3632	1.0305	2.6379	Very weak effect (negative)	Moderate effect	Very weak effect	Moderate effect
PT.Win_21d	0.8437	2.3632	1.0305	2.6645	Very weak effect (negative)	Moderate effect	Very weak effect	Moderate effect
PT.Win_28d	0.8694	2.3632	1.0305	2.6645	Very weak effect (negative)	Moderate effect	Very weak effect	Moderate effect
PT.Win_35d	0.8521	2.3396	1.0305	2.6645	Very weak effect (negative)	Moderate effect	Very weak effect	Moderate effect
PT.Win_42d	0.8106	2.3396	1.0305	2.6379	Very weak effect (negative)	Moderate effect	Very weak effect	Moderate effect
PT.Win_84d	0.8353	2.3164	1.0305	2.6379	Very weak effect (negative)	Moderate effect	Very weak effect	Moderate effect
PT.Win_168d	0.8869	2.2705	1.0305	2.8011	Very weak effect (negative)	Moderate effect	Very weak effect	Strong effect
RBM.Win_14d	1.0305	6.8895	1.0101	4.4817	Very weak effect	Strong effect	Very weak effect	Strong effect
RBM.Win_21d	1.2214	6.6859	1.0101	4.5267	Very weak effect	Strong effect	Very weak effect	Strong effect
RBM.Win_28d	1.1163	6.7531	1.0101	4.5722	Very weak effect	Strong effect	Very weak effect	Strong effect
RBM.Win_35d	1.2337	6.5535	1.0101	4.5267	Small effect	Strong effect	Very weak effect	Strong effect
RBM.Win_42d	1.1853	6.6194	1.0101	4.5267	Very weak effect	Strong effect	Very weak effect	Strong effect
RBM.Win_84d	1.1052	6.6859	1.0101	4.5267	Very weak effect	Strong effect	Very weak effect	Strong effect
RBM.Win_168d	1.1052	6.0496	1.0101	4.7588	Very weak effect	Strong effect	Very weak effect	Strong effect
RST.Win_14d	1.1275	4.0960	1.0408	2.5600	Very weak effect	Strong effect	Very weak effect	Moderate effect
RST.Win_21d	1.1275	4.0960	1.0408	2.5600	Very weak effect	Strong effect	Very weak effect	Moderate effect
RST.Win_28d	1.1618	3.9749	1.0408	2.6117	Very weak effect	Strong effect	Very weak effect	Moderate effect
RST.Win_35d	1.1853	4.0149	1.0408	2.6117	Very weak effect	Strong effect	Very weak effect	Moderate effect
RST.Win_42d	1.0833	4.0552	1.0408	2.5600	Very weak effect	Strong effect	Very weak effect	Moderate effect
RST.Win_84d	1.1735	4.0552	1.0408	2.5600	Very weak effect	Strong effect	Very weak effect	Moderate effect
RST.Win_168d	0.9048	3.9354	1.0408	2.6912	Very weak effect (negative)	Strong effect	Very weak effect	Moderate effect

Appendix F: DHR Model Summaries

PT DHR Models

[1] "Summary for: PT.Win_14d"

```
 Family: bernoulli
  Links: mu = logit
Formula: WinB ~ TDCs + DeltaAgr1 + DeltaPart + InitB + (1 | Adversary)
   Data: df_content (Number of observations: 957)
  Draws: 4 chains, each with iter = 2000; warmup = 1000; thin = 1;
         total post-warmup draws = 4000

Multilevel Hyperparameters:
~Adversary (Number of levels: 3)
              Estimate Est.Error l-95% CI u-95% CI Rhat Bulk_ESS Tail_ESS
sd(Intercept)     1.06      0.86     0.15     3.18 1.00     1207     1558

Regression Coefficients:
          Estimate Est.Error l-95% CI u-95% CI Rhat Bulk_ESS Tail_ESS
Intercept    -1.20      0.70    -2.50     0.42 1.00     1153     1410
TDCs         -0.15      0.09    -0.34     0.03 1.00     4015     2976
DeltaAgr1     0.86      0.28     0.32     1.42 1.00     3116     2866
DeltaPart     0.03      0.01     0.01     0.04 1.00     3640     2645
InitB         0.97      0.17     0.65     1.30 1.00     3401     2634

Draws were sampled using sampling(NUTS). For each parameter, Bulk_ESS
and Tail_ESS are effective sample size measures, and Rhat is the potential
scale reduction factor on split chains (at convergence, Rhat = 1).

    Estimate  Est.Error       Q2.5      Q97.5
R2 0.09952499 0.01806864 0.06471145 0.1358156

Probability of Direction

Parameter   |     pd
--------------------
(Intercept) | 94.53%
TDCs        | 95.12%
DeltaAgr1   | 99.92%
DeltaPart   | 99.70%
InitB       |   100%
```

[2] "Summary for: PT.Win_21d"

Family: bernoulli

  Links: mu = logit
Formula: WinB ~ TDCs + DeltaAgr1 + DeltaPart + InitB + (1 | Adversary)
   Data: df_content (Number of observations: 959)
  Draws: 4 chains, each with iter = 2000; warmup = 1000; thin = 1;
         total post-warmup draws = 4000

Multilevel Hyperparameters:
~Adversary (Number of levels: 3)
              Estimate Est.Error l-95% CI u-95% CI Rhat Bulk_ESS Tail_ESS
sd(Intercept)   1.10   1.00   0.12   3.70 1.00   956   1290

Regression Coefficients:
          Estimate Est.Error l-95% CI u-95% CI Rhat Bulk_ESS Tail_ESS
Intercept   -1.20   0.81   -2.56   0.74 1.00   1168   1342
TDCs   -0.17   0.09   -0.35   0.01 1.00   3335   2497
DeltaAgr1   0.86   0.27   0.35   1.38 1.00   3417   2858
DeltaPart   0.03   0.01   0.01   0.04 1.00   3466   2733
InitB   0.98   0.17   0.65   1.30 1.00   4111   2393

Draws were sampled using sampling(NUTS). For each parameter, Bulk_ESS
and Tail_ESS are effective sample size measures, and Rhat is the potential
scale reduction factor on split chains (at convergence, Rhat = 1).

    Estimate Est.Error   Q2.5   Q97.5
R2 0.09977536 0.01791887 0.06612948 0.1362894

Probability of Direction

Parameter | pd

(Intercept) | 93.00%
TDCs | 96.47%
DeltaAgr1 | 100%
DeltaPart | 99.72%
InitB | 100%

[3] "Summary for: PT.Win_28d"

```
 Family: bernoulli
  Links: mu = logit
Formula: WinB ~ TDCs + DeltaAgr1 + DeltaPart + InitB + (1 | Adversary)
   Data: df_content (Number of observations: 959)
  Draws: 4 chains, each with iter = 2000; warmup = 1000; thin = 1;
         total post-warmup draws = 4000

Multilevel Hyperparameters:
~Adversary (Number of levels: 3)
              Estimate Est.Error l-95% CI u-95% CI Rhat Bulk_ESS Tail_ESS
sd(Intercept)     1.09      0.88     0.15     3.40 1.01      881     1315

Regression Coefficients:
           Estimate Est.Error l-95% CI u-95% CI Rhat Bulk_ESS Tail_ESS
Intercept    -1.13      0.73    -2.40     0.56 1.00     1282     1644
TDCs         -0.14      0.09    -0.32     0.04 1.00     3815     2783
DeltaAgr1     0.86      0.28     0.33     1.41 1.00     2717     2417
DeltaPart     0.03      0.01     0.01     0.04 1.00     3325     2731
InitB         0.98      0.17     0.66     1.31 1.00     3547     2801

Draws were sampled using sampling(NUTS). For each parameter, Bulk_ESS
and Tail_ESS are effective sample size measures, and Rhat is the potential
scale reduction factor on split chains (at convergence, Rhat = 1).

    Estimate  Est.Error       Q2.5     Q97.5
R2 0.09874293 0.01787556 0.06443793 0.1349946

Probability of Direction

Parameter   |     pd
--------------------
(Intercept) | 92.40%
TDCs        | 93.30%
DeltaAgr1   | 99.95%
DeltaPart   | 99.72%
InitB       |   100%
```

[4] "Summary for: PT.Win_35d"

```
 Family: bernoulli
  Links: mu = logit
Formula: WinB ~ TDCs + DeltaAgr1 + DeltaPart + InitB + (1 | Adversary)
   Data: df_content (Number of observations: 959)
  Draws: 4 chains, each with iter = 2000; warmup = 1000; thin = 1;
         total post-warmup draws = 4000

Multilevel Hyperparameters:
~Adversary (Number of levels: 3)
              Estimate Est.Error l-95% CI u-95% CI Rhat Bulk_ESS Tail_ESS
sd(Intercept)     1.03      0.91     0.12     3.35 1.01      776     1340

Regression Coefficients:
           Estimate Est.Error l-95% CI u-95% CI Rhat Bulk_ESS Tail_ESS
Intercept    -1.19      0.70    -2.35     0.59 1.00     1137     1050
TDCs         -0.16      0.09    -0.35     0.02 1.00     3286     2561
DeltaAgr1     0.85      0.27     0.33     1.39 1.00     3128     2581
DeltaPart     0.03      0.01     0.01     0.04 1.00     3431     2343
InitB         0.98      0.16     0.67     1.29 1.00     3262     2515

Draws were sampled using sampling(NUTS). For each parameter, Bulk_ESS
and Tail_ESS are effective sample size measures, and Rhat is the potential
scale reduction factor on split chains (at convergence, Rhat = 1).

    Estimate  Est.Error       Q2.5     Q97.5
R2 0.09901632 0.01769241 0.06607106 0.1334639

Probability of Direction

Parameter   |     pd
--------------------
(Intercept) | 94.33%
TDCs        | 96.00%
DeltaAgr1   | 99.92%
DeltaPart   | 99.80%
InitB       |   100%
```

[5] "Summary for: PT.Win_42d"

```
 Family: bernoulli
  Links: mu = logit
Formula: WinB ~ TDCs + DeltaAgr1 + DeltaPart + InitB + (1 | Adversary)
   Data: df_content (Number of observations: 958)
  Draws: 4 chains, each with iter = 2000; warmup = 1000; thin = 1;
         total post-warmup draws = 4000

Multilevel Hyperparameters:
~Adversary (Number of levels: 3)
              Estimate Est.Error l-95% CI u-95% CI Rhat Bulk_ESS Tail_ESS
sd(Intercept)     0.99      0.87     0.11     3.34 1.00     1007     1416

Regression Coefficients:
          Estimate Est.Error l-95% CI u-95% CI Rhat Bulk_ESS Tail_ESS
Intercept    -1.21      0.69    -2.44     0.38 1.00     1085     1290
TDCs         -0.21      0.10    -0.40    -0.02 1.00     3806     2737
DeltaAgr1     0.85      0.27     0.32     1.38 1.00     3892     2572
DeltaPart     0.03      0.01     0.01     0.04 1.00     3610     2316
InitB         0.97      0.17     0.64     1.31 1.00     3572     2335

Draws were sampled using sampling(NUTS). For each parameter, Bulk_ESS
and Tail_ESS are effective sample size measures, and Rhat is the potential
scale reduction factor on split chains (at convergence, Rhat = 1).

    Estimate  Est.Error       Q2.5     Q97.5
R2 0.1010863 0.01820918 0.06757023 0.1382981

Probability of Direction

Parameter   |     pd
--------------------
(Intercept) | 94.62%
TDCs        | 98.52%
DeltaAgr1   | 99.90%
DeltaPart   | 99.80%
InitB       |   100%
```

[6] "Summary for: PT.Win_84d"

```
 Family: bernoulli
  Links: mu = logit
Formula: WinB ~ TDCs + DeltaAgr1 + DeltaPart + InitB + (1 | Adversary)
   Data: df_content (Number of observations: 957)
  Draws: 4 chains, each with iter = 2000; warmup = 1000; thin = 1;
         total post-warmup draws = 4000

Multilevel Hyperparameters:
~Adversary (Number of levels: 3)
              Estimate Est.Error l-95% CI u-95% CI Rhat Bulk_ESS Tail_ESS
sd(Intercept)     1.08      0.97     0.10     3.55 1.00      991     1454

Regression Coefficients:
           Estimate Est.Error l-95% CI u-95% CI Rhat Bulk_ESS Tail_ESS
Intercept    -1.17      0.73    -2.42     0.60 1.00     1142     1220
TDCs         -0.18      0.10    -0.39     0.01 1.00     3671     2755
DeltaAgr1     0.84      0.27     0.34     1.38 1.00     3504     2714
DeltaPart     0.03      0.01     0.01     0.04 1.00     4105     2771
InitB         0.97      0.16     0.64     1.29 1.00     3405     2674

Draws were sampled using sampling(NUTS). For each parameter, Bulk_ESS
and Tail_ESS are effective sample size measures, and Rhat is the potential
scale reduction factor on split chains (at convergence, Rhat = 1).

    Estimate  Est.Error       Q2.5     Q97.5
R2 0.09889027 0.01776929 0.06451173 0.1343085

Probability of Direction

Parameter   |     pd
--------------------
(Intercept) | 93.08%
TDCs        | 96.78%
DeltaAgr1   | 99.90%
DeltaPart   | 99.88%
InitB       |   100%
```

[7] "Summary for: PT.Win_168d"

Family: bernoulli

  Links: mu = logit
Formula: WinB ~ TDCs + DeltaAgr1 + DeltaPart + InitB + (1 | Adversary)
   Data: df_content (Number of observations: 947)
  Draws: 4 chains, each with iter = 2000; warmup = 1000; thin = 1;
         total post-warmup draws = 4000

Multilevel Hyperparameters:
~Adversary (Number of levels: 3)
              Estimate Est.Error l-95% CI u-95% CI Rhat Bulk_ESS Tail_ESS
sd(Intercept)   1.09   0.96   0.12   3.64 1.00   848   1088

Regression Coefficients:
          Estimate Est.Error l-95% CI u-95% CI Rhat Bulk_ESS Tail_ESS
Intercept   -1.20   0.78   -2.69   0.69 1.00   1419   1224
TDCs   -0.12   0.10   -0.31   0.06 1.00   3529   2831
DeltaAgr1   0.82   0.27   0.29   1.34 1.00   3256   2754
DeltaPart   0.03   0.01   0.01   0.04 1.00   3929   2856
InitB   1.03   0.17   0.70   1.36 1.00   3473   2853

Draws were sampled using sampling(NUTS). For each parameter, Bulk_ESS
and Tail_ESS are effective sample size measures, and Rhat is the potential
scale reduction factor on split chains (at convergence, Rhat = 1).

   Estimate Est.Error   Q2.5   Q97.5
R2 0.1014295 0.01804152 0.06677915 0.137624

Probability of Direction

Parameter | pd

(Intercept) | 93.47%
TDCs | 90.20%
DeltaAgr1 | 99.88%
DeltaPart | 99.85%
InitB | 100%

RBM DHR Models

[8] "Summary for: RBM.Win_14d"

Family: bernoulli

  Links: mu = logit
Formula: WinB ~ TDCs + DeltaAgr1 + DeltaPart + InitB + (1 | Adversary)
   Data: df_content (Number of observations: 833)
  Draws: 4 chains, each with iter = 2000; warmup = 1000; thin = 1;
         total post-warmup draws = 4000

Multilevel Hyperparameters:
~Adversary (Number of levels: 3)
              Estimate Est.Error l-95% CI u-95% CI Rhat Bulk_ESS Tail_ESS
sd(Intercept)   0.71   0.89   0.01   3.24 1.00   883   1602

Regression Coefficients:
          Estimate Est.Error l-95% CI u-95% CI Rhat Bulk_ESS Tail_ESS
Intercept   -1.40   0.61   -3.01   -0.24 1.00   1162   910
TDCs   0.03   0.07   -0.12   0.17 1.00   3691   2870
DeltaAgr1   1.93   0.29   1.38   2.48 1.00   3794   2843
DeltaPart   0.01   0.01   -0.01   0.03 1.00   3606   3006
InitB   1.50   0.17   1.17   1.84 1.00   3158   2964

Draws were sampled using sampling(NUTS). For each parameter, Bulk_ESS
and Tail_ESS are effective sample size measures, and Rhat is the potential
scale reduction factor on split chains (at convergence, Rhat = 1).

   Estimate Est.Error   Q2.5   Q97.5
R2 0.2159931 0.0193892 0.1768992 0.2527872

Probability of Direction

Parameter | pd

(Intercept) | 98.42%
TDCs | 63.73%
DeltaAgr1 | 100%
DeltaPart | 87.92%
InitB | 100%

[9] "Summary for: RBM.Win_21d"

Family: bernoulli

  Links: mu = logit
Formula: WinB ~ TDCs + DeltaAgr1 + DeltaPart + InitB + (1 | Adversary)
   Data: df_content (Number of observations: 837)
  Draws: 4 chains, each with iter = 2000; warmup = 1000; thin = 1;
         total post-warmup draws = 4000

Multilevel Hyperparameters:
~Adversary (Number of levels: 3)
              Estimate Est.Error l-95% CI u-95% CI Rhat Bulk_ESS Tail_ESS
sd(Intercept)   0.76   0.94   0.02   3.41 1.00   890   2059

Regression Coefficients:
          Estimate Est.Error l-95% CI u-95% CI Rhat Bulk_ESS Tail_ESS
Intercept   -1.46   0.62   -3.04   -0.33 1.00   1345   1104
TDCs   0.20   0.07   0.06   0.34 1.00   3787   2215
DeltaAgr1   1.90   0.29   1.31   2.48 1.00   2916   2763
DeltaPart   0.01   0.01   -0.01   0.03 1.00   4318   3103
InitB   1.51   0.17   1.17   1.83 1.00   3642   2890

Draws were sampled using sampling(NUTS). For each parameter, Bulk_ESS
and Tail_ESS are effective sample size measures, and Rhat is the potential
scale reduction factor on split chains (at convergence, Rhat = 1).

    Estimate Est.Error   Q2.5   Q97.5
R2 0.2261516 0.01934163 0.1866244 0.2619764

Probability of Direction

Parameter | pd

(Intercept) | 98.50%
TDCs | 99.65%
DeltaAgr1 | 100%
DeltaPart | 88.83%
InitB | 100%

[10] "Summary for: RBM.Win_28d"

Family: bernoulli

  Links: mu = logit
Formula: WinB ~ TDCs + DeltaAgr1 + DeltaPart + InitB + (1 | Adversary)
   Data: df_content (Number of observations: 837)
  Draws: 4 chains, each with iter = 2000; warmup = 1000; thin = 1;
         total post-warmup draws = 4000

Multilevel Hyperparameters:
~Adversary (Number of levels: 3)
              Estimate Est.Error l-95% CI u-95% CI Rhat Bulk_ESS Tail_ESS
sd(Intercept)   0.71   0.90   0.01   3.26 1.01   833   1604

Regression Coefficients:
          Estimate Est.Error l-95% CI u-95% CI Rhat Bulk_ESS Tail_ESS
Intercept   -1.43   0.58   -2.97   -0.29 1.01   1220   860
TDCs   0.11   0.07   -0.04   0.25 1.00   3265   2427
DeltaAgr1   1.91   0.29   1.35   2.49 1.00   3001   2544
DeltaPart   0.01   0.01   -0.01   0.03 1.00   4149   2877
InitB   1.52   0.18   1.18   1.87 1.00   2865   2342

Draws were sampled using sampling(NUTS). For each parameter, Bulk_ESS
and Tail_ESS are effective sample size measures, and Rhat is the potential
scale reduction factor on split chains (at convergence, Rhat = 1).

   Estimate Est.Error   Q2.5   Q97.5
R2 0.220755 0.02033339 0.1793028 0.2587081

Probability of Direction

Parameter | pd

(Intercept) | 98.67%
TDCs | 92.17%
DeltaAgr1 | 100%
DeltaPart | 88.20%
InitB | 100%

[11] "Summary for: RBM.Win_35d"

Family: bernoulli

  Links: mu = logit
Formula: WinB ~ TDCs + DeltaAgr1 + DeltaPart + InitB + (1 | Adversary)
   Data: df_content (Number of observations: 837)
  Draws: 4 chains, each with iter = 2000; warmup = 1000; thin = 1;
         total post-warmup draws = 4000

Multilevel Hyperparameters:
~Adversary (Number of levels: 3)
              Estimate Est.Error l-95% CI u-95% CI Rhat Bulk_ESS Tail_ESS
sd(Intercept)   0.71   0.92   0.01   3.44 1.00   970   1258

Regression Coefficients:
          Estimate Est.Error l-95% CI u-95% CI Rhat Bulk_ESS Tail_ESS
Intercept   -1.48   0.69   -3.25   -0.35 1.01   1166   812
TDCs   0.21   0.07   0.07   0.34 1.00   3021   2397
DeltaAgr1   1.88   0.29   1.33   2.45 1.00   3175   2584
DeltaPart   0.01   0.01   -0.01   0.03 1.00   3659   2686
InitB   1.51   0.18   1.18   1.87 1.00   3352   2429

Draws were sampled using sampling(NUTS). For each parameter, Bulk_ESS
and Tail_ESS are effective sample size measures, and Rhat is the potential
scale reduction factor on split chains (at convergence, Rhat = 1).

    Estimate Est.Error   Q2.5   Q97.5
R2 0.2267345 0.01955954 0.1878488 0.2638871

Probability of Direction

Parameter | pd

(Intercept) | 98.75%
TDCs | 99.90%
DeltaAgr1 | 100%
DeltaPart | 88.35%
InitB | 100%

[12] "Summary for: RBM.Win_42d"

Family: bernoulli

  Links: mu = logit
Formula: WinB ~ TDCs + DeltaAgr1 + DeltaPart + InitB + (1 | Adversary)
   Data: df_content (Number of observations: 837)
  Draws: 4 chains, each with iter = 2000; warmup = 1000; thin = 1;
         total post-warmup draws = 4000

Multilevel Hyperparameters:
~Adversary (Number of levels: 3)
              Estimate Est.Error l-95% CI u-95% CI Rhat Bulk_ESS Tail_ESS
sd(Intercept)   0.77   1.00   0.02   3.55 1.00   870   1947

Regression Coefficients:
          Estimate Est.Error l-95% CI u-95% CI Rhat Bulk_ESS Tail_ESS
Intercept   -1.47   0.67   -3.13   -0.15 1.00   1150   850
TDCs   0.17   0.07   0.04   0.31 1.00   3453   2603
DeltaAgr1   1.89   0.29   1.32   2.46 1.00   2549   3003
DeltaPart   0.01   0.01   -0.01   0.03 1.00   3335   2676
InitB   1.51   0.17   1.18   1.86 1.00   3263   2765

Draws were sampled using sampling(NUTS). For each parameter, Bulk_ESS
and Tail_ESS are effective sample size measures, and Rhat is the potential
scale reduction factor on split chains (at convergence, Rhat = 1).

    Estimate Est.Error   Q2.5   Q97.5
R2 0.2251016 0.01935536 0.1860251 0.2613587

Probability of Direction

Parameter | pd

(Intercept) | 97.97%
TDCs | 99.42%
DeltaAgr1 | 100%
DeltaPart | 89.30%
InitB | 100%

[13] "Summary for: RBM.Win_84d"

Family: bernoulli

  Links: mu = logit
Formula: WinB ~ TDCs + DeltaAgr1 + DeltaPart + InitB + (1 | Adversary)
   Data: df_content (Number of observations: 836)
  Draws: 4 chains, each with iter = 2000; warmup = 1000; thin = 1;
         total post-warmup draws = 4000

Multilevel Hyperparameters:
~Adversary (Number of levels: 3)
              Estimate Est.Error l-95% CI u-95% CI Rhat Bulk_ESS Tail_ESS
sd(Intercept)   0.71   0.92   0.01   3.39 1.00   809   1443

Regression Coefficients:
          Estimate Est.Error l-95% CI u-95% CI Rhat Bulk_ESS Tail_ESS
Intercept   -1.41   0.58   -2.86   -0.26 1.00   1234   1098
TDCs   0.10   0.07   -0.05   0.24 1.00   3413   2485
DeltaAgr1   1.90   0.29   1.35   2.48 1.00   3773   2670
DeltaPart   0.01   0.01   -0.01   0.03 1.00   3793   2948
InitB   1.51   0.18   1.16   1.86 1.00   3552   2702

Draws were sampled using sampling(NUTS). For each parameter, Bulk_ESS
and Tail_ESS are effective sample size measures, and Rhat is the potential
scale reduction factor on split chains (at convergence, Rhat = 1).

   Estimate Est.Error   Q2.5   Q97.5
R2 0.219737 0.01991058 0.1795028 0.2561654

Probability of Direction

Parameter | pd

(Intercept) | 98.58%
TDCs | 91.45%
DeltaAgr1 | 100%
DeltaPart | 88.42%
InitB | 100%

[14] "Summary for: RBM.Win_168d"

Family: bernoulli

  Links: mu = logit
Formula: WinB ~ TDCs + DeltaAgr1 + DeltaPart + InitB + (1 | Adversary)
   Data: df_content (Number of observations: 827)
  Draws: 4 chains, each with iter = 2000; warmup = 1000; thin = 1;
         total post-warmup draws = 4000

Multilevel Hyperparameters:
~Adversary (Number of levels: 3)
              Estimate Est.Error l-95% CI u-95% CI Rhat Bulk_ESS Tail_ESS
sd(Intercept)   0.72   1.02   0.01   3.33 1.01   766   1586

Regression Coefficients:
          Estimate Est.Error l-95% CI u-95% CI Rhat Bulk_ESS Tail_ESS
Intercept   -1.39   0.61   -2.76   -0.18 1.00   1012   985
TDCs   0.10   0.07   -0.03   0.24 1.00   3683   2745
DeltaAgr1   1.80   0.29   1.23   2.38 1.00   3668   2693
DeltaPart   0.01   0.01   -0.01   0.03 1.00   3703   2656
InitB   1.56   0.18   1.20   1.91 1.00   3344   2523

Draws were sampled using sampling(NUTS). For each parameter, Bulk_ESS
and Tail_ESS are effective sample size measures, and Rhat is the potential
scale reduction factor on split chains (at convergence, Rhat = 1).

    Estimate Est.Error   Q2.5   Q97.5
R2 0.2204617 0.01954448 0.1810816 0.2572626

Probability of Direction

Parameter | pd

(Intercept) | 98.28%
TDCs | 92.12%
DeltaAgr1 | 100%
DeltaPart | 86.78%
InitB | 100%

RST DHR Models

[15] "Summary for: RST.Win_14d"

Family: bernoulli

```
  Links: mu = logit
Formula: WinB ~ TDCs + DeltaAgr1 + DeltaPart + InitB + (1 | Adversary)
   Data: df_content (Number of observations: 428)
  Draws: 4 chains, each with iter = 2000; warmup = 1000; thin = 1;
         total post-warmup draws = 4000

Multilevel Hyperparameters:
~Adversary (Number of levels: 2)
              Estimate Est.Error l-95% CI u-95% CI Rhat Bulk_ESS Tail_ESS
sd(Intercept)     0.88      1.06     0.02     3.70 1.00      738     1152

Regression Coefficients:
          Estimate Est.Error l-95% CI u-95% CI Rhat Bulk_ESS Tail_ESS
Intercept    -0.87      0.71    -2.53     0.68 1.00     1297      777
TDCs          0.12      0.14    -0.16     0.39 1.00     3280     2239
DeltaAgr1     1.41      0.35     0.73     2.11 1.00     3751     2761
DeltaPart     0.04      0.01     0.02     0.06 1.00     3390     2567
InitB         0.94      0.22     0.51     1.36 1.00     3305     2651

Draws were sampled using sampling(NUTS). For each parameter, Bulk_ESS
and Tail_ESS are effective sample size measures, and Rhat is the potential
scale reduction factor on split chains (at convergence, Rhat = 1).

    Estimate  Est.Error       Q2.5     Q97.5
R2 0.1239328 0.02405053 0.07769567 0.1714394

Probability of Direction

Parameter   |     pd
--------------------
(Intercept) | 92.30%
TDCs        | 78.90%
DeltaAgr1   | 99.98%
DeltaPart   |   100%
InitB       |   100%
```

[16] "Summary for: RST.Win_21d"

```
 Family: bernoulli
  Links: mu = logit
Formula: WinB ~ TDCs + DeltaAgr1 + DeltaPart + InitB + (1 | Adversary)
   Data: df_content (Number of observations: 430)
  Draws: 4 chains, each with iter = 2000; warmup = 1000; thin = 1;
         total post-warmup draws = 4000

Multilevel Hyperparameters:
~Adversary (Number of levels: 2)
              Estimate Est.Error l-95% CI u-95% CI Rhat Bulk_ESS Tail_ESS
sd(Intercept)     0.82      0.97     0.02     3.50 1.00     1011     1663

Regression Coefficients:
           Estimate Est.Error l-95% CI u-95% CI Rhat Bulk_ESS Tail_ESS
Intercept    -0.86      0.71    -2.41     0.69 1.00     1380     1201
TDCs          0.12      0.14    -0.16     0.39 1.00     3582     2667
DeltaAgr1     1.41      0.35     0.76     2.13 1.00     2776     2618
DeltaPart     0.04      0.01     0.02     0.06 1.00     3581     2998
InitB         0.94      0.22     0.52     1.37 1.00     3148     3060

Draws were sampled using sampling(NUTS). For each parameter, Bulk_ESS
and Tail_ESS are effective sample size measures, and Rhat is the potential
scale reduction factor on split chains (at convergence, Rhat = 1).

    Estimate  Est.Error       Q2.5      Q97.5
R2 0.1249113 0.02397617 0.07844646 0.1721143

Probability of Direction

Parameter   |     pd
--------------------
(Intercept) | 92.55%
TDCs        | 80.50%
DeltaAgr1   |   100%
DeltaPart   | 99.98%
InitB       |   100%
```

[17] "Summary for: RST.Win_28d"

Family: bernoulli

  Links: mu = logit
Formula: WinB ~ TDCs + DeltaAgr1 + DeltaPart + InitB + (1 | Adversary)
   Data: df_content (Number of observations: 430)
  Draws: 4 chains, each with iter = 2000; warmup = 1000; thin = 1;
         total post-warmup draws = 4000

Multilevel Hyperparameters:
~Adversary (Number of levels: 2)
              Estimate Est.Error l-95% CI u-95% CI Rhat Bulk_ESS Tail_ESS
sd(Intercept)   0.87   1.06   0.01   3.62 1.00   778   1125

Regression Coefficients:
          Estimate Est.Error l-95% CI u-95% CI Rhat Bulk_ESS Tail_ESS
Intercept   -0.84   0.71   -2.37   0.80 1.00   1069   874
TDCs   0.15   0.15   -0.13   0.44 1.00   3175   2612
DeltaAgr1   1.38   0.35   0.69   2.09 1.00   3151   2751
DeltaPart   0.04   0.01   0.02   0.06 1.00   3172   2565
InitB   0.96   0.22   0.54   1.40 1.00   3178   2268

Draws were sampled using sampling(NUTS). For each parameter, Bulk_ESS
and Tail_ESS are effective sample size measures, and Rhat is the potential
scale reduction factor on split chains (at convergence, Rhat = 1).

    Estimate Est.Error   Q2.5   Q97.5
R2 0.1255483 0.02482156 0.07703517 0.172873

Probability of Direction

Parameter | pd

(Intercept) | 92.47%
TDCs | 84.75%
DeltaAgr1 | 100%
DeltaPart | 99.98%
InitB | 100%

[18] "Summary for: RST.Win_35d"

Family: bernoulli

  Links: mu = logit
Formula: WinB ~ TDCs + DeltaAgr1 + DeltaPart + InitB + (1 | Adversary)
   Data: df_content (Number of observations: 430)
  Draws: 4 chains, each with iter = 2000; warmup = 1000; thin = 1;
         total post-warmup draws = 4000

Multilevel Hyperparameters:
~Adversary (Number of levels: 2)
              Estimate Est.Error l-95% CI u-95% CI Rhat Bulk_ESS Tail_ESS
sd(Intercept)   0.84   1.04   0.02   3.73 1.00   911   1585

Regression Coefficients:
          Estimate Est.Error l-95% CI u-95% CI Rhat Bulk_ESS Tail_ESS
Intercept   -0.87   0.66   -2.43   0.54 1.01   1513   1080
TDCs   0.17   0.15   -0.12   0.47 1.00   3156   2390
DeltaAgr1   1.39   0.35   0.72   2.09 1.00   2726   2255
DeltaPart   0.04   0.01   0.02   0.07 1.00   3339   2507
InitB   0.96   0.22   0.52   1.42 1.00   3044   2227

Draws were sampled using sampling(NUTS). For each parameter, Bulk_ESS
and Tail_ESS are effective sample size measures, and Rhat is the potential
scale reduction factor on split chains (at convergence, Rhat = 1).

    Estimate Est.Error   Q2.5   Q97.5
R2 0.1265038 0.02458357 0.07965607 0.1751603

Probability of Direction

Parameter | pd

(Intercept) | 93.12%
TDCs | 86.67%
DeltaAgr1 | 100%
DeltaPart | 99.95%
InitB | 100%

[19] "Summary for: RST.Win_42d"

```
 Family: bernoulli
  Links: mu = logit
Formula: WinB ~ TDCs + DeltaAgr1 + DeltaPart + InitB + (1 | Adversary)
   Data: df_content (Number of observations: 429)
  Draws: 4 chains, each with iter = 2000; warmup = 1000; thin = 1;
         total post-warmup draws = 4000

Multilevel Hyperparameters:
~Adversary (Number of levels: 2)
              Estimate Est.Error l-95% CI u-95% CI Rhat Bulk_ESS Tail_ESS
sd(Intercept)     0.86      1.08     0.01     3.93 1.00      823     1318

Regression Coefficients:
           Estimate Est.Error l-95% CI u-95% CI Rhat Bulk_ESS Tail_ESS
Intercept    -0.82      0.74    -2.38     0.87 1.01      976      839
TDCs          0.08      0.15    -0.22     0.38 1.00     3694     2760
DeltaAgr1     1.40      0.36     0.71     2.10 1.00     2887     2556
DeltaPart     0.04      0.01     0.02     0.06 1.00     3413     2685
InitB         0.94      0.23     0.50     1.39 1.00     3238     2519

Draws were sampled using sampling(NUTS). For each parameter, Bulk_ESS
and Tail_ESS are effective sample size measures, and Rhat is the potential
scale reduction factor on split chains (at convergence, Rhat = 1).

    Estimate  Est.Error       Q2.5     Q97.5
R2 0.1226144 0.02448704 0.07530217 0.1703563

Probability of Direction

Parameter   |     pd
--------------------
(Intercept) | 92.12%
TDCs        | 69.38%
DeltaAgr1   |   100%
DeltaPart   | 99.92%
InitB       |   100%
```

[20] "Summary for: RST.Win_84d"

Family: bernoulli

  Links: mu = logit
Formula: WinB ~ TDCs + DeltaAgr1 + DeltaPart + InitB + (1 | Adversary)
   Data: df_content (Number of observations: 429)
  Draws: 4 chains, each with iter = 2000; warmup = 1000; thin = 1;
         total post-warmup draws = 4000

Multilevel Hyperparameters:
~Adversary (Number of levels: 2)
              Estimate Est.Error l-95% CI u-95% CI Rhat Bulk_ESS Tail_ESS
sd(Intercept)   0.82   1.01   0.02   3.54 1.00   788   1632

Regression Coefficients:
          Estimate Est.Error l-95% CI u-95% CI Rhat Bulk_ESS Tail_ESS
Intercept   -0.80   0.68   -2.16   0.79 1.01   1578   1312
TDCs   0.16   0.14   -0.12   0.44 1.00   3369   2479
DeltaAgr1   1.40   0.35   0.72   2.10 1.00   3463   2896
DeltaPart   0.04   0.01   0.02   0.06 1.00   3463   2693
InitB   0.94   0.22   0.52   1.36 1.00   3170   2703

Draws were sampled using sampling(NUTS). For each parameter, Bulk_ESS
and Tail_ESS are effective sample size measures, and Rhat is the potential
scale reduction factor on split chains (at convergence, Rhat = 1).

   Estimate Est.Error   Q2.5   Q97.5
R2 0.125136 0.02470908 0.07750048 0.1740081

Probability of Direction

Parameter | pd

(Intercept) | 90.97%
TDCs | 86.42%
DeltaAgr1 | 100%
DeltaPart | 100%
InitB | 100%

[21] "Summary for: RST.Win_168d"

```
 Family: bernoulli
  Links: mu = logit
Formula: WinB ~ TDCs + DeltaAgr1 + DeltaPart + InitB + (1 | Adversary)
   Data: df_content (Number of observations: 426)
  Draws: 4 chains, each with iter = 2000; warmup = 1000; thin = 1;
         total post-warmup draws = 4000

Multilevel Hyperparameters:
~Adversary (Number of levels: 2)
              Estimate Est.Error l-95% CI u-95% CI Rhat Bulk_ESS Tail_ESS
sd(Intercept)     0.91      1.04     0.02     3.80 1.00      832     1329

Regression Coefficients:
          Estimate Est.Error l-95% CI u-95% CI Rhat Bulk_ESS Tail_ESS
Intercept    -0.89      0.73    -2.49     0.77 1.00     1215     1075
TDCs         -0.10      0.18    -0.46     0.25 1.00     3101     2082
DeltaAgr1     1.37      0.35     0.69     2.09 1.00     3001     2366
DeltaPart     0.04      0.01     0.02     0.06 1.00     3278     2694
InitB         0.99      0.22     0.56     1.41 1.00     3068     2435

Draws were sampled using sampling(NUTS). For each parameter, Bulk_ESS
and Tail_ESS are effective sample size measures, and Rhat is the potential
scale reduction factor on split chains (at convergence, Rhat = 1).

    Estimate  Est.Error       Q2.5     Q97.5
R2 0.1255875 0.02439637 0.07911141 0.1730253

Probability of Direction

Parameter   |     pd
--------------------
(Intercept) | 92.22%
TDCs        | 71.20%
DeltaAgr1   |   100%
DeltaPart   | 99.98%
InitB       |   100%
```

Appendix G: DHR Posterior Distribution Plots

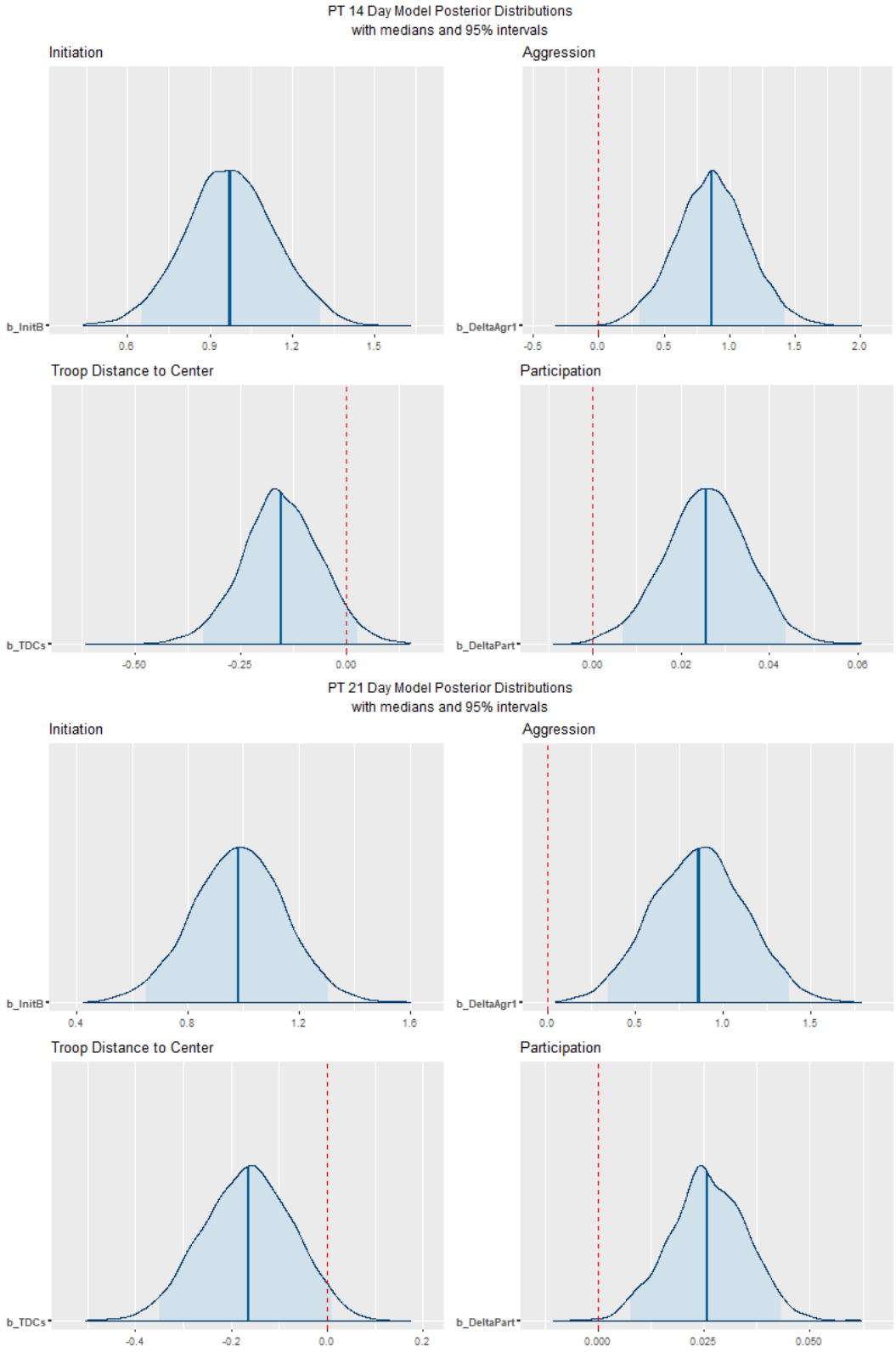

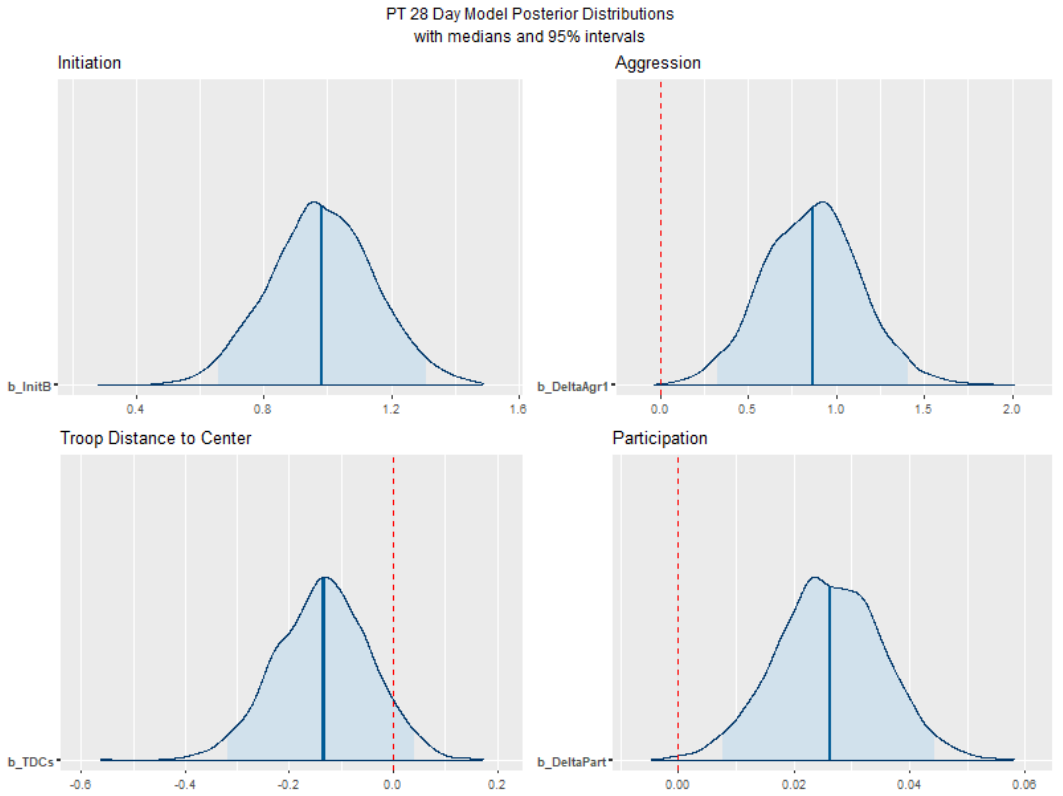
PT 28 Day Model Posterior Distributions
with medians and 95% intervals
Initiation
Aggression
b_InitB
b_DeltaAgr1
Troop Distance to Center
Participation
b_TDCs
b_DeltaPart

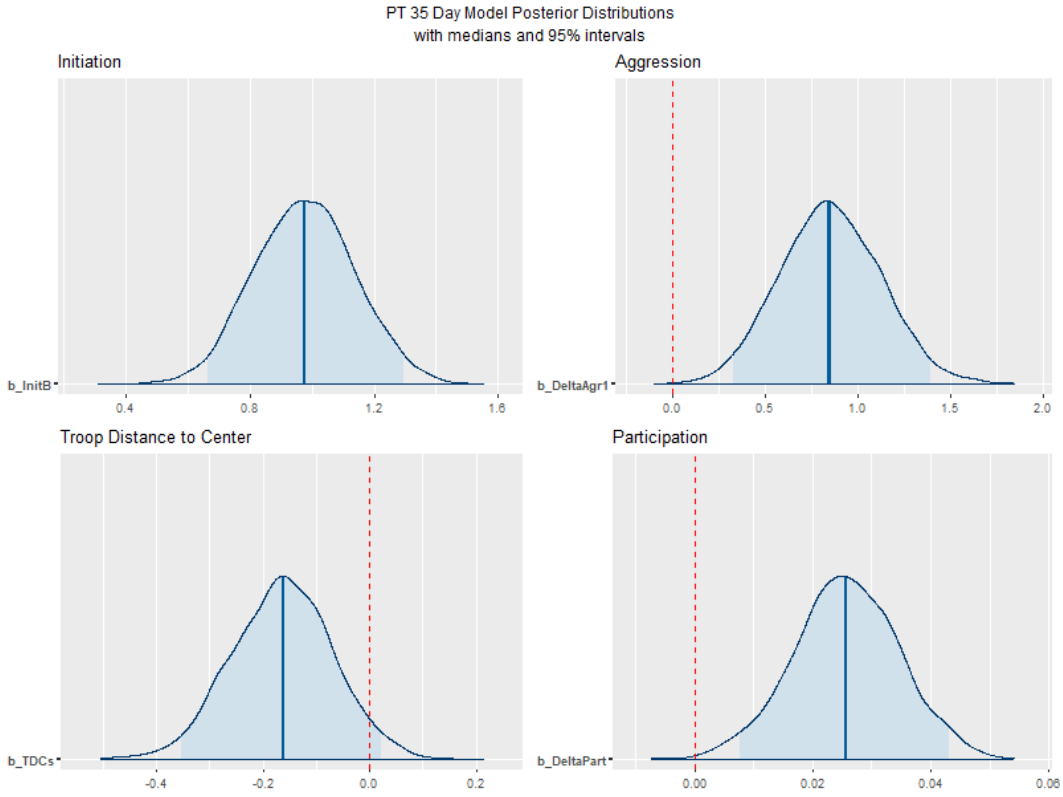
PT 35 Day Model Posterior Distributions
with medians and 95% intervals
Initiation
Aggression
b_InitB
b_DeltaAgr1
Troop Distance to Center
Participation
b_TDCs
b_DeltaPart

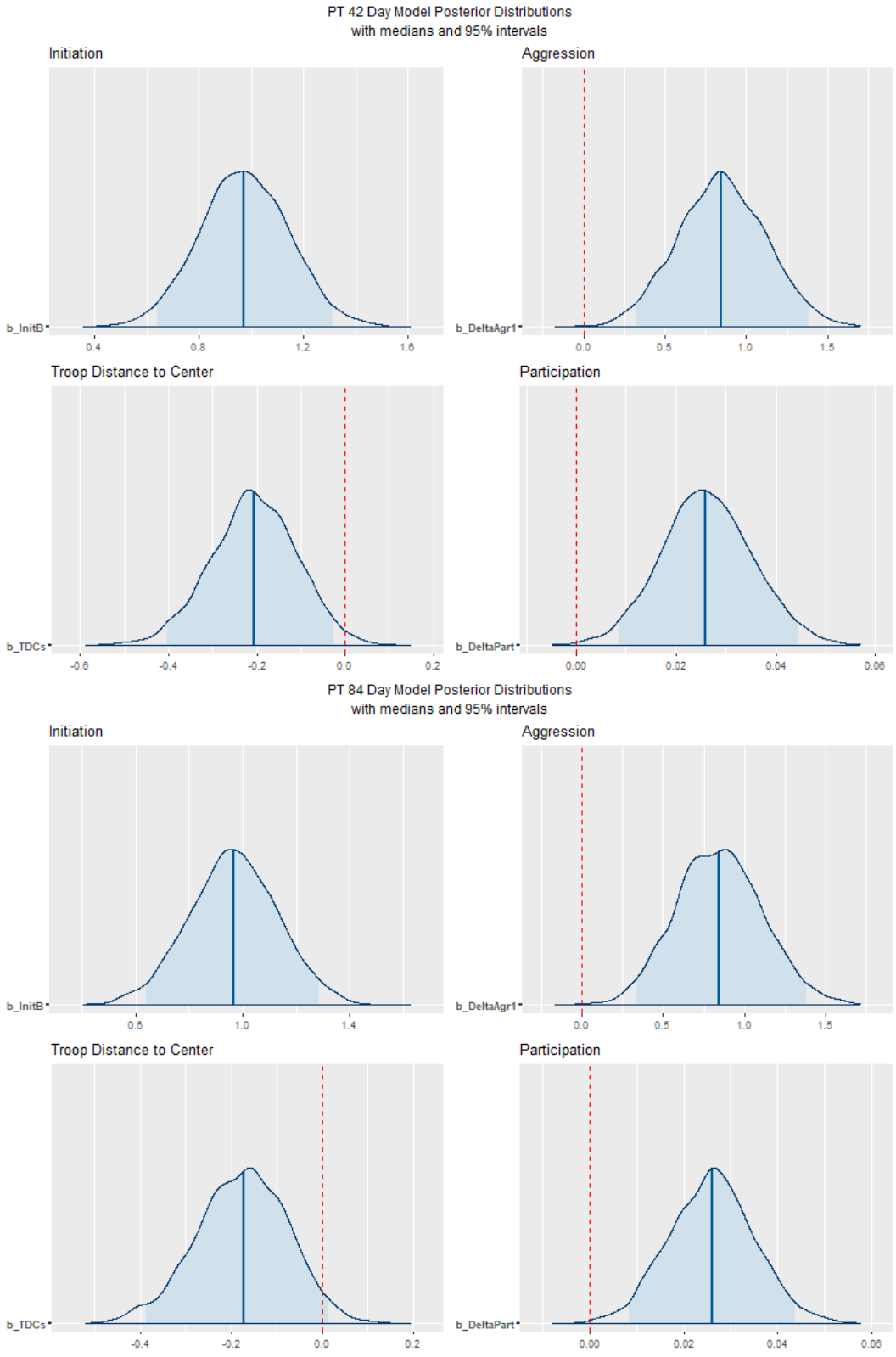
PT 42 Day Model Posterior Distributions
with medians and 95% intervals
Initiation
b_InitB
0.4
0.8
1.2
1.6
Aggression
b_DeltaAgr1
0.0
0.5
1.0
1.5
Troop Distance to Center
b_TDCs
-0.6
-0.4
-0.2
0.0
0.2
Participation
b_DeltaPart
0.00
0.02
0.04
0.06
PT 84 Day Model Posterior Distributions
with medians and 95% intervals
Initiation
b_InitB
0.6
1.0
1.4
Aggression
b_DeltaAgr1
0.0
0.5
1.0
1.5
Troop Distance to Center
b_TDCs
-0.4
-0.2
0.0
0.2
Participation
b_DeltaPart
0.00
0.02
0.04
0.06

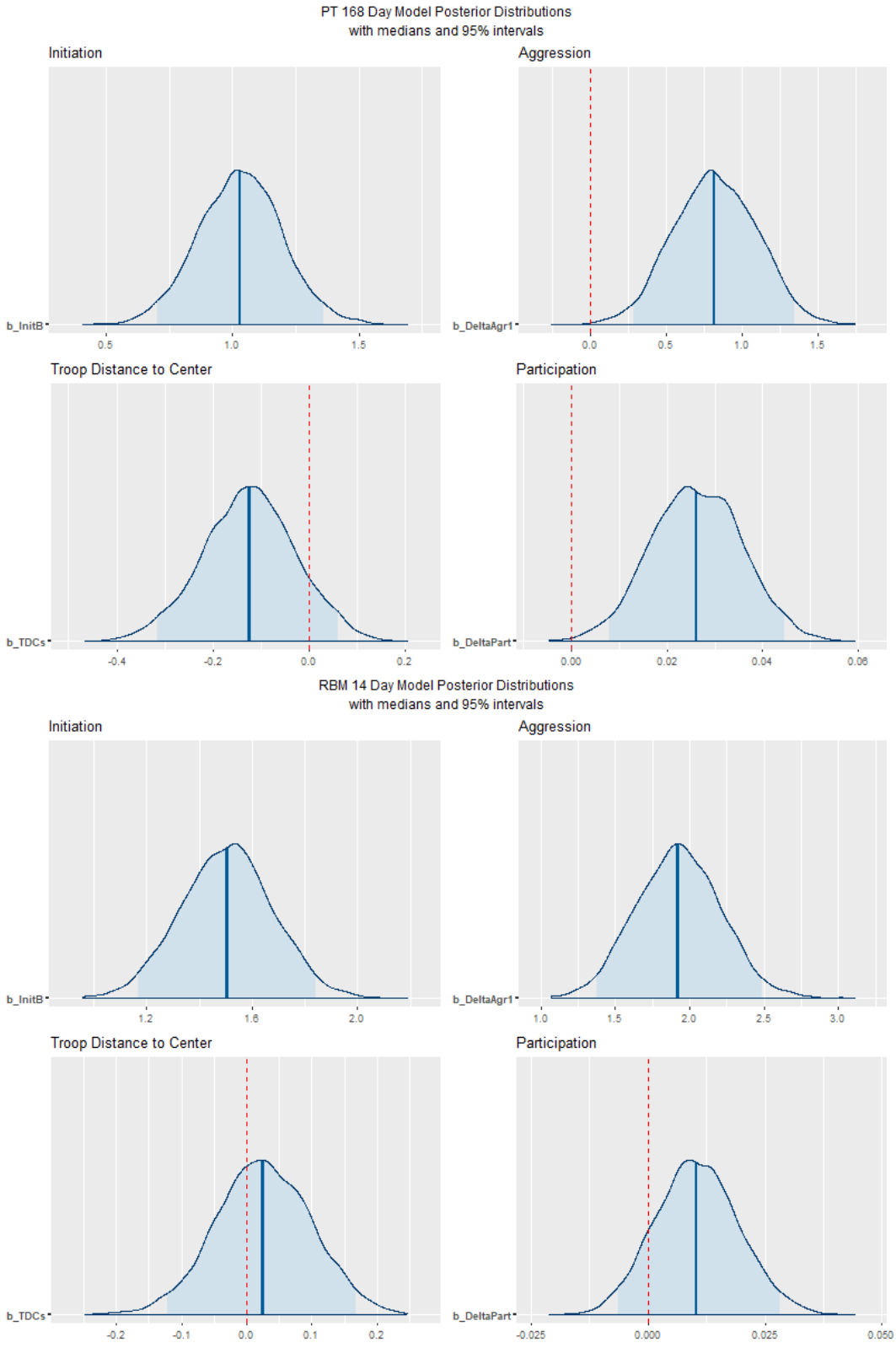
PT 168 Day Model Posterior Distributions
with medians and 95% intervals
Initiation
b_InitB
0.5
1.0
1.5
Aggression
b_DeltaAgr1
0.0
0.5
1.0
1.5
Troop Distance to Center
b_TDCs
-0.4
-0.2
0.0
0.2
Participation
b_DeltaPart
0.00
0.02
0.04
0.06
RBM 14 Day Model Posterior Distributions
with medians and 95% intervals
Initiation
b_InitB
1.2
1.6
2.0
Aggression
b_DeltaAgr1
1.0
1.5
2.0
2.5
3.0
Troop Distance to Center
b_TDCs
-0.2
-0.1
0.0
0.1
0.2
Participation
b_DeltaPart
-0.025
0.000
0.025
0.050

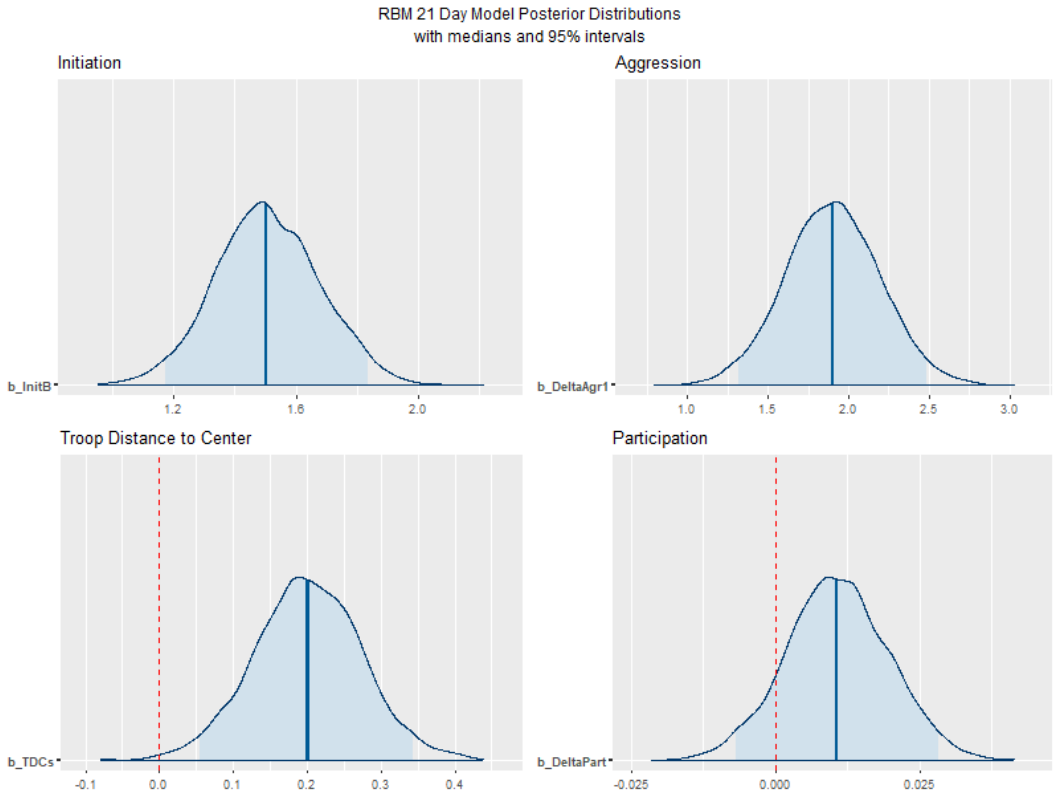
RBM 21 Day Model Posterior Distributions
with medians and 95% intervals
Initiation
b_InitB
1.2
1.6
2.0
Aggression
b_DeltaAgr1
1.0
1.5
2.0
2.5
3.0
Troop Distance to Center
b_TDCs
-0.1
0.0
0.1
0.2
0.3
0.4
Participation
b_DeltaPart
-0.025
0.000
0.025

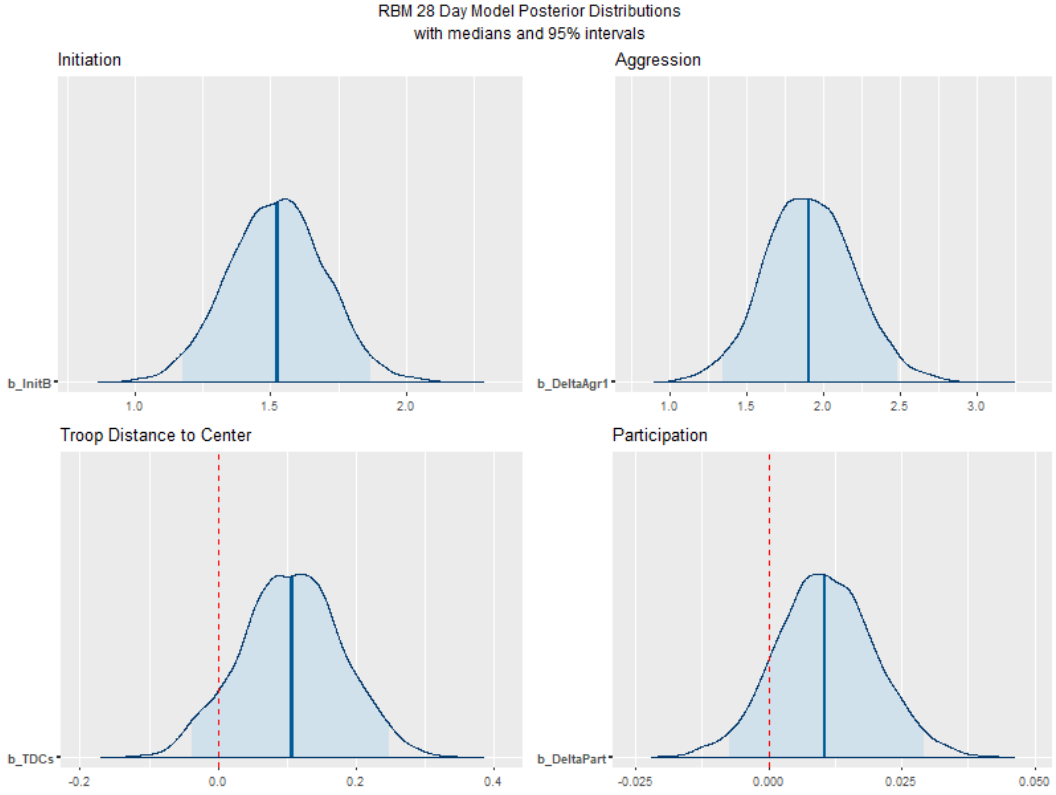
RBM 28 Day Model Posterior Distributions
with medians and 95% intervals
Initiation
b_InitB
1.0
1.5
2.0
Aggression
b_DeltaAgr1
1.0
1.5
2.0
2.5
3.0
Troop Distance to Center
b_TDCs
-0.2
0.0
0.2
0.4
Participation
b_DeltaPart
-0.025
0.000
0.025
0.050

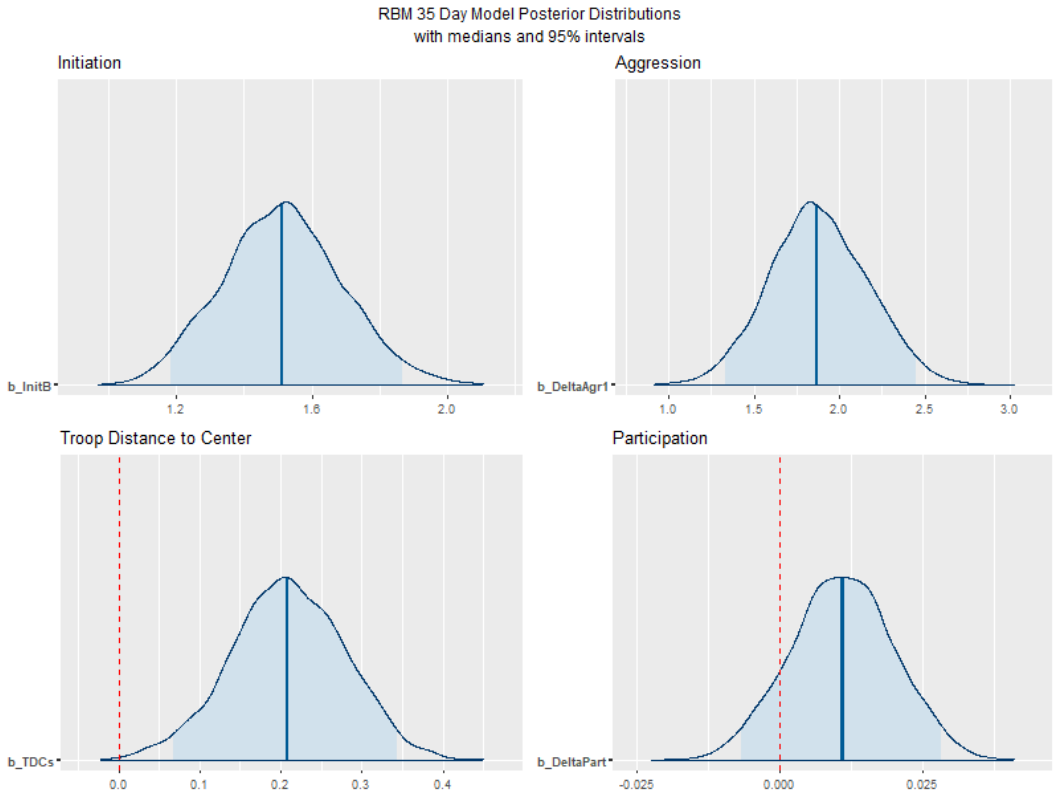
RBM 35 Day Model Posterior Distributions
with medians and 95% intervals
Initiation
b_InitB
1.2
1.6
2.0
Aggression
b_DeltaAgr1
1.0
1.5
2.0
2.5
3.0
Troop Distance to Center
b_TDCs
0.0
0.1
0.2
0.3
0.4
Participation
b_DeltaPart
-0.025
0.000
0.025

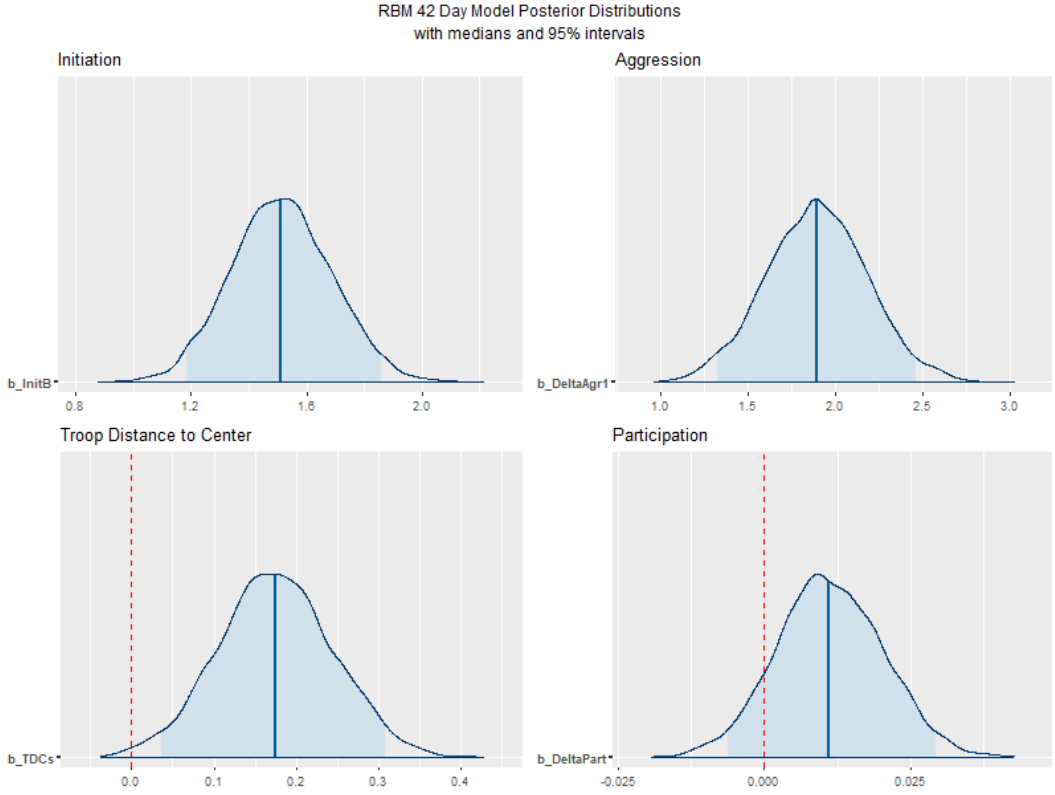
RBM 42 Day Model Posterior Distributions
with medians and 95% intervals
Initiation
b_InitB
0.8
1.2
1.6
2.0
Aggression
b_DeltaAgr1
1.0
1.5
2.0
2.5
3.0
Troop Distance to Center
b_TDCs
0.0
0.1
0.2
0.3
0.4
Participation
b_DeltaPart
-0.025
0.000
0.025

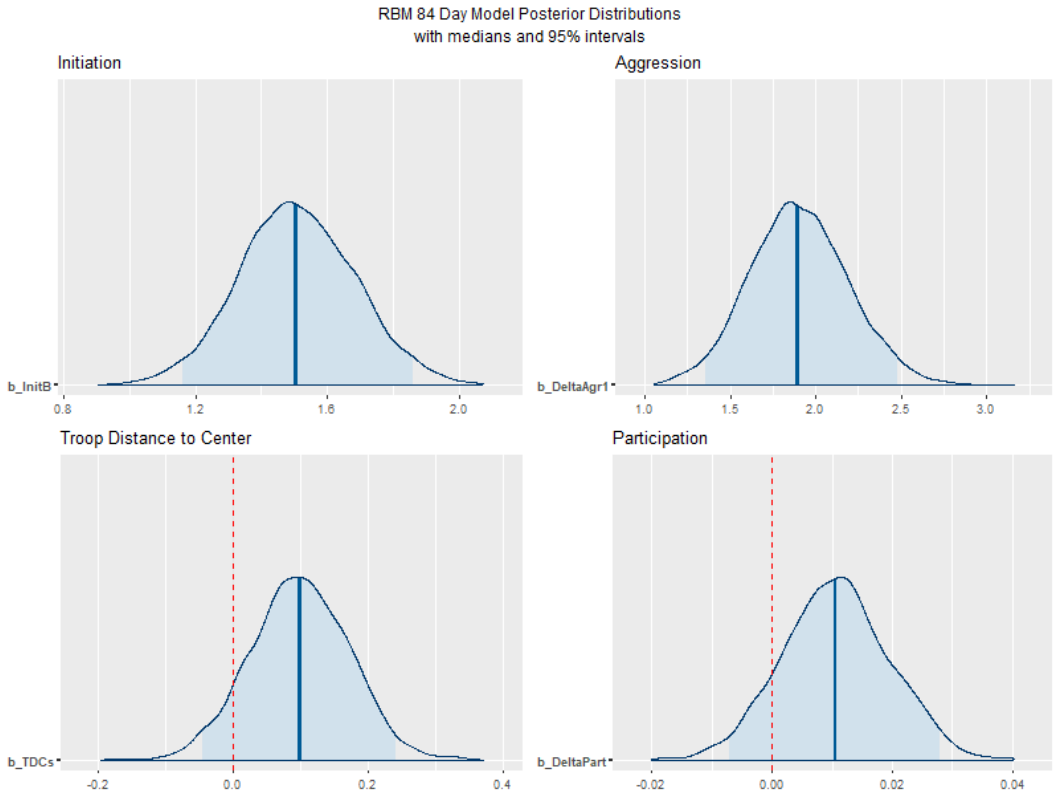
RBM 84 Day Model Posterior Distributions
with medians and 95% intervals
Initiation
b_InitB
0.8
1.2
1.6
2.0
Aggression
b_DeltaAgr1
1.0
1.5
2.0
2.5
3.0
Troop Distance to Center
b_TDCs
-0.2
0.0
0.2
0.4
Participation
b_DeltaPart
-0.02
0.00
0.02
0.04

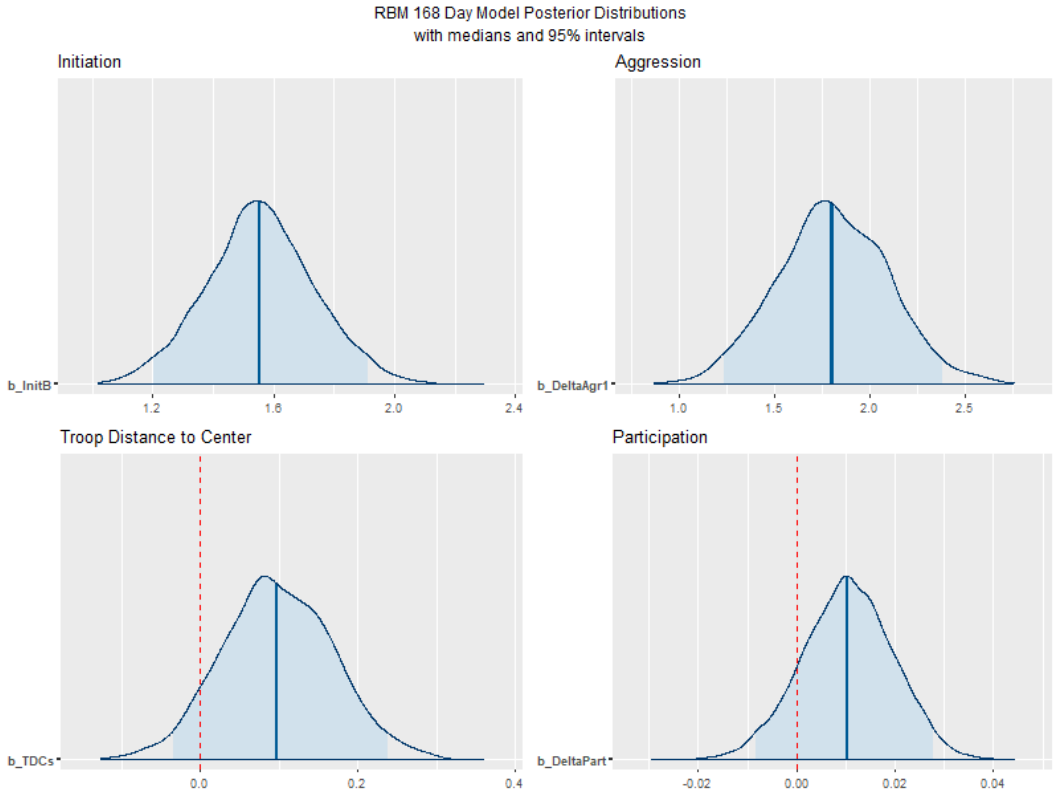
RBM 168 Day Model Posterior Distributions
with medians and 95% intervals
Initiation
b_InitB
1.2
1.6
2.0
2.4
Aggression
b_DeltaAgr1
1.0
1.5
2.0
2.5
Troop Distance to Center
b_TDCs
0.0
0.2
0.4
Participation
b_DeltaPart
-0.02
0.00
0.02
0.04

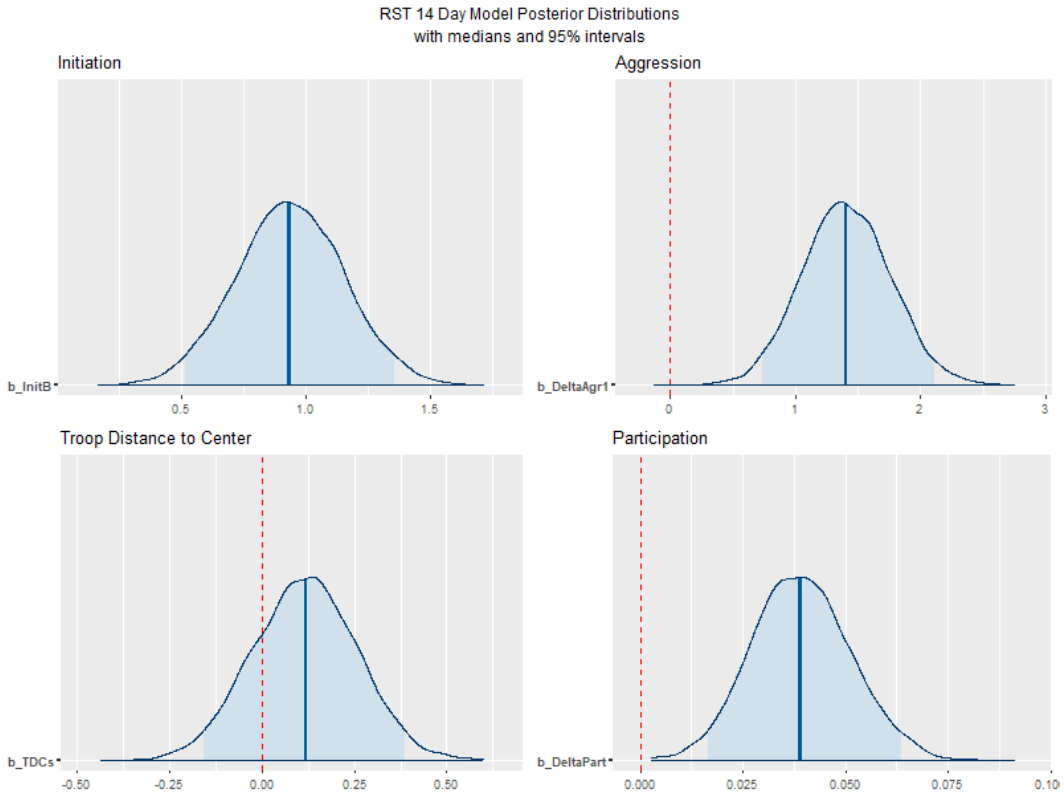
RST 14 Day Model Posterior Distributions
with medians and 95% intervals
Initiation
b_InitB
0.5
1.0
1.5
Aggression
b_DeltaAgr1
0
1
2
3
Troop Distance to Center
b_TDCs
-0.50
-0.25
0.00
0.25
0.50
Participation
b_DeltaPart
0.000
0.025
0.050
0.075

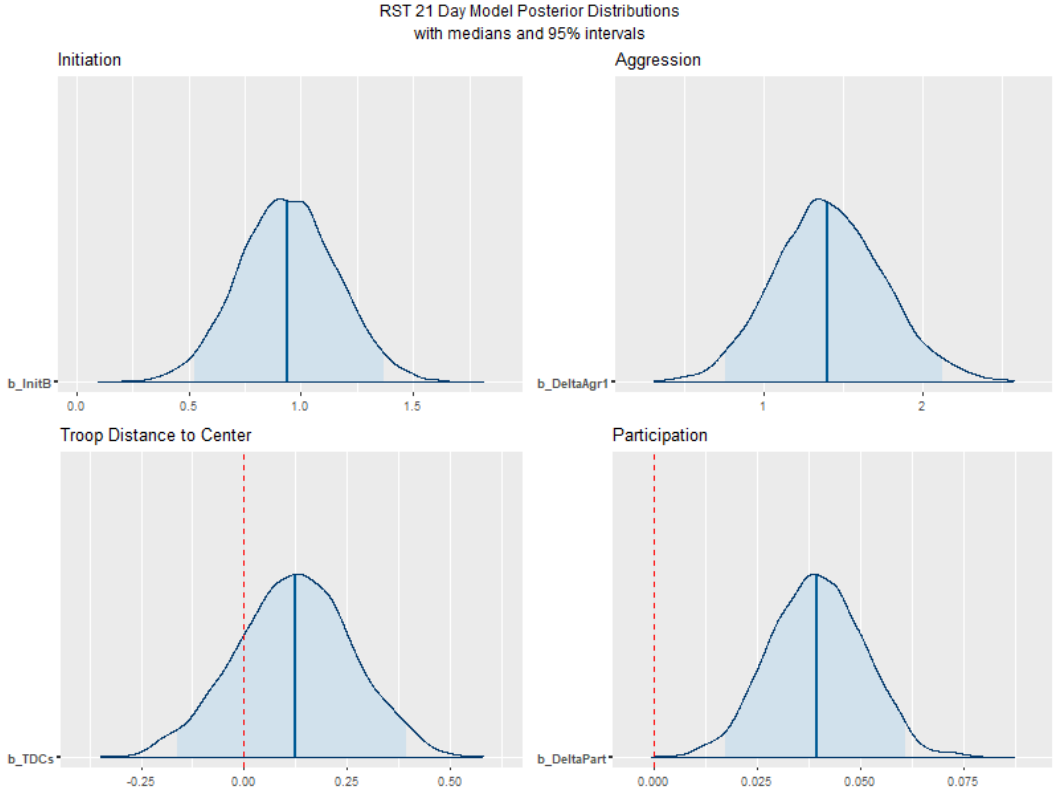
RST 21 Day Model Posterior Distributions
with medians and 95% intervals
Initiation
b_InitB
0.0
0.5
1.0
1.5
Aggression
b_DeltaAgr1
1
2
Troop Distance to Center
b_TDCs
-0.25
0.00
0.25
0.50
Participation
b_DeltaPart
0.000
0.025
0.050
0.075

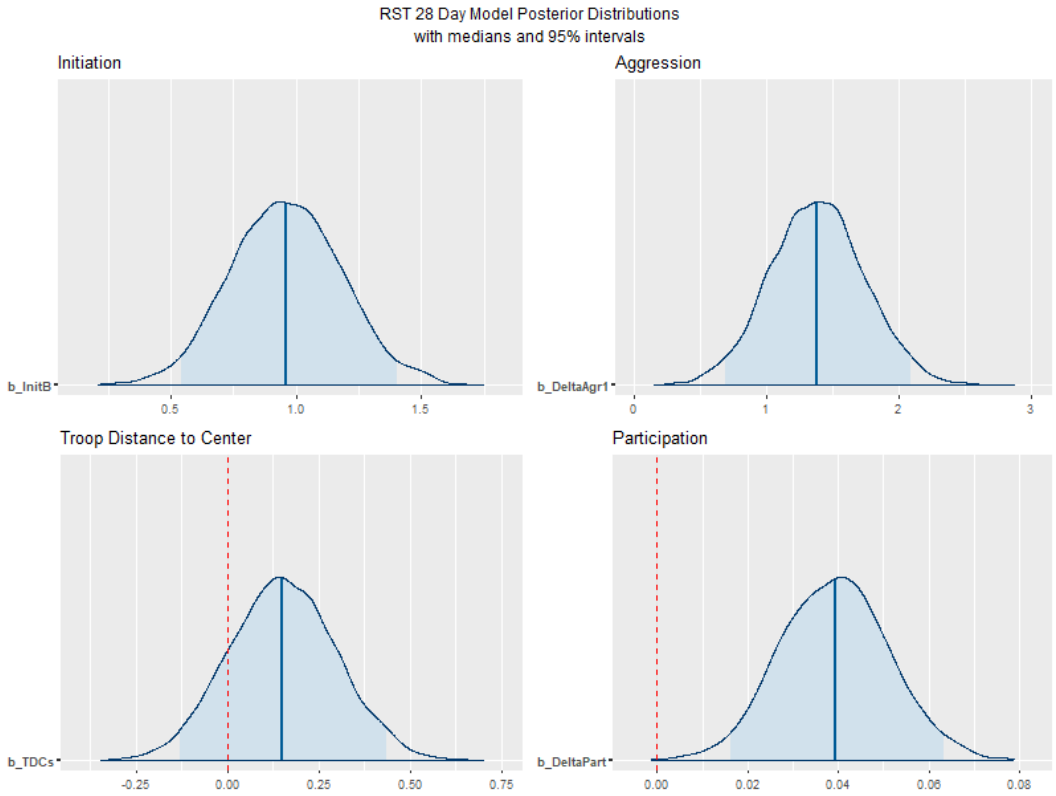
RST 28 Day Model Posterior Distributions
with medians and 95% intervals
Initiation
b_InitB
0.5
1.0
1.5
Aggression
b_DeltaAgr1
0
1
2
3
Troop Distance to Center
b_TDCs
-0.25
0.00
0.25
0.50
0.75
Participation
b_DeltaPart
0.00
0.02
0.04
0.06
0.08

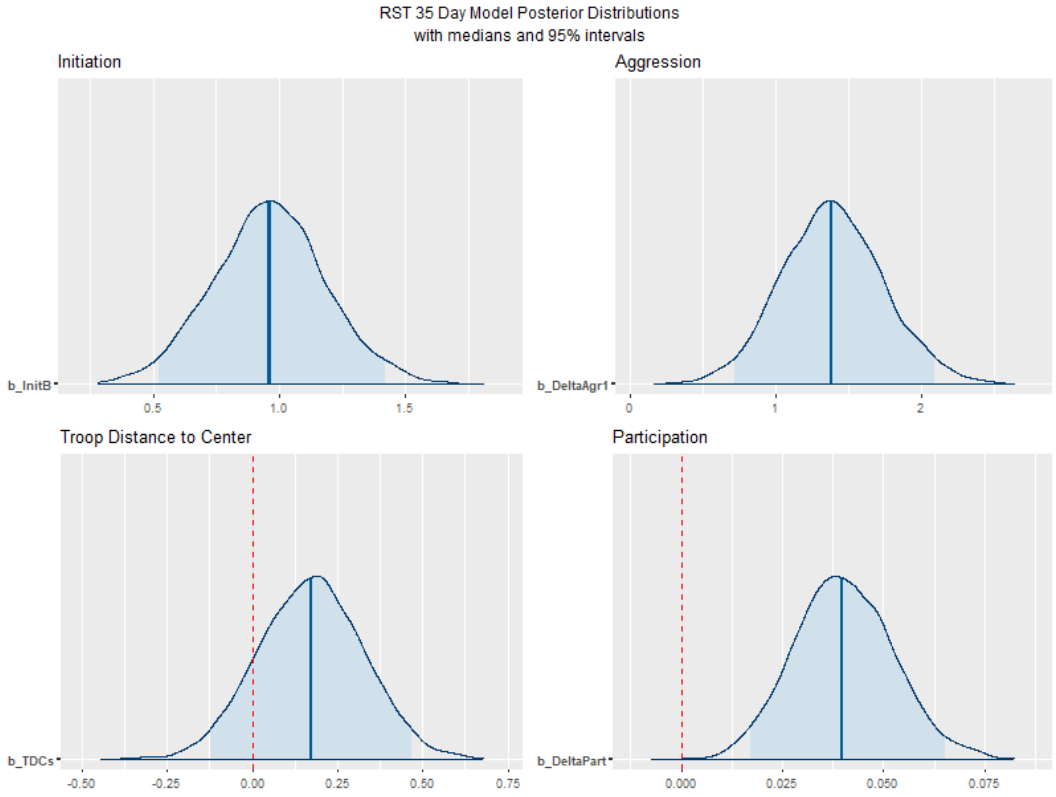
RST 35 Day Model Posterior Distributions
with medians and 95% intervals
Initiation
b_InitB
0.5
1.0
1.5
Aggression
b_DeltaAgr1
0
1
2
Troop Distance to Center
b_TDCs
-0.50
-0.25
0.00
0.25
0.50
0.75
Participation
b_DeltaPart
0.000
0.025
0.050
0.075

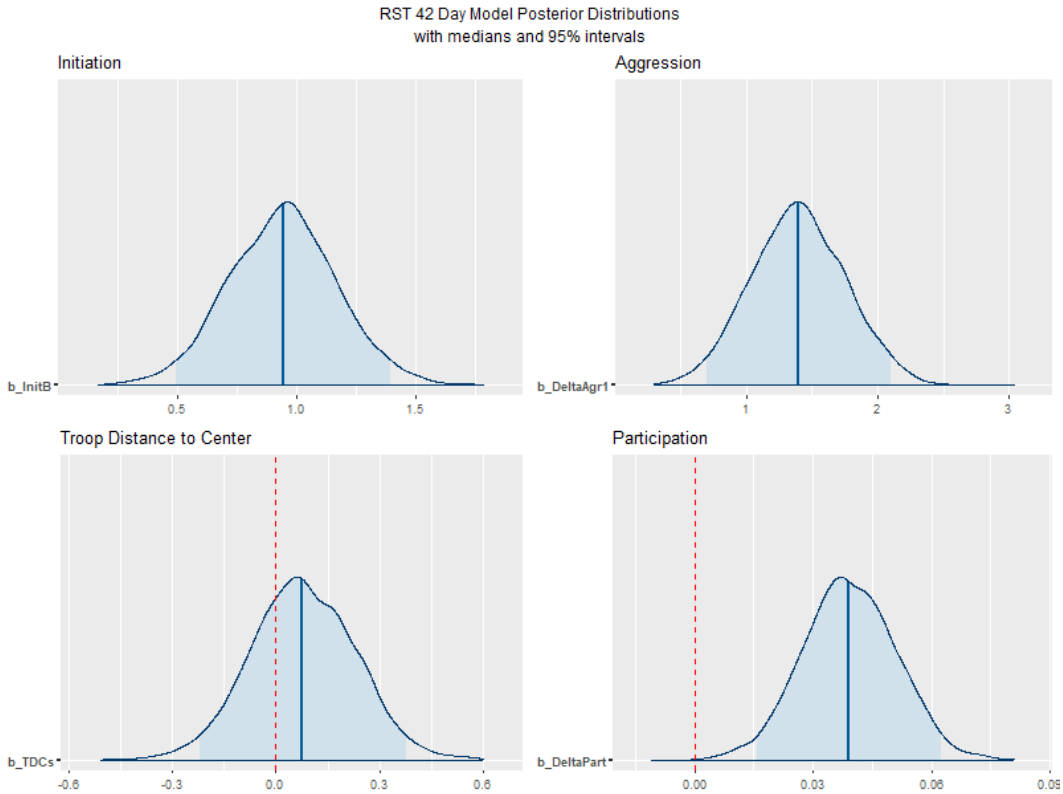
RST 42 Day Model Posterior Distributions
with medians and 95% intervals
Initiation
b_InitB
0.5
1.0
1.5
Aggression
b_DeltaAgr1
1
2
3
Troop Distance to Center
b_TDCs
-0.6
-0.3
0.0
0.3
0.6
Participation
b_DeltaPart
0.00
0.03
0.06
0.09

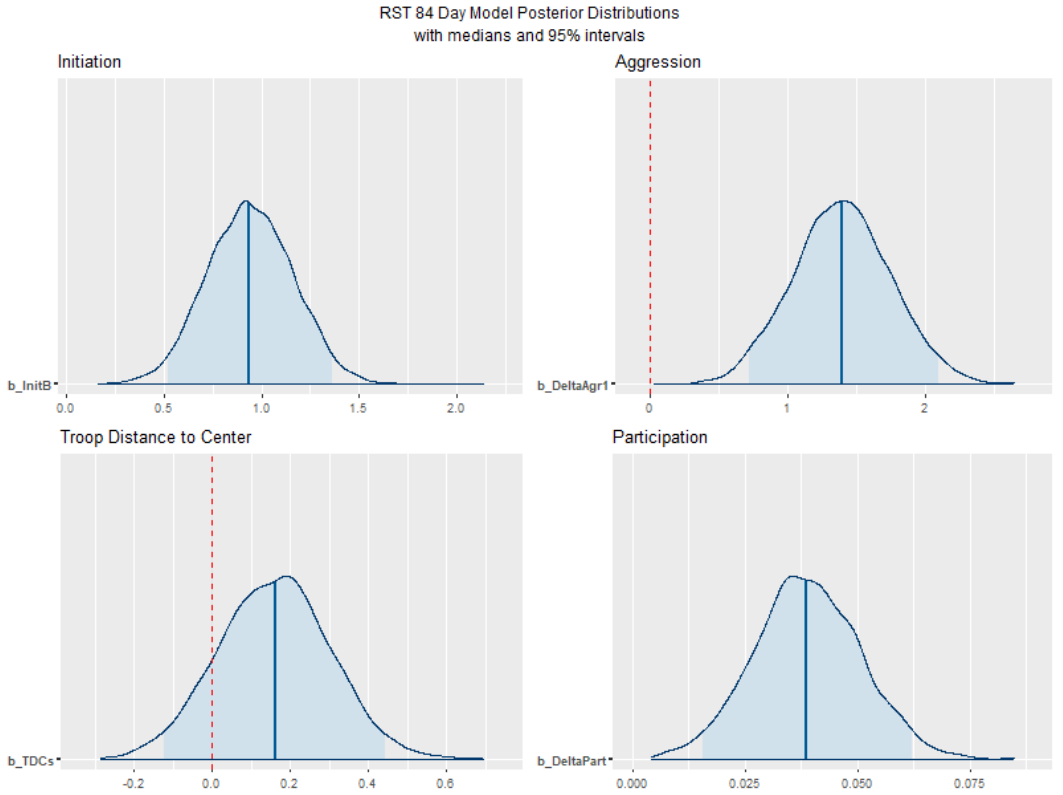
RST 84 Day Model Posterior Distributions
with medians and 95% intervals
Initiation
b_InitB
0.0
0.5
1.0
1.5
2.0
Aggression
b_DeltaAgr1
0
1
2
Troop Distance to Center
b_TDCs
-0.2
0.0
0.2
0.4
0.6
Participation
b_DeltaPart
0.000
0.025
0.050
0.075

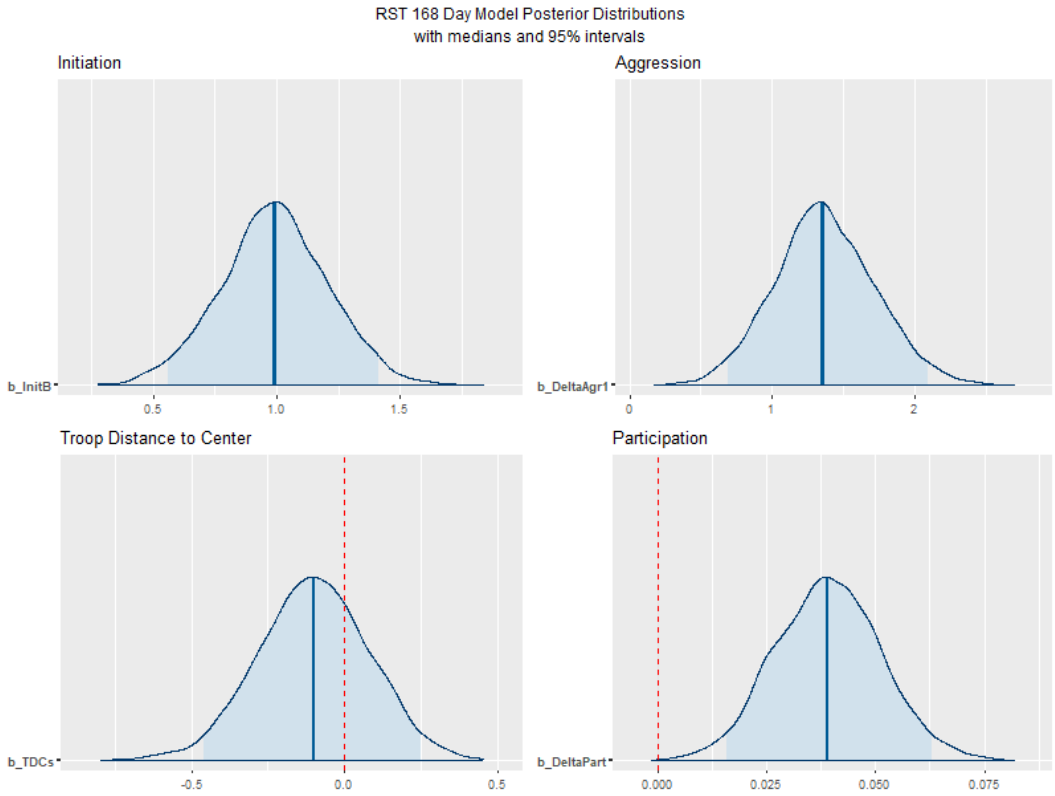

Figure 7.2: Dynamic home range posterior distribution plots, in order by Troop (PT, RBM, RST) and Window size (14, 21, 28, 35, 42, 84, 168 days). Each set contain Initiation (top left), Aggression (top right), Troop Distance to Centre (bottom left), Participation (bottom right).

Appendix H: Structure Models

Summaries

Winning

Time

```
Family: bernoulli
  Links: mu = logit
Formula: WinNum ~ 1 + s(DSS_S, by = Troop, bs = "fs", k = 10) + Troop
   Data: Win_Data (Number of observations: 2928)
  Draws: 4 chains, each with iter = 2000; warmup = 1000; thin = 1;
         total post-warmup draws = 4000

Smooth Terms:
                    Estimate Est.Error l-95% CI u-95% CI Rhat Bulk_ESS Tail_ESS
sds(sDSS_STroopPT_1)     2.67      1.23     0.79     5.63 1.00     1682     2541
sds(sDSS_STroopRBM_1)    4.25      2.22     1.70    10.26 1.00      856     1621
sds(sDSS_STroopRST_1)    3.48      1.30     1.71     6.67 1.00     1468     2478

Population-Level Effects:
                Estimate Est.Error l-95% CI u-95% CI Rhat Bulk_ESS Tail_ESS
Intercept          -1.35      0.08    -1.50    -1.19 1.00     4250     2269
TroopRBM            0.99      0.10     0.79     1.18 1.00     4902     2782
TroopRST            0.23      0.12    -0.01     0.46 1.00     4549     2930
sDSS_S:TroopPT_1    2.81      5.04    -5.50    14.19 1.00     2533     2057
sDSS_S:TroopRBM_1   0.23      5.71    -9.60    12.83 1.00     1831     2639
sDSS_S:TroopRST_1   7.74      5.86    -2.28    20.26 1.00     2479     2655

Draws were sampled using sampling(NUTS). For each parameter, Bulk_ESS
and Tail_ESS are effective sample size measures, and Rhat is the potential
scale reduction factor on split chains (at convergence, Rhat = 1).
    Estimate   Est.Error       Q2.5     Q97.5
R2 0.08806098 0.009651243 0.06942828 0.1077485
Using 10 posterior draws for ppc type 'dens_overlay' by default.
[1] "Number of Observations: 2928"
```

Space Time

```
Family: bernoulli
  Links: mu = logit
Formula: WinNum ~ 1 + t2(Point_X_S, Point_Y_S, DSS_S, by = Troop, bs = c("tp", "tp"), k =
c(25, 10), d = c(2, 1)) + Troop
   Data: Win_Data (Number of observations: 2928)
  Draws: 4 chains, each with iter = 2000; warmup = 1000; thin = 1;
         total post-warmup draws = 4000

Smooth Terms:
```

	Estimate	Est.Error	l-95% CI	u-95% CI	Rhat	Bulk_ESS	Tail_ESS
sds(t2Point_X_SPoint_Y_SDSS_STroopPT_1)	34.9503	4.6139	26.3555	44.6709	1.0006	6004	3016
sds(t2Point_X_SPoint_Y_SDSS_STroopPT_2)	1.0033	0.9936	0.0302	3.6807	1.0017	5617	2318
sds(t2Point_X_SPoint_Y_SDSS_STroopPT_3)	1.0179	1.0357	0.0214	3.8160	1.0005	4841	2065
sds(t2Point_X_SPoint_Y_SDSS_STroopRBM_1)	44.6861	5.4563	34.8245	56.0986	1.0002	4918	3008
sds(t2Point_X_SPoint_Y_SDSS_STroopRBM_2)	1.0006	1.0384	0.0162	3.8840	1.0005	5620	1984
sds(t2Point_X_SPoint_Y_SDSS_STroopRBM_3)	1.0234	1.0472	0.0243	3.9286	1.0002	4888	2046
sds(t2Point_X_SPoint_Y_SDSS_STroopRST_1)	34.2085	4.8739	25.3915	44.3814	1.0024	5225	3261
sds(t2Point_X_SPoint_Y_SDSS_STroopRST_2)	1.0055	0.9774	0.0308	3.5916	1.0010	6307	2133
sds(t2Point_X_SPoint_Y_SDSS_STroopRST_3)	1.0126	0.9886	0.0259	3.7468	1.0020	5354	2296

Population-Level Effects:

	Estimate	Est.Error	l-95% CI	u-95% CI	Rhat	Bulk_ESS	Tail_ESS
Intercept	1.3419	0.6867	0.0028	2.6996	1.0007	3309	2658
TroopRBM	0.3674	0.7964	-1.2474	1.9413	1.0002	6803	3123
TroopRST	-0.2034	0.8029	-1.7687	1.3642	1.0000	5921	3248
t2Point_X_SPoint_Y_SDSS_S:TroopPT_1	0.0810	0.5246	-0.9438	1.1085	1.0004	5034	2926
t2Point_X_SPoint_Y_SDSS_S:TroopPT_2	0.0219	0.2410	-0.4462	0.4980	1.0005	4881	3363
t2Point_X_SPoint_Y_SDSS_S:TroopPT_3	0.0652	0.1951	-0.3295	0.4380	1.0009	6453	3275
t2Point_X_SPoint_Y_SDSS_S:TroopPT_4	-0.0533	0.2244	-0.5037	0.3803	1.0014	4586	3069
t2Point_X_SPoint_Y_SDSS_S:TroopPT_5	-0.0897	0.1784	-0.4386	0.2571	1.0021	5257	3163
t2Point_X_SPoint_Y_SDSS_S:TroopRBM_1	0.2988	0.5533	-0.7899	1.3501	1.0002	4246	2822
t2Point_X_SPoint_Y_SDSS_S:TroopRBM_2	-0.0486	0.2400	-0.5098	0.4154	1.0003	5052	3011
t2Point_X_SPoint_Y_SDSS_S:TroopRBM_3	-0.2601	0.2015	-0.6689	0.1351	1.0000	5071	3563
t2Point_X_SPoint_Y_SDSS_S:TroopRBM_4	-0.1151	0.2235	-0.5580	0.3342	1.0011	4875	2965
t2Point_X_SPoint_Y_SDSS_S:TroopRBM_5	-0.2661	0.1688	-0.6136	0.0532	0.9996	5079	3085
t2Point_X_SPoint_Y_SDSS_S:TroopRST_1	-0.3259	0.5525	-1.4060	0.7169	1.0000	4202	2846
t2Point_X_SPoint_Y_SDSS_S:TroopRST_2	-0.1914	0.2263	-0.6485	0.2490	1.0001	5119	2649
t2Point_X_SPoint_Y_SDSS_S:TroopRST_3	-0.1790	0.2109	-0.6076	0.2213	1.0026	5072	3040

t2Point_X_SPoint_Y_SDSS_S:TroopRST_4 0.2351 0.2388 -0.2430 0.6916 1.0008 4664
2985
t2Point_X_SPoint_Y_SDSS_S:TroopRST_5 -0.0414 0.1973 -0.4482 0.3355 1.0005 5816
3319

Draws were sampled using sampling(NUTS). For each parameter, Bulk_ESS
and Tail_ESS are effective sample size measures, and Rhat is the potential
scale reduction factor on split chains (at convergence, Rhat = 1).
Using 10 posterior draws for ppc type 'dens_overlay' by default.
   Estimate Est.Error   Q2.5   Q97.5
R2 0.2334428 0.01293701 0.2074771 0.2582873
Output of model 'Win_ST':

Computed from 4000 by 2928 log-likelihood matrix

Monte Carlo SE of elpd_loo is 0.1.
Pareto k diagnostic values:
                         Count Pct.   Min. n_eff
(-Inf, 0.5]   (good)   2927 100.0% 3142
 (0.5, 0.7]   (ok)   1   0.0% 3721
   (0.7, 1]   (bad)   0   0.0% <NA>
   (1, Inf)   (very bad)   0   0.0% <NA>

All Pareto k estimates are ok (k < 0.7).

Output of model 'Win_Time':

Computed from 4000 by 2928 log-likelihood matrix

Monte Carlo SE of elpd_loo is 0.1.
All Pareto k estimates are good (k < 0.5).
See help('pareto-k-diagnostic') for details.

Model comparisons:
         elpd_diff se_diff
Win_ST   0.0   0.0
Win_Time -317.7   15.6
[1] "Number of Observations: 2928"

Initiation

Tim

Family: bernoulli
  Links: mu = logit
Formula: InitNum ~ s(DSS_S, by = Troop, bs = "fs", k = 10) + Troop
   Data: Init_Data (Number of observations: 4130)
  Draws: 4 chains, each with iter = 2000; warmup = 1000; thin = 1;
         total post-warmup draws = 4000

Smooth Terms:
                    Estimate Est.Error l-95% CI u-95% CI Rhat Bulk_ESS Tail_ESS
sds(sDSS_STroopPT_1)   8.78   2.46   4.68   14.34 1.01   986   1487
sds(sDSS_STroopRBM_1)   9.05   2.45   5.13   14.53 1.00   975   1416
sds(sDSS_STroopRST_1)   7.89   2.33   3.91   12.92 1.00   1361   2130

Population-Level Effects:
              Estimate Est.Error l-95% CI u-95% CI Rhat Bulk_ESS Tail_ESS
Intercept   -1.03   0.06   -1.14   -0.91 1.00   4211   3368
TroopRBM   0.84   0.08   0.68   0.99 1.00   5180   3454
TroopRST   0.19   0.10   0.01   0.38 1.00   4807   3083
sDSS_S:TroopPT_1   18.83   7.88   4.17   34.63 1.00   1686   2401
sDSS_S:TroopRBM_1   -3.20   6.67   -16.81   9.68 1.00   1922   2580
sDSS_S:TroopRST_1   3.94   8.64   -12.26   21.29 1.00   1847   2264

Draws were sampled using sampling(NUTS). For each parameter, Bulk_ESS
and Tail_ESS are effective sample size measures, and Rhat is the potential
scale reduction factor on split chains (at convergence, Rhat = 1).
   Estimate   Est.Error   Q2.5   Q97.5
R2 0.102418 0.008657597 0.08534743 0.1192784
Using 10 posterior draws for ppc type 'dens_overlay' by default.
[1] "Number of Observations: 4130"

Space Time

Family: bernoulli
  Links: mu = logit
Formula: InitNum ~ t2(Point_X_S, Point_Y_S, DSS_S, by = Troop, bs = c("tp", "tp"), k = c(25,
10), d = c(2, 1)) + (1 | Troop)
   Data: Init_Data (Number of observations: 4130)
  Draws: 4 chains, each with iter = 2000; warmup = 1000; thin = 1;
         total post-warmup draws = 4000

Smooth Terms:
                                          Estimate Est.Error l-95% CI u-95% CI   Rhat Bulk_ESS Tail_ESS
sds(t2Point_X_SPoint_Y_SDSS_STroopPT_1)   36.6868   4.4542 28.6192 46.1470 1.0016
4645   3112
sds(t2Point_X_SPoint_Y_SDSS_STroopPT_2)   1.0308   1.1190   0.0192   3.9937 1.0011
4806   2308
sds(t2Point_X_SPoint_Y_SDSS_STroopPT_3)   1.0065   0.9843   0.0271   3.5820 0.9997
4724   2338
sds(t2Point_X_SPoint_Y_SDSS_STroopRBM_1) 43.9817   5.1477 34.4068 54.7360 1.0030
4393   2802
sds(t2Point_X_SPoint_Y_SDSS_STroopRBM_2)   1.0327   1.0548   0.0291   3.7383 0.9993
6010   2408
sds(t2Point_X_SPoint_Y_SDSS_STroopRBM_3)   1.0444   1.0860   0.0217   4.0421 1.0001
4631   1586
sds(t2Point_X_SPoint_Y_SDSS_STroopRST_1) 43.1106   5.2058 33.6679 53.9304 1.0006
5490   3417

```
sds(t2Point_X_SPoint_Y_SDSS_STroopRST_2)   1.0008    1.0072   0.0292   3.6642 0.9999
5525     2405
sds(t2Point_X_SPoint_Y_SDSS_STroopRST_3)   1.0040    1.0218   0.0210   3.7057 1.0003
4948     2375

Group-Level Effects:
~Troop (Number of levels: 3)
              Estimate Est.Error l-95% CI u-95% CI   Rhat Bulk_ESS Tail_ESS
sd(Intercept)   0.8798    0.8113   0.0305   3.0685 1.0005     2620     2591

Population-Level Effects:
                                 Estimate Est.Error l-95% CI u-95% CI   Rhat Bulk_ESS Tail_ESS
Intercept                           1.3328    0.7644  -0.2171   2.9050 1.0009     2657     2260
t2Point_X_SPoint_Y_SDSS_S:TroopPT_1   -0.2493    0.4737  -1.1632   0.6626 1.0010     4286
2579
t2Point_X_SPoint_Y_SDSS_S:TroopPT_2   -0.1262    0.1960  -0.5277   0.2494 1.0010     3623
2036
t2Point_X_SPoint_Y_SDSS_S:TroopPT_3    0.0735    0.1423  -0.2082   0.3441 1.0000     4454
2848
t2Point_X_SPoint_Y_SDSS_S:TroopPT_4   -0.0128    0.1835  -0.3714   0.3487 1.0020     4902
2789
t2Point_X_SPoint_Y_SDSS_S:TroopPT_5   -0.1370    0.1346  -0.3988   0.1211 1.0003     4926
2796
t2Point_X_SPoint_Y_SDSS_S:TroopRBM_1   0.4906    0.4991  -0.5020   1.4719 0.9995     4160
2561
t2Point_X_SPoint_Y_SDSS_S:TroopRBM_2   0.0801    0.1991  -0.2993   0.4764 1.0013     3897
2520
t2Point_X_SPoint_Y_SDSS_S:TroopRBM_3  -0.2038    0.1661  -0.5301   0.1169 1.0013     4811
3118
t2Point_X_SPoint_Y_SDSS_S:TroopRBM_4  -0.1848    0.1843  -0.5548   0.1875 1.0005     4751
2882
t2Point_X_SPoint_Y_SDSS_S:TroopRBM_5  -0.1928    0.1389  -0.4730   0.0782 1.0001     4336
3198
t2Point_X_SPoint_Y_SDSS_S:TroopRST_1   0.2209    0.5667  -0.8876   1.3439 1.0005     4342
3171
t2Point_X_SPoint_Y_SDSS_S:TroopRST_2  -0.0939    0.2193  -0.5282   0.3413 1.0012     4993
2861
t2Point_X_SPoint_Y_SDSS_S:TroopRST_3  -0.1154    0.1979  -0.5095   0.2680 1.0013     5380
2708
t2Point_X_SPoint_Y_SDSS_S:TroopRST_4   0.1077    0.2253  -0.3264   0.5577 1.0010     4489
3140
t2Point_X_SPoint_Y_SDSS_S:TroopRST_5  -0.1406    0.1914  -0.5301   0.2363 1.0008     4934
3120

Draws were sampled using sampling(NUTS). For each parameter, Bulk_ESS
and Tail_ESS are effective sample size measures, and Rhat is the potential
scale reduction factor on split chains (at convergence, Rhat = 1).
Using 10 posterior draws for ppc type 'dens_overlay' by default.
   Estimate   Est.Error      Q2.5    Q97.5
R2 0.2197257 0.009814102 0.2005319 0.239137
```

```
Output of model 'Init_ST':
Computed from 4000 by 4130 log-likelihood matrix
------
Monte Carlo SE of elpd_loo is 0.1.
Pareto k diagnostic values:
                         Count Pct.    Min. n_eff
(-Inf, 0.5]   (good)     4128  100.0%  1907
 (0.5, 0.7]   (ok)         2    0.0%  2971
   (0.7, 1]   (bad)        0    0.0%  <NA>
   (1, Inf)   (very bad)   0    0.0%  <NA>
All Pareto k estimates are ok (k < 0.7).

Output of model 'Init_Time':
Computed from 4000 by 4130 log-likelihood matrix
------
Monte Carlo SE of elpd_loo is 0.1.
All Pareto k estimates are good (k < 0.5).

Model comparisons:
          elpd_diff se_diff
Init_ST      0.0       0.0
Init_Time -370.6      19.9
[1] "Number of Observations: 4130"
```

Aggression

Time

```
Family: zero_one_inflated_beta
  Links: mu = logit; phi = log; zoi = logit; coi = logit
Formula: Agr ~ 1 + s(DSSs, by = Troop) + Troop
         zoi ~ 1 + s(DSSs, by = Troop) + Troop
         coi ~ 1 + s(DSSs, by = Troop) + Troop
         phi ~ 1 + s(DSSs, by = Troop) + Troop
   Data: df.2023 (Number of observations: 5783)
  Draws: 4 chains, each with iter = 1000; warmup = 500; thin = 1;
         total post-warmup draws = 2000

Smooth Terms:
                          Estimate Est.Error l-95% CI u-95% CI Rhat Bulk_ESS Tail_ESS
sds(sDSSsTroopPT_1)           2.04      0.64     0.89     3.33 1.00      816      982
sds(sDSSsTroopRBM_1)          3.01      0.63     1.81     4.26 1.00     1146     1222
sds(sDSSsTroopRST_1)          0.86      0.50     0.10     2.05 1.00      731      505
sds(phi_sDSSsTroopPT_1)       0.84      0.83     0.02     3.09 1.01      488      960
sds(phi_sDSSsTroopRBM_1)      1.09      0.77     0.06     2.94 1.00      615      948
sds(phi_sDSSsTroopRST_1)      0.72      0.68     0.02     2.58 1.01      772     1127
sds(zoi_sDSSsTroopPT_1)       2.98      2.12     0.61     8.50 1.01      343      849
sds(zoi_sDSSsTroopRBM_1)      2.09      1.19     0.67     5.18 1.01      702     1080
sds(zoi_sDSSsTroopRST_1)      4.60      1.77     2.09     8.86 1.00      944     1441
sds(coi_sDSSsTroopPT_1)       0.72      0.52     0.03     2.01 1.00      958      879
```

```
sds(coi_sDSSsTroopRBM_1)     0.64      0.53     0.02     2.04 1.01      848      910
sds(coi_sDSSsTroopRST_1)     0.71      0.56     0.03     2.07 1.00      912      832

Population-Level Effects:
                 Estimate Est.Error l-95% CI u-95% CI Rhat Bulk_ESS Tail_ESS
Intercept           -1.00      0.03    -1.06    -0.95 1.00     2524     1270
phi_Intercept        1.78      0.05     1.68     1.87 1.00     1865     1506
zoi_Intercept        0.68      0.04     0.60     0.77 1.00     2935     1612
coi_Intercept       -3.46      0.15    -3.76    -3.17 1.00     1887     1403
TroopRBM             0.31      0.04     0.23     0.39 1.00     2572     1456
TroopRST             0.23      0.06     0.10     0.34 1.00     2442     1400
phi_TroopRBM        -0.13      0.07    -0.27    -0.00 1.00     2059     1317
phi_TroopRST        -0.22      0.09    -0.38    -0.05 1.00     2682     1461
zoi_TroopRBM        -0.25      0.06    -0.37    -0.12 1.00     3096     1641
zoi_TroopRST         0.34      0.08     0.18     0.50 1.00     2910     1661
coi_TroopRBM         0.78      0.18     0.44     1.15 1.00     2229     1586
coi_TroopRST         0.56      0.21     0.14     0.99 1.00     2466     1644
sDSSs:TroopPT_1     -0.40      0.96    -2.24     1.43 1.01     2500     1435
sDSSs:TroopRBM_1    -0.47      0.97    -2.27     1.41 1.00     2695     1537
sDSSs:TroopRST_1     0.34      0.84    -1.35     1.97 1.00     2162     1457
phi_sDSSs:TroopPT_1 -1.50      1.77    -5.22     2.14 1.00     1063      851
phi_sDSSs:TroopRBM_1 1.06      2.17    -3.17     5.65 1.00     1090     1083
phi_sDSSs:TroopRST_1 -0.20     1.97    -4.60     3.72 1.01      838      553
zoi_sDSSs:TroopPT_1  0.34      4.22   -10.48     7.03 1.00      741      710
zoi_sDSSs:TroopRBM_1 1.44      3.00    -4.33     7.73 1.00     1230     1162
zoi_sDSSs:TroopRST_1 1.46      5.52    -9.25    12.78 1.00     1647     1183
coi_sDSSs:TroopPT_1 -2.72      2.17    -6.98     2.38 1.00     1432     1122
coi_sDSSs:TroopRBM_1 -1.18     1.94    -5.95     1.92 1.01     1124      782
coi_sDSSs:TroopRST_1 -2.19     2.36    -8.04     1.35 1.00     1247      774

Draws were sampled using sampling(NUTS). For each parameter, Bulk_ESS
and Tail_ESS are effective sample size measures, and Rhat is the potential
scale reduction factor on split chains (at convergence, Rhat = 1).
    Estimate   Est.Error       Q2.5      Q97.5
R2 0.02212865 0.003553851 0.01592412 0.02953976
Using 10 posterior draws for ppc type 'dens_overlay' by default.
[1] "Number of Observations: 5783"
```

Space Time

```
Family: zero_one_inflated_beta
  Links: mu = logit; phi = log; zoi = logit; coi = logit
Formula: Agr ~ 1 + t2(Point_X_S, Point_Y_S, DSS_S, by = Troop, k = c(25, 10), d = c(2, 1)) +
Troop
       zoi ~ 1 + t2(Point_X_S, Point_Y_S, DSS_S, by = Troop, k = c(25, 10), d = c(2, 1)) + Troop
       coi ~ 1 + t2(Point_X_S, Point_Y_S, DSS_S, by = Troop, k = c(25, 10), d = c(2, 1)) + Troop
       phi ~ 1 + t2(Point_X_S, Point_Y_S, DSS_S, by = Troop, k = c(25, 10), d = c(2, 1)) + Troop
   Data: df.sp.sub (Number of observations: 5783)
  Draws: 4 chains, each with iter = 1000; warmup = 500; thin = 1;
       total post-warmup draws = 2000
```

Smooth Terms:

	Estimate	Est.Error	l-95% CI	u-95% CI	Rhat	Bulk_ESS	Tail_ESS
sds(t2Point_X_SPoint_Y_SDSS_STroopPT_1)	10.09	3.65	3.42	17.79	1.01	470	349
sds(t2Point_X_SPoint_Y_SDSS_STroopPT_2)	7.55	5.71	0.28	21.83	1.01	451	521
sds(t2Point_X_SPoint_Y_SDSS_STroopPT_3)	8.37	6.96	0.35	26.20	1.01	493	876
sds(t2Point_X_SPoint_Y_SDSS_STroopRBM_1)	12.26	3.46	6.61	20.20	1.01	701	1007
sds(t2Point_X_SPoint_Y_SDSS_STroopRBM_2)	5.70	4.75	0.21	17.65	1.00	734	986
sds(t2Point_X_SPoint_Y_SDSS_STroopRBM_3)	8.67	7.08	0.38	27.31	1.01	557	872
sds(t2Point_X_SPoint_Y_SDSS_STroopRST_1)	16.56	7.03	2.72	31.49	1.02	305	195
sds(t2Point_X_SPoint_Y_SDSS_STroopRST_2)	9.80	8.35	0.37	30.98	1.00	786	965
sds(t2Point_X_SPoint_Y_SDSS_STroopRST_3)	12.22	13.69	0.28	51.68	1.01	423	364
sds(phi_t2Point_X_SPoint_Y_SDSS_STroopPT_1)	3.06	2.84	0.07	10.11	1.01	613	937
sds(phi_t2Point_X_SPoint_Y_SDSS_STroopPT_2)	5.91	5.14	0.27	18.56	1.00	838	1087
sds(phi_t2Point_X_SPoint_Y_SDSS_STroopPT_3)	9.25	8.44	0.30	31.32	1.01	604	950
sds(phi_t2Point_X_SPoint_Y_SDSS_STroopRBM_1)	3.38	2.41	0.22	8.98	1.00	669	984
sds(phi_t2Point_X_SPoint_Y_SDSS_STroopRBM_2)	6.35	4.66	0.29	17.41	1.00	492	617
sds(phi_t2Point_X_SPoint_Y_SDSS_STroopRBM_3)	11.83	10.24	0.61	37.60	1.00	573	1023
sds(phi_t2Point_X_SPoint_Y_SDSS_STroopRST_1)	3.21	2.83	0.15	10.92	1.00	1090	850
sds(phi_t2Point_X_SPoint_Y_SDSS_STroopRST_2)	6.44	5.50	0.27	20.45	1.00	1184	946
sds(phi_t2Point_X_SPoint_Y_SDSS_STroopRST_3)	9.03	8.41	0.28	32.40	1.00	1032	975
sds(zoi_t2Point_X_SPoint_Y_SDSS_STroopPT_1)	7.88	5.66	0.36	20.93	1.01	309	692
sds(zoi_t2Point_X_SPoint_Y_SDSS_STroopPT_2)	14.93	10.17	0.97	40.20	1.01	437	930
sds(zoi_t2Point_X_SPoint_Y_SDSS_STroopPT_3)	172.87	29.98	121.42	238.56	1.00	973	1359
sds(zoi_t2Point_X_SPoint_Y_SDSS_STroopRBM_1)	19.42	7.77	4.98	36.26	1.01	358	395
sds(zoi_t2Point_X_SPoint_Y_SDSS_STroopRBM_2)	6.83	5.95	0.14	21.98	1.00	692	644
sds(zoi_t2Point_X_SPoint_Y_SDSS_STroopRBM_3)	185.23	33.14	130.63	255.56	1.00	701	1028

sds(zoi_t2Point_X_SPoint_Y_SDSS_STroopRST_1) 13.53 5.22 5.72 26.16 1.00 845 984
sds(zoi_t2Point_X_SPoint_Y_SDSS_STroopRST_2) 7.78 6.97 0.25 25.40 1.00 903 1001
sds(zoi_t2Point_X_SPoint_Y_SDSS_STroopRST_3) 197.15 40.88 130.05 290.93 1.00 1118 1289
sds(coi_t2Point_X_SPoint_Y_SDSS_STroopPT_1) 3.88 3.78 0.11 14.46 1.00 968 858
sds(coi_t2Point_X_SPoint_Y_SDSS_STroopPT_2) 5.27 4.43 0.18 16.16 1.00 1325 866
sds(coi_t2Point_X_SPoint_Y_SDSS_STroopPT_3) 69.04 29.93 16.44 138.67 1.00 514 398
sds(coi_t2Point_X_SPoint_Y_SDSS_STroopRBM_1) 8.12 8.17 0.16 30.25 1.00 444 830
sds(coi_t2Point_X_SPoint_Y_SDSS_STroopRBM_2) 6.25 5.53 0.14 21.17 1.01 904 568
sds(coi_t2Point_X_SPoint_Y_SDSS_STroopRBM_3) 142.33 45.80 69.10 248.31 1.01 682 870
sds(coi_t2Point_X_SPoint_Y_SDSS_STroopRST_1) 8.28 7.13 0.39 26.83 1.00 1022 988
sds(coi_t2Point_X_SPoint_Y_SDSS_STroopRST_2) 7.44 6.54 0.28 23.86 1.00 1345 813
sds(coi_t2Point_X_SPoint_Y_SDSS_STroopRST_3) 288.80 101.65 136.26 533.53 1.00 639 978

Population-Level Effects:

	Estimate	Est.Error	l-95% CI	u-95% CI	Rhat	Bulk_ESS	Tail_ESS
Intercept	-1.03	0.25	-1.56	-0.45	1.00	926	593
phi_Intercept	1.76	0.28	1.08	2.30	1.00	842	843
zoi_Intercept	-5.28	2.11	-9.71	-1.51	1.00	748	1180
coi_Intercept	-0.13	1.43	-2.92	2.84	1.00	667	426
TroopRBM	0.18	0.35	-0.60	0.90	1.01	791	683
TroopRST	-0.05	0.43	-0.96	0.82	1.01	811	671
phi_TroopRBM	-0.01	0.43	-0.98	0.91	1.01	837	785
phi_TroopRST	0.09	0.42	-0.72	1.00	1.01	697	752
zoi_TroopRBM	-0.05	1.01	-2.03	1.93	1.00	1953	1340
zoi_TroopRST	0.01	1.00	-1.99	1.95	1.00	2331	1597
coi_TroopRBM	0.27	0.94	-1.59	2.07	1.00	2071	1673
coi_TroopRST	0.17	0.98	-1.73	2.17	1.00	2306	1671
t2Point_X_SPoint_Y_SDSS_S:TroopPT_1	0.01	0.27	-0.58	0.57	1.01	614	541
t2Point_X_SPoint_Y_SDSS_S:TroopPT_2	0.04	0.11	-0.17	0.27	1.00	1678	1440
t2Point_X_SPoint_Y_SDSS_S:TroopPT_3	0.07	0.13	-0.18	0.33	1.00	1598	1617
t2Point_X_SPoint_Y_SDSS_S:TroopPT_4	-0.03	0.06	-0.16	0.09	1.00	1321	1068
t2Point_X_SPoint_Y_SDSS_S:TroopPT_5	0.00	0.07	-0.15	0.15	1.00	1344	1183
t2Point_X_SPoint_Y_SDSS_S:TroopRBM_1	0.15	0.27	-0.49	0.66	1.01	764	654

t2Point_X_SPoint_Y_SDSS_S:TroopRBM_2 0.12 0.11 -0.11 0.34 1.00 1589
1532
t2Point_X_SPoint_Y_SDSS_S:TroopRBM_3 -0.53 0.14 -0.80 -0.26 1.00 1461
1424
t2Point_X_SPoint_Y_SDSS_S:TroopRBM_4 0.13 0.06 -0.00 0.25 1.00 1229
1019
t2Point_X_SPoint_Y_SDSS_S:TroopRBM_5 0.04 0.07 -0.09 0.18 1.00 1397
1044
t2Point_X_SPoint_Y_SDSS_S:TroopRST_1 -0.33 0.40 -1.02 0.58 1.00 876
582
t2Point_X_SPoint_Y_SDSS_S:TroopRST_2 -0.42 0.19 -0.76 -0.06 1.00 861
610
t2Point_X_SPoint_Y_SDSS_S:TroopRST_3 0.02 0.22 -0.41 0.42 1.00 1489
1360
t2Point_X_SPoint_Y_SDSS_S:TroopRST_4 -0.40 0.17 -0.73 -0.05 1.00 799
609
t2Point_X_SPoint_Y_SDSS_S:TroopRST_5 0.28 0.22 -0.13 0.68 1.00 1027
918
phi_t2Point_X_SPoint_Y_SDSS_S:TroopPT_1 0.24 0.28 -0.29 0.88 1.01 927
734
phi_t2Point_X_SPoint_Y_SDSS_S:TroopPT_2 -0.11 0.16 -0.43 0.21 1.01 1826
1324
phi_t2Point_X_SPoint_Y_SDSS_S:TroopPT_3 -0.09 0.20 -0.50 0.29 1.00 1758
1773
phi_t2Point_X_SPoint_Y_SDSS_S:TroopPT_4 0.03 0.10 -0.15 0.24 1.00 1263
1079
phi_t2Point_X_SPoint_Y_SDSS_S:TroopPT_5 0.10 0.10 -0.10 0.29 1.00 1382
1554
phi_t2Point_X_SPoint_Y_SDSS_S:TroopRBM_1 -0.02 0.35 -0.88 0.66 1.00 627
357
phi_t2Point_X_SPoint_Y_SDSS_S:TroopRBM_2 0.02 0.17 -0.31 0.36 1.00 1521
1183
phi_t2Point_X_SPoint_Y_SDSS_S:TroopRBM_3 0.11 0.21 -0.30 0.50 1.00 1795
1592
phi_t2Point_X_SPoint_Y_SDSS_S:TroopRBM_4 -0.02 0.09 -0.17 0.16 1.00 1337
1018
phi_t2Point_X_SPoint_Y_SDSS_S:TroopRBM_5 -0.10 0.09 -0.29 0.06 1.00 1564
1093
phi_t2Point_X_SPoint_Y_SDSS_S:TroopRST_1 0.33 0.36 -0.42 1.01 1.00 909
796
phi_t2Point_X_SPoint_Y_SDSS_S:TroopRST_2 0.17 0.22 -0.28 0.60 1.00 1888
1540
phi_t2Point_X_SPoint_Y_SDSS_S:TroopRST_3 0.21 0.29 -0.35 0.78 1.00 1698
1562
phi_t2Point_X_SPoint_Y_SDSS_S:TroopRST_4 0.17 0.18 -0.18 0.53 1.00 1730
1517
phi_t2Point_X_SPoint_Y_SDSS_S:TroopRST_5 -0.35 0.23 -0.78 0.11 1.00 1541
1594
zoi_t2Point_X_SPoint_Y_SDSS_S:TroopPT_1 -0.02 0.98 -1.95 1.87 1.00 1353
1424

zoi_t2Point_X_SPoint_Y_SDSS_S:TroopPT_2 0.11 0.38 -0.62 0.84 1.00 1106
1152
zoi_t2Point_X_SPoint_Y_SDSS_S:TroopPT_3 0.20 0.38 -0.53 0.94 1.00 917
1160
zoi_t2Point_X_SPoint_Y_SDSS_S:TroopPT_4 0.11 0.33 -0.59 0.76 1.01 882
1111
zoi_t2Point_X_SPoint_Y_SDSS_S:TroopPT_5 -0.05 0.34 -0.69 0.65 1.00 812
832
zoi_t2Point_X_SPoint_Y_SDSS_S:TroopRBM_1 -0.03 0.95 -1.86 1.87 1.00 1120
1353
zoi_t2Point_X_SPoint_Y_SDSS_S:TroopRBM_2 -0.29 0.39 -1.06 0.48 1.00 899
1213
zoi_t2Point_X_SPoint_Y_SDSS_S:TroopRBM_3 0.18 0.41 -0.61 0.99 1.00 1050
1182
zoi_t2Point_X_SPoint_Y_SDSS_S:TroopRBM_4 -0.03 0.32 -0.65 0.57 1.00 879
997
zoi_t2Point_X_SPoint_Y_SDSS_S:TroopRBM_5 0.14 0.36 -0.57 0.88 1.00 760
1154
zoi_t2Point_X_SPoint_Y_SDSS_S:TroopRST_1 0.01 0.98 -1.92 1.91 1.00 1227
1131
zoi_t2Point_X_SPoint_Y_SDSS_S:TroopRST_2 -0.09 0.47 -1.04 0.82 1.00 1262
1595
zoi_t2Point_X_SPoint_Y_SDSS_S:TroopRST_3 -0.02 0.49 -0.98 0.91 1.00 1243
1324
zoi_t2Point_X_SPoint_Y_SDSS_S:TroopRST_4 0.21 0.46 -0.67 1.10 1.00 1181
1124
zoi_t2Point_X_SPoint_Y_SDSS_S:TroopRST_5 0.13 0.48 -0.81 1.08 1.00 1357
1465
coi_t2Point_X_SPoint_Y_SDSS_S:TroopPT_1 0.18 0.83 -1.43 1.84 1.00 1018
1314
coi_t2Point_X_SPoint_Y_SDSS_S:TroopPT_2 0.09 0.25 -0.40 0.62 1.00 1203
1069
coi_t2Point_X_SPoint_Y_SDSS_S:TroopPT_3 -0.07 0.26 -0.55 0.46 1.00 1258
861
coi_t2Point_X_SPoint_Y_SDSS_S:TroopPT_4 -0.14 0.24 -0.61 0.37 1.01 1012
892
coi_t2Point_X_SPoint_Y_SDSS_S:TroopPT_5 0.01 0.25 -0.52 0.51 1.00 1223
1270
coi_t2Point_X_SPoint_Y_SDSS_S:TroopRBM_1 0.01 0.95 -1.87 1.91 1.00 1260
1243
coi_t2Point_X_SPoint_Y_SDSS_S:TroopRBM_2 0.08 0.39 -0.70 0.88 1.00 1274
1356
coi_t2Point_X_SPoint_Y_SDSS_S:TroopRBM_3 -0.06 0.39 -0.87 0.72 1.00 1152
1378
coi_t2Point_X_SPoint_Y_SDSS_S:TroopRBM_4 0.13 0.36 -0.57 0.83 1.00 1066
1222
coi_t2Point_X_SPoint_Y_SDSS_S:TroopRBM_5 0.14 0.35 -0.54 0.89 1.01 1213
1099
coi_t2Point_X_SPoint_Y_SDSS_S:TroopRST_1 0.01 0.97 -1.88 1.82 1.00 1314
1564

```
coi_t2Point_X_SPoint_Y_SDSS_S:TroopRST_2   -0.01      0.61   -1.21     1.20 1.00     1206
1505
coi_t2Point_X_SPoint_Y_SDSS_S:TroopRST_3   -0.11      0.60   -1.28     1.08 1.00     1452
1396
coi_t2Point_X_SPoint_Y_SDSS_S:TroopRST_4   -0.14      0.61   -1.37     1.04 1.00     1322
1286
coi_t2Point_X_SPoint_Y_SDSS_S:TroopRST_5   -0.14      0.62   -1.38     1.12 1.00     1557
1454

Draws were sampled using sampling(NUTS). For each parameter, Bulk_ESS
and Tail_ESS are effective sample size measures, and Rhat is the potential
scale reduction factor on split chains (at convergence, Rhat = 1).
Using 10 posterior draws for ppc type 'dens_overlay' by default.
   Estimate  Est.Error       Q2.5     Q97.5
R2 0.1233749 0.02279844 0.08862468 0.1793226
Warning: Found 667 observations with a pareto_k > 0.7 in model 'ASTS'. It is recommended to
set 'moment_match = TRUE' in order to perform moment matching for problematic observations.
Output of model 'ASTS':

Computed from 2000 by 5783 log-likelihood matrix
------
Monte Carlo SE of elpd_loo is NA.
Pareto k diagnostic values:
                  Count Pct.    Min. n_eff
(-Inf, 0.5]   (good)     4640  80.2%   57
 (0.5, 0.7]   (ok)       476   8.2%   50
   (0.7, 1]   (bad)      327   5.7%   13
   (1, Inf)   (very bad) 340   5.9%   0
See help('pareto-k-diagnostic') for details.

Output of model 'ATM':
Computed from 2000 by 5783 log-likelihood matrix
------
Monte Carlo SE of elpd_loo is 0.2.
Pareto k diagnostic values:
                  Count Pct.    Min. n_eff
(-Inf, 0.5]   (good)     5782  100.0%  641
 (0.5, 0.7]   (ok)         1    0.0%  226
   (0.7, 1]   (bad)        0    0.0%  <NA>
   (1, Inf)   (very bad)   0    0.0%  <NA>
All Pareto k estimates are ok (k < 0.7).

Model comparisons:
     elpd_diff se_diff
ATM       0.0       0.0
ASTS -23995.8    7028.8
[1] 5783
```

Appendix H: AI Assistance Disclosure

Artificial intelligence tools (Microsoft Copilot, based on the GPT-5 model) were used during the preparation of the Intertroop Encounters (ITE) Chapter of this dissertation for limited editorial support. Assistance was restricted to proofreading for grammar and clarity, suggesting stylistic improvements, and providing feedback on sentence structure and organization. All edits and recommendations were made with the explicit intent to preserve the author's voice and writing style. In some cases, the tool offered suggestions for improving logical flow and transitions between sections. No original research content, new arguments, or substantive ideas were generated by AI. All intellectual contributions, interpretations, and conclusions presented in this work are solely those of the author.

The above disclosure paragraph was generated wholly by Microsoft Copilot. Full transparency of AI-assisted interactions can be provided by me from my M365 Copilot account at o365.uleth.ca, assuming institutional logging of conversations is retained.

Summary of Key Prompts for Committee Review

To ensure transparency, here is a concise summary of the types of prompts I provided to Copilot during the writing process, this was also generated by Copilot AI:

1. **Proofreading and Language Refinement**
    - Asked Copilot to check grammar, clarity, and conciseness of academic text.
    - Requested stylistic improvements while maintaining my voice and tone.

2. **Structural and Organizational Feedback**
    - Suggested edits for logical flow and coherence.
    - Helped improve transitions between sections for better readability.

3. **Summarization Within the Paper**
    - Condensed sections of the paper for clarity and brevity.
    - All summarization was for the paper itself, not for abstracts or presentations.

4. **Formatting and Presentation Guidance**
    - Provided advice on headings and academic formatting.
    - Suggested outline structures for sections.

5. **Meta-Disclosure and Transparency**
    - Asked Copilot to summarize all prior prompts for disclosure purposes.
    - Requested drafting of this disclosure paragraph.

Verification of Scope:

At no point did AI generate original research content, new arguments, or substantive ideas. Assistance was limited to editorial improvements such as transitions, clarity, and style preservation.